**Upgrading Old Movable Bridges with FRP Deck Application:**

**The case study of Wilhelminabrug**

by

Klodian Gradeci

July 2013

A Master Thesis Report

Submitted to the

Faculty of Civil Engineering and Geosciences,

in partial fulfillment of

the requirements for the degree of

Master of Science in Civil Engineering

by

Klodian Gradeci (4184580)

Faculty of Civil Engineering and Geosciences
Delft University of Technology
Delft, The Netherlands
July 2013

Thesis Committee:

**Prof. F.S.K. Bijlaard**, Professor at Delft University of Technology, Faculty of Civil Engineering and Geosciences, Department of Design and Construction, Section Steel & Composite Structures

**Dr. M.H. Kolstein**, Associate Professor at Delft University of Technology, Faculty of Civil Engineering and Geosciences, Department of Design and Construction, Section Steel & Composite Structures

**Dr. M.A.N. Hendriks**, Assistant Professor at Delft University of Technology, Faculty of Civil Engineering and Geosciences, Department of Design and Construction, Section Structural Mechanics

**Ir. W.P.J. Langedijk**, Chief Engineer at Iv-Infra B.V, Section of Steel Structures

# Abstract

Fibre Reinforced Polymer bridge decks, thanks to their beneficial properties and various advantages over traditional materials, have great potential as a material used in bridge engineering. They exercise high specific strength and stiffness-to-weight-ratio, a property particularly interesting from the point of view of designers, as it provides the possibility to consider new design concepts and what´s more significant, enables dead load savings, which is particularly important while retrofitting existing structures by replacing old bridge decks. Over the last 30 years, many authors have studied and conducted research for FRP composite bridge deck which are gaining greater acceptance as the materials of choices for civil and infrastructure applications. Nevertheless, many aspects still need to be addressed before a widespread introduction of this new technology is possible.

The purpose of this research is to provide an overview and investigate the performance of FRP decking system used to upgrade old movable bridges when composite action is provided between the deck adhesively bonded with the main girders. This thesis will firstly introduce the literature research investigating the structural analysis of FRP decking systems. Afterwards, the efficiency of using FRP decks for upgrading old movable bridges is investigated through three-dimensional finite element models based on the use of commercial software Abaqus. Three different FRP decks, Ecosafe from Lightweight Structures BV, ASSET from Fiberline and Duraspan from Martin Marietta Composites are used to investigate the upgrading and deck replacement of the old movable bridge, Wilhelminabrug located in Zaandam, The Netherlands. Due to the deterioration of the steel superstructure, a preliminary investigation for each deck is computed using three different configuration of steel superstructure, alternating the main girder span and the availability of cross beams, during the static analysis in order to find the most suitable solution. The composite behaviour of the bridge and lateral load distribution are further examined for each of three decks using the strain distribution. Moreover, the fatigue life assessment is analyzed using the cumulative damage method for the FRP deck and the simplified λ-method for the steel superstructure. Lastly, the effect of temperature differences in vertical deflection is considered and a small parametric study is considered.

Based on the results of this research, it can be concluded that FRP decking systems offer remarkable potential when low self-weight is a crucial demand of the project. The investigation

suggests that the deflection (SLS) governs the design as opposed to strength (ULS), although with the right superstructure configuration the requirements can be met. Composite action and lateral load distribution are additional advantages that adhesively bonded FRP decks offer in bearing the external loadings. Upgrading old movable bridges with FRP decks acting compositely with steel girders is to be considered as a feasible option their rehabilitation.

Key words: Fiber Reinforced Polymer FRP, FRP deck, composite bridge, hybrid bridge, composite action. effective width, adhesive bonded connection, lateral distribution, fatigue

## Acknowledgements

*I would like to express my deepest appreciation to all those who provided me the possibility to complete this thesis.*

*First of all, I would like to express my great appreciation to Ir. W.P.J. Langedijk, my daily supervisor at Iv-Infra, for his valuable advice and assistance during the planning and development of this research work. His willingness to give his time so generously has been much appreciated. My grateful thanks are also extended to Prof. F.S.K. Bijlaard, Dr. M.H. Kolstein, and Dr. M.A.N. Hendriks for accepting to be part of this graduation committee, for their professional guidance and constructive suggestions enriching the quality of this master thesis.*

*I would like to thank Iv-Infra, especially to Mr. Langedijk and Mr. van Lierop, for giving me the opportunity and trusting me to conduct this research. In addition, I am grateful to the "Excellence Fund" for funding my master studies at TU Delft.*

*I would particularly show gratitude to my family for all the faith they have in me and their encouragement in pursuing my academic aspiration. My final word goes for Mirza Balaj as the reason I embarked on this extraordinary experience, that she made more cheerful every day.*

# Contents

# List of Figures

## List of Tables

## Notations

**Roman upper case letters**

$A$ is the cross section area

$D_{annual}$ is the obtained annual damage

$D_{fac}$ dynamic amplification factor

$D_i$ is the damage obtained for stress range i

$D_{TOT}$ is the total obtained damage

$D_\lambda$ is the total damage obtained by the λ-coefficient method

E is the modulus of elasticity

G is the modulus of shear

LL is the live load

$Q_{ik}$ is the magnitude of characteristic axle load on notional lane number ($i$=1, 2, 3…) of a road bridge

Y is the distance from neutral axis


**Roman lower case letters**

$f_u$ is the ultimate limit strength

$f_y$ is the yield strength

$q_{ik}$ is the magnitude of characteristic vertical distributed load on notional lane number ($i$=1, 2, 3…) of a road bridge

$k1$ is a coefficient affecting the fatigue strength or while assessing reinforcement steel with the cumulative damage method, a the slope of the S-N relation until $N*$

$k2$ is the slope of the S-N-line or while assessing reinforcement steel with the cumulative damage method, the slope of the S-N relation after $N*$

$m$ is the slope of the S-N relation

$ni$ is the number of stress cycles

$n$ is the number of stress cycles with constant amplitude corresponding to the characteristic fatigue strength equal to the stress range $ri$ σ


**Greek upper case letters**

Δσ is the reference normal stress range

$Δσ_C$ is the stress amplitude that will cause failure after 2 million cycles

$Δσ_D$ is the stress amplitude that will cause failure after five million cycles

$Δσ_E$ is the equivalent stress range corresponding to $n$ cycles

$Δσ_{E2}$ is the equivalent stress range related to 2 million cycles

$Δσ_L$ is the stress amplitude that will cause failure after 100 million cycles

$Δσ\,p$ is the reference stress range determining the damage effects of the stress range spectrum

$Δσ_{s,71}$ is the steel stress range caused by a load model 71

$\Delta\sigma_{S,Ec}$ is the stress range obtained while the $\lambda$-coefficient fatigue load model is applied to the bridge with axle loads amplified

$\sigma_{S,equ}\Delta\sigma$ is the equivalent stress range in the reinforcement corresponding to $n$ cycles

$\Delta\tau$ is the reference shear stress range

$\Delta\tau_C$ is the shear stress amplitude that will cause failure after 2 million cycles

$\Delta\tau_L$ is the shear stress amplitude that will cause failure after 100 million cycles

$\Phi$ is the damage equivalent impact factor

$\Phi2$ is the damage equivalent impact factor, carefully maintenance

$\Phi3$ is the damage equivalent impact factor, standard maintenance

**Greek lower case letters**

$A_{Qi}$ is the adjustment factor for characteristic axle load on notional lane number ($i$=1, 2, 3…) of a road bridge

$\alpha_{qi}$ is the adjustment factor for characteristic vertical distributed load on notional lane number ($i$=1, 2, 3…) of a road bridge

$\gamma_{F,fat}$ is a partial coefficient taking the uncertainties in the fatigue load model into account

$\gamma_{S,fat}$ is the partial coefficient taking material uncertainties into account

$\gamma_{Mf}$ is a partial coefficient for fatigue strength

$\lambda$ is the damage equivalence factor

$\lambda_1$ is the coefficient representing the damage effect of the traffic

$\lambda_2$ is the coefficient representing the traffic volume

$\lambda_3$ is the coefficient representing the design life of the bridge

$\lambda_4$ is the coefficient representing the influence from traffic on other lanes

$\lambda_{max}$ is the the maximum value taking into account of the fatigue limit

$\upsilon$ is the poisson's ratio

$\sigma$ is the normal stress

$\gamma_F$ is the partial load safety factor

**Abbreviations**

CFRP    Carbon fibre reinforced polymers

FEM     Finite element model

FRP     Fibre reinforced polymers

GFRP    Glass fibre reinforced polymers

SLS     Serviceability limit state

ULS     Ultimate limit state

i

# 1. INTRODUCTION

Over the last few years, investigations have proven that a growing number of old bridges in Europe are classified as structurally deficient, obsolete bridges and require the need for rehabilitation. The need to maintain, renew, strengthen and upgrade this part of the infrastructure will increase dramatically in the near future. Deterioration of bridge decks is mainly caused by corrosion of steel due to de-icing agents, both in concrete and steel decks, fatigue and the insufficient load carrying capacity. The latter is originated from the increased traffic load in combination with new code requirements and when the bridge have to elongated or widened. With regard to insufficient load carrying capacity of these old bridges, effective and efficient solutions need to be developed presenting new options in bridge construction.

Construction of a new bridge is a potential alternative, however it is considered expensive and construction time needed are not acceptable. Moreover, old movable bridges in cities are often key objects and landmarks of the urban architecture and are a vital part of a city's infrastructure which may require a preservation of the structure. Competitive alternatives is the repair and strengthening of the old bridge by deck replacement, complete replacement of the structure (with or without the counter weight in case of movable bridges) or rebuild of the substructure. The current practice when refurbishing these old movable bridges is the replacement of the old deteriorated deck with a new one with the same material. However, this poses new difficulties that are crucial during the selection procedure. Firstly, the construction time, especially in urban areas, should be minimized due to traffic disruption. Moreover, due to the increase of the traffic in the recent years and higher static loading requirements in codes/regulations the weight of the bridge is considered the most important issue. Especially in movable bridges the latter can lead to an increase of weight and/or change of the counterweight. The reasons stated above make it very difficult the option to re-use the same materials as for the old bridge and poses the demand to search for other alternatives.

Hybrid structures made with FRP decks and steel girders are expected to be a potential alternative in replacement and refurbishment of old decks while maintaining the current substructure. Properties such as low self-weight, high strength and stiffness-to-weight-ratio, rapid erection time, fatigue resistance and little inspection for FRP products prerequisites make this type of construction very attractive. Although these kinds of structures have increased their

market in the recent years, the lack of knowledge of their behavior and the lack of standards or design codes have limited their application. Moreover, many technical problems related to the structural design of bridges with pultruded FRP decks have still not been solved/ investigated, or at least only partially. This includes the connection between the main steel girders and FRP deck which mostly is designed as a non-composite action, leading toward economical deficiencies. Adhesive bonding, shear studs and bolting are the main connection methods used for joining FRP structural components to the superstructure, offering different/contrasting structural behaviors. Adhesive bonding, besides offering the possibility of composite action, is a more material-adapted connection method since larger surface can be linked together and can eliminate stress concentration, thus ensuring reduced stresses and smoother load transfer for brittle and anisotropic material such as FRP.

In this research Wilheminabrug, a bascule bridge long 14 m and wide 16 m located in Zaandam, Netherlands will serve as a feasibility study. Three deck alternatives, a solid core sandwich and two hollow core sandwich sections, will be studied as potential options to upgrade this old movable bridge.

## 1.1. Problem Statement

FRP decking systems, although with higher material costs compared to traditional ones, are developing into a promising alternative construction solution to upgrade old movable bridges where the advantages of FRP outweigh its initial costs. Further research is required in order to effectively exploit the advantages of this new decking system, including its structural efficiency and cost analysis, in the particular case of old movable bridges where of big interest is maintaining the same counterpart when additional increase of traffic loading takes place. Moreover, how far the advantages of hybrid bridges when composite behaviour takes place is yet to be discussed.

## 1.2.Project motivation and aim

The driving force of this thesis is the set of advantages that FRP bridge decks offer, from which they have found the way onto the market. The most significant advantages leading to their practical implementation in the refurbishment of old bridges which are applicable to movable bridges too, are summarized below:

- High strength and stiffness-to-weight-ratio
- Relatively small dead load, approximately 20% of a comparable concrete bridge deck
- Rapid installment decreasing the traffic interruption
- Low maintenance costs due to their environmental resistance features, especially corrosion
- Bridge widening, due to their decrease of dead load
- Noise reduction

Moreover, additional advantages can be delivered depending on the connection used. In bridges with FRP deck built to date, almost all connections methods involve mechanical fastening due to previous experience of such application in other materials. Nevertheless, adhesively-bonded connections compared to traditional methods have the following advantages:

- *Composite action* resulting from the bonded connection between the bridge deck and steel girder. This action can significantly increase the stiffness and strength of the whole hybrid structure, which can lead to a reduction of the material used for steel girders, or an increase in traffic acceptance.
- *Prevention of high stress concentrations*, due to larger areas which are linked to each other.
- *Reduction of labor costs*. Mechanical fastening (bolts, clamps or shear studs) require additional work in the construction site which can increase considerably the construction time.

A more detailed description and clarification of the advantages stated above will be treated in the following chapters.

### 1.3.Objectives and Research Questions

The main objective of this thesis is the description of the structural behavior of a hybrid FRP deck- steel girders structure used as a refurbishment technique when upgrading old steel movable bridges. Existing knowledge regarding the behavior of FRP decks, especially the proposed ones, will be integrated into the investigations carried out in this research. The achievements of this objective involve addressing the following research lines:

- Verification of the Whilehelminabrug in correlation with stresses and deflections

- The advantages of using FRP decks in relation in self-weight reduction
- Assessment of fatigue life of the FRP deck and steel superstructure
- Demonstration of the feasibility and development of adhesively bonded deck-to-girder connection to provide composite action

## 1.4. Methodology

To accomplish the objectives discussed above a method based on the integration of literature study and analytical work is used. Numerical analyses by means of finite element modelling using Abaqus software are utilized to assess the overall structural behavior and load carrying capacity of the bridge. Static and fatigue loading according to the Eurocodes and national Dutch codes are used to evaluate the code verifications. Simple analytical analyses are employed to assess the effective width of the deck and the lateral distribution factors. The general organization of this research outline is illustrated in the graphs in Figure 1-1 and Figure 1-2.
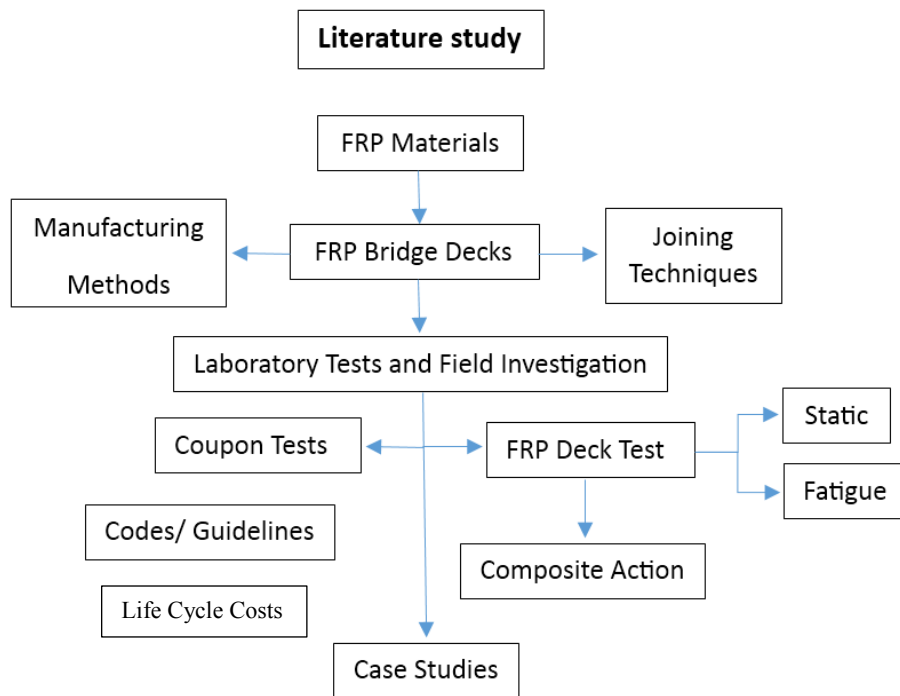


Figure 1-1 Organization chart of literature study
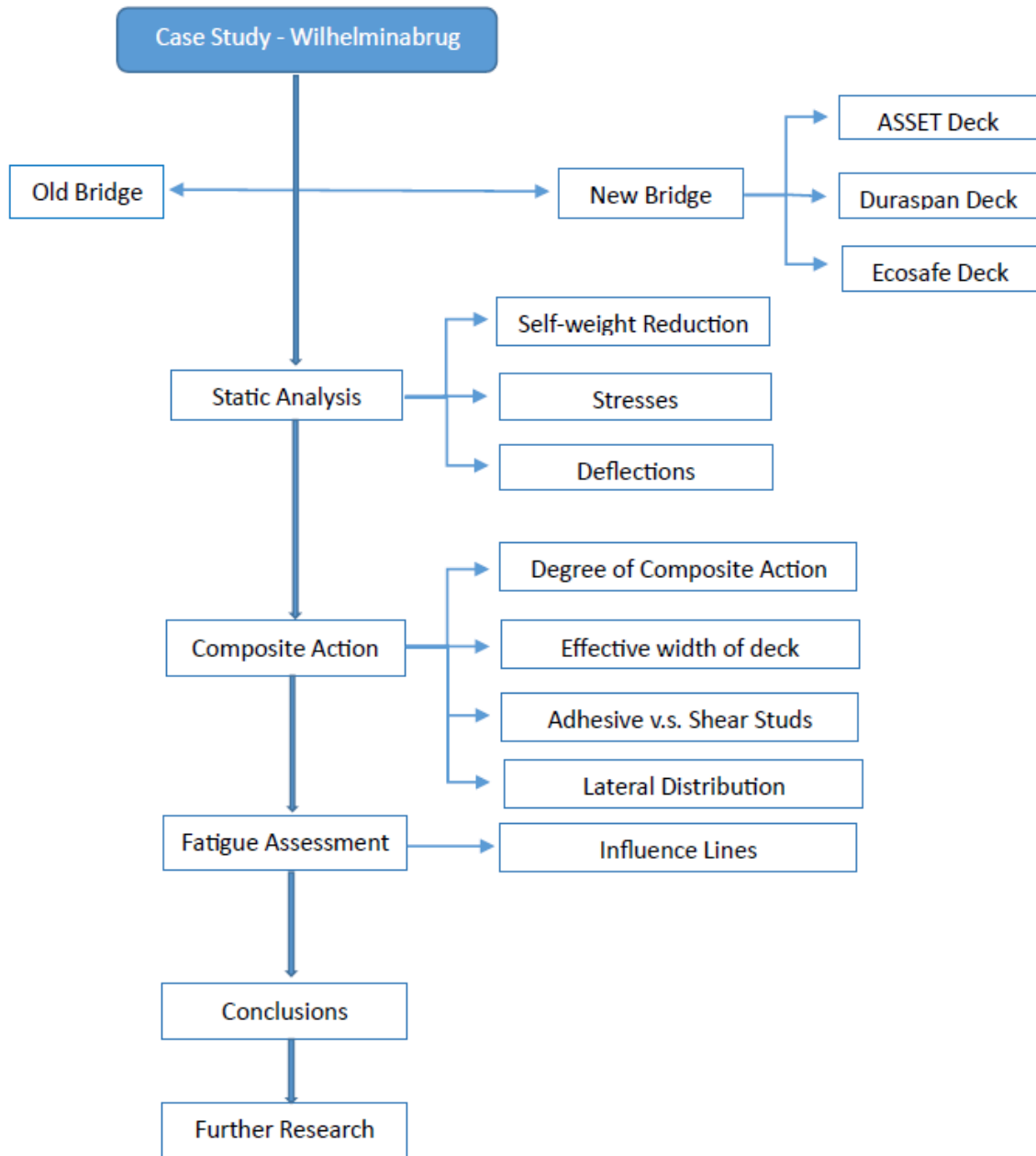
Figure 1-2 Organization chart of application study

**1.5.Outline of the thesis**

The thesis is divided into four parts:

**Part I** - *Introduction*, introducing the key issues involved in the subject.

**Part II** - *State of the Art*, describing a detailed literature review of the use of FRP decks in bridge construction. It begins with presentation of the constituent materials of FRP in civil engineering applications focusing on FRP decks, their manufacturing methods and joining techniques. Following with the results of laboratory tests and field investigations, it presents a clear study of the main issues concerning the behavior of hybrid bridges while demonstrating the need for research of adhesively bonded connections between steel girders and FRP deck. Other issues such as design codes and guidelines, deflection criteria and environmental effects are discussed. Similar case studies and their installation process are presented in the last part of this chapter.

**Part III** - *Analytical part* of the thesis. It comprises two chapters:

*Chapter 3* provides a description of the bridge to be studied and the applied loads based on the Eurocodes and national Dutch codes. It follows with a detailed overview of the finite element modelling and the used approaches.

*Chapter 4* presents the feasibility study of upgrading Wilheminabrug covering different scenarios. Firstly, it starts with the description of the current bridge. Following the latter, three difference case scenario of steel structure configuration will be integrated with three proposed FRP decks. The structural behaviour of each of the before mentioned case scenarios will be studied in function of reduction of self-weight, stresses and local/global deflection. Summary of the results and comparison between decks will be discussed in the end.

*Chapter 5* presents the study of the composite action between the steel girders and FRP decks. The degree of composite action and the effective width of the deck will be addressed for the three proposed decks. An investigation analyzing the difference between the two joining techniques, adhesive bonding and shear studs, will take place. Moreover, the lateral distribution factors will be investigated. Summary of the results and comparison between decks will be discussed in the end.

*Chapter 6* investigates the behaviour of the decks under fatigue loading and asses the fatigue life expectation of the bridge.

*Chapter 7 and 8* study further characteristics of the system. The effect e temperature difference in the vertical deflection is further investigated. Additionally, by simulating parametric studies through numerical analysis the influence of flange thickness of FRP decks will be considered in this study.

**Part IV** – Conclusions and Further Research

*Conclusions* drawn in this thesis and suggestions for *further research*.

*Appendix* containing additional information, figures and tables.

# 2. LITERATURE REVIEW – FRP BRIDGE DECKS

## 2.1. Introduction to FRP

Composite is defined as a mechanically separable combination of two or more component materials, different at the molecular level, mixed purposefully in order to obtain a new material with optimal properties, different than the properties of the components (Potyrała, 2011). Composite materials have been used in construction for centuries. Although the use of molten glass fibres dates 3000 years ago, their potential as reinforced materials was not recognized until the introduction of plastics during this century (M.H.Kolstein, 2008). The new class of composite materials gaining acceptance from civil engineers in the recent years, both for the rehabilitation of existing structures and the construction of new ones, are Fibre Reinforced Polymer (FRP) composites. Fibre Reinforced Polymer composites consist of the fibres, acting as the load bearing function, embedded in the matrix.

Fibre Reinforced Polymers (FRP) have been applied in a variety of ways in bridge construction because of the many advantages they offer. They are used as reinforcing bars for concrete, in all possible shapes of prestressing members (internal prestressing in concrete and external prestressing for new bridges and for strengthening purposes, stay cables, cables for suspension bridges, ground anchors, etc.), as strips and sheets for strengthening, as beams sections or in the form of trusses and as bridge deck slabs both for repair work and for new bridges. Some applications are already well established, above all for strengthening, for example adhesive strips or the sheet technology for strengthening columns (Keller T. , 2003). FRP bridge deck is the alternative to heavy traditional material used in bridge deck such as steel or concrete. These decks are beneficial for maintenance purposes and case of the replacement of the deck to accommodate any increased traffic demand (Stankiewicz, 2012).

### 2.1.1. Reinforcing Fibres

The fibres in FRP composite materials consist of thousand individual filaments used with resin system to improve the mechanical properties of cured resin and provide usable components. They usually occupy 30-70% of the volume of the composite and 50% of its weight. To perform their function of carrying the load and provide stiffness, strength, thermal stability and other structural properties of FRP material they must have high modulus of elasticity, high ultimate strength, and low variation of strength among fibres, high stability of their strength during

handling and high uniformity of diameter and surface dimension among fibres (Potyrała, 2011). The most common types of fibres are glass, carbon and aramid fibres.

Glass based fibres are used for some FRP products such as reinforcing concrete bars strengthening fabrics, and FRP structural profiles. Different grades of glass fibres are distinguished by their letter nomenclature respectively E, A, C and S as shown in Table 2-1. Glass fibres are usually manufactured by the extrusion method. There are five forms of glass fibres used as the reinforcement of the matrix material: chopped fibres, chopped strands, chopped strand mats, woven fabrics, and surface tissue. Although the existence of different types, in the building industry above all the fairly inexpensive E-glass fibres are used, which are shown in Figure 2-1. The disadvantages of glass fibres are the relatively low Young's modulus, the low humidity and alkaline resistances as well as the low long-term strength due to stress rupture. Protection by resin is an important issue for glass based fibres due to sensitivity of these fibres to moisture (Keller T. , 2003).

Table 2-1 Approximate properties of common grades of glass fibres. (Bank, 2006)

| Grade of Glass Fibre | Density | Tensile Modulus | Tensile Strength | Max. Elongation |
|:---:|:---:|:---:|:---:|:---:|
| | $[g/cm^3]$ | [Gpa] | [Mpa] | [%] |
| E | 2.57 | 72.5 | 3400 | 2.5 |
| A | 2.46 | 73 | 2760 | 2.5 |
| C | 2.46 | 74 | 2350 | 2.5 |
| S | 2.47 | 88 | 4600 | 3 |



Figure 2-1Glass fibre fabric/ photo from (Tap Plastics, n.d.)

9

Carbon based fibres shown in Figure 2-2 are used in many structural engineering application such as FRP strengthening sheet and fabrics, FRP strengthening strips, and FRP pre-stressing tendons and are a type of high-performance fibre. Carbon fibres are produced in different grades, namely standard, high strength, high modulus, and ultrahigh modulus as shown in Table 2-2. Carbon fibres can be said to be a durable material due to their ability to perform very well in hot and moist condition, and resistance to fatigue loads. The disadvantages of carbon fibres are the inherent anisotropy (reduced radial strength), comparatively high energy requirements in their production as well as the relatively high costs (Keller T. , 2003).
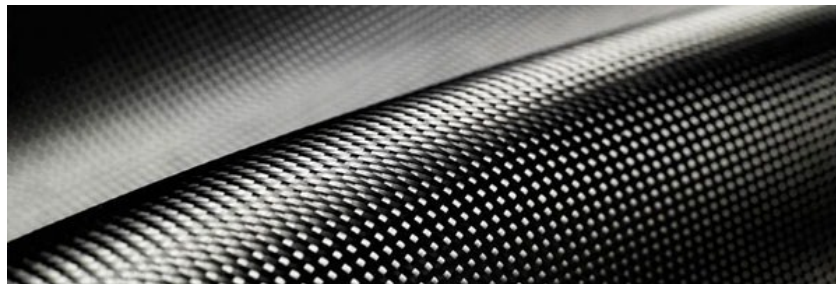


Figure 2-2 Carbon fibre fabrics/ photo from (KEROCK, n.d.)

Table 2-2 Approximate properties of common grades of glass fibres. (Bank, 2006)

| Grade of Carbon Fibre | Density | Tensile Modulus | Tensile Strength | Max. Elongation |
|---|---|---|---|---|
| | [g/cm$^3$] | [Gpa] | [Mpa] | [%] |
| Standard | 1.7 | 250 | 3700 | 1.2 |
| High Strength | 1.8 | 250 | 4800 | 1.4 |
| High Modulus | 1.9 | 500 | 3000 | 0.5 |
| Ultra High Modulus | 2.1 | 800 | 2400 | 0.2 |

Aramid fibres shown in Figure 2-3 are mostly used for FRP wrap in column strengthening. A combination of their expensive price, low melting point, difficulty in processing, and poor compressive properties have made aramid based fibres infamous for FRP structural engineering applications. In fact, their advantages to absorb energy have made them applicable for bullet proof vests, helmets, and automotive safety technology. The disadvantages of aramid fibres are the low compressive strength (500-1,000 MPa), the reduced long-term strength (stress rupture) as well as their sensitivity to UV radiation (Keller T. , 2003) .
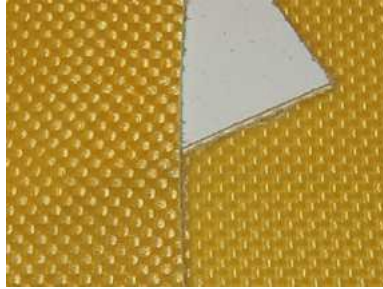
Figure 2-3Aramid fibre fabric/ photo from (The RC, n.d.)

A comparative quantitative evaluation of the individual fibres (in laminates) is shown in Table 2-3.

Table 2-3 Quantitative rating of fibre types (rating: 3 = very good, 2 = good, 1 = adequate, 0 = inadequate) (Keller T. , 2003)

| Criterion | Weighting factor | Weighted rating for laminates with fibres of: | | |
|---|---|---|---|---|
| | | Carbon | Aramid | E-glass |
| Range of weighting factor | 1 to 3 | Carbon | Aramid | E-glass |
| Tensile strength | 3 | 9 | 9 (= 3×3) | 9 |
| Compressive strength | 2 | 6 | 0 (= 2×0) | 4 |
| Young's modulus | 3 | 9 | 6 | 3 |
| Long-term behaviour | 3 | 9 | 6 | 3 |
| Fatigue behaviour | 2 | 6 | 4 | 2 |
| Bulk density | 2 | 4 | 6 | 2 |
| Alkaline resistance | 2 | 6 | 4 | 0 |
| Cost | 3 | 6 | 6 | 9 |
| Total points | | 55 | 41 | 32 |
| Ranking | | 1 | 2 | 3 |

In civil engineering and infrastructure applications glass and carbon fibres have demonstrated to own the most attractive qualities. In particular, E-type glass fibres and carbon fibres are used in the construction of FRP decks. Due to the economical solution that E glass fibres have shown they provide a good alternative in bridge deck application. On the other hand, carbon fibres application in bridge decks is very limited due to economic reasons, and are only used in particular situation when a high strength-to-weight ratio and fatigue strength are required.

The typical forms of reinforcement available to the manufactures for fibreglass, carbon and other fiber materials according to (NCHRP, 2006) are the followings:

1- Continues Roving

They consist of hundreds of monofilament threads gathered to form a thicker strand called "roving" (See Figure 2-4). Components which have the roving in only one directions are characterized by a highly uniderectional mechanical properties. They are used as structural reinforcement in proccesses such as filament winding and pultrusion (See section 2.2).



Figure 2-4  Spools of continuous fiberglass roving (NCHRP, 2006)

2- Discontinuous Roving

Discontinuous roving or chopped strand glass (see Figure 2-5), usually produced by spray-up method, may be chopped into very small lengths (1⁄2 in. to 2 in.). This form of reinforcement is most often used where low fiber volume and reduced mechanical properties are acceptable.



Figure 2-5  Chopped strand glass (NCHRP, 2006)

3- Woven Rovings

Woven roving is produced by weaving fiberglass roving into fabric through the process of hand lay-up and panel molding. In order to create highly orthotropic properties, the weave can be made with more strands in one direction as shown in Figure 2-6.
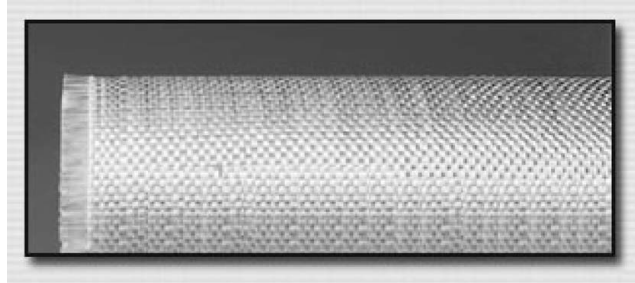


Figure 2-6  Woven roving fabric (NCHRP, 2006)

4- Mats

Mats are produced as continuous or chopped strand mats by depositing strands and binding them to each other (see Figure 2-7). The continuous strand mat has better strength characteristics than a chopped mat.
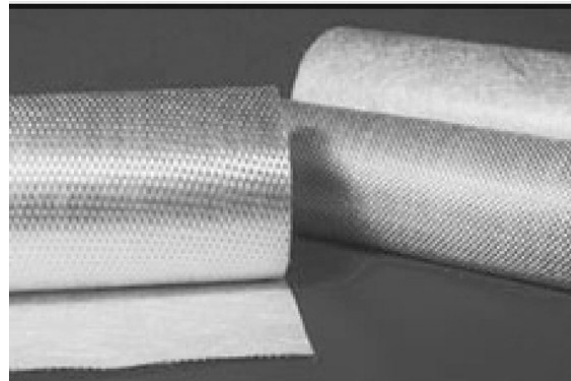


Figure 2-7  Chopped strand mat fabric (NCHRP, 2006)

5- Non-crimp Fabric

By stitching or knitting the reinforcement strands together using lightweight threads, sheets of fabric as shown in Figure 2-8 can be made without weaving to produce straight, non-crimped, layers of fibers. This form of sheet reinforcement has become very popular for deck fabrication because it allows large quantities of fibre reinforcement on single spools. Compared to woven fabric, non-crimped fiber strands maintain their straightness and hence, have higher stiffness and

strength retention. These are the most expensive form. They are manufactured in multiple layers, so in essence they themselves are sub-laminates.
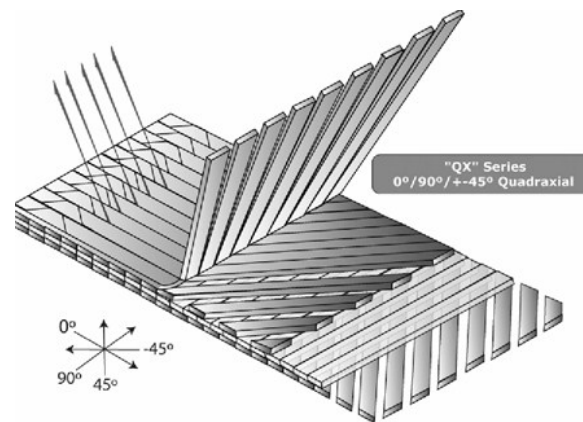


Figure 2-8  Non-crimp fabric construction (NCHRP, 2006)

### 2.1.2. Matrix Resin

Whereas the fibres exercise the actual load-bearing function, according to (Keller T. , 2003) the polymer matrix essentially has four functions:

-   Fixing the fibres in the desired geometrical arrangement,
-   Transferring the forces to the fibres,
-   Preventing buckling of the fibres under compressive actions,
-   Protecting the fibres from humidity, etc.

Type of matrix material and its compatibility with the fibres also significantly affect the failure mode of the structure. The components of the matrix are resins, fillers and additives. The function of fillers is to fill out the form of a profile in order to reduce the use of more expensive reinforcement and matrix materials. They make it possible to reduce the price of finished product. Additives are constituent components that may be added to the composite matrix to modify its properties and in general, enhance its performance (Potyrała, 2011). Resins are the main component of a matrix and are dived in thermoplastics and thermosetting polymers (thermosets) based on the manufacturing method and properties. For FRP structures today mainly thermosets are used (Keller T. , 2003).

The most important thermosetting resins being used in industry are mentioned below according to (NCHRP, 2006):

1- Orthophthalic Polyesters

2- Isophthalic Polyesters

3- Vinyl Esters

4- Epoxies

Their properties are shown in Table 2-4.

Table 2-4  Typical Mechanical Properties of Common Resins[1]

| Resin System | | Compressive Strength ksi | Tensile Strength ksi | Tensile Modulus Msi | Heat Deflection Temp °F |
|---|---|---|---|---|---|
| Orthophthalic | Without reinforcement [2] | NA | 7.2–8.5 | 0.45–0.66 | 175 |
| | With fiberglass reinforcement [3] | NA | 22 | 1.7 | |
| Isophthalic | Without reinforcement [2] | 17 | 10–11.7 | 0.45–0.65 | 195 |
| | With fiberglass reinforcement [3] | 30 | 23 | 1.7 | |
| Vinyl ester | Without reinforcement [2] | NA | 11–12.7 | 0.46–0.57 | 212 |
| | With fiberglass reinforcement [3] | 30 | 23 | 1.6 | |
| Epoxy | Without reinforcement [4] | NA | 7–8 | 0.43–0.55 | 120–220[5] |
| | With fiberglass reinforcement [3,4] | 35 | 30 | 1.8 | |

[1]Hancox and Mayer, *Design Data for Reinforced Plastics*, Chapman and Hall, London, UK, 1994.
[2]Typical range after full cure, dry. Not normally used in structure without reinforcement.
[3]Based on fiberglass mat reinforcement at 40% fiber volume.
[4]Room temperature cure epoxy systems, heated systems will be slightly higher.
[5]Low value is for room temperature cure, high value for heated process.

An experimental study was conducted to evaluate the endurance properties of GFRP decks according to the type of applied resin (Park, Hwang, Lee, & Jung, 2007). It was shown that vinyl esters which are more expensive, exhibit higher material strength and environmental resistance than the polyesters. Epoxies are used only in special occasions due to their high price. For bridge deck applications, iso-polyesters offer the most favorable conditions due to their low cost and environmental properties (corrosion and moisture resistance).

---

[1] The heat deflection temperature (HDT) is the temperature at which the resin will "soften" and lose strength.

## 2.2. Manufacturing Methods of FRP Decks

When manufacturing FRP composites besides shaping, removing and joining materials such as for traditional materials, it should be taken into consideration that the material and the physical component are manufactured at the same time. This process should be taken into consideration in the early stage of the design process for FRP bridge deck and the latter reflects among the designer's mixing of constituent and composition of the laminate(s). The methods to produce FRP bridge decks are the following:

- Hand laminating
- Pultrusion
- Vacuum assisted resin transfer moulding (VARTM)
- Filament winding

### 2.2.1. Hand lay-up or Open Molding

The hand lay-up process is the most fundamental method of manufacturing still widely used in all industries. The basic procedure is shown in Figure 2-9 and a bridge deck system produced with this method is shown in Figure 2-10. Fiber reinforcement is placed in position on the mold or plate and then saturated with resin. A crew then uses specialized rollers and paddles to work the resin into the fabric, fully wetting the layer. After determining that the layer is fully wetted, the crew repeats the process on succeeding layers until the lamination is complete. The component is then left to cure thoroughly, which takes from a few hours to overnight. The advantage of hand lay-up is its low capital equipment costs and the low-to-moderate labor skill it requires. These factors usually make it the least expensive method for one of- a-kind or limited production work. For complex parts, this may be the only feasible method. The disadvantage of this process is the variability in procedure and material properties due to the manual labor involved.

Dry filament placement                    Fabric saturation

Figure 2-9  Hand lay-up process (NCHRP, 2006)



Figure 2-10  Kansas Structural Composites Honeycomb Deck Section (FHWA, n.d.)

### 2.2.2. Pultrusion

Pultrusion is a process enabling continual production of FRP profiles with constant cross sections and material properties manufactured for specific purposes.  According to (Potyrała, 2011), so far it´s the only known method that ensures sufficiently consistent quality. The process in its basic form has been used for almost 60 years.

The pultrusion process involves pulling raw materials, which usually consists of a liquid resin mixture and flexible textile reinforcing fibers, through a heated steel-forming die using a continuous rolling device. As the reinforcement is saturated with the resin mixture in the resin bath and pulled through the die, heat from the die initiates the gelation of the resin. In the end, a rigid cured profile corresponding to the shape of the die is formed. The process is shown in Figure 2-11and in Figure 2-12.

Figure 2-11  Fiberline Pultrusion Equipment (NCHRP, 2006)
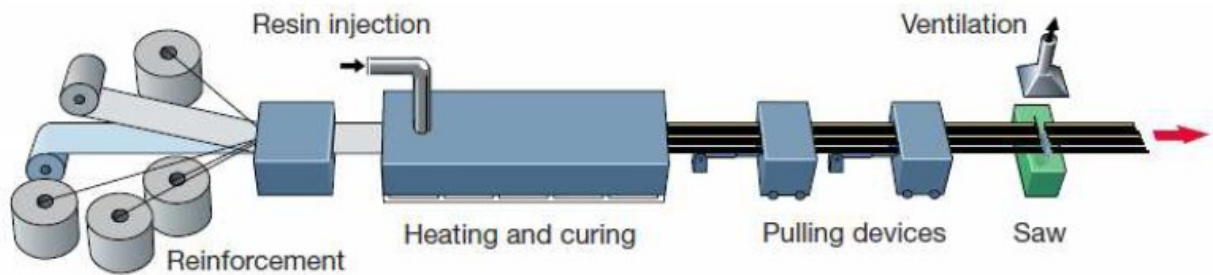


Figure 2-12  Pultrusion Process (NCHRP, 2006)

The advantage of pultrusion is the well-controlled and consistent dimensional profile of the structural components coming out of the die. Since it is the most automated process now in use, it requires little hands-on labor. Internal die segments allow open or wrap-around shapes to be designed and details such as hollow tubes and trapezoids to be produced. It enables very high fibre contents to be achieved using continuous yarn, woven cloth or mat reinforcement. Open and closed profiles can be produced to close tolerances and quite intricate detail can be achieved.

All features mentioned above make pultrusion the most common process to manufacture bridge deck such as the one shown in Figure 2-13.
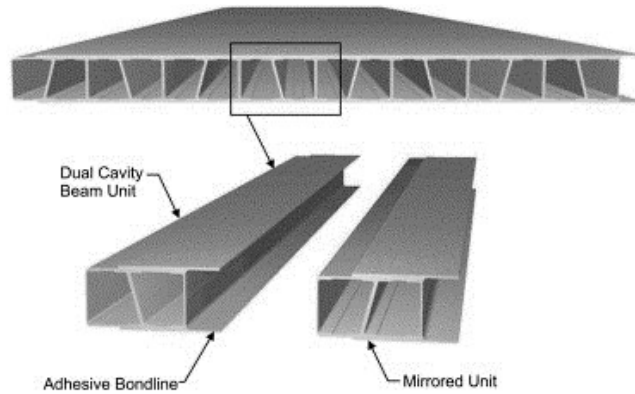
Figure 2-13  Pultruted Bridge Deck (Keller & Schollmayer, 2004)

The disadvantage is that pultrusion produces long, narrow "barlike" profiles, so deck designs employing pultrusion must consider how to combine pultruded elements to create the necessary width.

### 2.2.3.  Vacuum-Assisted Resin-Transfer Molding (VARTM)

The VARTM method employs a soft bag over the part to seal the mold so that a vacuum can be drawn under the bag. Once vacuum is achieved, the part is pressed onto the hard tool by atmospheric pressure. Resin ports on feed tubes are then opened to permit resin to flow into the mold and infiltrate the dry fabric reinforcement, as shown in Figure 2-14.
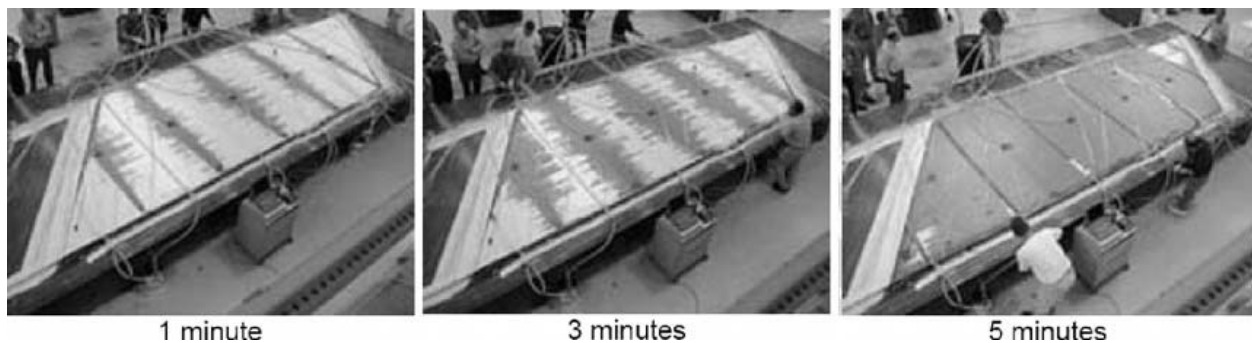


Figure 2-14  Vacuum infusion process on Tycor reinforced bridge deck (NCHRP, 2006)

The advantage of VARTM is the rapid infusion of large parts when the procedure works. As seen in Figure 2-14, infusion of large sections can be accomplished in minutes. Because the fiber reinforcement is compressed and locked in place by atmospheric pressure on the soft bag side, high fiber volume can be achieved. Good dimensional tolerance also is achieved because excess

resin can just flow out of the vacuum ports. This process is used to manufacture sandwich systems where a core is bonded between top and bottom face sheets.

However, because the resin flows indiscriminately under vacuum, the VARTM process requires volumetrically nearly solid sections in order to avoid forming resin-rich areas or resin pools in cavities. Also, any nonstructural materials such as foam core must be able to sustain the atmospheric pressure without crushing.

### 2.2.4. Filament Winding

Filament winding (see Figure 2-15) is a process in which resin-impregnated fibres are wound over a rotating mandrel at the desired angle. Therefore, starting materials for this process are continuous glass, carbon or aramid fibres. Liquid thermoset resins used in this process are epoxy, polyester and vinyl ester. The composite unit is then removed from the mandrel and cured by being placed in an oven enclosure at 60°C for 8 hours. This manufacturing process is commonly used to fabricate tubular structures and pipes. It is a low-cost process because low-cost materials and tooling are used. However, it is limited to producing closed and convex structures and gives comparatively low volume fraction of fibres.
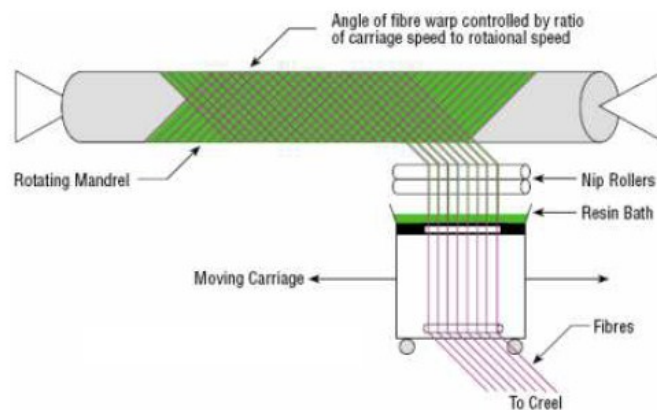


Figure 2-15  Filament Winding Process (ALE, n.d.)

### 2.3. FRP Bridge Decks

FRP composite structures for use as vehicular bridge decks have successfully transitioned from the experimental to the commercial stage over the past decade. Many FRP decks have been installed in Europe and in USA. These are basically characterized by low self-weight (about 20% of a comparable concrete slab), high resistance to corrosion and fatigue and they can be installed

quickly with a minimum of interruption to traffic (Keller T. , 2003). Bridge decks are usually made of fibreglass and polyester or vinyl resin. Most of them are formed in the pultrusion process, but hand lay-up and vacuum assisted resin transfer moulding. Since the deflection always governs the design due to the relatively low Young's modulus (similar to concrete) – the stresses in the glass fibres under permanent loads are never in the critical range of stress rupture. Since the majority of these deck systems are manufactured by pultrusion technique as shown in Table 2-5 deck thicknesses are constant and are limited about 120-225 mm. Therefore, due to the deflection requirements the possible span lengths reach a maximum of only about 2.7m, which necessitates a primary a primary load-bearing structure consisting of underlying girders. In case of deck replacement the existing girders (concrete or steel) can be used (Keller T. , 2003).

Based on their composition, FRP decks can be divided into three categories (NCHRP, 2006):

1- Type 1: Honeycomb Sandwich

The FRP decks both use identical sine wave web patterns in their core construction which provides considerable flexibility in tailored depth. However, the hand lay-up process now employed requires painstaking attention to quality control in the bonding of the top and bottom face sheets to the core. Among these decks are included the one produced by Kansas Structural Composites and Infrastructure Composites, Inc. as shown in Figure 2-16 and Figure 2-19.
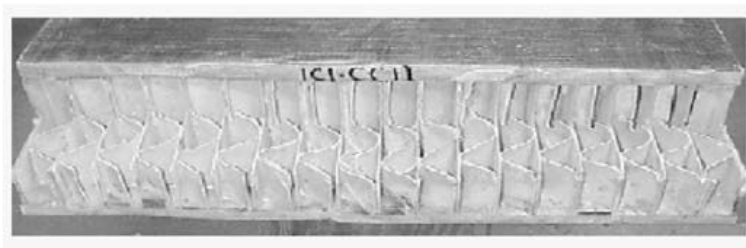


Figure 2-16  Honeycomb sandwich configuration (NCHRP, 2006)

2- Type 2: Solid Core Sandwich

Solid core decks have foam or other fillers in the cores and they are generally manufactured by VARTM process. The FRP decks shown in Figure 2-17 use both use solid core sections. Among

these decks are included the decks produced by Hardcore Composites and WebCore Technologies as shown in Figure 2-19.
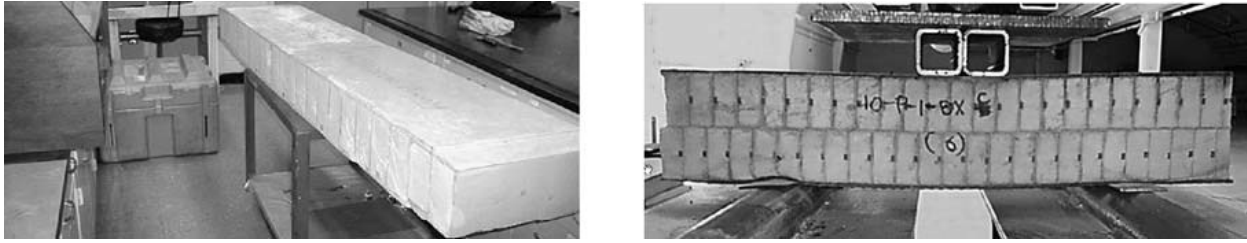


Figure 2-17  Solid core sandwich configuration (NCHRP, 2006)

3- Type 3: Hollow Core Sandwich

These FRP decks consists of pultruded shapes fabricated together to form deck sections which typically have continuous hollow core patterns as shown in Figure 2-18. These types of decks are used from Martin Marietta Materials (Durapsan) and Fiberline (ASSET).
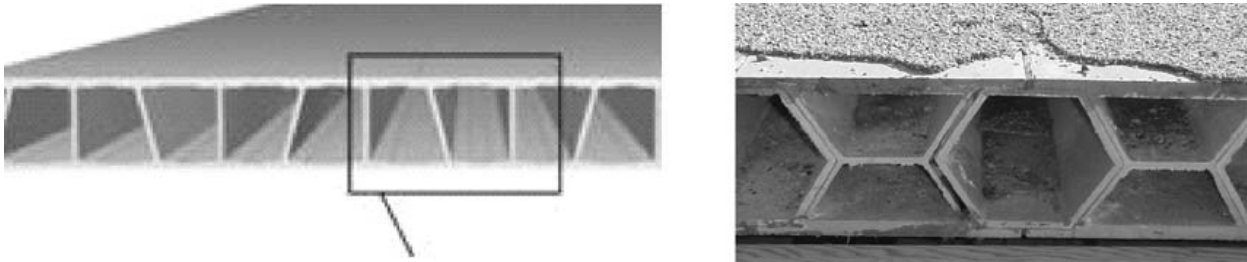


Figure 2-18  Pultruded hollow core sandwich configuration (NCHRP, 2006)

An overview of the FRP deck systems on the market in USA and Europe is shown in Table 2-5 and in Figure 2-19 in the following page.

Table 2-5  Comparison of FRP deck slab systems (Keller T. , 2003)

## Comparison of FRP Deck Slab Systems

| Bridge system | No. of bridges | Deck thickness | On girders | Element connection | Girder connection | Cross slope | Guide rails | Produc-tion |
|---|---|---|---|---|---|---|---|---|
| Hardcore deck | 10 | variable | no (yes) | glued | inserts if necessary | integrated | insert connections | variation VARTM |
| Kansas deck | 3 | variable | no (yes) | glued | clamps if necessary | integrated | pockets integrated | hand-laminated |
| Super-deck | 8 | 203 mm constant | yes | glued | glued + blind bolts | not integrated | on longit. girders | pultruded |
| DuraSpan deck | 9 | 194 mm constant | yes | glued | shear stud connectors | not integrated | dowelled | pultruded |
| Strong-well deck | 1 | 171 mm constant | yes | glued + mechan. | bolted | not integrated | not yet solved | pultruded |
| EZ-Span deck | 1 | 216 mm constant | yes | glued | not yet solved | not integrated | not yet solved | pultruded |
| «Manito-ba» deck | 0 (under develop.) | ~ 200 mm constant | yes | glued | not yet solved | not integrated | not yet solved | filament wound |
| Asset deck | 0 (under develop.) | 225 mm constant | yes | glued | not yet solved | not integrated | not yet solved | pultruded |
| ACCS system | 4 | variable (boxes) | no | mechan. + glued | not foreseen | not integrated | only railing | pultruded |
| Total | 36 | | | | | | | |



Hardcore (Hardcore Composites, USA)

Kansas (Kansas Structural Composites, Inc., USA)

Superdeck (Creative Pultrusion, Inc., USA)

ASSET (Fiberline A/S, Dania)

DuraSpan (Martin Marietta Composites, USA)

Virginia Tech (Strongwell, USA)

EZ-Span (Creative Pultrusion, Inc., USA)

ACCS (Maunsell Structural Plastics, Wielka Brytania)
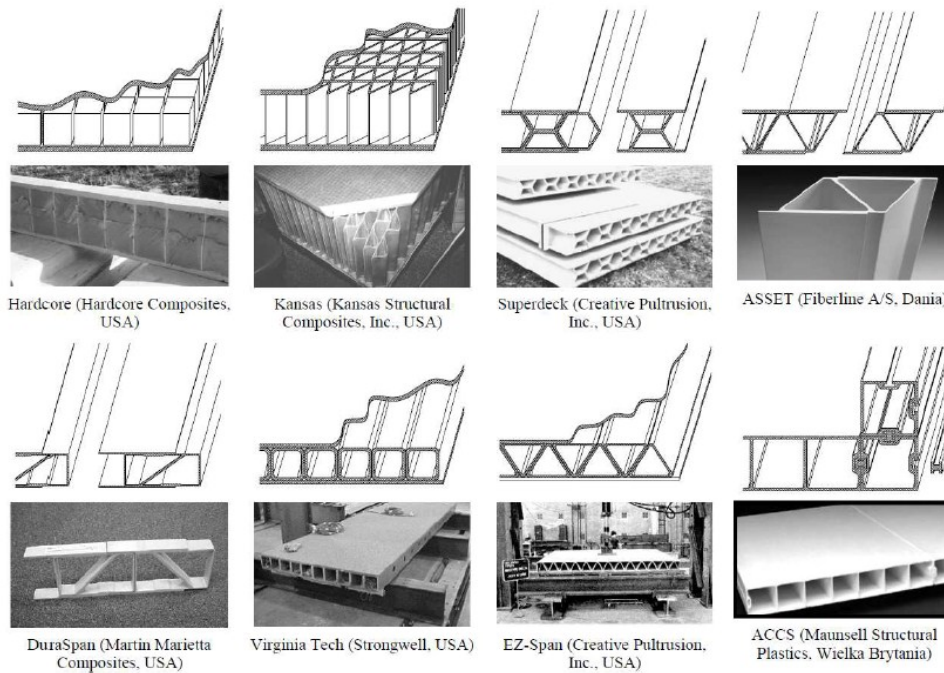
Figure 2-19  Various FRP deck systems (Potyrała, 2011)

## 2.4. Joining Techniques

In civil engineering applications of fiber reinforced polymer structures, connections are inevitable due to the requirements and limitations on shape size and transportations. Connections for FRP bridge decks include primary and secondary load-carrying joints, which are most concerned in construction, and non-structural joints. FRP bridge decks are usually provided in modular panel forms connected to their supports and transfer the loads transversely to the supports that usually bear on abutments. They shall be designed to meet the requirements of safety, serviceability with regards to durability, economy, future inspections and aesthetics. The advantages of FRP composites used in bridge construction would be efficiently used only if the connections are properly understood and designed (Zhou & Keller, 2005). According to the Eurocomp Design Code and Handbook (EUROCOMP, 1996), three classes of connections involved in composite construction are identified:

- Primary joints (Joints that carry major strength and stiffness to an assembly for the whole-life of the structure)

- Secondary structural joints (Joints whose failure would be only local failure without comprising the entire structure)

- Non-structural joints (Connections with the main purpose to exclude the external environment.)

In FRP bridge deck applications all these connections have been developed. However the primary and secondary load-carrying connections that are mostly of concern according to (Zhou & Keller, 2005) include the followings:

1. Component- component connections to form FRP bridge deck panels (referred as component level connection or with abbreviation CLC)

2. Panel-panel connections to form FRP bridge deck systems (referred as panel level connection or PLC)

3. FRP deck-to-supports connections to form bridge superstructures (referred as system level connection or SLC)

Mechanically fasteners and adhesive bonding or their combination are the methods used to join FRP composites. Adhesive bonding is usually used in component-component level to connect permanent FRP deck components due to the simplifications of processing and easy in geometry implementation. In panel and system levels all the types of connection mentioned before are used and are discussed below.

### 2.4.1. Component level connections for FRP bridge deck panels (CLC)

The main objective in this type of connections is ensuring the integrity of the deck panel and the load transfer efficiency between the jointed components while satisfying specified limit states (deflection and strength criterion) and taking into account the ease of processing and environmental attacks (Zhou & Keller, 2005). As already stated, adhesive bonding is used as a joining technique to produce deck panels. However, mechanically fasteners have been proposed and tested, although studies have shown that adhesive bonded joints are easier to design and provide larger safety margins (Zetteberg & Astrom, 2001). (See Figure 2-20 )



Figure 2-20  Deck panels through various joining techniques. (a) Bonded pultrusion shapes (b) Bonded sandwich (c) Bonding with fastening (Zhou & Keller, 2005)

Laboratory tests and field investigation have shown that failure occurs in fiber reinforced components other than adhesive bonding. According to (Zhou & Keller, 2005), after testing bonded cellular deck panes, there was no clear relationship between the load-carrying capacity of the modular FRP deck panels and the ultimate strength of the adhesively bonded connections. Some of the failure modes of bonded cellular deck panels are shown in Figure 2-21.
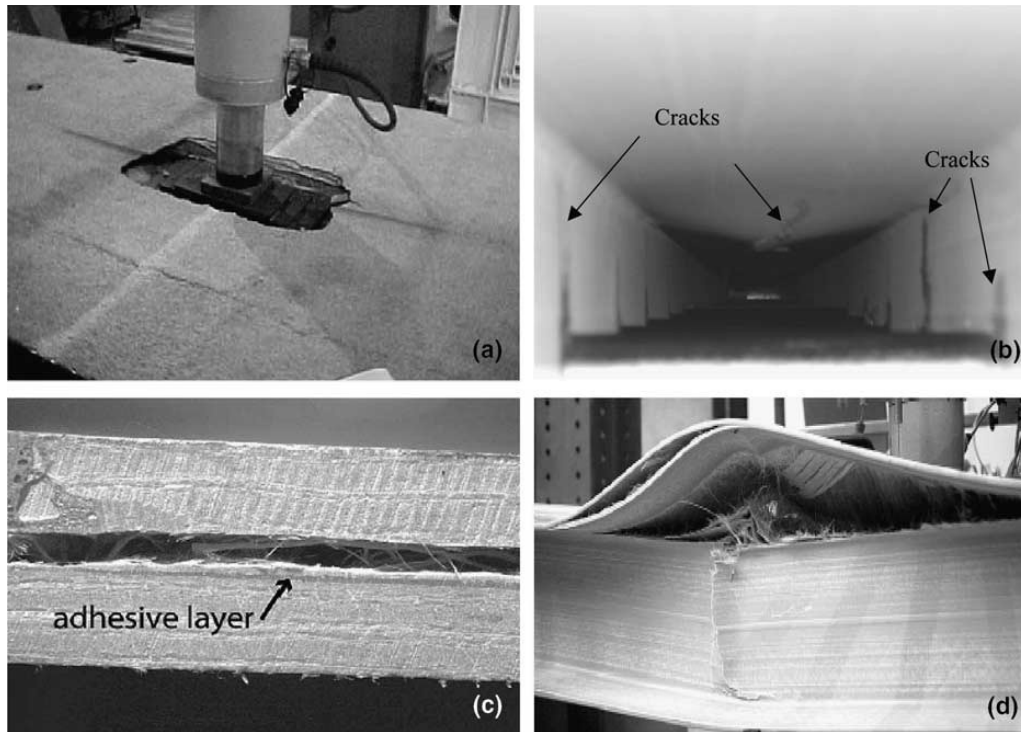
Figure 2-21  Failure modes of bonded cellular deck panels. (a) Surface failure (b) Internal failure (c) Delamination (d) Delamination and buckling (Zhou & Keller, 2005)

### 2.4.2.  Panel level connections of FRP bridge decks (PLC)

This connection ensures the deck system's load transferring and carrying capability (bending moment and shear force, resistance to dynamic loads); ensures deformation compatibility due to thermal effect and the ease of on-site installation, sometimes including the possibility of disassembly in case of repair. The techniques developed for panel connections are the splicing tongue-groove connection and the clip-joint connection via mechanical fixing (Zhou & Keller, 2005). Bonded joints have more efficient load transfer and failure resistant capability but offer the disadvantage of disassembly compared to mechanical fixing. Results from constructed projects have shown the cracks mostly appear in the shear key connection as shown in Figure 2-22.
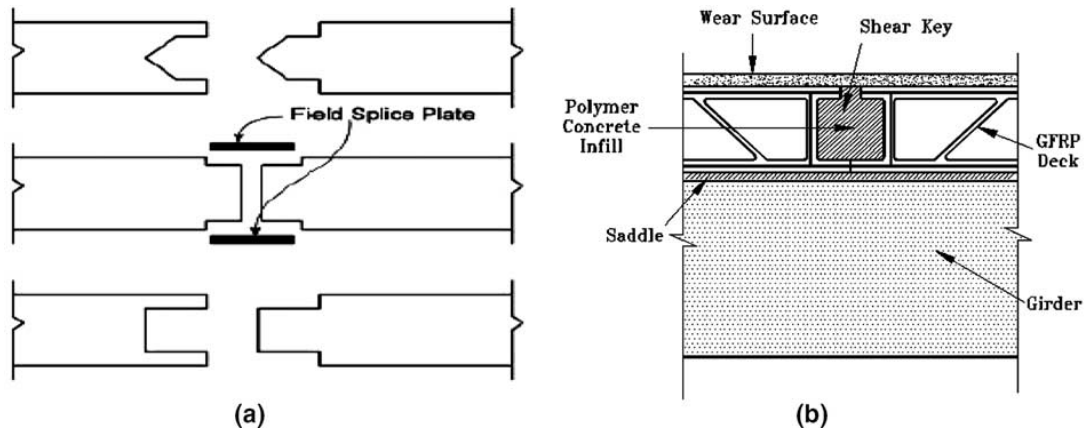
Figure 2-22  Typical panel connections for FRP deck systems. (a) Adhesive-bonding (b) Mechanical shear key (Zhou & Keller, 2005)

### 2.4.3.  System level connections for FRP composite bridge superstructures (SLC)

This system level connection is the most important and challenging topic in the development of FRP bridge connections since its efficiency governs the overall behavior of the formed superstructure and affects the economical solutions. Depending on the requirements of the specific project, the deck-to-girder connection can be designed with or without composite action between the deck and its supports. When no composite action is intended, which is usually a mechanical fastener, easy in assembling and disassembling is opted for. In case of aiming composite action mechanical fasteners and adhesive bonding or their combination can be used. For practical purposes these connections can be divided in three categories: adhesively bonded, shear-stud and mechanical (bolted or clamped) connections. Some examples of connection deck-to-girder are shown in the Figure 2-23.
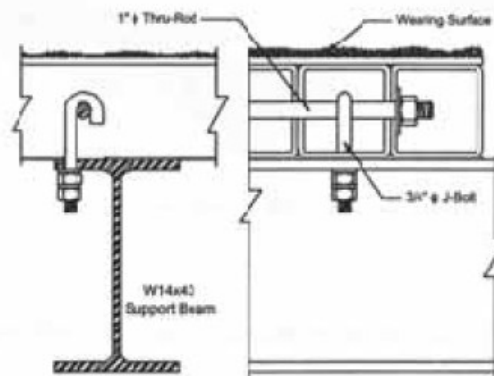


a) Bolted connection (Gurtler, 2004)

27
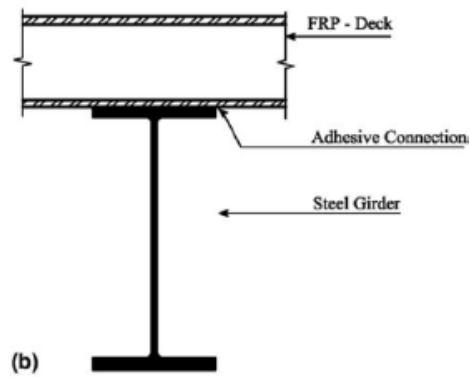
b) Adhesive bonded connection (Keller, Th; Gurtler, H, 2004)
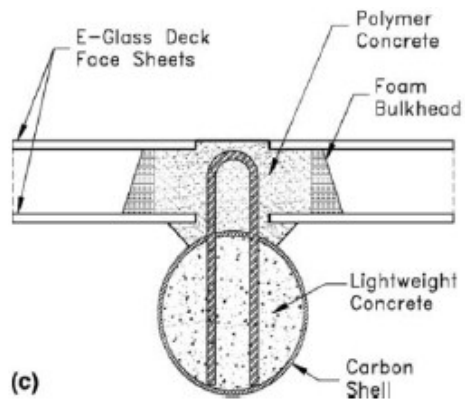


c) Hybrid connection (Burgueno, Seible, Karbhari, Davol, & Zhao, 1999)



(a) Elevation view; (b) Cross section
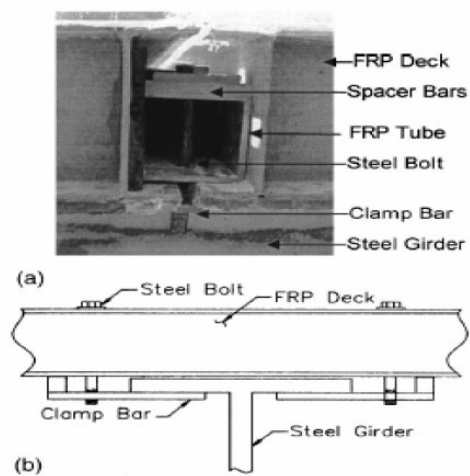
d) Clamped connection used by KSCI (Righman J. , 2002)
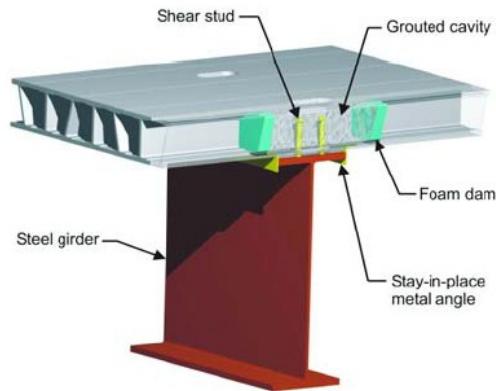
e) Detailed deck-girder connection (Zhou & Keller, 2005)

Figure 2-23  Examples of connection deck-to-girder

The majority deck-to-girder connections due to their proven history in civil engineering applications are the shear studs and stirrups as shown in Figure 2-23 c) and e). Shear-stud deck-to-girder connection has the following advantages: ease of construction by utilizing concepts that are widely used in the history of construction; partial composite action between deck and girders, which can contribute to the stiffness of the superstructure; and good capacity to secure the deck in place and prevent uplift under vertical vehicular loads and horizontal braking force. However, some disadvantages and concerns still exist, including the difficulty of disassembly for repair and low durability of the grout under fatigue loading (Liu, 2007). Adhesively bonded connections as shown in Fig b) offer the advantages of easy construction, uniform stress distribution and fatigue resistance (Zhou & Keller, 2005). Bolted connections have the advantages of easy assembly and disassembly, easy replacement and cost effectiveness but they do not offer composite action due to the high modular ratio between FRP deck and steel girder. An example is shown in Figure 2-23a) where the connection is approximated as simply supported. Due to non-composite behavior a large portion of impact loads are taken by the deck, which makes this design suitable for rehabilitation when the reduction of loading impacts is required (Zhou & Keller, 2005). Another example of non-composite behavior is shown in Figure 2-23 d) where the clamped connection prevents the deck from uplifting. This type of connection might not be a good solution since they are quite labor intensive and have to be protected from the dirt and water

leakage which might cause durability problems. Table 2-6 and Table 2-7 shown the comparison and some typical features of different connection between FRP members from Eurocomp (1996).

Table 2-6 Typical features of different connections between FRP members (from Eurocomp 1996 Design Manual)

| Mechanical connections | |
|---|---|
| **Advantages** | **Disadvantages** |
| - requires no special surface preparation<br>- can be disassembled<br>- ease of inspection<br>- quasi-ductile behaviour | - low strength to stress concentrations<br>- special practices required in assembly<br>- fluid and weather tightness normally requires special gaskets or sealants<br>- corrosion of metallic fasteners |
| **Bonded connections** | |
| **Advantages** | **Disadvantages** |
| - high joint strength can be achieved<br>- low part count<br>- fluid and weather tightness<br>- potential corrosion problems are minimized<br>- smooth external surfaces<br>- stiffness | - cannot be disassembled<br>- requires special surface preparation<br>- difficulty of inspection<br>- temperature and high humidity can affect joint strength<br>- brittle |
| **Combined connections** | |
| **Advantages** | **Disadvantages** |
| - bolts provide support and pressure during assembly and curing<br>- growth of bondline defects is hindered by bolts | - structurally bolts act as backup elements – in an intact joint, bolts carry no load |

Table 2-7 Characteristics of different joint categories (from Eurocomp 1996 Design Manual)

| | Mechanical | Bonded | Combined |
|---|---|---|---|
| **Stress concentration at joint** | high | medium | medium |
| **Strength/weight ratio** | low | medium | medium |
| **Seal (water tightness)** | no | yes | yes |
| **Thermal insulation** | no | yes | no |
| **Electrical insulation** | no | yes | no |
| **Aesthetics (smooth joints)** | bad | good | bad |
| **Fatigue endurance** | bad | good | good |
| **Sensitive to peel loading** | no | yes | no |
| **Disassembly** | possible | impossible | impossible |
| **Inspection** | easy | difficult | difficult |
| **Heat or pressure required** | no | yes/no | yes/no |
| **Tooling costs** | low | high | low |
| **Time to develop full strength** | immediate | long | long |

30

## 2.5. Codes and Design Guidelines: current status

In contrast to traditional materials such as concrete and steel, whose properties do no vary very much, FRP structures are distinguished from each other from their composition materials (fibre types, matrices, fibre architecture and combination of fibres with matrices). From this great variety of products that are achieved mandatory and end-to-use design procedures or application codes are still missing today.

### 2.5.1. Codes

In some countries, especially in Canada and Japan, the first codes for some very specific applications are prepared, mainly for FRP reinforced and strengthened concrete. In Europe, no official Design Code is still available. The only existing Eurocode referring to FRP composites is the European Standard EN 13706 giving directions regarding testing and notification of GFRP pultruded profiles (Potyrała, 2011). It applies solely to pultruded profiles for "structural purposes", which according to the standard are defined as cases "where the load-bearing characteristic is the major criterion of design and where the product is part of a load-bearing system. The standard specifies the minimum requirements for the quality, tolerances, strength, stiffness and surface of structural profiles and basically divides pultruded structural profiles into two classes. The standard broadly consists of three parts:

**EN 13706-1** establishes a data block system for the designation of pultruded profiles made from FRP composites classified based on a system information about selection of materials (type of polymer matrix used, the reinforcement material, the type of reinforcement) and the additional in-service performance features (e.g. fire retardancy, UV stability, surface treatment).

**EN 13706-2** specifies the general requirements applicable to the specification of all types of pultruded profiles falling within the scope of this specification as defined in EN 13706-1. It indicates testing methods and tolerances for pultruded structural profiles and gives guidelines for quality and quality assurance.

**EN 13706-3** introduces the specification (properties which shall be specified and the level to be obtained for each grade of profile) of pultruded profiles. It indicates minimum values for the technical properties of structural profiles (see Table 2-8) in relation to the standard's two classes described by short form code. E23－having the most stringent requirements to quality; and E17

31

⁻having more lenient requirements to quality (Effective Flexural Modulus of the profile measured by testing a length of the complete profile).

Table 2-8 Minimum values for the technical properties of structural profiles E17 and E23[2] (Potyrała, 2011)

| Characteristic properties | Test method | Minimum requirements | |
|---|---|---|---|
| | | E17 | E23 |
| Modulus of elasticity for the whole unit [GPa] | EN 13706-2 | 17 | 23 |
| Tensile modulus - longitutional [GPa] | EN ISO 527-4 | 17 | 23 |
| Tensile modulus - transverse [GPa] | EN ISO 527-4 | 5 | 7 |
| Tensile strngth - longitutional [MPa] | EN ISO 527-4 | 170 | 240 |
| Tensile strength - transverse | EN ISO 527-4 | 30 | 50 |
| Pin-bearing strength - longitutional | EN 13706-2 | 90 | 150 |
| Pin-bearing strength - transverse [MPa] | EN 13706-2 | 50 | 70 |
| Bending strength - longitutional [MPa] | EN ISO 14125 | 170 | 240 |
| Bending strength - transverse [MPa] | EN ISO 14125 | 70 | 100 |
| Shear strength – longitutional [MPa] | EN ISO 14130 | 15 | 25 |

### 2.5.2. Guidelines

As already discussed, there are no accepted and official guidelines for the design of structures using conventional or custom FRP profiles. According to various sources, (Bank, 2006) and (Keller T. , 2003), very little have changed in this issue for many years. There exist two general design manuals for structural engineers: the Structural Plastics Design Manual and the Eurocomp Design Code and Handbook (Potyrała, 2011). While the evidence is sufficient to confirm that the analytical equations in these two references are suitable for use in designing structures with profiles, there is little consensus about what safety and resistance factors to use. One option proposed by (Keller T. , 2003) to insert such guidelines is to have manufacturer-independent application codes geared to civil engineering practice. Some manufacturers offer the most comprehensive in-house design manuals intended for use with their respective profile products, for instance:

---

[2] E - Effective Flexural Modulus of the profile measured by testing a length of the complete profile
E23 ⁻ having the most stringent requirements to quality
E17 ⁻ having more lenient requirements to quality

- Bedford Reinforced Plastics, Inc. Design Guide and Design Guide Appendum (Bedford, 2010)
- Fiberline Design Manual by Fiberline Composites A/S (Fiberline)
- EXTREN DWB® DESIGN GUIDE (Corporation, 2003)

Apart from these, some general guidelines referring to deflections, vibrations, allowable stress limitations and fatigue provisions are available at AASHTO Guideline Specifications for Design of FRP Pedestrian Bridges (AASHTO, 2008).

## 2.6. Deflection/Design Criteria

Due to the low modulus of elasticity that characterize FRP material, the design of FRP decks is more often governed by deflection criteria rather than strength criteria. The resulting structures may possess very high factors of safety for strength, but the deflection criteria does not allow to fully exploit this strength. Although there are no specific guidelines regarding the design criteria in service limit state (SLS) much research has been conducted on the static behaviour of FRP deck. Currently the Eurocodes has not given any limit design criteria regarding the deflection of the structure. The FHWA report, "FRP Decks and Superstructures: Current Practice" by the U.S. Department of transportation Federal Highway Administration gives guidance that the deflection should be kept at 1/800 of the supporting length (Hoffard & Malvar, 2005). Moreover, the predicted strains under design load should be less than 20% of the FRP composites minimum guaranteed ultimate strength (base on coupon testing). Canadian guidelines suggest that this limit should be kept under 1/600 of the supporting length. While many other researchers provides less conservative approach limiting the deflection on 1/400 of the supporting length. In many reports the deflection criteria is based on the existing deflection limitations of "plate girder with slab" situation. Test results have shown that the failure mechanisms are the delamination at the outer free edges and/or at the inner drop-offs on the compressive flange (Hoffard & Malvar, 2005). Research is still going on to determine safety factors and implement design guidelines regarding deflection criteria.

## 2.7. Test on Coupon Level

FRP bridge deck designs taking place in the early 1990s used parallel rectangular tubes bonded together and covered with face sheets to create a sandwich type structure. After several investigations it was found that although these configurations were sufficiently stiff, this type of

structure was unstable in the lateral direction due to the lack of lateral support (Montley, Castanos, & Klang). This led to the introduction of trapezoidal tubes creating, in effect, a mix of diagonal webs and vertical webs, where the diagonal webs contributed significantly to the local and global response of the bridge deck material. During some tests performed at the University of Delaware, this type of design without additional face sheets on the tubes proved that local failure occurs under fatigue loading. Adding face sheets to the deck solved the fatigue problem but increased the cost significantly (Montley, Castanos, & Klang). One of the solutions considered to improve this behaviour was to change the angle of the diagonal web; this would reduce the span between the vertical and diagonal webs and improve the capacity of the diagonal web to carry bending loading. The concerns with the modification were that elimination of additional face sheets could produce a significant decrement in the global stiffness (transverse deflection) and lateral stiffness of the deck. This behaviour was studied by (Costanos, 2000), where four different element models were created for the understanding of the effects of a web angle change, properly 45, 60, 75 and 90-degree angle web models for Duraspan Deck (See Figure 2-24).



a)                                    b)
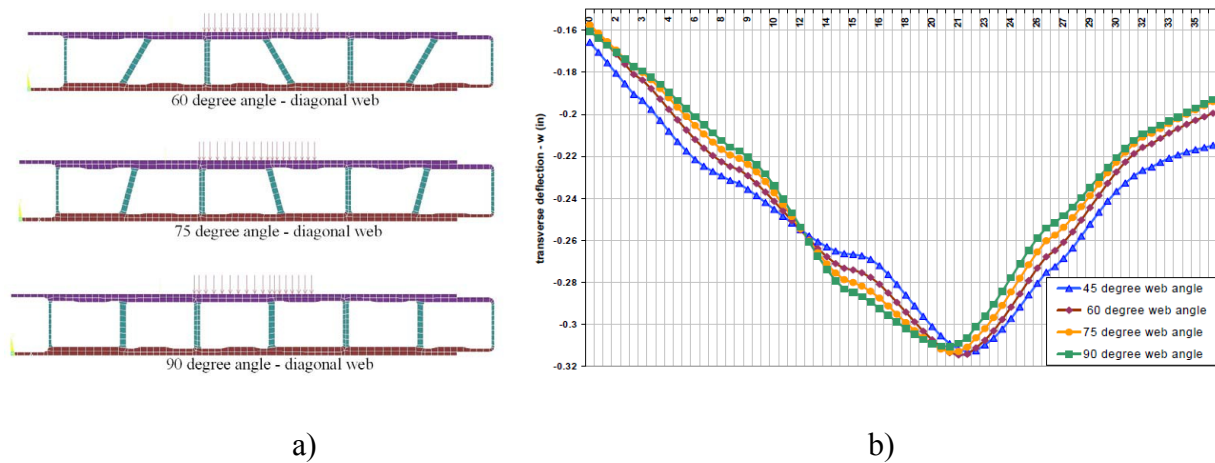
Figure 2-24 a) Finite element models of Duraspan bridge deck with 60, 75, and 90-degree web angles b) Transverse deflection of the different web angle models (Montley, Castanos, & Klang)

According to the graph presented in Figure 2-24 it shows that the maximum deflection remained the same for all cases, concluding that the changes in the diagonal web angle did not present a significant variation in the global stiffness of the deck. In general, it was observed that the reactions at the supports became less distributed as the diagonal web angle changes from 45 to

90 degrees. According to (Montley, Castanos, & Klang), a 75-degree diagonal web angle was selected to be the best configuration for the redesign of the deck, which resulted from a compromise between the reduction of the distance between the webs in order to improve the local fatigue resistance and provide sufficient lateral stiffness in the deck.

In order to investigate basic physical properties and durability of FRP deck by applied resin types, (Park, Hwang, Lee, & Jung, 2007) performed various durability tests including the physical properties (tensile, compressive and shear strength, modulus of elasticity) in the direction of fiber and the perpendicular direction to fiber of the flange and web which comprise the FRP deck. The geometry, physical properties and fiber architecture of the FRP deck studied are shown in Figure 2-25 and Figure 2-26. The design fiberglass volume ratio constituting the flange and web was 65%. In webs, $\pm45^{\circ}$ woven mats were added to resist against in-plane shear deformation in the deck. Design fibreglass volume ratio constituting the flanges and webs was 65%.



| Description | | Flange (Upper & low : 18 & 16mm) | Web (11 mm) |
|---|---|---|---|
| Elastic modulus (GPa) | $E_{11}$ | 25.491 | 23.610 |
| | $E_{22}$ | 23.663 | 15.785 |
| Poisson ratio | $v_{12}$ | 0.255 | 0.255 |
| Shear modulus (GPa) | $G_{12}, G_{13}$ | 7.131 | 9.865 |
| | $G_{23}$ | 4.258 | 6.584 |

(Units: mm)
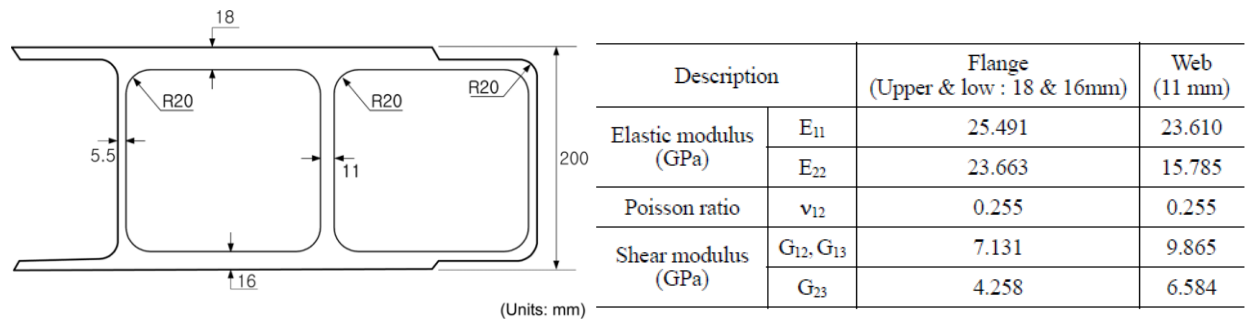
Figure 2-25 Shape of FRP Bridge Deck and Design Material Properties (Park, Hwang, Lee, & Jung, 2007)
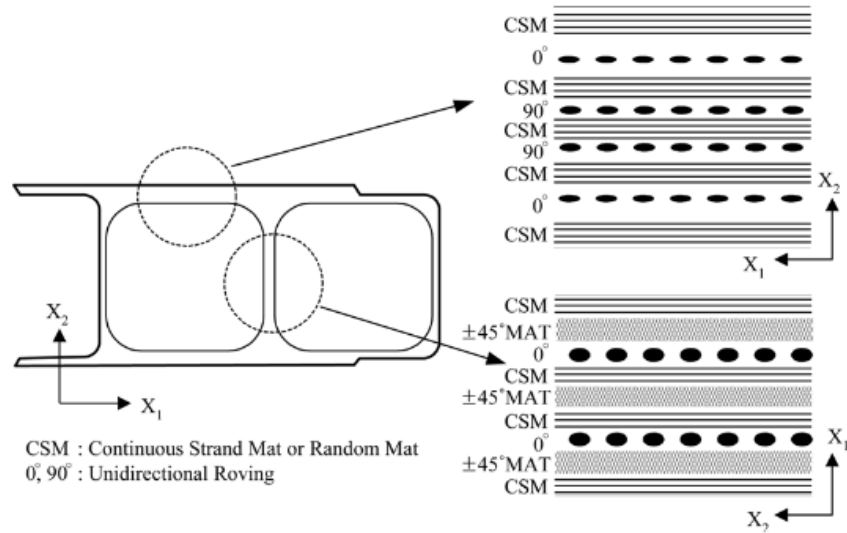
Figure 2-26 Pattern Design of Flange and Web (Park, Hwang, Lee, & Jung, 2007)

Three test specimens for each test were prepared for the tension, compression and shear strength of the FRP deck flange and web in the directions of fiber and perpendicular to the fiber. Table 2-9 to Table 2-11 respectively presents the results of tensile, compressive and in-plane shear test.

Table 2-9 Results of Tensile Test (Park, Hwang, Lee, & Jung, 2007)

| Description | Flange | | | | | | | | Web | | | | | | | |
|---|---|---|---|---|---|---|---|---|---|---|---|---|---|---|---|---|
| | Fiber Dir | | | | Transverse Dir | | | | Fiber Dir | | | | Transverse Dir | | | |
| | Tensile Strength | | Tensile Elastic Modulus | | Tensile Strength | | Tensile Elastic Modulus | | Tensile Strength | | Tensile Elastic Modulus | | Tensile Strength | | Tensile Elastic Modulus | |
| | $V^{1)}$ | $P^{2)}$ | V | P | V | P | V | P | V | P | V | P | V | P | V | P |
| Specimen 1 | 0.316 | 0.394 | 36.6 | 32.4 | 0.0973 | 0.1820 | 14.5 | 23.1 | 0.306 | 0.319 | 31.5 | 22.4 | 0.0746 | 0.0889 | 12.5 | 20.8 |
| Specimen 2 | 0.379 | 0.387 | 31.3 | 31.8 | 0.0577 | 0.1860 | 17.6 | 22.6 | 0.366 | 0.274 | 23.4 | 19.8 | 0.0585 | 0.0652 | 12.7 | 14.2 |
| Specimen 3 | 0.311 | 0.402 | 30.8 | 33.0 | 0.0973 | 0.1770 | 14.6 | 20.4 | 0.305 | 0.309 | 26.0 | 20.7 | 0.0721 | 0.0924 | - | 17.0 |
| Avg(A) | 0.314 | 0.394 | 31.1 | 32.4 | 0.0972 | 0.1817 | 14.6 | 22.0 | 0.306 | 0.301 | 24.7 | 21.0 | 0.0734 | 0.0822 | 12.6 | 17.3 |
| Design Elastic Modulus (B) | | | 25.491 | | | | 23.663 | | | | 23.610 | | | | 15.785 | |
| A/B | | | 1.22 | 1.27 | | | 0.61 | 0.93 | | | 1.05 | 0.89 | | | 0.80 | 1.10 |

1) Vinylester
2) Polyester

36

Table 2-10 Results of Compressive Test (Park, Hwang, Lee, & Jung, 2007)

| Description | Flange | | | | Web | | | |
|---|---|---|---|---|---|---|---|---|
| | Fiber Dir | | Transverse Dir | | Fiber Dir | | Transverse Dir | |
| | V [1] | P [2] | V | P | V | P | V | P |
| Specimen 1 | 0.182 | 0.248 | 0.105 | 0.085 | 0.156 | 0.342 | 0.107 | 0.153 |
| Specimen 2 | 0.192 | 0.264 | 0.083 | 0.076 | 0.098 | 0.265 | 0.064 | 0.202 |
| Specimen 3 | 0.158 | 0.244 | 0.082 | 0.078 | 0.170 | 0.267 | 0.096 | 0.193 |
| Average | 0.177 | 0.252 | 0.090 | 0.080 | 0.141 | 0.291 | 0.089 | 0.183 |

1) Vinylester
2) Polyester

Table 2-11 Results of In-plane Shear Test (Park, Hwang, Lee, & Jung, 2007)

| Description | Flange | | Web | |
|---|---|---|---|---|
| | V [1] | P [2] | V | P |
| Specimen 1 | 62.7 | 64.6 | 96.9 | 45.9 |
| Specimen 2 | 64.2 | 65.1 | 94.8 | 49.3 |
| Specimen 3 | 65.6 | 65.4 | 75.8 | 50.0 |
| Average | 64.2 | 65.0 | 95.9 | 48.4 |

1) Vinylester
2) Polyester

The measurements of the tensile modulus of elasticity of the FRP deck in this study member showed that, vinylester satisfies the modulus of elasticity required in the direction of the fiber (the direction of the design span of decks), while the polyester cases failed to satisfy the design modulus of elasticity in the web fiber direction. When compared with the modulus of elasticity of steel (Es = 210 GPa), the stiffness of the FRP deck member are, in vinylester and polyester respectively, 14.8% and 15.4% in the fiber direction in the flange. In the compressive tests, it was shown that the compressive strength in the fiber direction of the flange, which was applied with polyester, was higher than the case of vinylester. In the webs, the ratios between the compressive strengths in the fiber direction and perpendicular direction to fiber showed similar values in the cases of vinylester and polyester resins (approx. 1.58~1.59). Tests performed to study the in-plane shear failure demonstrated that the failure of fiber was the main cause of failure. In the cases of flanges, the two resin cases showed similar results, while in the cases of web, vinylester showed about 2 times on average higher than polyester.

Bridge decks, as a structural member exposed to the environment, are affected by the surrounding conditions. (Smith, 2001) and (Montley, Castanos, & Klang) performed some environmental testing on pultruded structural shapes to study their behaviour under temperature, humidity effects. In the thermal expansion tests, for the vinylester specimens, the thermal expansion coefficient in the fiber directions in flanges and webs turned out to be approximately 1/2 of those of steel and concrete, while in the directions perpendicular to the fiber, the coefficients were $10.5 \times 10^{-6}$ and $10.9 \times 10^{-6}$ respectively, which were similar to those of steel and concrete. In the heat and cold resistance tests, no significant change in the modulus of elasticity or strength was observed at low temperatures, while rapid decrease in the modulus of elasticity and strength was identified at high temperatures. The FRP deck specimens made with vinylester showed less modulus of elasticity and strength to be compared with the control than the specimens made with polyester. In the chemical resistance test, vinylester displayed better properties of flexural strength and flexural elastic modulus, while polyester showed better tensile strength. Flexural strength was weakened more by chemical immersion than tensile test.

Comparing the FRP deck members made with vinylester and polyester, polyester showed unfavorable results in thermal, chemical, and weathering resistance properties to vinylester. Therefore, if chemical and thermal resistance can be improved, vinylester will be more suitable than polyester for the FRP deck material which is subject to long term exposal to the environment (Park, Hwang, Lee, & Jung, 2007).

(Alnahhal & Chiewanichakorn, 2006) studied the thermal behaviour of FRP deck under fire loading. Thermal simulations showed that FRP bridge decks are sensitive to the effect of elevated temperatures. As compared with steel or concrete bridges, FRP bridges exhibited lower heat resistance (See Figure 2-27). At the most critical fire scenario reported in this study, the top face skin starts failure after 440s of a burning truck on deck. Therefore, any FRP bridge under fire incident has to be vacant from people and vehicles quickly, and the damaged region of an FRP bridge should be repaired before any further use.
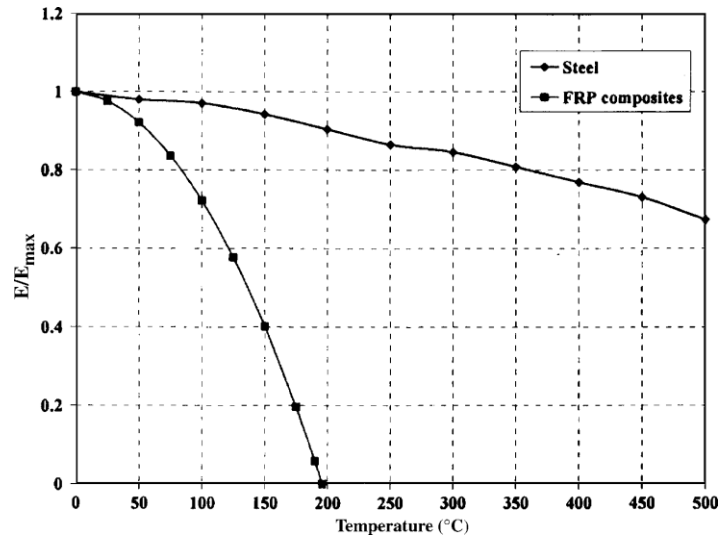
Figure 2-27 Stiffness-temperature curve of FRP and steel at elevated temperature (Alnahhal & Chiewanichakorn, 2006)

## 2.8. Laboratory test of FRP Decks

This section provides information regarding laboratory tests performed on FRP deck with different configuration and properties. Kansas, Duraspan, ASSET and Ecosafe deck are presented.

(Camata & Shing, 2005) investigated Kansas deck system made of two stiff plates and a sinusoidal shape core by hand lay-up process as shown in Figure 2-28.
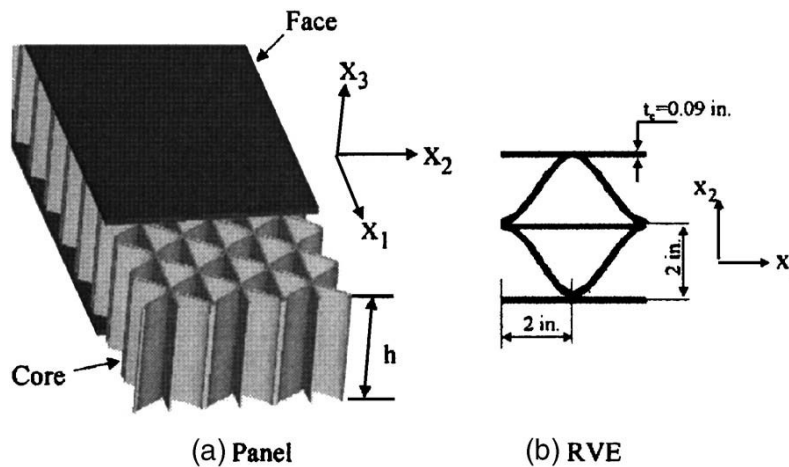


Figure 2-28 Configuration of the Kansas deck system (Camata & Shing, 2005)

Crushing tests on four beams of this type of deck were performed with three-point loading test to investigate the crushing loads. Failure loads of the beams varied from 175 to 587 kN, and this scatter was due to adhesive bonding quality between the core and the plates. Load-deflection response of the four beams is shown in Figure 2.31
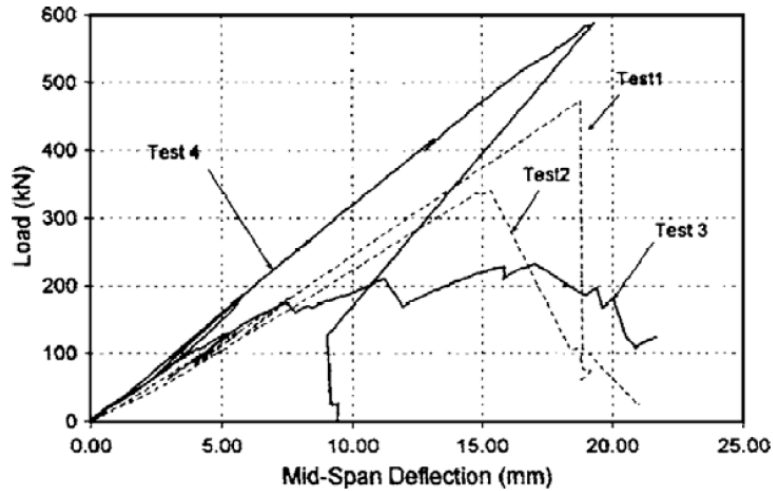


Figure 2-29 Load-deflection curve of the beams (Camata & Shing, 2005)

It was observed that failure modes were brittle and were caused due to the delamination of the flanges and debonding of the flanges from the webs. Delamination started in the top flange followed by debonding non-uniformly and buckling of the core in the back side. This change and scatter in results is due to the manufacture process since these decks are manufactured by hand lay-up process which leads to imperfections and nonuniformities in the bonding. The load-displacement curves as shown in Figure 2-29 are linear up to failure expect for test 3 which was pseudo-ductile different from the others. The failure mode of the compressive crushing tests was buckling of the cores. Ultimate crushing capacity of the specimens was approximately 72.1 kN. The average actual core stress was 64.7 MPa and the nominal stress when considering the whole loading area was computed as 7.1 MPa.

Other decking system test were performed by (Keller & Gurtler, 2006), where the selected FRp decks were Duraspan and ASSET as shown in Figure 2-30.
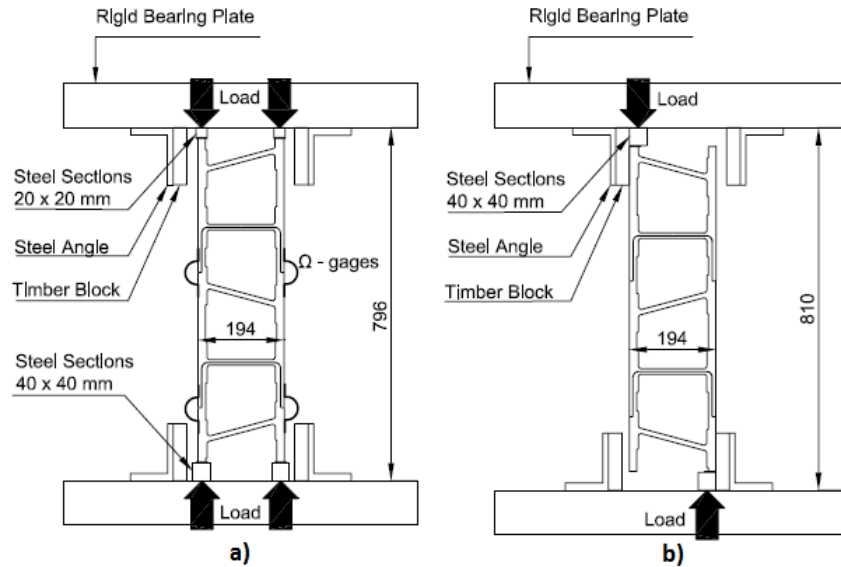
Figure 2-30 Experimental set-up for a) in-plane compression; b) in-plane shear (Keller & Gürtler, 2006)

Tests were performed to find out in-plane[3] properties of these decks which might act as a top chord of bridge girders in case of composite action between the deck and the girders and the results are shown in Table 2-12. In-plane compression and in-plane shear tests were carried out on panels made of three adhesively bonded components.

Table 2-12 In-plane compression and shear results for trapezoidal deck system (average values ± standard deviation) (Keller & Gurtler, 2004)

| Type of in-plane loading | Ultimate failure load (kN) | (a) Elastic modulus machine (GPa) | (b) Elastic modulus strain gages (GPa) | (c) Elastic modulus $\Omega$-gages (GPa) | Maximum differential displacement (mm) | System shear modulus (GPa) |
|---|---|---|---|---|---|---|
| Compression (three specimens) | 736 ± 19 | 8.1 ± 0.3 | 14.1 ± 2.4 | 6.9 ± 1.0 | – | – |
| Shear (three specimens) | 59 ± 3 | – | – | – | 33 ± 8 | 0.005 ± 0.001 |

The failure mode of ASSET deck was brittle and linear elastic up to failure, while Duraspan deck exhibited some ductility. The so called 'elastic limits' marks the beginning of the local delamination failures. In tests of in-plane compression, Duraspan deck was deformed laterally while loading and delamination in the flanges of the deck started propagating. In ASSET deck delamination in the stepped joint caused failure as shown in Figure 2-31. Failure modes of in-

---

[3] The term 'in-plane' in this context means the properties in the deck plane and the tests are done transverse to the pultrusion direction.

plane shear tests were web delamination and joint failure for Duraspan and failure in the stepped joint for ASSET deck as demonstrated in Figure 2-32. In Table 2.5 it can be observed that the strength and stiffness of ASSET deck system are higher than Duraspan deck system. The difference is more significant for in-plane shear stiffness and capacity. The configuration of ASSET deck is triangular compared to trapezoidal configuration of Duraspan system, which makes possible the transfer of forces mostly by truss action, in case of Duraspan deck is mainly by Vierendeel action. Thus, ASSET deck has much higher in-plane shear stiffness and strength than Duraspan deck.



Figure 2-31 Failure modes of Duraspan in the left and ASSET deck in the right for in-plane compression tests (Keller & Gürtler, 2006)
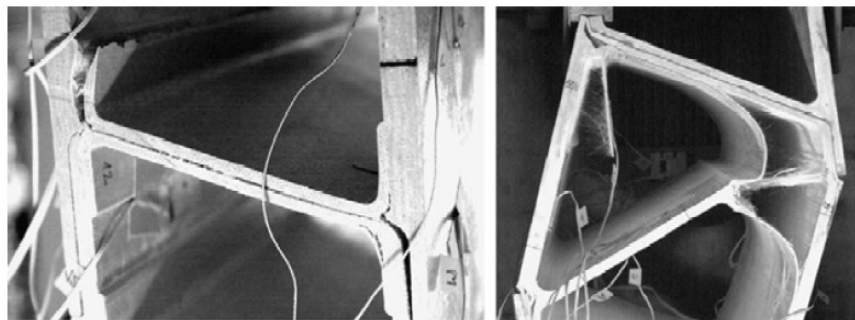


Figure 2-32 Failure modes of Duraspan in the left and ASSET deck in the right for in-plane shear tests (Keller & Gürtler, 2006)

In-plane tension tests were executed on Duraspan deck system, to examine the deck acting as a top chord in continuous bridges with negative moment regions (Keller & Schollmayer, 2006). Failure mode in this case was failure in the stepped joints as shown in Figure 2-33.

Figure 2-33 Failure in the joint for in-plane tension test in Duraspan deck (Keller & Schollmayer, 2006)

Static test performed on Duraspan decks, wide 1.1016 to 1.626, spanning 1.9-2.7 m to investigate the bending behavior are presented in Figure 2-34. The results showed that global load-deflection response was linear-elastic up to ultimate limit state loads. Failure of the deck occurred around the area of the patch load where buckling of the upper face sheet and the webs started as shown in Figure 2-35. Thereafter, delamination between the flanges and the webs were observed. The maximum resulting stress was 194 MPa at failure.



Figure 2-34 Experimental set-up for static tests performed by (Keller & Schollmayer, 2004)
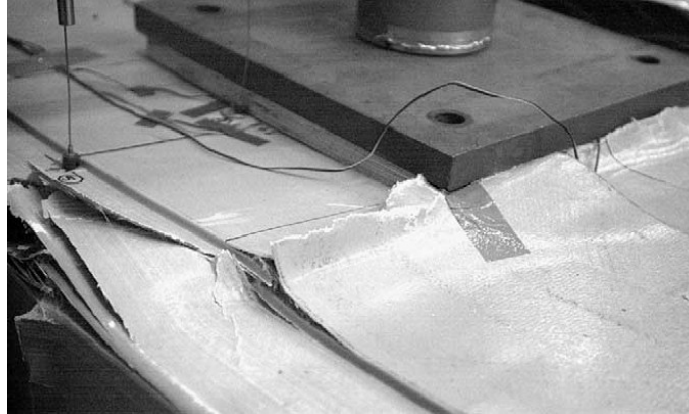
Figure 2-35 Failure mode of Duraspan deck: buckling and delamination (Keller & Schollmayer, 2004)

Tests on Ecosafe deck were performed by (Jiang, Kolstein, & Bijlaard, 2013). The FRP-to-steel adhesively-bonded joints were experimentally investigated under tensile loading as shown in Figure 2-37and Figure 2-39.
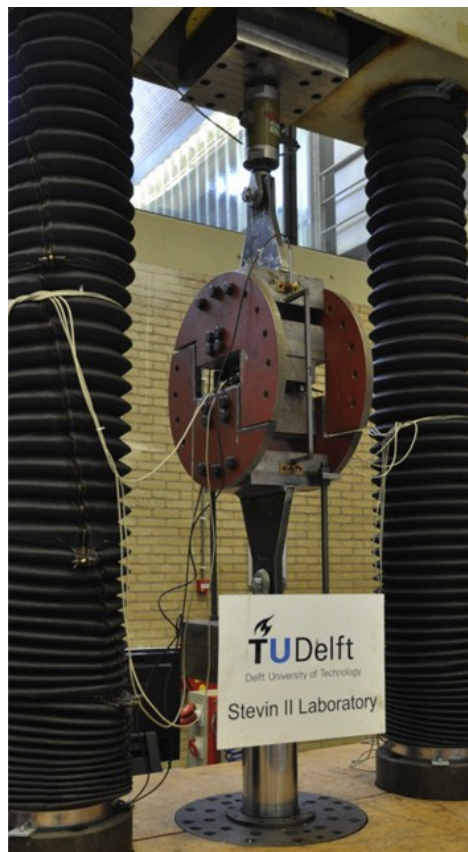


Figure 2-36 Experimental set-up (Jiang, Kolstein, & Bijlaard, 2013)
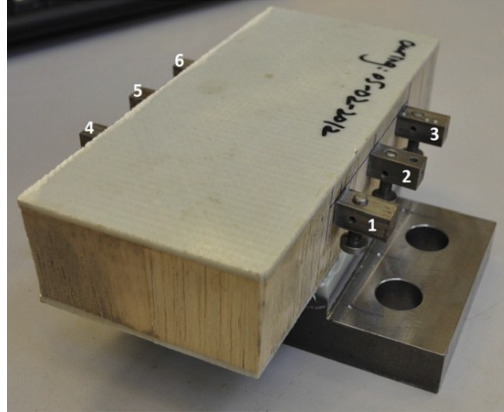
Figure 2-37 Adhesive joint specimen (Jiang, Kolstein, & Bijlaard, 2013)

The mechanical behavior of adhesive joint specimens with surface pretreatment (SP) and un-pretreatment (UP) were compared. For UP-specimens, the joints failed in a brittle mode as shown in Figure 2-38, which occurred between FRP sandwich deck and adhesive layer. The average ultimate failure load of UP-specimens was 16.04 kN; the results are presented in Table 2-13. For SP-specimens, the failure of adhesive joint was triggered by delamination of FRP composites. The average ultimate failure load of SP-specimens was 9.83% higher than that of UP-specimens.

Table 2-13 Ultimate failure loads of six adhesive joints (Jiang, Kolstein, & Bijlaard, 2013)

|  | UP-01 | UP-02 | UP-03 | Average | Deviation |
|---|---|---|---|---|---|
| Failure load (kN) | 15.69 | 16.43 | 16.04 | 16.05 | 2.37% |
|  | SP-01 | SP-02 | SP-03 | Average | Deviation |
| Failure load (kN) | 19.37 | 17.93 | 15.57 | 17.62 | 11.63% |



Figure 2-38 Delamination failure of SP-specimen01 (Jiang, Kolstein, & Bijlaard, 2013)

## 2.9. Composite action between the deck and the girders

One of the most important issues when studying the hybrid bridges made with steel girders and FRP decks is the degree of the composite action between the deck and the girders. Composite action refers to amount of the degree that horizontal shear forces are transferred between the girder and the deck. When full composite action is relieved 100% of the horizontal force is transferred between the girder and the deck. Contrary to the latter, no horizontal shear forces are transferred in a non-composite section. Moreover, partial composite action refers to the situation when a portion of this horizontal shear force is transferred between the deck and the girders. Full composite action is regarded as a plane strain distribution in the composite section, consequently fulfilling the hypothesis of Bernoulli as explained by (Gurtler, 2004) (See Figure 2-39).
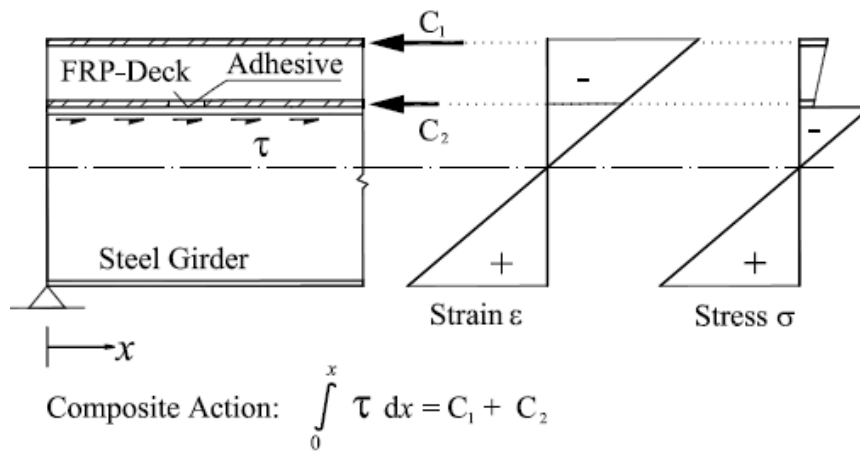


Figure 2-39 Theory of the composite action in a composite section (Gurtler, 2004)

Due to the composite action between the steel girder and FRP deck the neutral axis will shift up toward the FRP deck. The shifted neutral axis due to additional FRP deck on top of the steel girder will change the moment of inertia and section modulus of the whole member resulting in the decrease of the stress in the top flange of the girder.

The development of connections between FRP decks and girders is challenging in order to achieve full composite action. This composite action between bridge decks and the underlying girders gives a substantial increase in overall stiffness and load resistance of the system, leading to a more efficient and economical structure. In addition, composite action between a bridge FRP deck, which is considered as a brittle material and bridge girders with a more ductile behaviour

will contribute to an enhanced ductility of the bridge structure. The load transfer in deck-girder adhesively bonded joints is complex and not yet precisely understood. Most of the constructed bridges consisting of FRP decks with steel girders are constructed with shear connectors. In the recent years adhesive bonding is used to connect steel girders with FRP decks due to the good fatigue behavior. The design of the girders in these bridges is done without considering the contribution of the FRP deck and the FRP deck itself is assumed to have composite action. This design is conservative since the decks contribute to the load-carrying capacity of the girders. The major reason of considering this conservative design is due to lack of design methods and complex load-bearing behaviour.

FRP decks must participate in the bridge's longitudinal direction as part of upper flange of the main girders in addition to providing transversal load-carrying action between the bridge girders. The degree of composite action between the girders and the FRP deck, apart from the connection between these two elements, depends also on the in-plane shear stiffness and in-plane axial stiffness of the FRP deck in the longitudinal bridge direction between the supports and in-plane tensile stiffness over the inner supports in case of continuous bridges (Keller & Gurtler, In-plane tensile performance of a cellular FRP bridge deck acting as top chord of continuous bridge girders., 2006). The determination of the composite action between the deck and the girder was be determined by testing the hybrid girder. Tests were performed by Keller and Gurtler on adhesively bonded hybrid FRP-steel girders. ASSET and Duraspan deck systems were utilized. The test set-up is shown in Figure 2-40 for ASSET deck, which is the equivalent for Duraspan deck system as well. The composite action of the deck itself was examined by comparing the strains and the differential shifts between the top and bottom deck panels.

According to the results driven (Gurtler, 2004) shown in Figure 2-41, the strains in the top flange are reduced to some extent for ASSET and significantly reduced for Duraspan. Thus, it is concluded that ASSET deck has a slight reduction of participation of the top flange in the composite action of the deck and Duraspan possesses a considerable reduction. This is verified by differential shifts between the panels as well, were the shifts of Duraspan were approximately 40 times larger than those of ASSET deck.

47
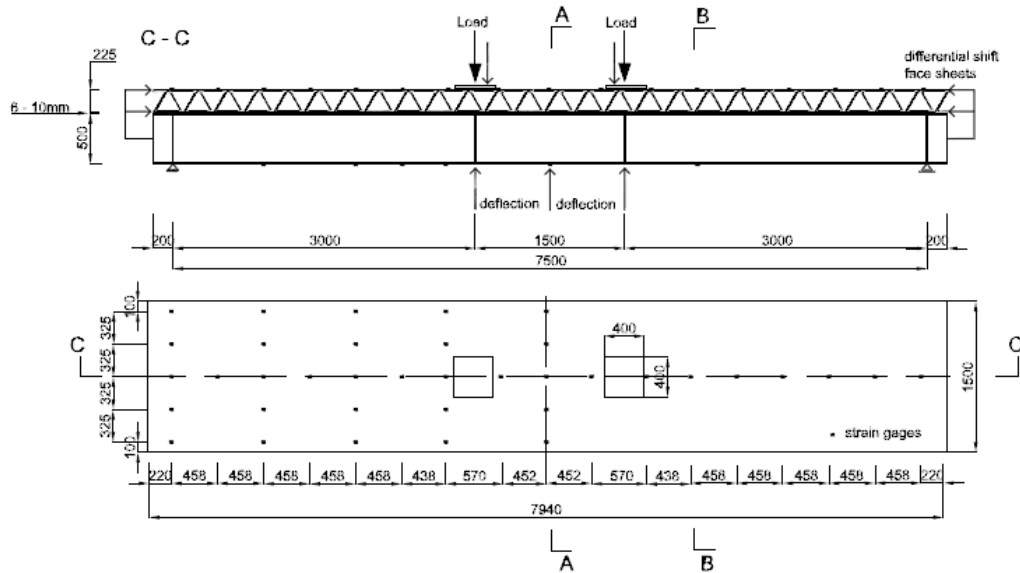
Figure 2-40 Test set-up of adhesively bonded hybrid FRP-steel girders (Keller & Gurtler, In-plane tensile performance of a cellular FRP bridge deck acting as top chord of continuous bridge girders., 2006)
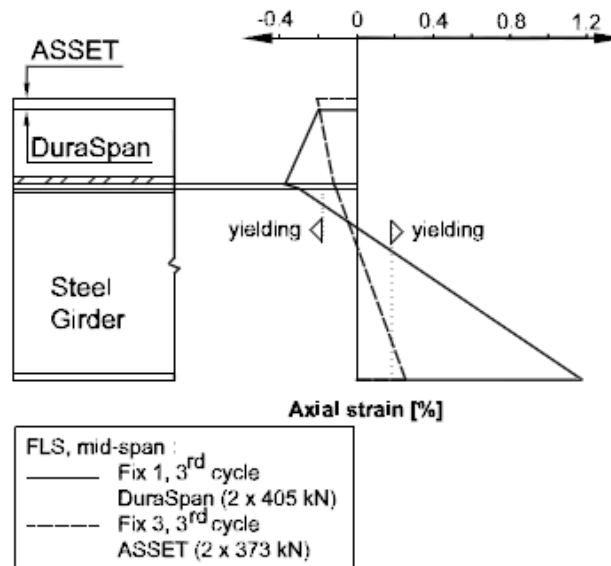


Figure 2-41 Strain and stress distribution in the mid-span of the ASSET and Duraspan hybrid Girders[4] (Gurtler, 2004)

The participation of the upper deck panel was less pronounced for ASSET deck since it exhibits much higher in-plane shear stiffness as described. In sections where there are shear forces the

---

[4] Fix 3 and Fix 4 are the names of the composite beams tested under SLS loading.

strain distribution is different (See Figure 2-42) due to secondary moments in the deck itself caused by shear forces. This effect is more pronounced near the support where the global moment is small and the secondary moment of the deck caused by shear forces is high enough to cause tensile strains in top flange of the deck.
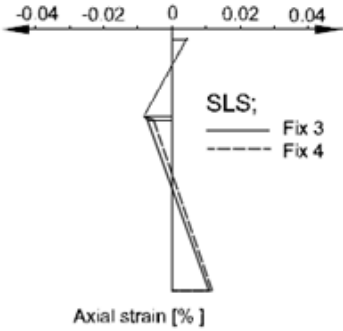


Figure 2-42 Axial strain distributions between the support and the load (Gurtler, 2004)

In a composite deck-girder system, the portion of the deck assumed to contribute to the flexural capacity of the longitudinal girder is characterized by the effective width of the deck. The effective deck width in the study performed by (Gurtler, 2004) was checked by measuring the axial strains on deck plates along the transverse direction. The strains are shown in Figure 2-43for serviceability limit state (SLS) and failure limit state (FLS).

As it can be observed in the Figure 2-43 the strains in SLS for both decks are almost linear along the whole width of the deck. This indicates that the decks fully participate as top chords in the SLS state. In FLS this participation is reduced and the strains are not linear along the whole width but they decease in the ends of the deck width. This is more noticeable in the bottom panels.

a) Asset hybrid girder  b) DuraSpan hybrid girder
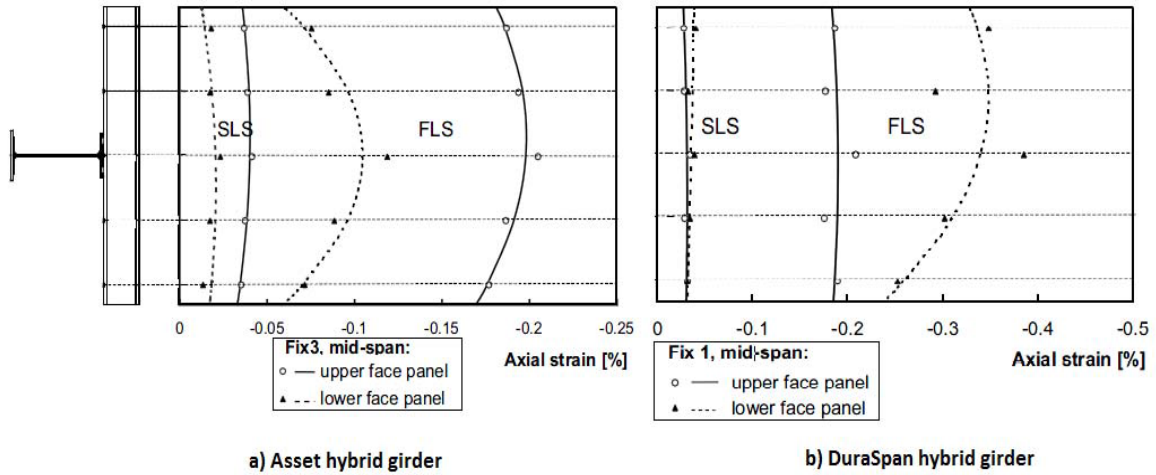
Figure 2-43 The axial strains in transverse direction of the hybrid girders in midspan to evaluate the effective widths (Gurtler, 2004)

The tests indicated that the deflections of the FRP-steel hybrid girders were decreased and the failure loads increased compared to just steel girders. The load-deflection curves for hybrid girders and steel girder are illustrated in Figure 2-44.
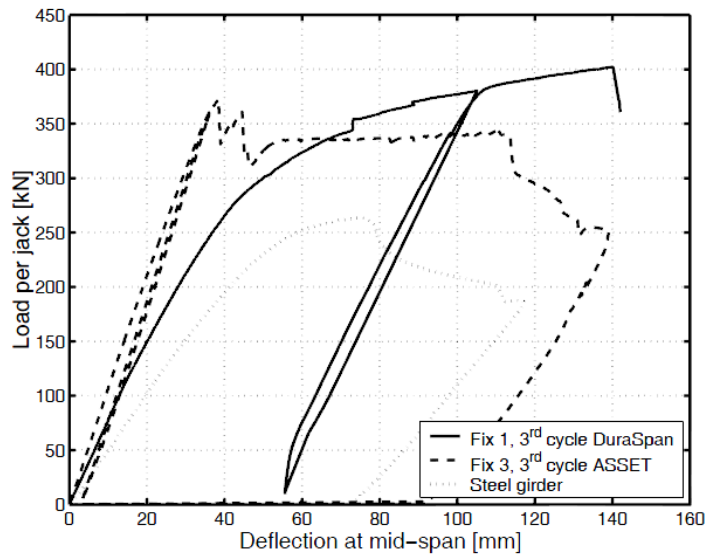


Figure 2-44 Comparison of load-deflection curves for hybrid and steel girders (Gurtler, 2004)

### 2.9.1. Adhesive Bonding

Adhesive material used for bonding FRP deck with steel girders has shown an increase in fatigue life. In general a thickness from 6mm to 10 mm is used. Experiments to investigate the

performance of epoxy bonded balanced double-lap and single-lap joints between pultruded GFRP flat sections were performed by (Keller & T., 2005a) (Keller & Vallee, 2005b) and where the joints were subjected to quasi-static axial tensile loading.
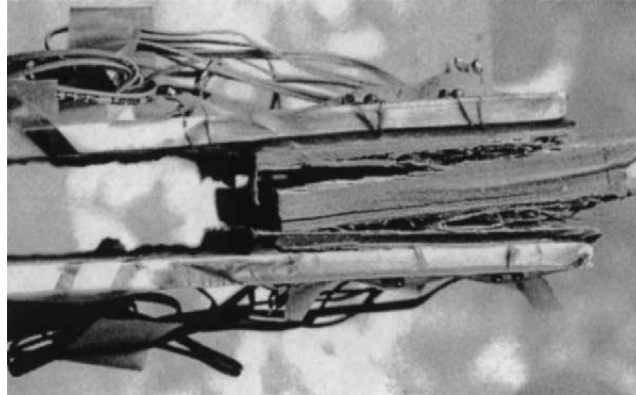


Figure 2-45 Fibre tear failure of adhesively bonded lap joints

As a conclusion, the failure was initiated as a result of combination of peeling tensile stresses combined with shear stresses. It was observed that failure modes were the delamination in the outer fibre of mat region of FRP coupon and not in the adhesive connection as shown in Figure 2-45. Through-thickness strength of the adhesive-adhered interface was higher than that of interface between the fibre mats. The adhesive thickness with changes from 1- 3mm had a small influence in the distribution of the stresses.

FRP coupons were tested using a shear-tensile method device to predict the strength of these joints which allows the measurements of through-thickness tensile stresses and shear strength as shown in Figure 2-46 (Keller & Vallée, 2005b). The resulting combined through-thickness tensile and shear strength is given in Figure 2-47.
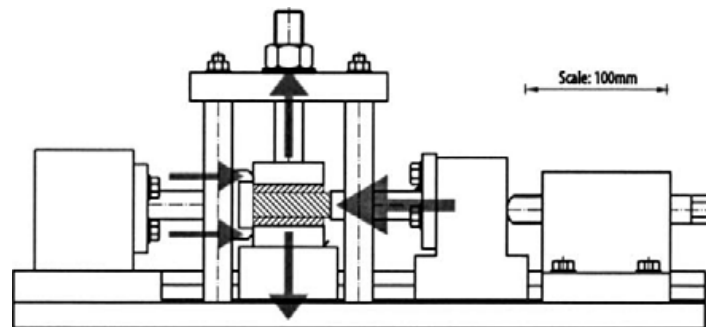


Figure 2-46 Shear-tensile device used to test the bonded FRP coupons (Keller & Vallée, 2005b)

It was observed that the failure mode was the classical fibre-tear failure in the outer mats of adherends as previously discussed. The joint strength was principally determined by the low tensile peeling stress of the adherends. The calculated partial material safety factor was 1.34.
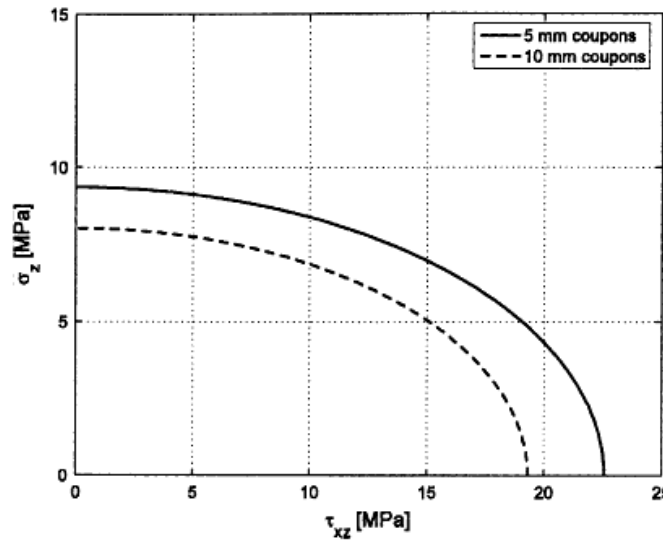


Figure 2-47 Combined through-thickness tensile and shear strength of 5mm and 10 mm thick FRP coupons (Keller & Vallée, 2005b)

In the adhesively bonded FRP decks (ASSET and Duraspan) to steel girders tests was observed that the adhesive bonding connection was stiff enough to guarantee full composite action between the girder and the bottom face panel of the deck up to failure (Keller & Gurtler, 2005). Keller et al. 2005 observed also that even flexible adhesives in layers up to 50 mm thick gave full composite action between the bottom face panel of FRP decks and steel girders. In these test the adhesives were subjected to just longitudinal shear stresses and these stresses were far below the ultimate stresses at failure. Peeling stresses were absent in this test.

The performance of adhesive joints subjected to peeling forces was investigated further by Keller & Schollmayer (2009). Tensile peeling forces in the adhesives are developed due to uplift forces created by the load-bearing behaviour in the transverse direction of the bridge as shown in Figure 2-48. Experimental tests were performed on steel girders adhesively bonded to Duraspan deck subjecting to tensile forces as illustrated in Figure 2-49.
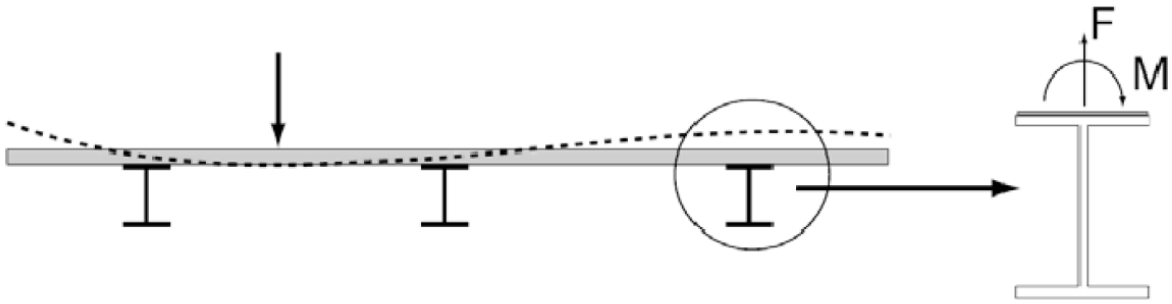
Figure 2-48 Resulting uplift forces and moments due to load-behaviour of the deck in the transverse direction of the bridge (Keller & Schollmayer, 2009)
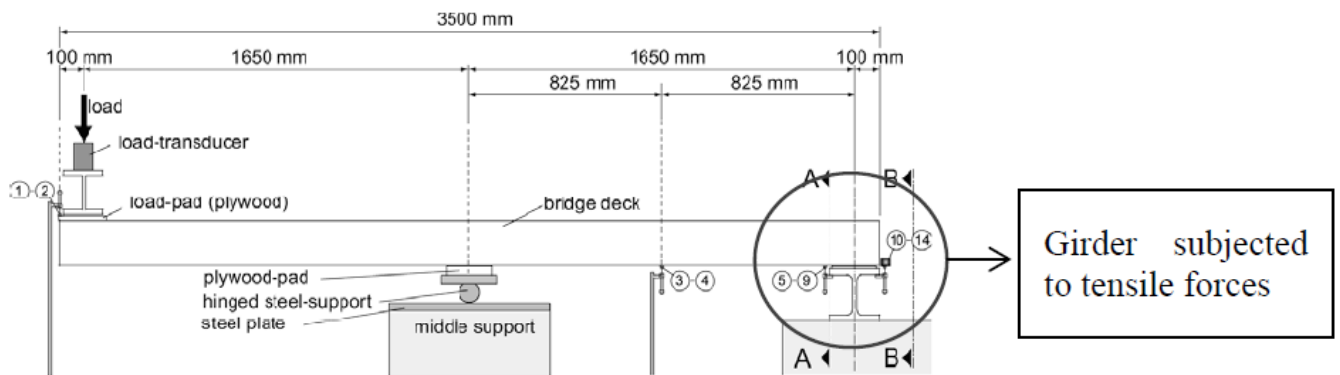


Figure 2-49 Test set-up of the hybrid girder subjected to tensile forces (Keller & Schollmayer, 2009)

The girders were loaded up to failure. The failure mode was observed to be fibre-tear failure in the outer mat layers of the deck flanges, shown in Figure 2-50. This was consistent with the failure modes of the lap joints presented above.



53
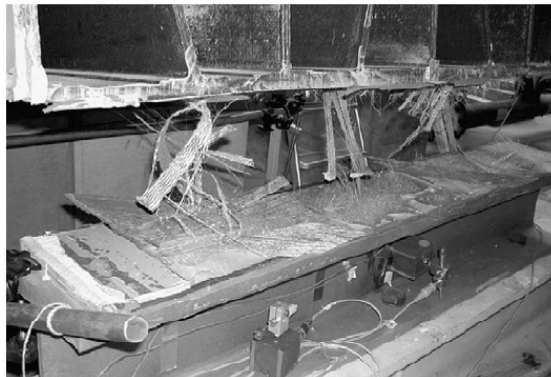
Figure 2-50 Fibre-tear failure of the outer mat layers of the adhesively bonded FRP deck to steel girders subjected to tensile forces (Keller & Schollmayer, 2009)

Keller & Schollmayer, 2009 performed a numerical analysis with a portion of deck adhesively bonded to the girders in order to understand the stress in the joints. The FEM model, presented in Figure 2-51, showed that peak stress concentrations were present under vertical and inclined webs. As shown in Figure 2-52, these stress concentrations are more pronounced under the vertical web. This indicates that the loads are transferred directly from the webs through the adhesive joints to the girders. The average joint uplift stress at failure was determined as 0.79 MPa by the experimental results. The joint tensile failure stress of 9.1 MPa is determined by multiplying this value with the stress concentration factor, calculated as 12.4 from numerical analysis. This tensile failure stress corresponds to the tensile failure stress determined in lap joint tests under pure tensile loading (See Figure 2-47).
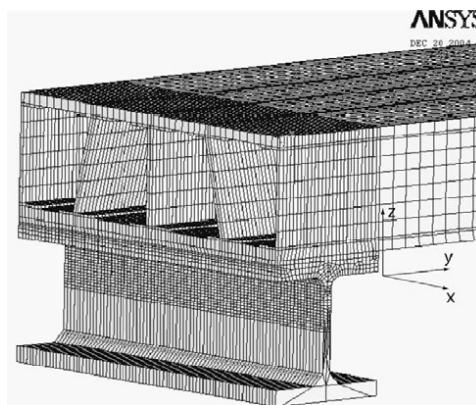


Figure 2-51 FEM modeling of deck adhesively connected to steel girder (Keller & Schollmayer, 2009)
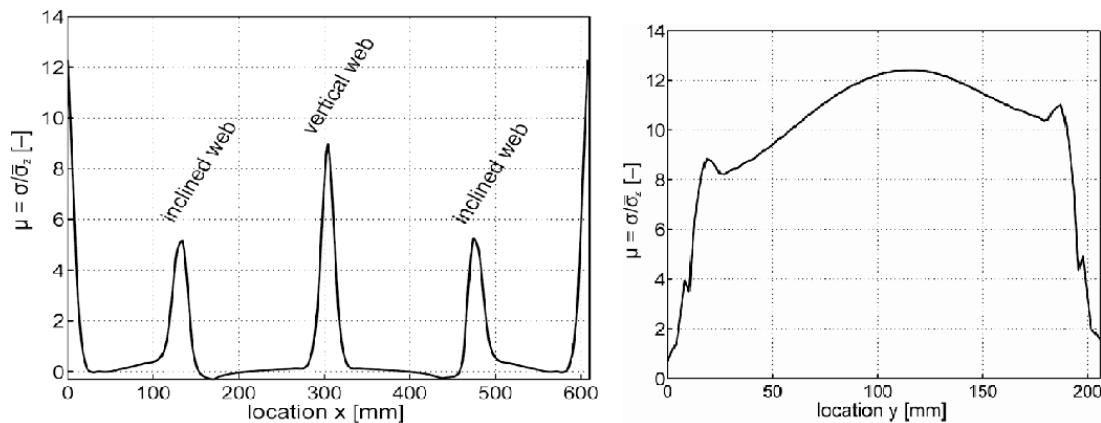
Figure 2-52 The results of normalized through-thickness tensile stress distribution in the adhesive joints; left: along the longitudinal direction, right: along transverse direction under a vertical web (Keller & Schollmayer, 2009)

In addition, the adhesive joint was tested for fatigue loading up to 10 million cycles during static test analysis as well. No stiffness degradation was observed but the ultimate load was significantly decreased. The deflection response of the hybrid girder subjected to fatigue loading is shown in Figure 2-53. The deflection response is almost linear during the fatigue load cycles which show that the stiffness is not degraded. The load-displacement responses of two hybrid girder are depicted in Figure 2-54.
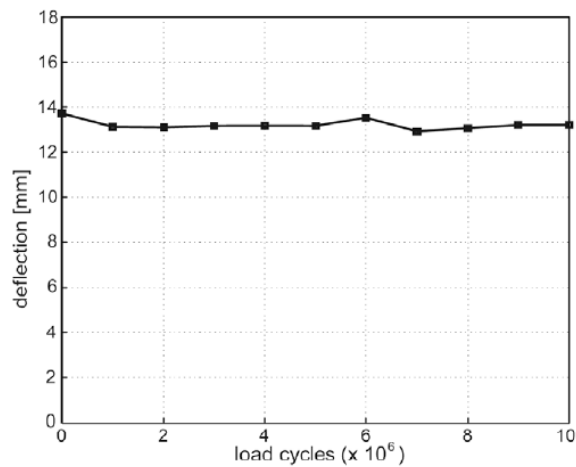


Figure 2-53 Deflection response of the hybrid Duraspan-steel girder subjected to 10 million fatigue cycles (Keller & Schollmayer, 2009)
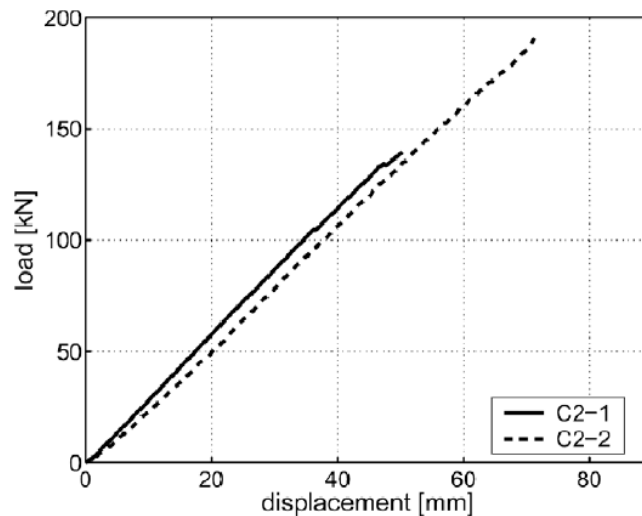
Figure 2-54 Load-displacement responses of two hybrid girders (Keller & Schollmayer, 2009)

C2-1 hybrid girder was subjected to fatigue loading of 10 million cycles then to static loading while the other hybrid girder C2-2 was subjected to just static loading. As it can be observed, the ultimate load for C2-1 is lower than for C2-2.

The investigations show that when the deck is adhesively bonded to the girders fibre tear failure mode is observed due to low through-thickness strength of FRP plates. Moreover, stress concentrations are attained under the webs.

## 2.10. Fatigue tests of FRP structures

Long term performance of fiber reinforced polymer composite bridge decks is dependent on progressive damage in the materials (due to change in the internal stress state and material state) and still a subject of considerable interest as there is lack of understanding of the underlying mechanisms. Because of the relatively large number of possible failure mechanisms in FRP composite materials, the prediction of fatigue life in a component is not simple. In a composite material, fatigue damage can take the form of any or all of the following: delamination, matrix cracking, fiber failure, matrix crazing, fiber-matrix debonding and void growth. It is dependent on variables associated with the testing conditions and the construction and composition of the material (Majumdar, 2008). Determination of strength and failure mode under actual service conditions plays a pivotal role for predicting possible damage initiation areas and eventually life of the bridge deck. Many researchers have conducted laboratory experiments to predict the fatigue life of FRP decks. Duraspan and ASSET deck bonded adhesively to steel girders were tested by (Keller & Gürtler, 2005). The results of static experiments during fatigue indicated no signs stiffness degradation as a result of the 10 million fatigue cycles, corresponding to 75 years. No signs of bond or material deterioration could be observed. However, it is stated that long term fatigue loading behaviour of the adhesive bond must be further researched. Another fatigue experiment performed on Duraspan deck bonded adhesively to steel girders was conducted by (Cassity, Richards, & Gillispie, 2002) on a specimen that was 3.66 m long and consisted of 3 pultruded tubes bonded together as shown in Figure 2-55. The configuration of the deck was chosen to induce both negative and positive flexure in the specimen that was calibrated to the actual demonstration bridge and was subjected to 10.5 million cycles of fatigue loading. The deck was tested without the presence of the overlay in order to achieve a conservative estimate.

The results showed that the connection survived fatigue without failure. Although the negative moment region survived fatigue without damage, the deck showed some fatigue sensitivity. Local bending of the top face sheet in the vicinity of the tire patch resulted in interlaminar shear cracking on the underside of the top face sheet at a ply drop-off detail and mid-depth of the top face sheet as shown in Figure 2-56. According to (Cassity, Richards, & Gillispie, 2002), the localized cracking of the deck may not have occurred if an overlay was present.



Figure 2-55 Global fatigue specimen (Cassity, Richards, & Gillispie, 2002)
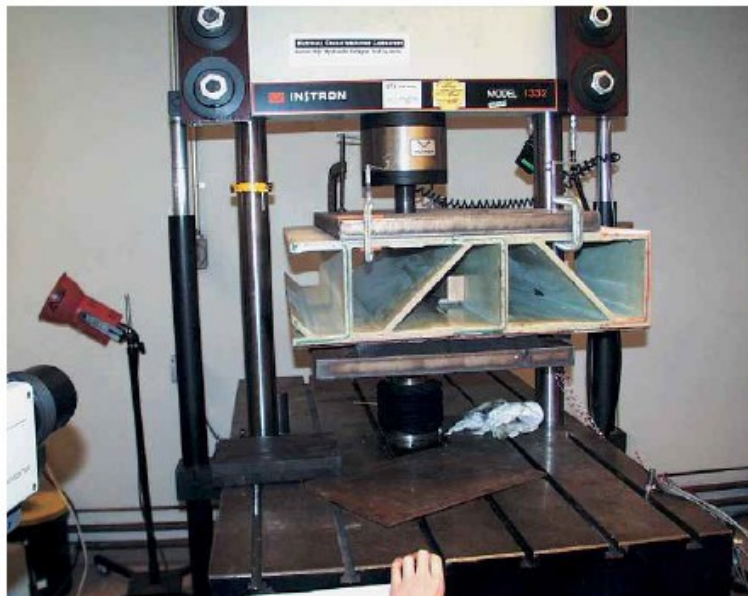
Figure 2-56 Local fatigue testing of deck (load is applied from the bottom) (Cassity, Richards, & Gillispie, 2002)

Degradation of the stiffness on FRP decks has been observed in some other tests conducted by (Brown & Berman, 2010). Two different deck types up to 2 million cycles were tested as shown in Figure 2-57. Deck A was composed of adhesively bonded tubes sandwiched by adhesively bonded top and bottom plates. Deck B had a bottom section consisting of I-profiles and a mechanically connected top plate.
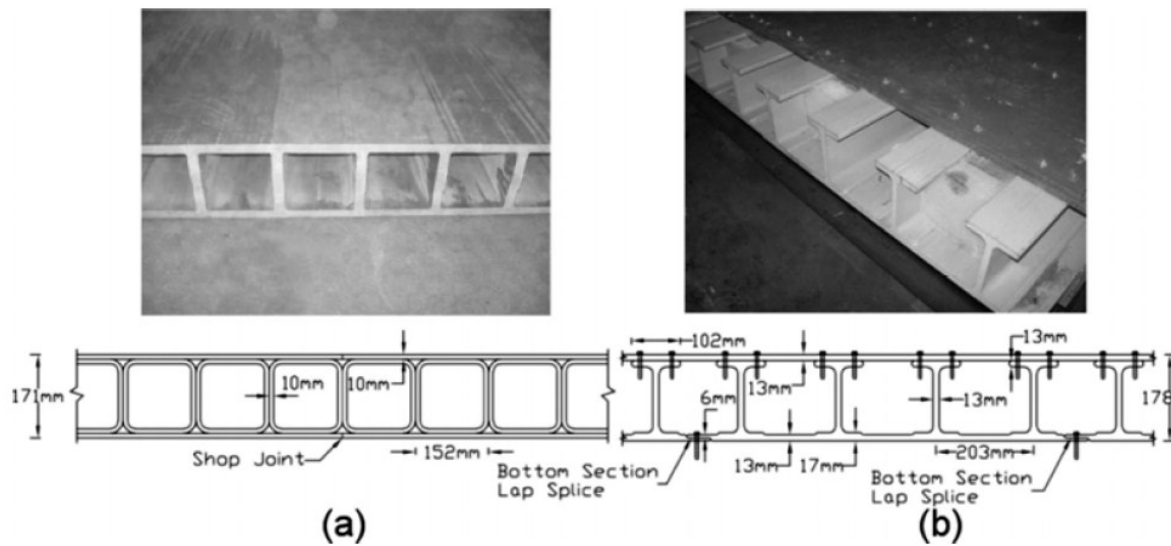


Figure 2-57 Deck types a) Deck A b) Deck B tested for fatigue evaluation by (Brown & Berman, 2010)

Different connections of these decks to steel girders were utilized as shown in Figure 2-58. The spacing between the connections in deck A was 1.8 m and in deck B 0.36m.
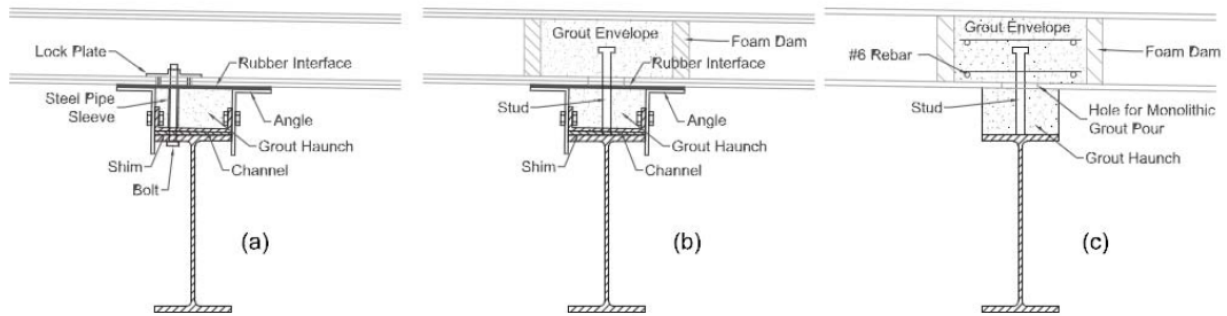
Figure 2-58 Deck to girder connections: a) Bolt and lock plate used for deck A b) Shear stud used for deck A c) Shear studs used for deck B (Brown & Berman, 2010)

Degradation of the stiffness was observed in both decks during fatigue loading, although more pronounced in deck A. The higher degradation of deck A was due to failure of the shop joint (panel level connections) during loading, the scarceness and flexibility of system level connections and imperfections at the adhesive joints between the deck panels. Deck type B showed less degradation of stiffness which might be due to bearing deformations of the screwed connection of the upper panel. Some degradation of the composite action between the girders and the decks was detected by comparing the location of the neutral axis.

Another laboratory investigation was performed by (Gleason & Dusicka, 2012) to study the behavior of Morrison Bridge of Portland when replacing the steel deck with FRP deck. Three different decks were chosen and four fatigue tests were conducted. Of the four tests, three completed the full amount of cycles while one of the modified ZellComp tests failed at 1.4 million cycles. The maximum deflection per cycle is shown for all four tests in Figure 2-59. Fatigue displacement degradation measured between 9% and 13% for the three completed fatigue tests.
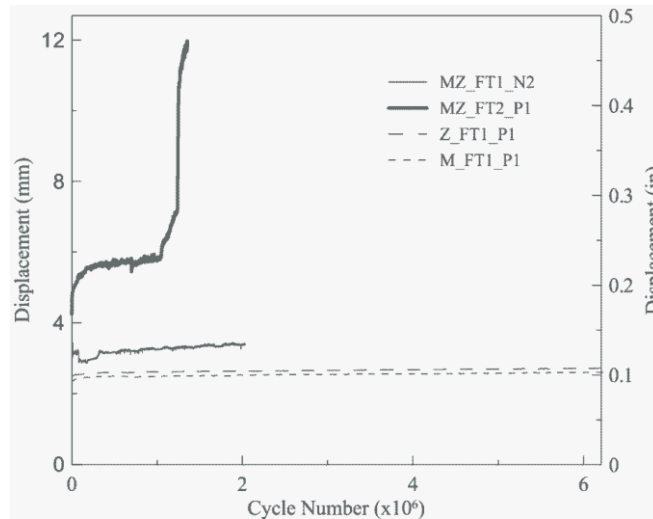
Figure 2-59 Fatigue comparison (Gleason & Dusicka, 2012)

The four fatigue tests showed that the Martin Marietta (Duraspan Deck) and ZellComp decks resulted adequate for the Morrison Bridge. Unfortunately, there were insufficient data to make the same determination for the modified ZellComp option. The modified ZellComp deck failed in fatigue testing according to the HITEC fatigue testing procedure. However, this procedure was found to not be representative of the Morrison Bridge. In both modified ZellComp fatigue tests, bolt failures occurred and should therefore be monitored in field situations. Fatigue testing cracked the overlay over the lap joints in the modified ZellComp fatigue tests, but fatigue was not found to damage the overlay in other places on the deck (Gleason & Dusicka, 2012).

In case of composite bridges when replacing the concrete deck by a FRP deck particular care must be taken if there are fatigue prone details. The lighter FRP deck will likely result in lower total stresses in the supporting girders, but due to the reduced composite action and effective width and increased distribution factors, the live load induced stress range is likely to be increased. (Harries & J.Moses, 2007) studied this behavior and it was observed some increase in live load stress range. The increased transient stress range must be considered if there are prone fatigue details in the bridge. Thus, existing fatigue-prone details may become a concern and require additional attention in the design.

A methodology and strategy has been proposed for fatigue damage assessment and life prediction of bridge-deck sections with online structural health monitoring data (Chan & Li, 2001). A fatigue damage model based on the continuum damage mechanics (CDM) is developed

for evaluating accumulative fatigue damage of existing bridges. For accurate estimation of fatigue life, the nonlinear fatigue model based on CDM may be better than Miner's rule. However, this needs further verification on structural fatigue tests although it has been verified by material fatigue tests (Majumdar, 2008). Chiewanichakorn studied the behavior of a FRP deck in truss bridge using finite element models (Chiewanichakorn & Aref, 2007). FE models were employed to conduct dynamic time-history analyses with a moving AASHTO fatigue truck over the bridge. Fatigue life was evaluated based on fatigue resistance formulae specified in AASHTO-LRFD design specifications.

Another fatigue testing of different cross sections of FRP decks as shown in Figure 2-60 under extremely high ($50^{o}$C) and low temperatures ($-30^{o}$C) was performed to evaluate the FRP deck performance by (Dutta, Lopez-Anido, Kwon, & Durell, 2003). Degradation of the stiffness of FRP deck following 10 million cycles under the two extreme temperatures was observed. The degradation of the stiffness of the FRP decks is believed to be more affected by the extreme temperature levels. The decks are affected more by the high temperatures. The degradation of stiffness in low temperature was not as significant as in high temperature.
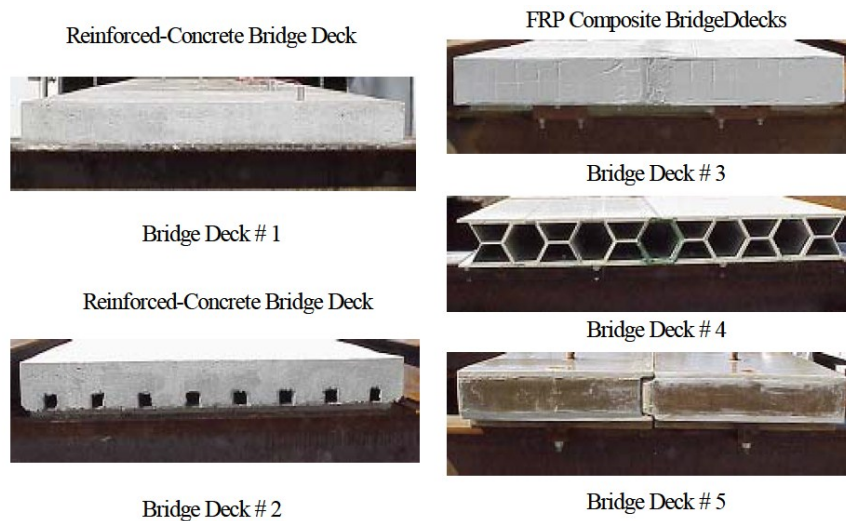


Figure 2-60 Cross-section of FRP deck systems (Dutta, Lopez-Anido, Kwon, & Durell, 2003)

## 2.11. Cost Analysis and Environmental Issues

While initial costs for a FRP bridge, both for complete structure or in combination with steel, may be slightly higher than a steel equivalent, once the benefits of easier installation and reduced maintenance are taken into account, the total cost will be considerable comparable for FRP option. Christian Scholze from Fiberline Composites, according to (Kendall, 2008), showed this

conclusion graphically in Figure 2-61. Moreover, he presented the potential environmental benefit of FRP compared to other traditional materials showing the energy consumed in
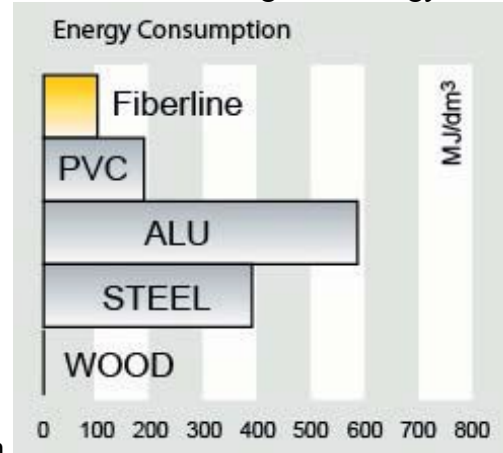


producing other materials by the graph shown in Figure 2-62Figure 2-61. Fiberline recommends painting pultrusion used in external applications to provide additional environmental protection and a 30-year life to repainting is normally achieved.
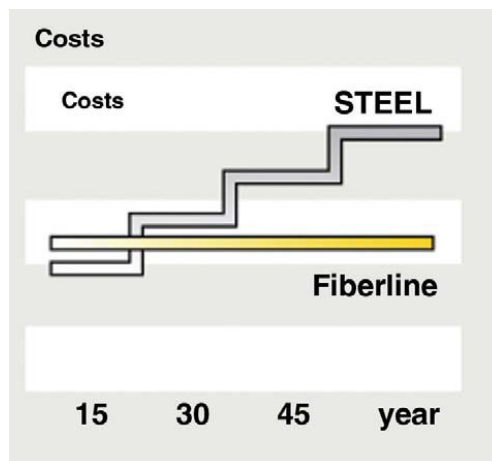


Figure 2-61 Relative costs of steel and FRP bridges through life (Kendall, 2008)



62
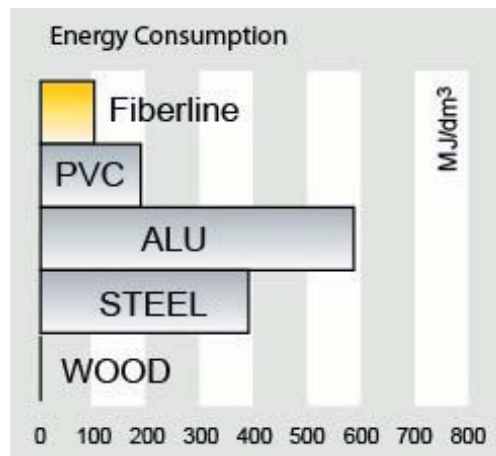
Figure 2-62 Energy consumption in the manufacture of materials (Kendall, 2008)

The environmental issue in the construction industry is becoming increasingly important during the material selection process. According to Dr Sue Halliwell from Net Composites at (Kendall, 2008), both legislation and ASSET owners are demanding improved environmental performance and longer service life with reduced maintenance. She explained how FRP could assist in meeting the environmental challenge as follows:

- ideal for modular, factory-based production, leading to better quality control
- inherently thermal insulating, eliminating thermal bridging
- resistant to passage of water vapour
- joints can be vapour- and air-tight
- thermal stability improves long-term performance in relation to air-tightness
- composite materials can be tailored to contain reflective coatings on strategic surfaces to reduce solar gain.

As a case study she presented the 13.5 m bridge Noord Footbridge a complete FRP bridge located in the Netherlands. According to Table 2-14, combining initial and maintenance costs structural steel is the cheapest option, followed by FRP. On the other hand, the environmental analysis of embodied energy put FRP as a clear winner with each other option using more than twice the energy required for FRP. Moreover, the same result is achieved when assessing pollution impacts.

Table 2-14 Assessments of candidate materials for bridge construction (Kendall, 2008)

| Criterion | Material of the bridge | | | |
| --- | --- | --- | --- | --- |
| | Structural steel | Stainless steel | Plastics | Aluminium |
| Initial costs (€) | Painted: **40 000**<br><br>Aluminium-coated: **50 000** | In steel AISI 316L: **110 000**<br>In steel AISI 304L: **96 000** | Pultruded sections GRP: **70 000** | **77 000** |
| Maintenance costs (€) for a 50-year life | Painted: **30 000**<br><br>Aluminium coated: **6000** | In steel AISI 316L: **6000**<br><br>In AISI 304L: more, life cycle shorter | Estimated: **17 000** | Estimated: **19 000** |
| Embodied energy (MJ) | 270 000 | 299 600 | 120 000 | 268 700 |
| Environment: critical volume of polluted ... | water: **674.5 m³**<br>air: **7.326·10⁶ m³** | Not investigated but certainly more water and air pollution than for structural steel. | water: **34.8 m³**<br>air: **17.660·10⁶ m³** | water: **237.2 m³**<br>air: **53.570·10⁶ m³** |

Another cost comparison by Fiberline is formulated in the table below shown in Figure 2-63 for FRP deck systems and other traditional materials. As it can be observed FRP decking systems require higher initial cost comparing to other materials. However to get a more realistic estimation of the total costs, installation time (that reflects directly to the disruption and delay costs) and maintenance costs should be provided as well. Jon Shave at (Kendall, 2008), presented the business case of Mount Pleasant Bridge. The latter is constructed on two spans of 26 m, with an FRP deck on steel beams, supporting a single vehicle lane. He concluded that although the structure costs for the FRP deck was more than a conventional one, the additional costs is offset by significant savings in the scheme cost and whole life cost.
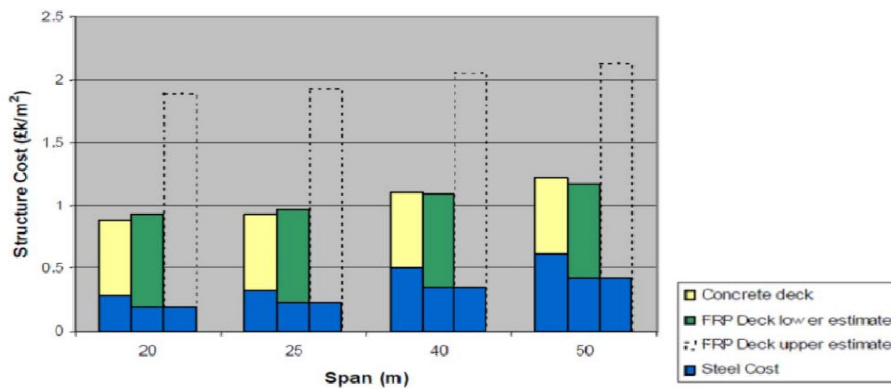


Figure 2-63 Cost comparison of FRP concrete and steel decks in different spans (Mara V. , 2011)

He also studied the costs when longer bridge span with a constant width of 6 m are required. He concluded that the extra structure costs is balanced by installation savings (see Figure 2-64).
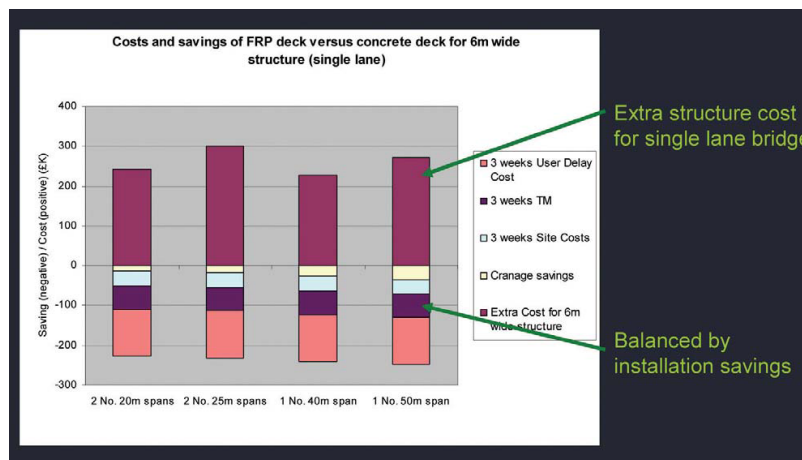


Figure 2-64 FRP bridge deck costs and savings for a single-lane bridge (Kendall, 2008)

64

A sustainability analysis was performed on two refurbishment options in a case study bridge in Sweden as shown in Figure 2-65 from (Mara & Haghani, 2012). One of the option including replacement of the existing deck with an FRP deck (alternative 1) and replacement of the entire superstructure with a prefabricated concrete deck on steel girders (alternative 2). It was concluded that substantial cost savings can be achieve considering FRP decks as a refurbishment option for functionally obsolete bridges instead of replacing the entire superstructure. The refurbishment method with the FRP deck results in lower environmental impact, the total amount of carbon emissions for FRP deck option decreased by 16,5 % than replacement of the entire superstructure option whereas the embodied energy consumption decreased by 30 % (see Figure 2-65 and Figure 2-66).
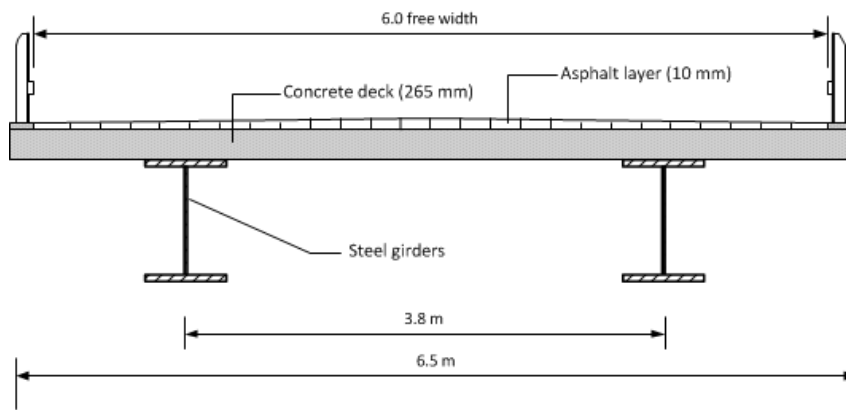


Figure 2-65 Cross-section of Rokån Bridge (Mara & Haghani, 2012)
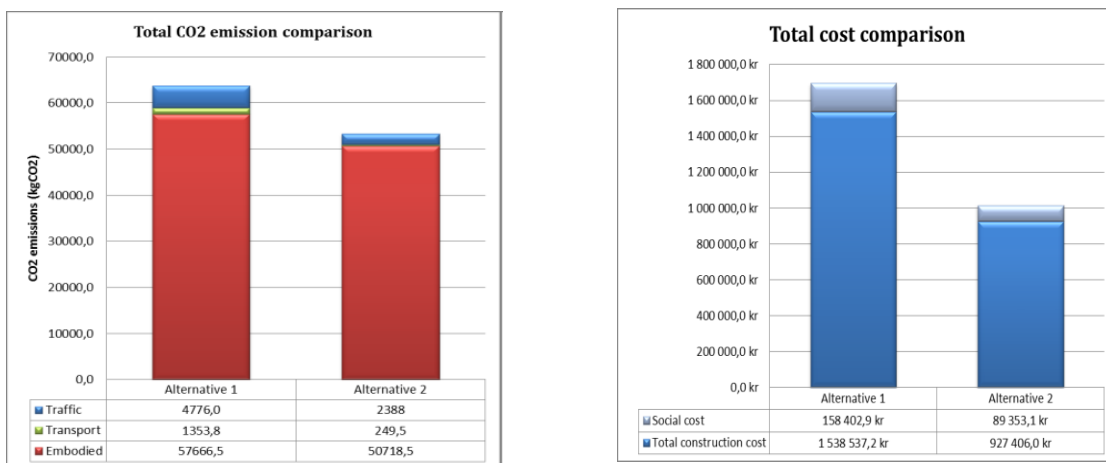


Figure 2-66 Total cost comparison and carbon emissions for the two alternatives (Mara & Haghani, 2012)

An interesting cost analysis is found for the Johnson bascule bridge shown in (MMM Group, 2011). The study compares the initial and maintenance cost between 6 propositions in replacing the deck in Johnson Street Bridge, Victoria, USA. The deck solutions are shown in Table 2-15 with the initial cost while additional cost are shown in Table 2-16.



Figure 2-67 Johnson Street Bridge (MMM Group, 2011)

Table 2-15 Options of deck replacement of Johnson Street Bridge – Initial Costs (MMM Group, 2011)

| **Option 1a: Traditional Steel Orthotropic Deck** | |
|---|---|
| Deck Fabrication | $1,550 / m$_2$ |
| Deck Shipping and Installation | $450 / m$_2$ |
| Floor Beams at 5.0m centres* | $200 / m$_2$ |
| Proprietary Lightweight Wearing Surface** | $150 / m$_2$ |
| Sub-Total Cost = $1.9 Million $2,350 / m$_2$ | |
| **Option 1b: Proprietary Steel Orthotropic Deck** | |
| Deck Fabrication | $1,200 / m$_2$ |
| Deck Shipping and Installation | $450 / m$_2$ |
| Floor Beams at 5.0m centres* | $200 / m$_2$ |
| Proprietary Lightweight Wearing Surface ** | $150 / m$_2$ |
| Sub-Total Cost = $1.6 Million† $2,000 / m$_2$ | |
| **Option 2: Open Grid Steel Deck** | |
| Steel Grid Fabrication | $400 / m$_2$ |
| Deck Shipping and Installation | $400 / m$_2$ |
| Floor Beams at 5.0m centres c/w Stringers* | $300 / m$_2$ |
| Sub-Total Cost = $0.9 Million† $1,100 / m$_2$ | |
| **Option 3: Half-Filled Grid Deck with Overfill** | |
| Steel Grid Fabrication | $400 / m$_2$ |
| Deck Shipping and Installation | $400 / m$_2$ |
| Floor Beams at 2.5m centres* | $400 / m$_2$ |
| Lightweight Concrete Infill | $250 / m$_2$ |
| Sub-Total Cost = $1.2 Million† $1,450 / m$_2$ | |
| **Option 4: Exodermic$_{TM}$ Deck** | |
| Steel Grid Fabrication | $400 / m$_2$ |

66

Deck Shipping and Installation                                  $400 / m$_2$
Floor Beams at 4.0m centres*                                    $350 / m$_2$
Reinforced Lightweight Concrete                                 $400 / m$_2$
     Sub-Total Cost = $1.25 Million† $1,550 / m$_2$

## Option 5: Fibre Reinforced Polymer Deck

FRP Deck Materials                                              $850 / m$_2$
Deck Shipping and Installation                                  $300 / m$_2$
Floor Beams at 5.0m centres c/w Stringers*                      $300 / m$_2$
Polymer Concrete Wearing Surface***                             $200 / m$_2$
     Sub-Total Cost = $1.4 Million† $1,650 / m$_2$

## Option 6: Sandwich Plate System

Deck Fabrication                                                $1,250 / m$_2$
Deck Shipping and Installation                                  $400 / m$_2$
Floor Beams at 5.0m centres c/w Stringers*                      $300 / m$_2$
Proprietary Lightweight Wearing Surface ***                     $150 / m$_2$
     Sub-Total Cost = $1.7 Million† $2,100 / m$_2$

Table 2-16 Additional Costs Related to Bridge Deck System Weights (MMM Group, 2011)

| Deck Option | Additional Counterweight Costs | Additional Mechanical Costs | Additional Pier Foundation Costs |
|---|---|---|---|
| 1a – Traditional Orthotropic | $46,000 | $20,000 | $7,000 |
| 1b – Proprietary Orthotropic | $128,000 | $54,000 | $19,000 |
| 2 – Open Grid Steel Deck | $68,000 | $29,000 | $10,000 |
| 3 – Half-filled Grid Deck | $546,000 | $232,000 | $82,000 |
| 4 – Exodermic™ Deck | $760,000 | $322,000 | $114,000 |
| 5 – FRP Deck | $0 | $0 | $0 |
| 6 – SPS Deck | $485,000 | $206,000 | $73,000 |

Each of the evaluation criteria were given a weighting which when multiplied by the ranking number and added up to determine the final ranking for the each deck system. The first and second criteria are related to costs (initial deck costs and additional costs due to deck weight) and weighted at 20% and 25% resulting in a total weighting for cost comparisons of 45%. Deck and wearing surface maintenance was weighted at 25% and long term performance risk was given a weighting of 30%. The bridge deck systems with the lowest final ranking numbers provide the best solutions for the Johnson Street Bridge roadway deck. The results are shown in Table 2-17.

When all the variables are included in the study the FRP deck (Zell Comp) results with a rating 3.05 while the orthotropic results in 2.1 and the open grid case in 2.6. However, in this study the

long term performance risks of the FRP deck are considered high. If this risk is considered low as for the case of orthotropic deck, the rating of the FRP deck is 2.15, while for orthotropic is 2.1 and for the open grid case 2.6.

Table 2-17 Bridge deck system ranking evaluation (MMM Group, 2011)

| Ranking Criteria | Weight | 1b Orthotropic | 2 Open Grid | 3 Half-filled Grid | 4 Exodermic™ | 5 FRP | 6 SPS |
|---|---|---|---|---|---|---|---|
| | | 1=best meets criteria, 2=better than average, 3=average, 4=less than average, 5=poorly meets criteria | | | | | |
| Deck Initial Cost | 20% | $1.6M | $0.9M | $1.20M | $1.25M | $1.4M | $1.7M |
| | | 4 | 1 | 2 | 2 | 3 | 4 |
| Deck Weight & Additional Costs Relative to FRP Deck Weight | 25% | 285 kg/m² | 245 kg/m² | 400 kg/m² | 470 kg/m² | 220 kg/m² | 380 kg/m² |
| | | $0.20M | $0.11M | $0.86M | $1.2M | $0 | $0.76M |
| | | 2 | 1 | 4 | 5 | 1 | 4 |
| Deck & Wearing Surface Maint. | 25% | Good | Very Poor | Very Good | Very Good | Very Poor | Good |
| | | 2 | 5 | 1 | 1 | 5 | 2 |
| Risk (Long-term Performance) | 30% | Low | Moderate | Low | Low | High | Very High |
| | | 1 | 3 | 2 | 2 | 4 | 5 |
| | 100% | Weighted Score (Lowest Best Meets Criteria) | | | | | |
| | | 2.1 | 2.6 | 2.25 | 2.5 | 3.3 | 3.8 |
| Final Ranking | | 1 | 4 | 2 | 3 | 5 | 6 |

## 2.12. Construction Process

Advanced fiber-reinforced polymer composite bridge decks offer tremendous potential to meet critical needs for rehabilitation and upgrading of existing old bridges. As a conclusion from literature research on FRP hybrid bridges built to date, they are easy to work with and offer rapid installation process. This amount of time depends mostly on the experience of the contractor. A general overview of the construction process is presented below:

### A. Fabrication and Pre-work procedures

Part of the preparation work before the assembly procedure is

- Pre-fabrication

This process is already treated in Section 2.2 on page 16.

- Remove of existing construction and preparation of sub-structure

Depending on the existing substructure different actions should be taken into consideration when preparing it for assembly. Figure 2-68 shows an example when the existing structure was removed and metal shell piles were driven for the new piers. The metal shell piles were filled and encased with concrete as shown in Figure 2-68. The pier caps and abutments were formed and finished, followed by placement of the steel plate girders.



Figure 2-68 Concrete Encased Metal Shell Piles (left) and Angle Irons Tack Welded to the Girder Top Flange (right) (Winkelman, 2002)

- Shipping of materials

After the manufacturing of FRP decks takes place off-site including installation guidelines regarding connections, shipping takes place.



Figure 2-69 Panel Delivery by Tractor-Trailer (Winkelman, 2002) (Craing & Sweet, 2005)

*B. Assembly*

- Preparation of Epoxy (if needed)



Figure 2-70 Mixing of Adhesives (Winkelman, 2002), (Craing & Sweet, 2005)

- Clean areas that would become part of field joint with acetone wash
- Applying adhesive primer to bond line surfaces (male and female parts)
- Screed off excess adhesive
- Erect FRP panels
- Push panels together using jacks

C. *Connection deck-to-girder*

As already mentioned in the section before, the connection deck-to-girder can be adhesively bonding or with mechanical fastening. In case of adhesive bonding, the selected adhesive is applied to the steel girders and after the panel are placed a curing time for the adhesive is aimed for. When mechanical fastening takes place the pockets for the shear studs are already pre-fabricated. Once the panels are erected, the shear studs are installed through the holes in the deck using an automatic welding gun. The pockets should be sized to allow enough clearance to insert the stud gun from the top of the deck and weld each stud. Welding the studs after the panels are erected eliminates the potential for misalignment of the studs and pockets. In addition, the pockets do not have to be oversized to accommodate sliding of the panels during bonding and provide adequate clearance to preinstalled studs. Depending on case and contractors choice, haunches can be formed using plywood after the panels are erected and studs are installed as shown in Figure 2-71. The gout can be mixed to a fluid constituency using an automatic grout

mixer and pump. After that the grout can be pumped into the haunch and pockets. Once all panels are erected, this follows by the application of a vinyl ester resin and the composite material strip over the joint. The deck panels should be cleaned and lightly blasted to create a rough/ abraded surface to ensure a good bond to the epoxy adhesive. Approved blasting methods according to (Cassity, Richards, & Gillespie, 2002), include high-pressure water blasting with abrasives in the water, abrasive blasting with containment or vacuum abrasive blasting.



Figure 2-71 Compression of the Field Joints with Hydraulic Hand Jacks (left) and Composite Doweling of the Field Joints (right) (Winkelman, 2002)



Figure 2-72 Applying Field Splice Joints (left) and Shear Studs (Right) (Craing & Sweet, 2005)

Figure 2-73 Installation of Grout (Craing & Sweet, 2005)



Figure 2-74 Vinyl Ester Resin Application to Field Joint (left) and Composite Material Strip Used over Field Joints (right) (Winkelman, 2002)

### D. Finishing Procedures

The guardrails and curb can be installed directly on the top of the FRP decks, or attached to an existing structure which is adjacent or connected to FRP decks. After this, as the last process an application of wearing surface takes place.

Figure 2-75 Wearing Surface (Craing & Sweet, 2005)

## 2.13. Case Studies

### 2.13.1. Friedberg Bridge, Germany

Friedberg Bridge is a hybrid bridge built in April 2008, marking the first composite FRP-steel bridge built in Germany (Knippers & Gabler, 2006). The structure chosen to connect a span of 21.5 m was selected to as a hybrid bridge with two steel girders covered by a pultruded multi cellular FRP deck (ASSET). The adhesive used for bonding purposes is SIKADUR 30 from Sika Deutschland GmbH, Stuttgart. The overall spans 27 m with a width of upper lane 3,5 m and emergency pavement 2x0,75m as shown in Figure 2-76 and Figure 2-77. Unlike other FRP bridges built to the date of construction of Friedberg Bridge, the latter is a hybrid bridge where a composite action of the bridge deck and the steel girders takes place. When this composite action is achieved the vertical displacement is reduced by approximately 20% compared to the steel stringers alone.
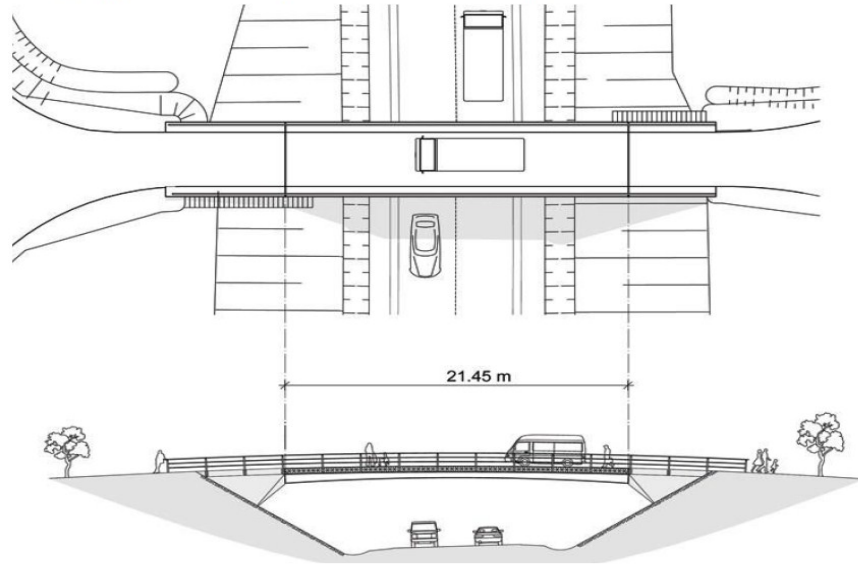
Figure 2-76 Elevation and plan view of Friedberg Bridge (Knippers & Gabler, 2006)
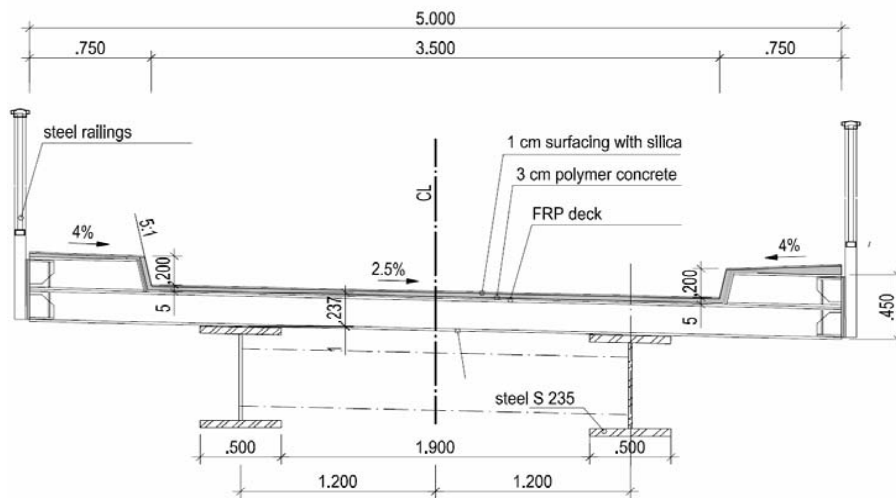


Figure 2-77 Cross Section of the bridge (Knippers & Gabler, 2008)

A comparison of three superstructures suitable to the same span and loading conditions shows the low weight of an FRP deck. While a pre-stressed concrete superstructure has a dead load of approximately 84 kN/m, a steel-concrete composite bridge has 62 kN/m and the finally chosen FRP deck 14 kN/m without wearing and railings (see Figure 2-78).
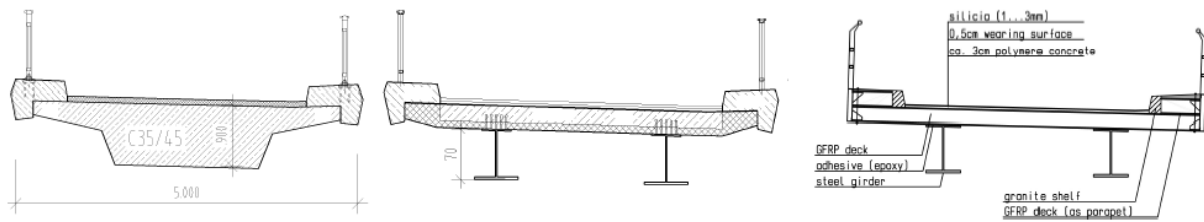
Figure 2-78 Cross section of Friedberg bridge – design as pre-stressed concrete, steel composite and FRP superstructure (Knippers & Gabler, 2006)

## 2.13.2. The Grasshopper Bridge, Denmark

The Grasshopper Bridge is a small bascule bridge located in Zealand, Denmark originally built in 1936 (See Figure 2-79). The bridge has a counter weight of about 100 tons and has a badly rotted timber deck whose planking had to be replaced about every five years creating a lot of maintenance work and traffic disruption. In June 2011 the old bridge deck was replaced with FRP deck panels marking the first road bridge built up with an FRP deck in Denmark (Fiberline).

The authorities in charge of the maintenance decided to replace the old deck with a new fibreglass bridge deck, ASSET deck, manufactured from Fibreline. Due to the lightweight-strength ratio offered from these decks it was possible to widen the road by 30 cm and have still enough room to attach a 160 cm footbridge.



Figure 2-79 Side view of the Grasshopper Bridge, Denmark (Fiberline)

Another consideration for choosing ASSET deck is the ease in installation. The fibreglass bridge decks weigh significantly less than conventional structures and could be prefabricated, brought

to site and installed in next to no time (See Figure 2-80 and Figure 2-81). In this case the assembly time lasted one night.



Figure 2-80 Preparation for work (Fiberline)
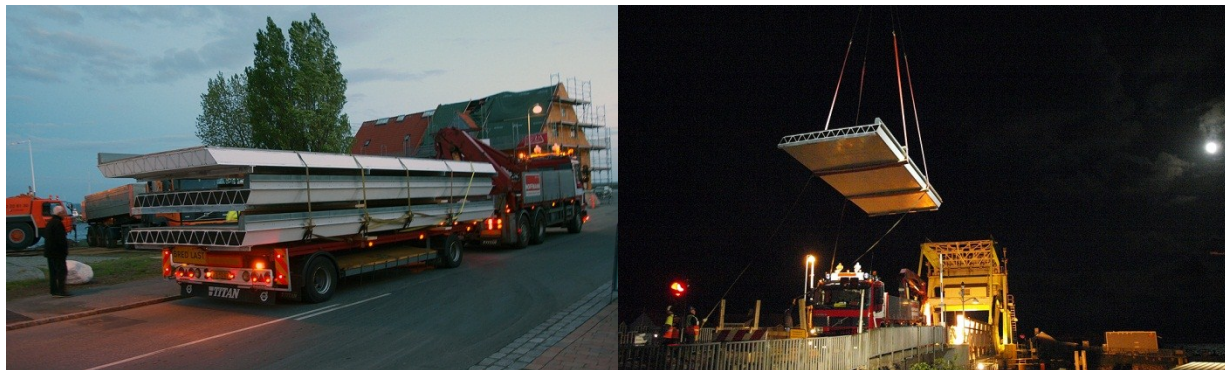


Figure 2-81 Rapid Assembly of the bridge (Fiberline)

## 2.13.3. Broadway Bridge, USA

The Broadway Bridge shown in Figure 2-82, also the seventh longest bascule bridge in the world spanning approximately 42 m, over the Willamette River in Portland is a vital structure to its surrounding areas. This historic bridge carries four lanes of traffic with an average daily volume of 30,000 vehicles (Sams, 2005). Built in 1912, the bridge has served Portland's marine (river) traffic and vehicular traffic quite well for over 90 years. However, its age and frequent use, especially the aggressive traffic, left it with a long list of repair needs. One element that justified considerable attention was the bascule span's steel grid deck which was selected for replacement.

Figure 2-82 View of the Broadway Bridge (Wikipedia, 2012)



Figure 2-83 Traffic on Broadway bridge (Busel, 2012)

The selection and execution of the grid replacement was a complicated procedure due to some constraints. Firstly, the designers needed to match the weight of the existing steel grid as closely as possible due to complicated re-word of the bascule span's mechanical drive system. Another significant constraint was the execution time. Because of the bridge's critical importance to commerce and the traveling public, its owner applied strict limitations to the project's construction schedule, holding the bridge's vehicular traffic closure to a defined 60-day period. Moreover the bridge should be available for opening every fourth day within the aggressive 60-day vehicular closure. This meant that a new deck must not only be installed quickly, but must

be modular in nature and securable if a bascule opening was required during construction. With these requirements in mind, the bridge owner selected Duraspan FRP bridge deck system (manufactured by Martin Marietta Composites) to replace the worn steel grid on the bascule span (Hamrick, 2012).

Broadway Bridge utilized conventional shear studs and grout-filled cavities to connect the new deck to the bridge's longitudinal beams as shown in Figure 2-84. According to (Sams, 2005), its attachment method had a proven track record in static testing, fatigue testing, and in place performance. Grout was poured through the deck into a cavity formed by stay-in-place metal angles, providing a variable haunch along each longitudinal beam (See Figure 2-84). However, no consideration of composite action was applied when the beams carry the loads during the design processed.
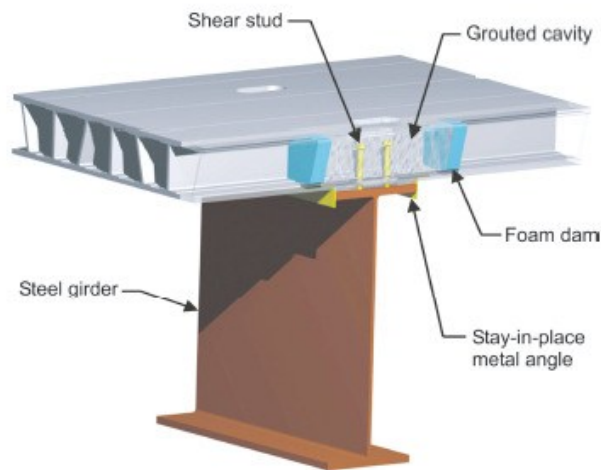


Figure 2-84 The FRP deck panel was attached above steel girder with shear stud. (Sams, 2005)

Two forklifts worked together to bring the FRP deck panel (weight 2720 kg) with maintaining tight clearances from each side of the bridge, as is shown in Figure 2-85. Total 32 deck panels were applied. The deck panels should have been secured to the beams with temporary attachments before the bascule opening on the day fourth. The procedure of this construction is shown in more details in Figure 2-85 to Figure 2-87.

Figure 2-85 The Bridge's longitudinal stringers were prepared for placement of FRP panels (Sams, 2005)
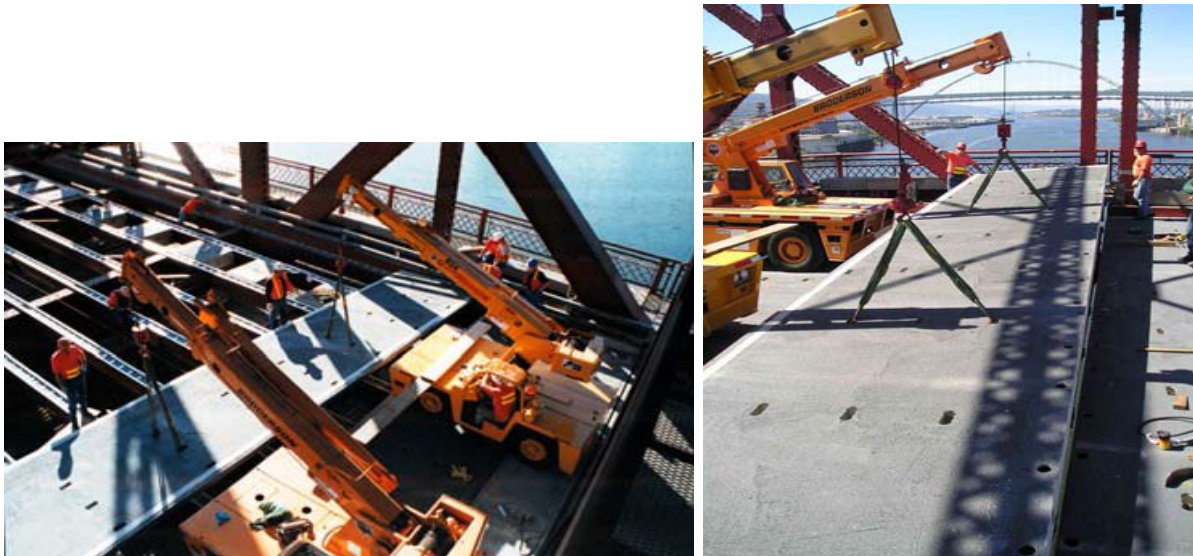


Figure 2-86 FRP deck panels were set in place with dual forklifts. (Sams, 2005)

Figure 2-87 Installation of bottom sections and top sheets (ZellComp, sd)

## 2.14. Disadvantages of FRP decking systems

Although fiber reinforced polymer (FRP) composite decking is a viable option for highway bridges, there are still some remaining issues to be addressed:

- Cost: The initial unit cost of an FRP deck is higher compared to other traditional materials
- Supply & Demand: There are few suppliers of FRP bridge decks. Demand has been intermittent, making it difficult for suppliers to remain in business and be profitable.
- Sole Source: FRP deck systems that are on the market today are proprietary systems. Repeatedly specifying and/or purchasing the sole source products is contrary to the regulations and policies of most government agencies, which complicates their typical contracting practices.

- Technical: Although the decks used to date have generally performed satisfactorily, there have been some technical issues associated with implementing this new technology.

- Guidelines: Due to the variety of products of FRP decks in use and limited laboratory test and field investigation exists a lack of guidelines and codes. This influences very much the use of FRP decking systems.

## 2.15. Conclusions

The use of Fiber Reinforced Polymer decks has a great potential in bridge engineering. Different types of deck systems have been proposed by many researchers over the past 30 years. Most of the research works have been carried out on structural component level at the laboratory and less at full scale laboratory investigation of FRP deck in a bridge structure. Moreover, analytical works using finite elements methods have considered FRP decks as orthotropic plates which yielded satisfactory results correlating with field investigation for studying the global response but the local effects remain unknown is this context. Effectiveness of uniform steel patch loading and corresponding analyses of deck response may be inadequate to capture true long term degradation mechanism. Furthermore, most research validated the design according to the deflection criteria on the structure, some of them have considered the possibility of limiting criteria based on relative deflection of the deck itself.

Fatigue life prediction methodologies are mostly well developed based on coupon level experimental data and there are a few studies providing the experimental work on system or structural level work. Some researchers have only performed some fatigue tests on structural components up to a certain number of cycles at service load level and verified structural integrity while others have employed nonlinear damage models to predict life of FRP composite bridge deck. Sources show positive results providing the required lifetime under fatigue loading.

The methods used to connect pultruded FRP bridge decks to steel girders to date involve either mechanical fastening (bolts or shear studs) or, as used in the latest years, adhesive bonding. Mechanical fastenings are generally very time-consuming in the construction process not letting exploit the advantages of rapid installation of FRP deck and therefore can be more expensive. Furthermore, they are not adapted to the very brittle properties of FRP materials, since high stress concentrations occur at connection points in the bridge decks. Bonding is a connection method that can allow several of the disadvantages related to the aforementioned. Furthermore,

81

experimental results from laboratory studies and field investigation have proven the composite action of steel girder with FRP bridge decks increasing significantly the load bearing capacity of the hybrid bridge.

Life Cycle Cost analysis is the best process to answer the competitiveness of FRP bridge deck on a cost basis; nevertheless there is not enough data to conduct such research to give a clear overview of the total cost of bridge using FRP decks. It is observed that different case studies provide contrary conclusions regarding the cost analysis. However, most of them agree that the initial costs of FRP decks are significantly higher than other traditional materials. Hence, the initial costs of FRP decks must be reduced to be cost competitive with the SRC decks on a life cycle cost basis. Sources give positive feedback regarding the maintenance cost which may reduce the total life cost to a lower value compared to traditional materials.

Based on the literature review, it can be concluded that there is lack of adequate research in the following areas of potential interest. (a) Lack of codes and guidelines for the application of FRP composite deck systems (b) Performance evaluation of FRP deck systems through full scale laboratory experiments utilizing tire patch loading and FEA simulation to investigate local effects (c) Strength and Fatigue life prediction of FRP deck systems (d) consequences of environmental effects. This thesis will therefore attempt to address some of the critical issues in these areas.

# 3. BRIDGE BACKGROUND AND FINITE ELEMENT MODELING

This chapter presents the background of the bridge used as the case study of upgrading movable bridges with FRP decks. In addition, details and properties of the three applied FRP decks will be revealed. Further, it gives a short description of loading conditions applied to the bridge and the proposed configuration for the superstructure. In the end, the key features for the finite element modeling are presented.

## 3.1. Bridge Background and Design Requirements

Wilhelmina Bridge (Wilhelminabrug in Dutch) is located in the city of Zaandam, Zaanstad, Noord-Holland, The Netherlands as shown in Figure 3-1 providing an important connection for the urban traffic. Originally built 70 years ago Wilhelminabrug is a single leaf bascule bridge.
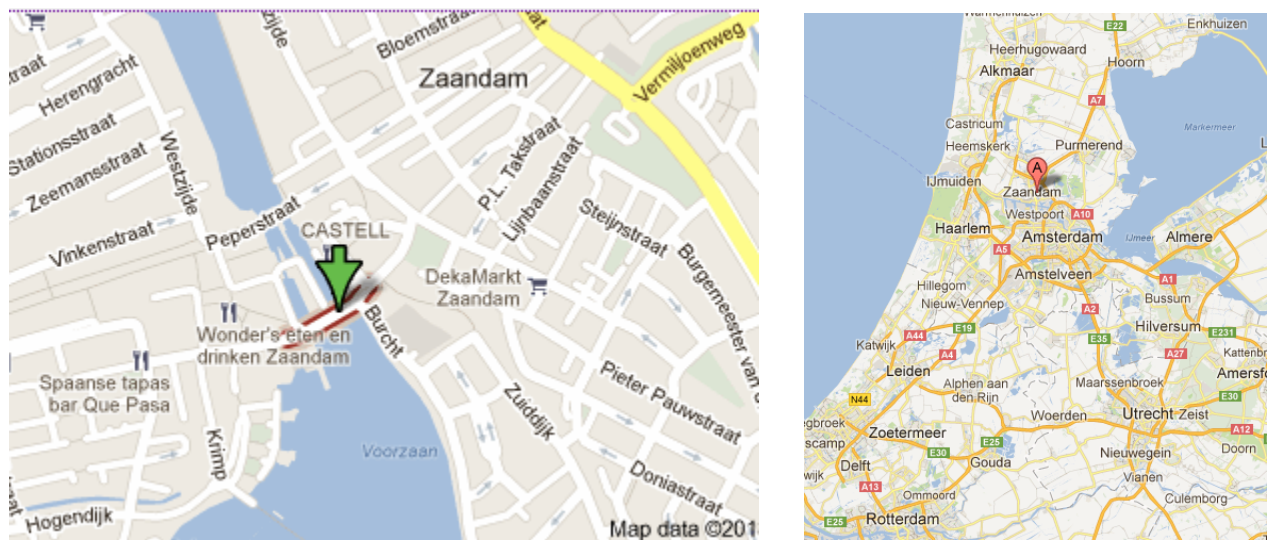


Figure 3-1  Location of Wilhelmina Bridge

Actually, it spans 13 m longitudinally with a width of 16.17 m accommodating two vehicular lanes of approximately 3.5 m, two cyclic lanes and sidewalks in two directions as shown in the figures below. The structure consists of four main girders linked to the ballast supporting 6 cross beams spanning 2.465 m. The deck made with wooden planks is supported by steel stringers that are supported on the cross beams. A detailed view is given in Figure 3-2 to Figure 3-5.

The responsible agency requires the rehabilitation of this bridge while laying down some design constraints. The bridge span should be enlarged from 13.155 m to 15.15 m. The bridge should be

designed as a total road bridge in case its function will be changed in the near future. The construction height should remain the same due to constraint for underline passage and the bridge should be concentric in height with the road. The rotating part should remain the same while the steel structure and the deck shall be changed (due to field investigation) but the center line distance between the main girders should equal the actually distance. Different repairing possibilities are studied due to economical and self-weight constraints, including steel orthotropic deck and FRP decks with no composite behaviour. FRP decks with no composite actions have proven to be very expensive, while the orthotropic steel deck have increased the total self-weight (120 tons) very much, leading towards the improvement of the mechanical part.



Figure 3-2   Wilhelmina Bridge



Figure 3-3 Street view of Wilhelmina Bridge
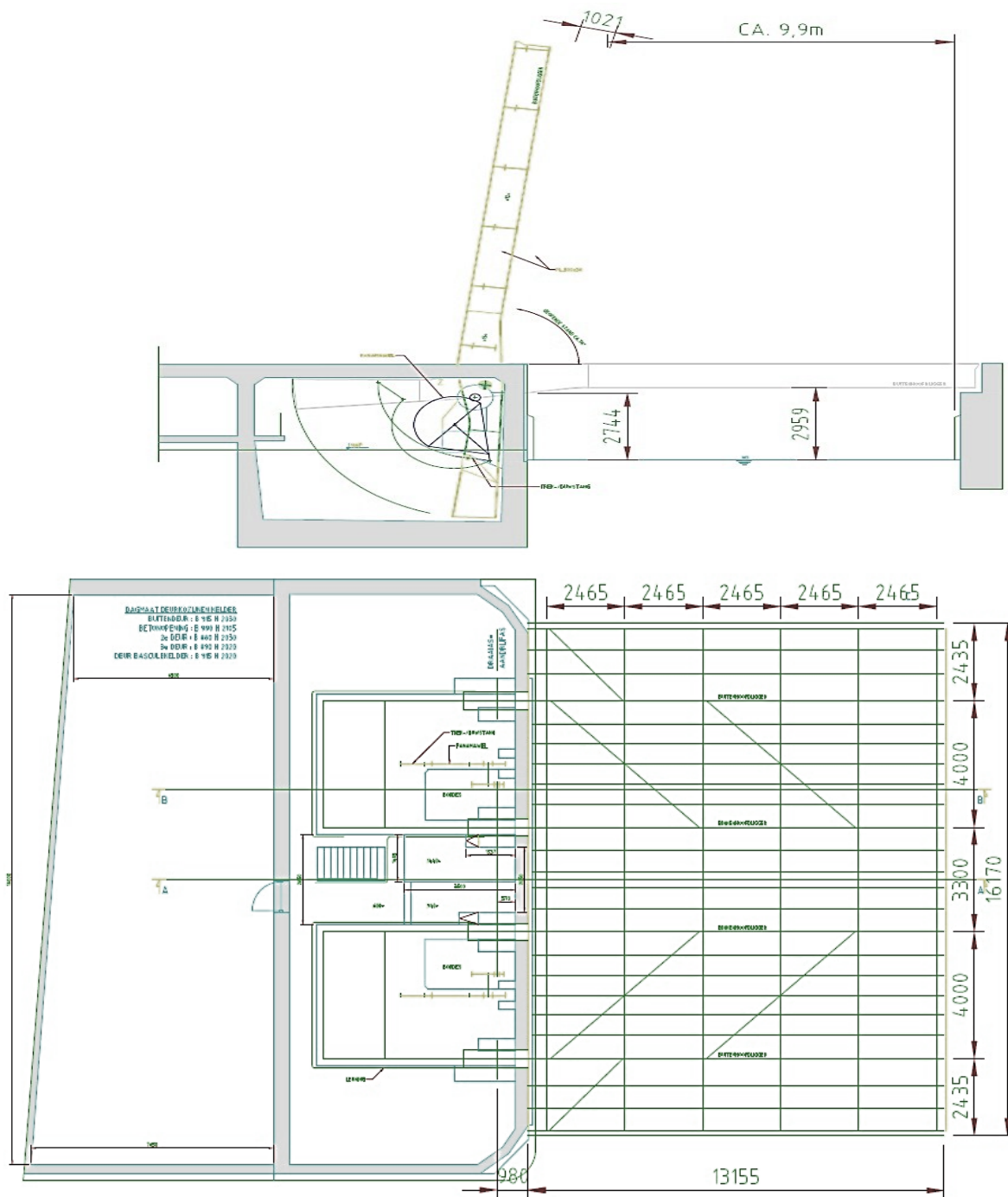
Figure 3-4 Front view and side view of Wilhelminabrug
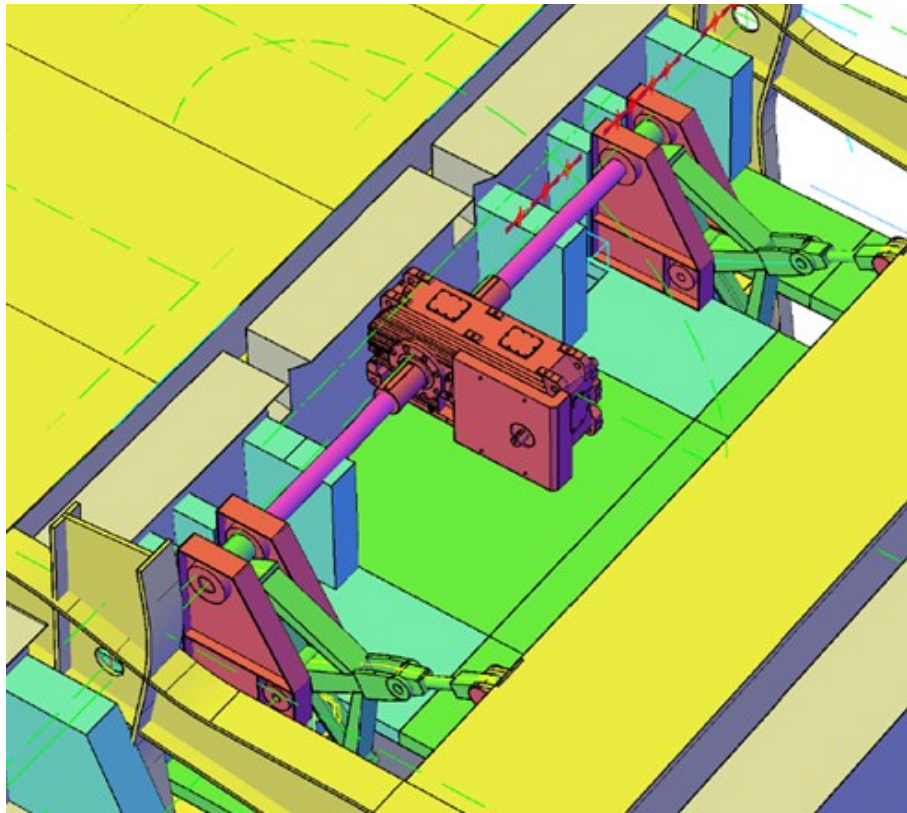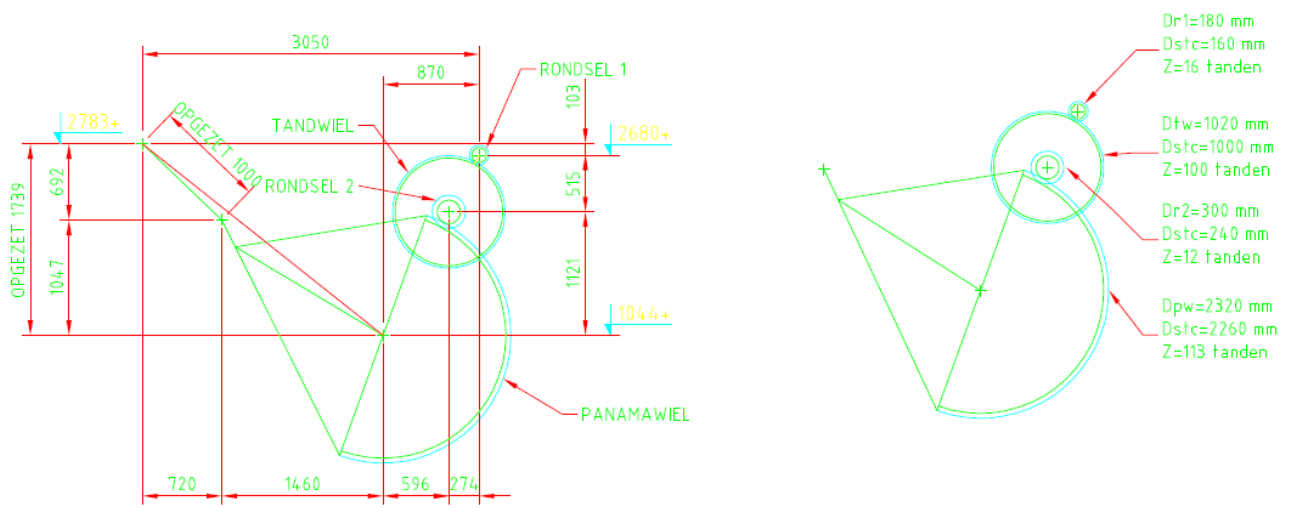
Figure 3-5 Rotating device of movable bridge

## 3.2. Materials

The new bridge deck design will consist of a new steel structure supporting FRP deck adhesively bonded together. Three types of different FRP decks, ASSET deck from Fiberline, Denmark;

Duraspan 766 deck from Martin Marietta Composites, USA and Ecosafe deck from Lightweight Structure, Netherlands are selected as potential substitutions for the old wooden deck. They are shown in Figure 3-6 to Figure 3-8.



Figure 3-6 Ecosafe deck (Jiang, Kolstein, & Bijlaard, 2013)
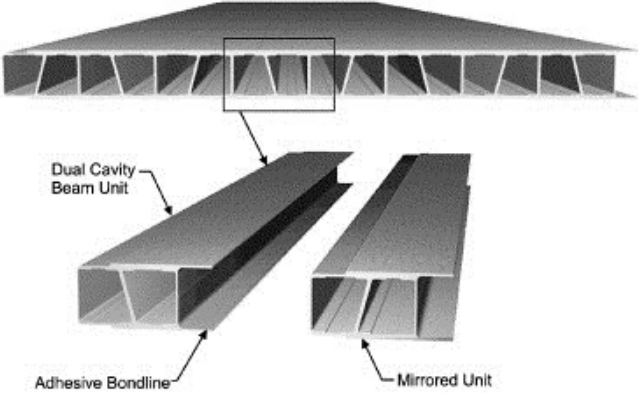


Figure 3-7 Duraspan deck (Keller & Gurtler, 2005)



Figure 3-8 ASSET deck (Fiberline)

ASSET deck is a hollow core pultruded FRP deck with a constant depth of 225 mm and is formed by assembling 299 mm long interlocking components to form any length of deck necessary. It consists of two FRP flanges connected with inner and outer FRP webs forming a panel as shown in Figure 3-9. These panels are glued with each other to form the deck. The dimensions of ASSET deck are presented in Figure 3-9 and Table 3-1. Duraspan deck is a

hollow core pultruded deck consisting of two FRP flanges connected by inclined and straight webs with a constant depth of 195 mm as presented in Figure 3-10. Ecosafe deck is a sandwich core deck with variable thickness. It consists of two FRP flanges glued together with a core section made with balsa wood. For this application study the thickness of the flanges is selected 15.6 mm and the core part 225mm.



Figure 3-9  ASSET Deck Panel (Fiberline)

Table 3-1  Dimensions of ASSET Deck (Fiberline)

| ASSET Deck | |
|---|---|
| | [mm] |
| H | 225 |
| B | 521 |
| $B_{eff}$ | 299 |
| $B_1$ | 260,5 |
| $B_2$ | 260,5 |
| $H_1$ | 112,5 |
| $H_2$ | 112,5 |

Figure 3-10 Duraspan deck dimensions (Gurtler, 2004)

The representative properties of each deck are presented in the table 3-2 to 3-5.

Table 3-2  Properties of FRP laminates for ECOSAFE deck (Jiang, Kolstein, & Bijlaard, 2013)

| Ecosafe | |
|---|---|
| Property[5] | Face Panels |
| | [MPa] |
| Elastic Modulus 11 | 17257 |
| Elastic Modulus 22 | 17257 |
| Elastic Modulus 33 | 11000 |
| Poisson Ratio 12 | 0.33 |
| Poisson Ratio 23 | 0.3 |
| Poisson Ratio 13 | 0.18 |
| Shear Modulus 12 | 6986 |
| Shear Modulus 23 | 3400 |
| Shear Modulus 31 | 3400 |

Table 3-3 Properties of core material for ECOSAFE deck (Jiang, Kolstein, & Bijlaard, 2013)

| Ecosafe | |
|---|---|
| Property | Core Material |
| | [MPa] |
| Elastic Modulus | 5759 |
| Poisson Ratio | 0.35 |
| Shear Modulus | 309 |

---

[5] 1 – pultrusion direction; 2 – transvers direction; 3 – vertical direction
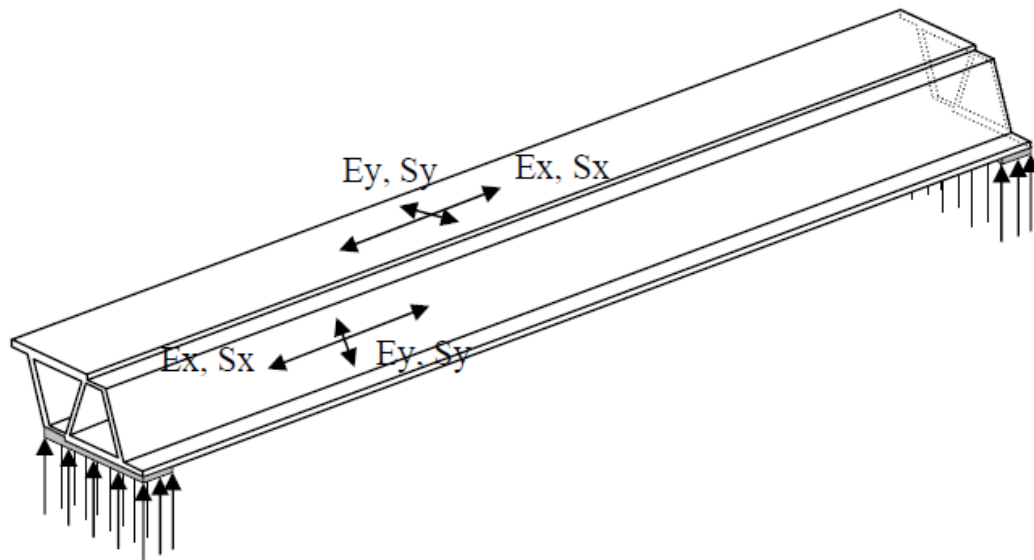
Figure 3-11  ASSET Deck (Fiberline)

Table 3-4  Properties of FRP laminates for ASSET deck (Fiberline)[6]

| ASSET Deck | | | |
|---|---|---|---|
| Properties | Face Panels | Outer Web | Inner Web |
| | [Mpa] | [Mpa] | [Mpa] |
| Elastic Modulus x | 23000 | 17300 | 16500 |
| Elastic Modulus y | 18000 | 22700 | 25600 |
| Shear Modulus xy | 2600 | 3150 | 2000 |
| Shear Modulus xz | 600 | 600 | 600 |
| Shear Modulus yz | 600 | 600 | 600 |
| Poison ratio xy | 0.3 | 0.3 | 0.3 |

Table 3-5 Duraspan Deck properties (Gurtler, 2004)

---

[6] x- pultrusion direction; y- transverse direction z-through thickness

90

| Deck Location | Top sheet **1** | Web walls **2** | Bottom sheet **3** | Equivalent Slab [3] (Bending prop) |
|---|---|---|---|---|
| Lay-up [2] | Web + [0(60)/90(20)/+-45(20)] | [0(33)/+-45(66)] | Web + [0(60)/90(20)/+-45(20)] | |
| Thickness (mm) | 12.70 | 6.35 (vert leg) 12.70 (diag leg) | 12.70 | 190.50 |
| $E_L$ ($10^3$ MPa) | 21.24 | 17.38 | 21.24 | 8.53 |
| $E_T$ ($10^3$ MPa) | 11.79 | 9.65 | 11.79 | 4.14 |
| $E_Z$ ($10^3$ MPa) | 4.14 | 4.14 | 4.14 | 0.69 |
| $G_{LT}$ ($10^3$ MPa) | 5.58 | 7.17 | 5.58 | 0.69 |
| $G_{LZ}$ ($10^3$ MPa) | 0.60 | 0.60 | 0.60 | 0.69 |
| $G_{ZT}$ ($10^3$ MPa) | 0.60 | 0.60 | 0.60 | 0.69 |
| $v_{LT}$ | 0.32 | 0.3 | 0.32 | 0.33 |
| $v_{LZ}$ | 0.3 | 0.3 | 0.3 | 0.33 |
| $v_{ZT}$ | 0.3 | 0.3 | 0.3 | 0.33 |
| $\varepsilon C_L$ (%) | -1.23 | -1.24 | -1.23 | - |
| $\varepsilon T_L$ (%) | 1.23 | 1.27 | 1.23 | - |
| $\varepsilon C_T$ (%) | -1.27 | -1.97 | -1.27 | - |
| $\varepsilon T_T$ (%) | 1.25 | 1.35 | 1.25 | - |
| $\gamma$ (%) | 2.53 | 2.53 | 2.53 | - |
| $FC_L$ (MPa) | -261.210 | -215.455 | -261.210 | - |
| $FT_L$ (MPa) | 261.210 | 220.668 | 261.210 | - |
| $FC_T$ (MPa) | -149.739 | -190.164 | -149.739 | - |
| $FT_T$ (MPa) | 147.381 | 130.316 | 147.381 | - |
| $FS_{LT}$ (MPa) | 70.650 | 90.711 | 70.650 | - |
| ILS (MPa) | 41.370 | 41.370 | 41.370 | - |
| Bond shear, $FB_{LT}$ (MPa) [5] **4** | 6.89 | | | |

Notes: [1] Laminate stiffnesses and strengths calculated from actual test data of similar thick laminates; failure based on first ply failure criteria

Notation: $E_L$, $E_T$, $E_Z$ – extensional moduli; $G_{LT}$, $G_{LZ}$, $G_{ZT}$ – shear moduli
$v_{LT}$, $v_{LZ}$, $v_{ZT}$ – poisson's ratios
$\varepsilon C_L$, $\varepsilon T_L$, $\varepsilon C_T$, $\varepsilon T_T$, $\gamma$ – strain allowables (c – compression. τ – tension)
$FC_L$, $FT_L$, $FC_T$, $FT_T$, $FS_{LT}$ – laminate ultimate strengths
ILS – nominal interlaminar shear stress

Subscripts: L – longitudinal direction; T – transverse direction; Z – through thickness
[2] Fiber orientation, [θ°], expressed in percent (%) of laminate thickness
[3] Effective flexural properties for equivalent slab of same thickness
[4] 60% fiber content by weight
[5] 90% of average failure load from preliminary lap shear tests

Steel S355 is used for the main girders and cross beams. The main girders and cross beams are selected I-shaped cross sections according to the dimensions as for the old bridge deck with dimensions (h x b x $t_w$ x $t_f$) of (1000x500x15x30) mm and (1000x350x15x25) mm respectively. The cross sections with dimensions are presented in Figure 3-12.

Main Girder          Cross Beam
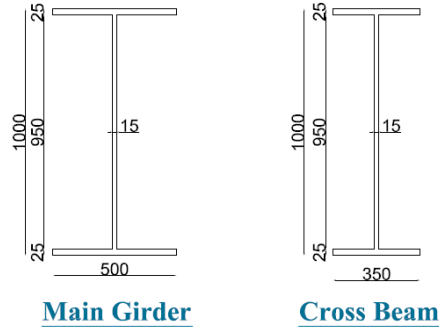
Figure 3-12 Cross sections of main girder and cross beam

For the adhesive, bonding the steel girders with the FRP deck, Sikadur 330 with height of 6 mm is chosen and its properties are shown below in Figure 3-13.



Figure 3-13 Properties of adhesive Sikadur 330 at $23^0$C (Gurtler, 2004)

A cross section profile of the deck decks is shown below in Figure 3-14.



ECOSAFE Deck          ASSET Deck          Duraspan  Deck

Unit: mm
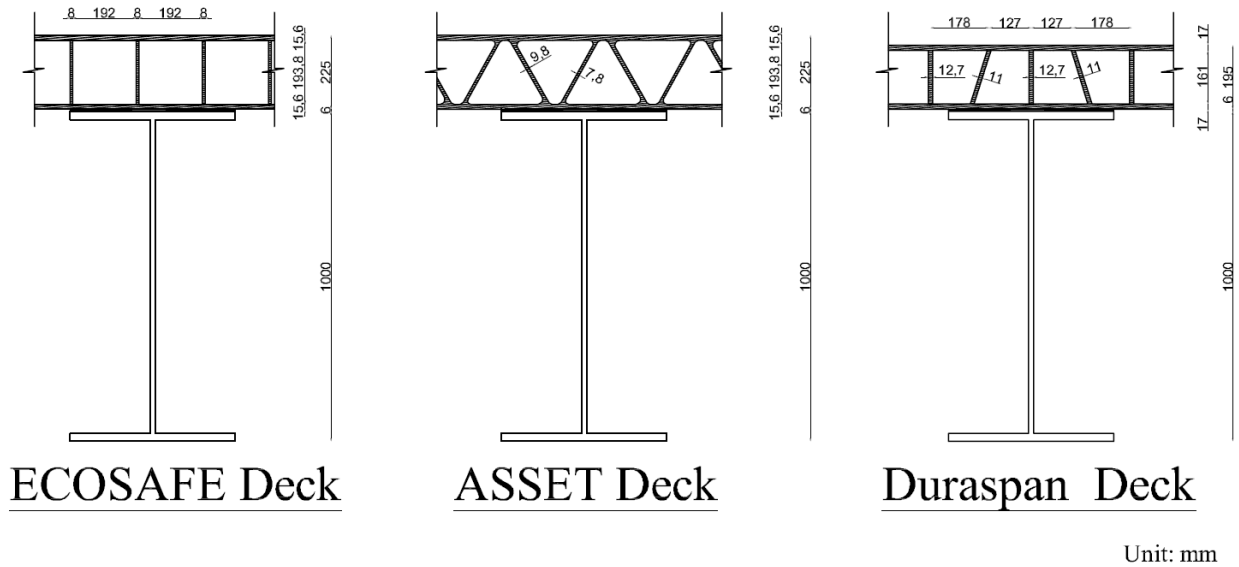
Figure 3-14  Section profile of each deck spanning over main girders

### 3.3. Loading Conditions

Several loading conditions according to Eurocode 1 are considered for the analysis of the bridge and presented in the following sub-chapters.

### 3.3.1. Combination of actions (not applicable for fatigue design)

For ULS verifications: characteristic load combination according to EN 1990 is used.

$1.35*DL + 1.5*LL$

For deflections (SLS): frequent load combination according to EN 1990 is used.

$1*DL + 1*LL$

Where,

DL- dead load consisting of the self-weight including the asphalt layer

LL- live load according to the sections 3.3.2, 3.3.3.

### 3.3.2. Vertical Loading

In order to simulate the traffic load acting on the bridge, Load Model 1 according to Eurocode 1 was utilized (EN-1991-2, 2003). This model consists of concentrated and uniformly distributed loads, which cover most of the effects of the traffic of lorries and cars. It is represented by a double-axle concentrated load, each axle having the following weight $\alpha_Q Q_k$, where $\alpha_Q$ are adjustment factors. In addition a uniformly distributed load having the weight per square meter of notional lane $\alpha_Q q_k$.

The loading scheme is presented in Figure 3-15. The characteristic values of Load Model 1 are presented in Table 3-6 while the values of $\alpha_Q$ are taken 1. The loading is positioned taking into account the most unfavorable situation. A section cut including the vertical positioning of loadings and divisions of the lanes is shown in Figure 3-16.

Table 3-6 Load Model 1: Characteristic values (EN 1991-2, 2003)

| Location | Tandem system *TS* | UDL system |
|---|---|---|
| | Axle loads $Q_{ik}$ (kN) | $q_{ik}$ (or $q_{ik}$) (kN/m$^2$) |
| Lane Number 1 | 300 | 9 |
| Lane Number 2 | 200 | 2,5 |
| Lane Number 3 | 100 | 2,5 |
| Other lanes | 0 | 2,5 |
| Remaining area ($q_{rk}$) | 0 | 2,5 |
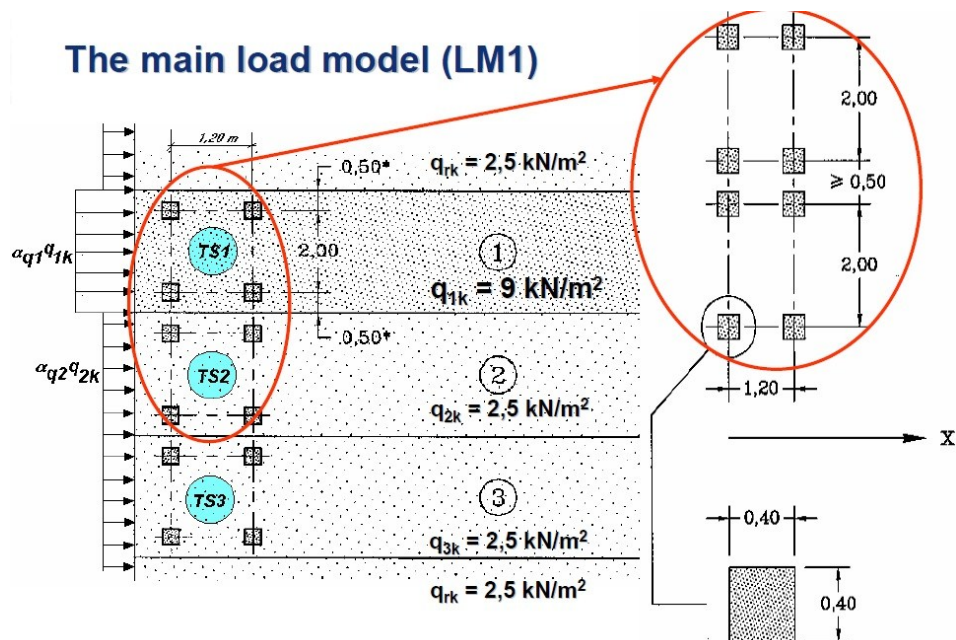


Figure 3-15  Application of Load Model 1 (EN 1991-2, 2003)
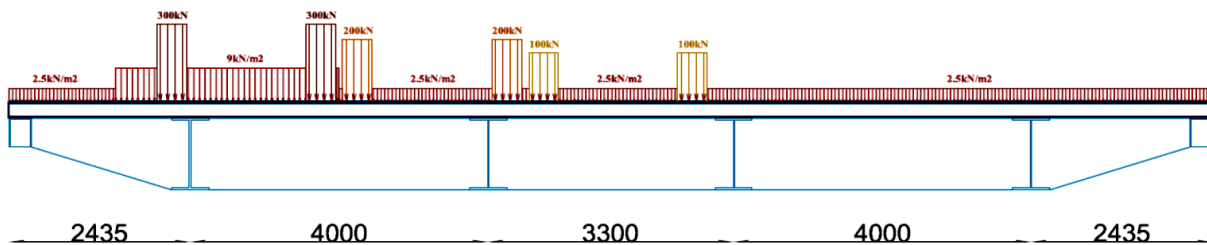


Figure 3-16  Schematic of Load Model 1 application

94

### 3.3.3. Fatigue Loading

The fatigue loading is presented in Chapter 6.

### 3.4. Proposed Configuration of the Steel Structure

As a first step for the upgrade design of this movable bridge three types of configuration of the superstructure are selected and studied. They are presented in the figures below (Figure 3-18 to Figure 3-20) including the position of load model 1. Configuration type 1 consists of four main girders supporting the FRP deck and two cross beams in the beginning and end of the bridge deck. In configuration type 2 additional steel girders are added to reduce the spanning distance of the bridge deck. They consists of I-shaped cross section with dimensions ($h \times b \times t_w \times t_f$) equal to (500x300x10x15) mm. In the third configuration additional cross beams in the transverse direction are added spanning 2800 mm. The decks of each configuration are orientated in such way that the pultrusion direction of the fiber reinforced polymer structure is transverse to the direction of the main girders corresponding to the strongest direction. This illustration is presented in Figure 3-17. The cross section of the main girders and the cross beams are as discussed in section 3.2.
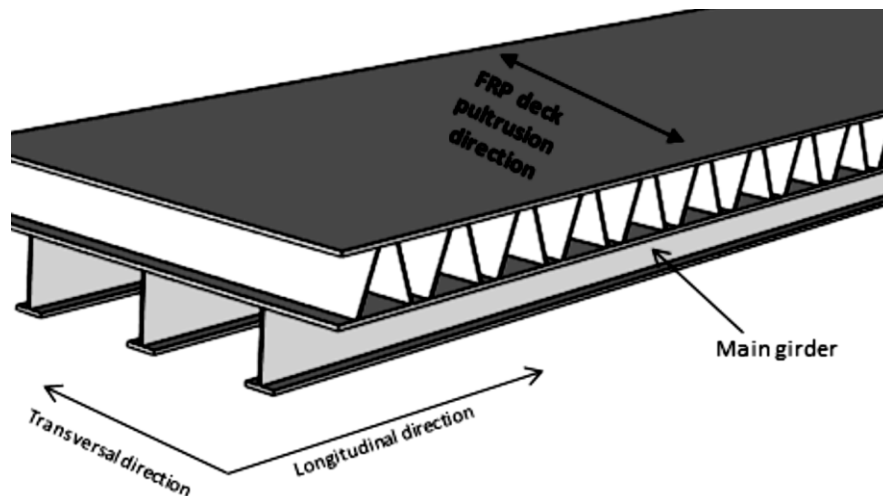


Figure 3-17  Orientation of FRP decks

95
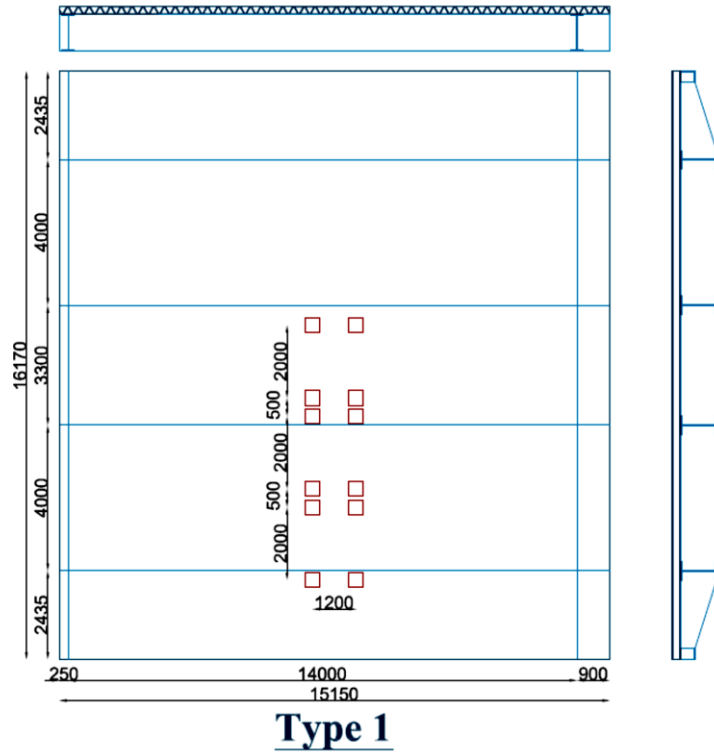
Figure 3-18  Configuration type 1
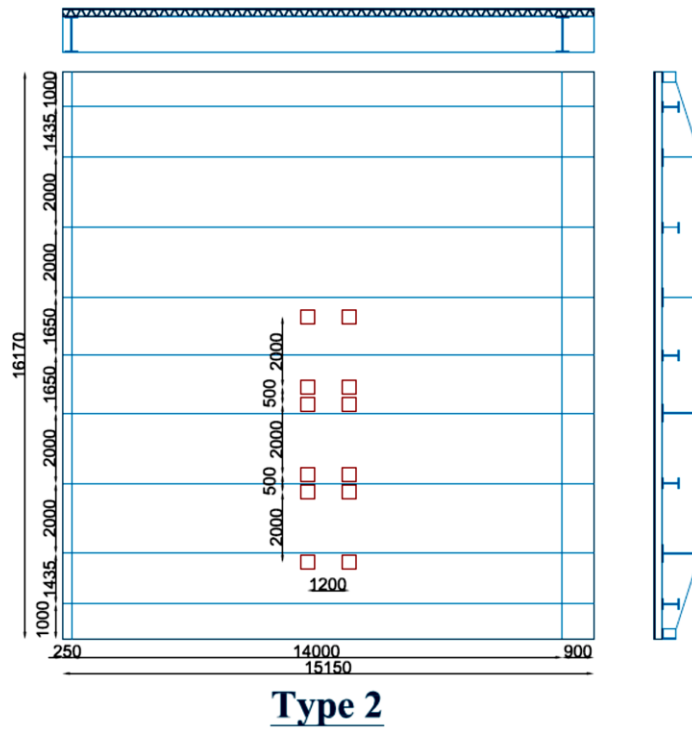


Figure 3-19  Configuration type 2

96
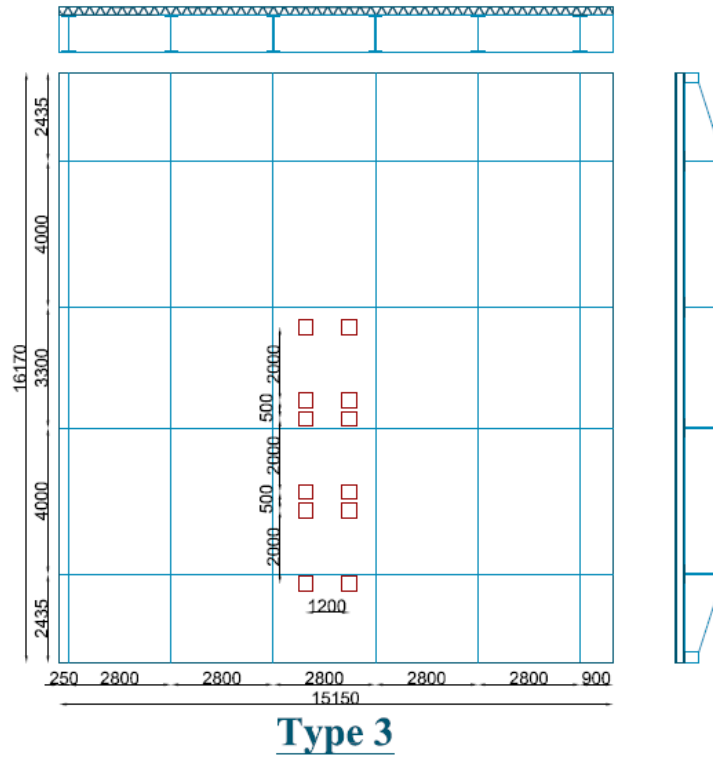
Figure 3-20  Configuration type 3

## 3.5. Finite Element Modeling

The finite element method is a general procedure useful to conduct a structural analysis. In the FEM, the solution of a problem in continuum mechanics is approximated by the analysis of an assembly of finite elements interconnected at a finite number of nodal points and represents the solution field of the problem.

In this study the software ABAQUS (ver. 6.10) was used to compute the models of the bridge. Several authors, as discussed in this thesis, after examining have stated the accurate and precise results that this software achieves when comparing with experimental studies in case of FRP decks on steel girders. A complete ABAQUS analysis usually consists of three distinct stages: preprocessing, simulation, and post processing. These three stages are linked together by files as shown below.

97
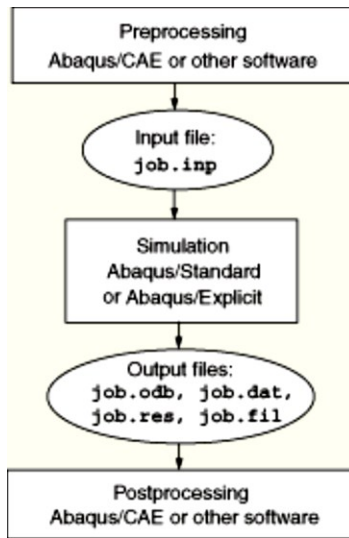
Figure 3-21  Abaqus analysis

A complete analysis using Abaqus requires a description of the material, the model configuration, boundary conditions, and loading as generally used for FEM software. For service-load simulations, at least two material constants are required to characterize the linear elastic behavior of the material: Young's modulus (E) and Poisson's ratio (v). Boundary conditions that represent structural supports specify values of displacement and rotation variables at appropriate nodes. Abaqus can provide response information at the nodes and element stresses at designated integration points within the element. Stresses at various points through the thickness of the element can also be provided, which is particularly important for this study.

### 3.5.1. Elements

The model consists of three physical parts and the rest of the conditions are applied as loads and boundary conditions. These parts are the steel girders and cross beams, the FRP decking systems and the adhesive or shear studs. Abaqus/CAE embeds the part in the *X, Y, and Z* coordinate system. A three-dimensional part can contain any combination of solid, shell, wire, cut, round, and chamfer features but for this study two type of elements are utilized to model the whole bridge, shell and solid three dimensional elements as shown in Figure 3-22.
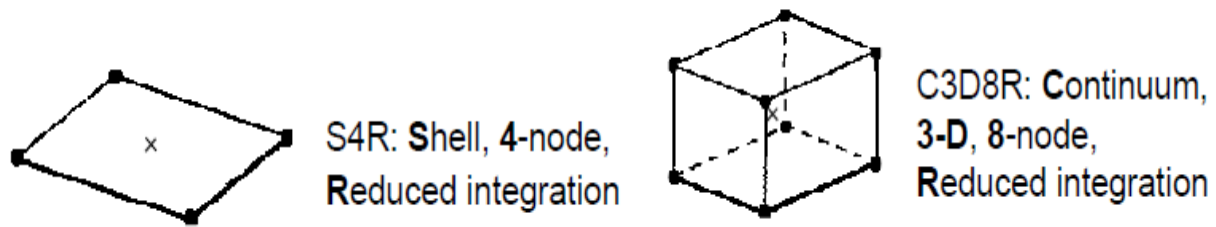
Figure 3-22  Elements used: left, shell S4R and right, Solid C3D8R

The steel beams are modelled with 3D deformable shell elements (4 nodes), S4R with reduced integration since the structure is mainly dominated by flexure behaviour. The plates of different dimensions are first input as parts and then assembled by rotating and translating them into their place as if they are welded together. After the process of assembly, the whole girders and cross beams are merged so that the parts don't act independent by each other. The latter is elaborated in the following sections. For the steel members a Young's modulus of 210 GPa and a Poisson's ratio of 0.3 was utilized. The density of the steel is 7850 kg per m3.

The FRP decking system, Ecosafe, is modelled using 3D deformable solid elements (8 nodes), C3D8R with reduced integration due to the solid continuous section profile. Orthotropic material properties are utilized with the characteristics as discussed in section 3.2. Material orientation is specified for every component with local coordinate systems. On the other hand, for ASSET and Duraspan deck 3D deformable shell elements (4 nodes) are used due to the more detailed implicit hollow configuration. It should be mentioned that the webs and flanges of the deck are modelled as straight surfaces in Abaqus, while in reality curved shaped connection exists as shown in Figure 3-23 for ASSET deck. The latter holds for Duraspan deck as well. This curvature helps in reduction of stress concentration. Necessary partitions in the deck flange where the load is applied and meshing are also made.
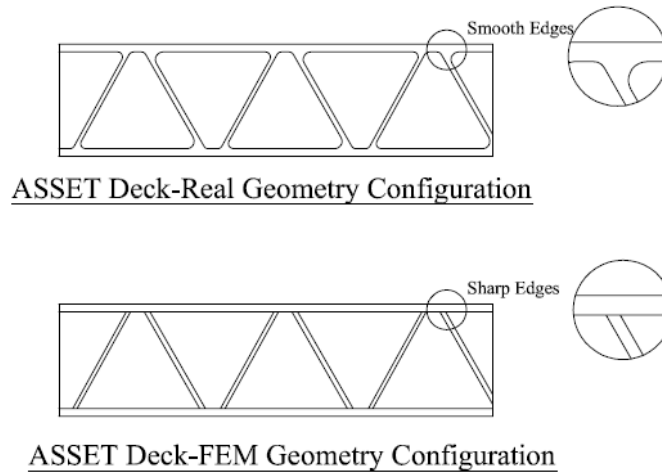
Figure 3-23  ASSET Deck simulation

### 3.5.2.  Modelling the interface

In order to simulate the adhesive action and the shear studs between the steel girders and FRP deck different procedures presented in the Abaqus documentation and applied from several authors are examined.

#### 3.5.2.1.       Adhesive Modeling

'Tie Constraints', 'Surface-to-Surface' interaction with cohesive behaviour and modelling the adhesive as 3D solid element are the three options studied to represent the adhesive connection according to Abaqus documentation.

- 'Tie Constraints' provide a fully bonded rigid connection between steel girders and the corresponding area of the deck flange which directly transmits all stress between both connected elements without slipping. The interface is independent of the meshing properties of the two neighboring parts. This modeling technique was validated with experimental work by (Vovesný́a & Rottera, 2012). It is a surface based constraint using master-slave formulation meaning that the nodes on one surface (the slave) cannot penetrate the segments that make up the other surface (the master), as shown in Figure 3-24. The algorithm places no restrictions on the master surface; it can penetrate the slave surface between slave nodes, as shown in Figure 3-24.
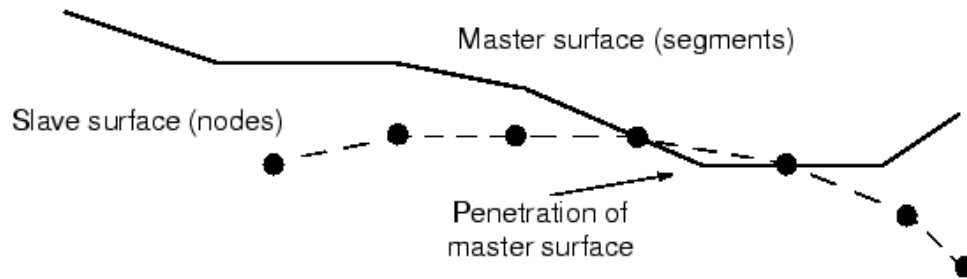
Figure 3-24 The master surface can penetrate the slave surface (Abaqus CAE, 2010)

Due to the strict master-slave formulation, it should be careful to select the slave and master surfaces correctly in order to achieve the best possible contact simulation. Some simple rules according to (Abaqus CAE, 2010) follow as:

- the slave surface should be the more finely meshed surface

- if the mesh densities are similar, the slave surface should be the surface with the softer underlying material

The top flange of the girders are modeled as master surface while the corresponding area of the bottom flange of the deck is modelled as slave surface.

 - The surface to surface interaction behaviour is a very similar option to tie constraints. It was adopted by (Mara & Al-Emrani2012) to connect ASSET deck with steel girders. It allows for a transition from shell element modeling to solid element modeling. It couples the motion of a "line" of nodes along the edge of a shell model to the motion of a set of nodes on a solid surface (or shell surface). The tangential behaviour is assigned as frictionless, meaning that no slip can occur, while the normal behaviour was assigned as 'hard' contact with constraint enforcement method as penalty, meaning that pressure exists between the two connected parts. Under eligible slave nodes any slave nodes experiencing contact was used. This means the cohesive behaviour not only for all nodes of the slave surface that are in contact with the master surface at the start of a step, but also for slave nodes that are not initially in contact but may come in contact during the course of a step was used in contact property of the interaction (Abaqus User's manual). This technique requires time to run the analysis, but contrary to 'tie constraint' gives information on interaction stresses.

101

- The last method models the adhesive as a linear elastic 3D element with orthotropic material properties and then uses 'tie constraint' to bond it with the flanges of the girders and FRP deck. The lowest E-modulus shown in Figure 3-13 is selected. Figure 3-25 shows an example where this technique is used. As it can be seen different meshing variables are used for the adhesive and neighboring parts.
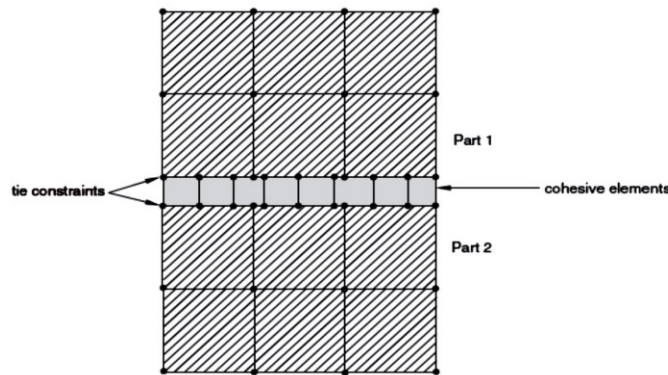


Figure 3-25  Independent meshes with tie constraints

During this analysis the third model is implemented since is faster than surface to surface interaction and gives a more detailed results (including the adhesive stresses) rather than 'tie constraints'. For each case study the appropriate clearance between the top flange of the girder and the bottom face of the deck or adhesive was provided representing the real geometry of the bridge. Figure 3-26 to Figure 3-28 show a detailed description of the finite element modeling of each cross section.
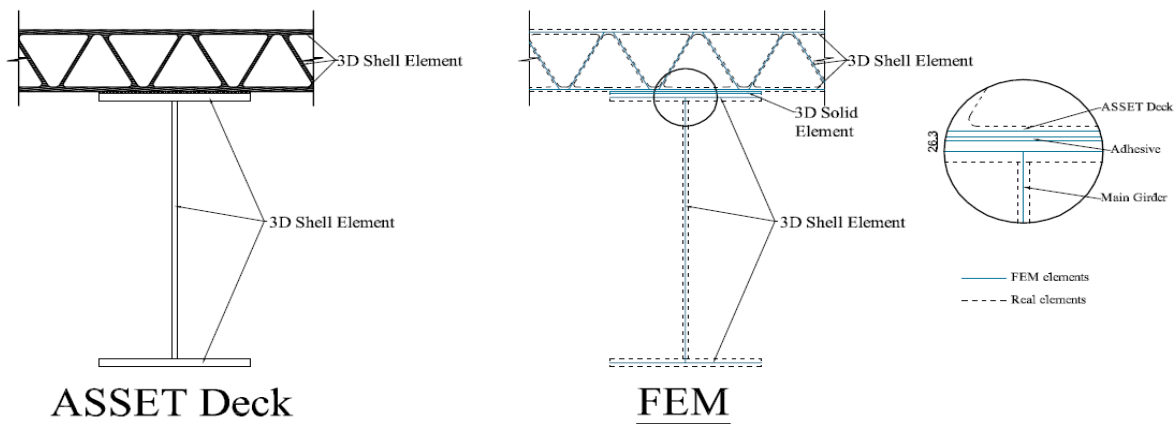


Figure 3-26 Finite element modeling of ASSET deck
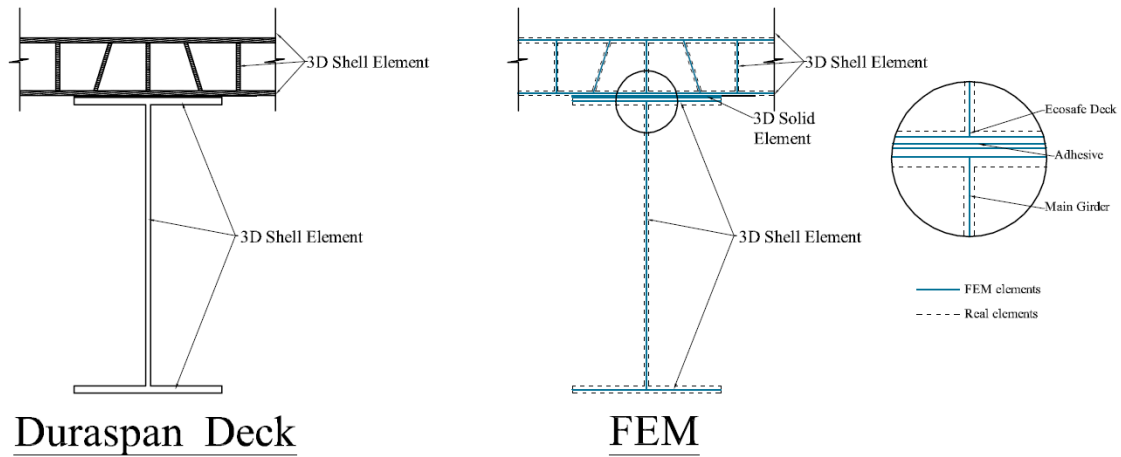
Figure 3-27 Finite element modeling of Duraspan deck
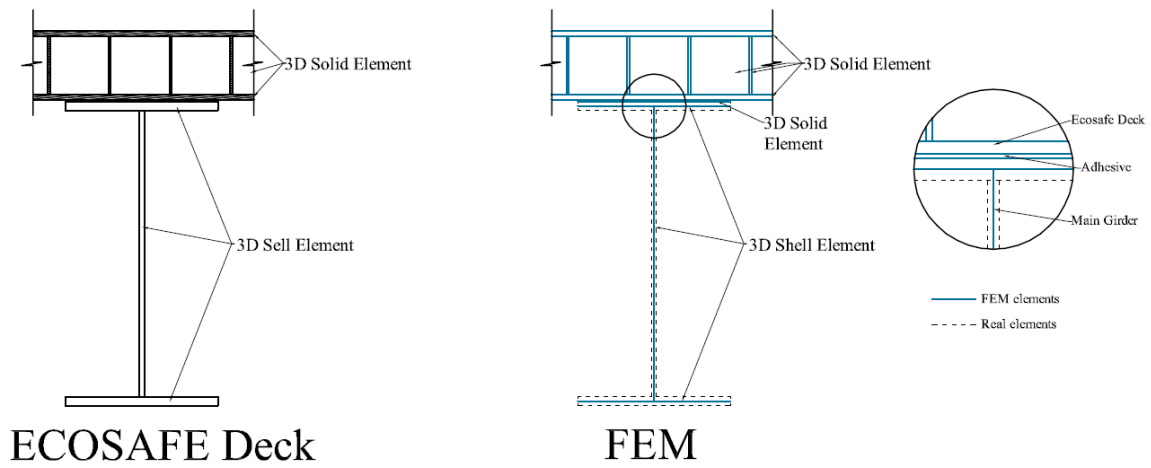


Figure 3-28 Finite element modeling of Ecosafe deck

### 3.5.2.2.  Shear studs modeling

A 25 mm gap center-to-center distance is provided between the bottom face of the FRP deck and the top face of the girder flange representing the geometry of the real bridge. The grout haunch is not modeled. In order to simulate the interaction between FRP deck and the steel girders joined by shear studs multiple-point constraint connector elements (CONN3D2 in Abaqus) among the common nodes over the sector contact section between the top flange of the beam and the bottom of the deck. Each connector element extended between the center-line of the beam flange thickness and the center-line of the deck thickness.  To achieve full composite action all three rotational degrees of freedom (x, y and z direction) are coupled between the beam and the deck, meaning no relative rotation, and all three displacement (x, y and z direction) are coupled. This

technique was used and validated with experimental studies by (Chen & Davalos, 2012). Figure 3-29 shows a transparent view of the bridge and the application of shear studs (marked with green color).
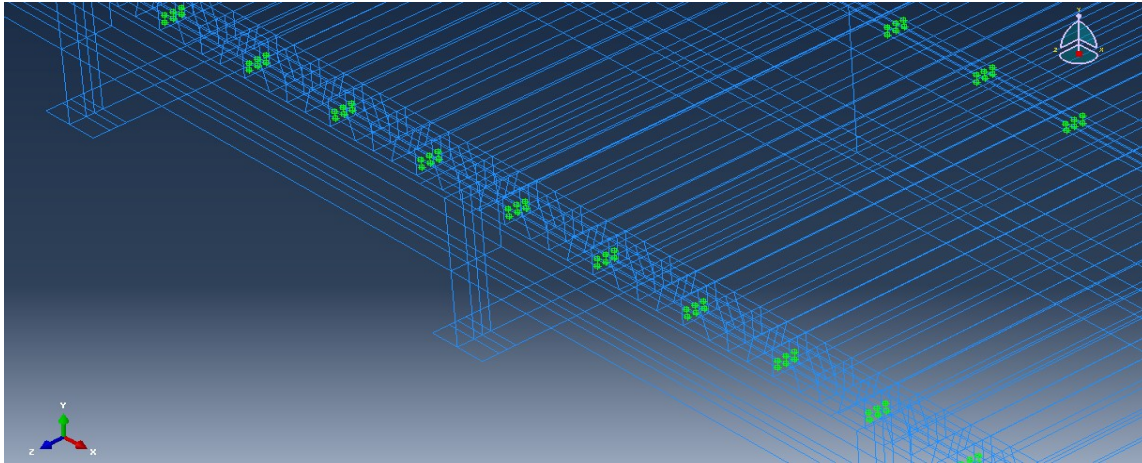


Figure 3-29 Shear studs (green color) application in Abaqus (transparent view of deck)

### 3.5.3. Boundary Conditions

In the Wilhelminabrug there are 6 supports in total, four in the main girders near the ballast where the bridge is prevented to move in vertical and longitudinal direction and two in the opposite direction that prevent the vertical translation of the bridge, according to the requirements set by the responsible company. Figure 3-30 shows the position of such constraints (orange color) and Table 3-7 gives the representative constraint.

Table 3-7 Boundary Condition[7]

|  | Displacement | | | Rotation | | |
|---|---|---|---|---|---|---|
|  | x | y | z | x | y | z |

| B.C. 1 | Fixed | Fixed | Fixed | Free | Free | Free |
|---|---|---|---|---|---|---|
| B.C. 2 | Fixed | Fixed | Free | Free | Free | Free |
| B.C. 3 | Fixed | Fixed | Free | Free | Free | Free |
| B.C. 4 | Fixed | Fixed | Free | Free | Free | Free |
| B.C. 5 | Free | Fixed | Free | Free | Free | Free |
| B.C. 6 | Free | Fixed | Free | Free | Free | Free |
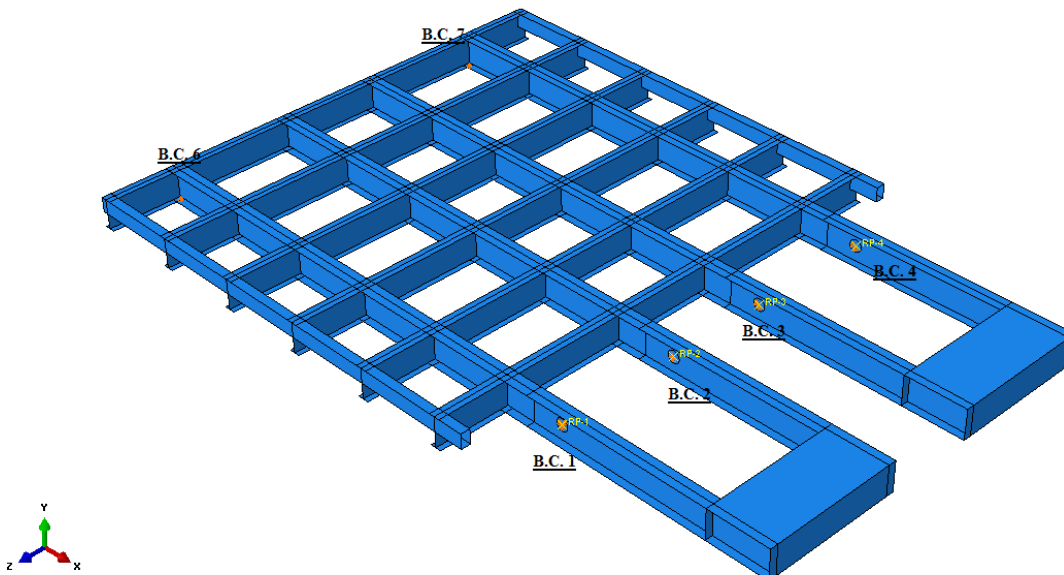
Figure 3-30  Boundary Conditions

To present the boundary conditions of the rotating part a circular cut with diameter d=400mm was modeled to the webs of the main girders. This surface was attached to a representing node through the option multi-point constraint (MPC - Link). The center node of the circular profile was assigned as controlling point while the circle was assigned as the slave nodes. Figure 3-31 shows the way this option is applied for the boundary condition BC 5-6 and BC 1-4.
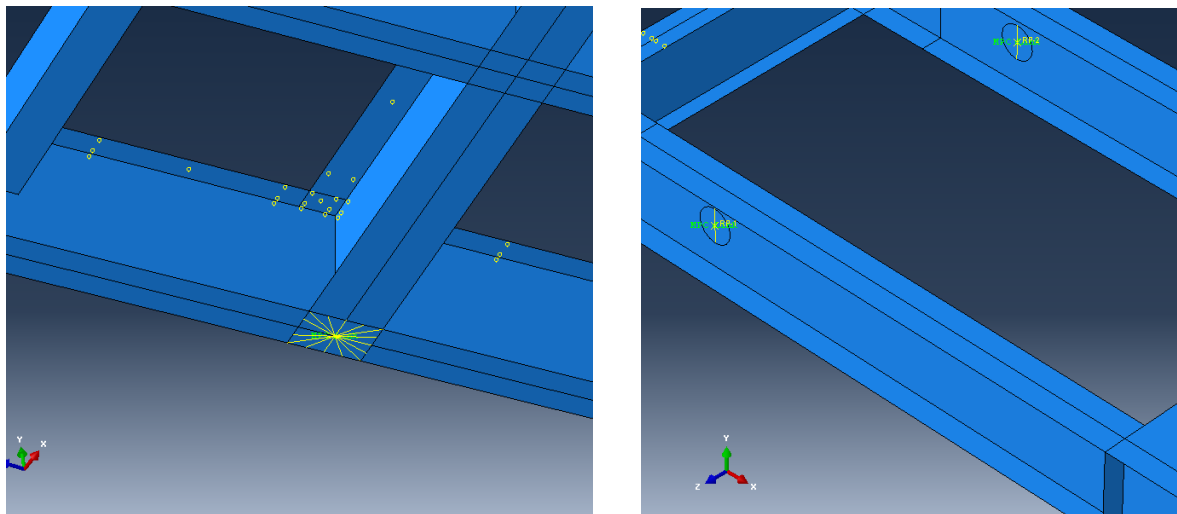


a – MPC at boundary condition (BC 1-4)          b – MPC at boundary condition (BC 5&6)

Figure 3-31 Multi point constraint application

### 3.5.4.  Loading

In order to model the loading conditions according to EC1 sections with surface 400x400 mm were created in the top of the deck where the wheel loads were applied. Load Model 1 is applied

as a pressure load over these surfaces. Figure 3-32 presents the loading configuration when type 3 structure is applied.
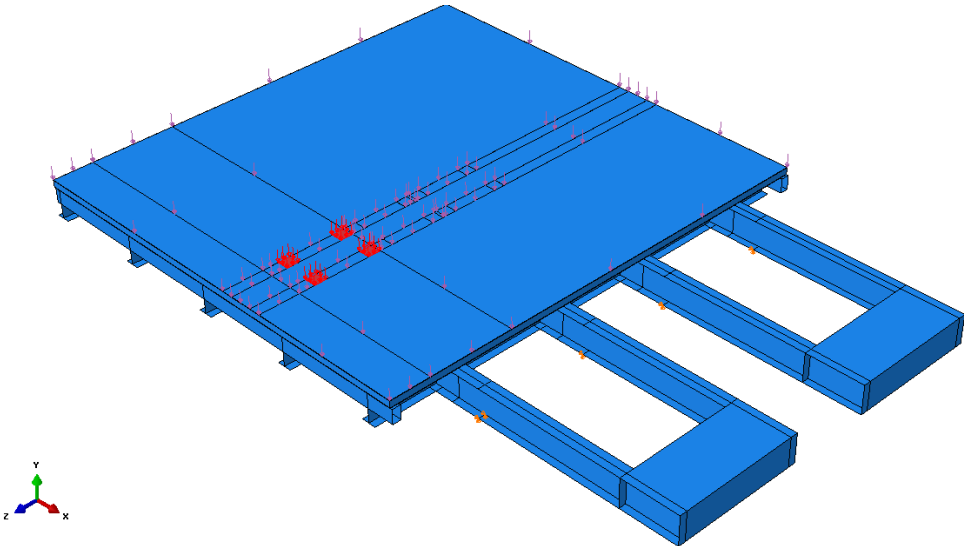


Figure 3-32  Loading application during FEM procedure

### 3.5.5.  Mesh

The mesh varied in size due to the requirements from the software Abaqus where the slave surfaces should have a finer mesh than master surfaces in order to obtain better results and shorten the time of the analysis. In general, a maximum of 100 mm size element were used (see
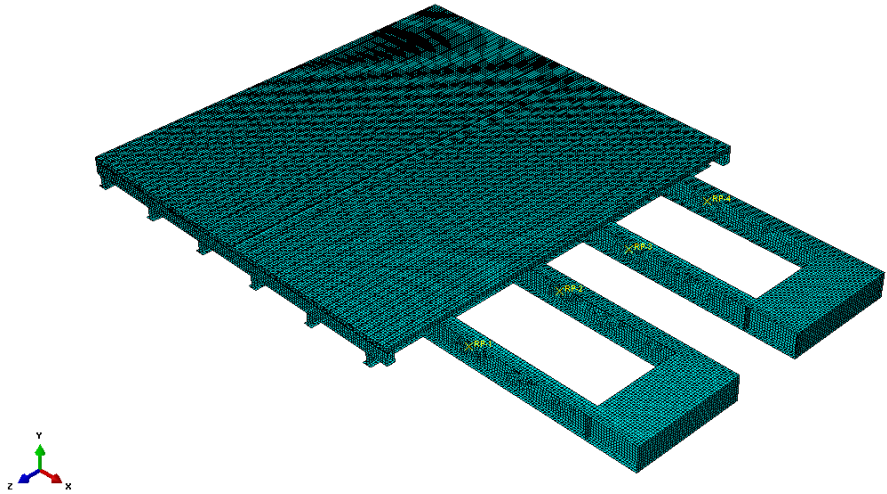


Figure 3-33 and Figure 3-34 to Figure 3-36 for a zoomed view). Mesh controls were assigned where the element shape was used quad-dominated under free and structured technique. In the

end a verification of the mesh was performed in order to satisfy the requirements for accurate results. The number of elements after meshing for each of the configurations is shown in Table 3-8, Table 3-9 and Table 3-10.

Table 3-8  Number of finite elements when Ecosafe deck is applied

| | Ecosafe deck applied | | | |
|---|---|---|---|---|
| | Deck | Steel | Adhesive | Total |
| Type | C3D8R | S4R | C3D8R | |
| 1 | 147572 | 35519 | 5170 | 188261 |
| 2 | 147572 | 53622 | 6876 | 208070 |
| 3 | 147572 | 46622 | 6284 | 200478 |

Table 3-9  Number of finite elements when Duraspan deck is applied

| | Duraspan deck applied | | | |
|---|---|---|---|---|
| | Deck | Steel | Adhesive | Total |
| Type | S4R | S4R | C3D8R | |
| 1 | 81972 | 35519 | 5170 | 122661 |
| 2 | 81972 | 53622 | 6876 | 142470 |
| 3 | 81972 | 46622 | 6284 | 134878 |

Table 3-10  Number of finite elements when ASSET deck is applied

| | ASSET deck applied | | | |
|---|---|---|---|---|
| | Deck | Steel | Adhesive | Total |
| Type | S4R | S4R | C3D8R | |
| 1 | 99954 | 35519 | 5170 | 140643 |

| | | | | |
|---|---|---|---|---|
| 2 | 99954 | 53622 | 6876 | 160452 |
| 3 | 99954 | 46622 | 6284 | 152860 |
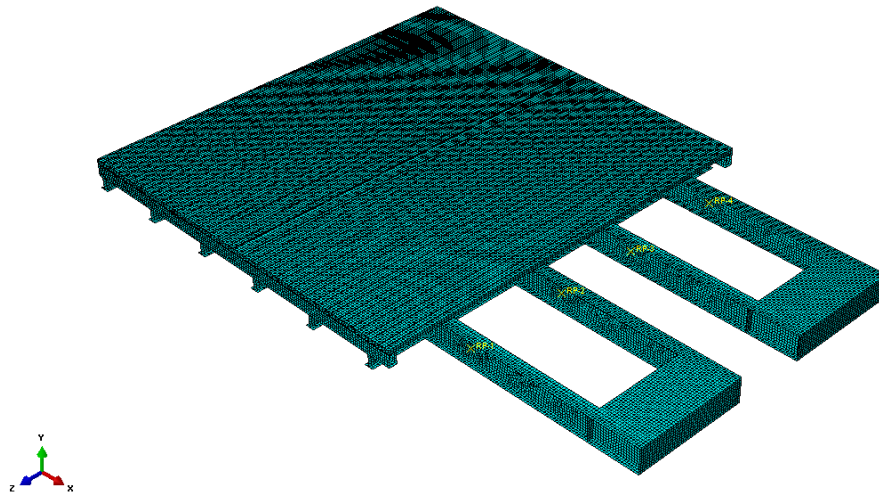


Figure 3-33  Meshing of the structure (type 3 with Duraspan deck applied)
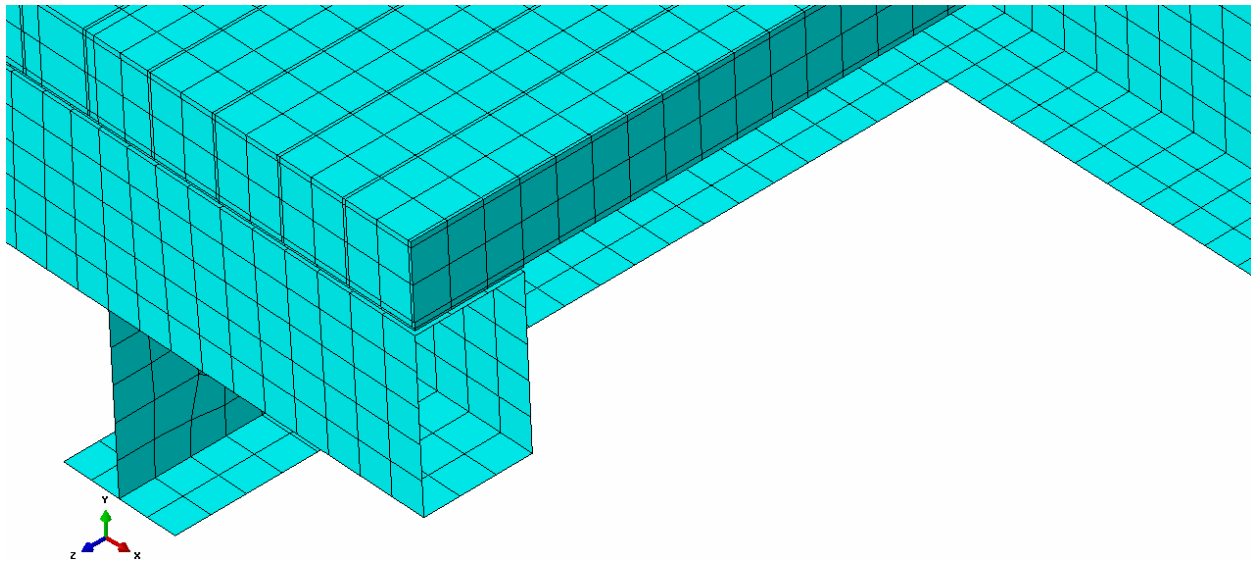


Figure 3-34 Zoomed mesh view when Ecosafe deck is applied
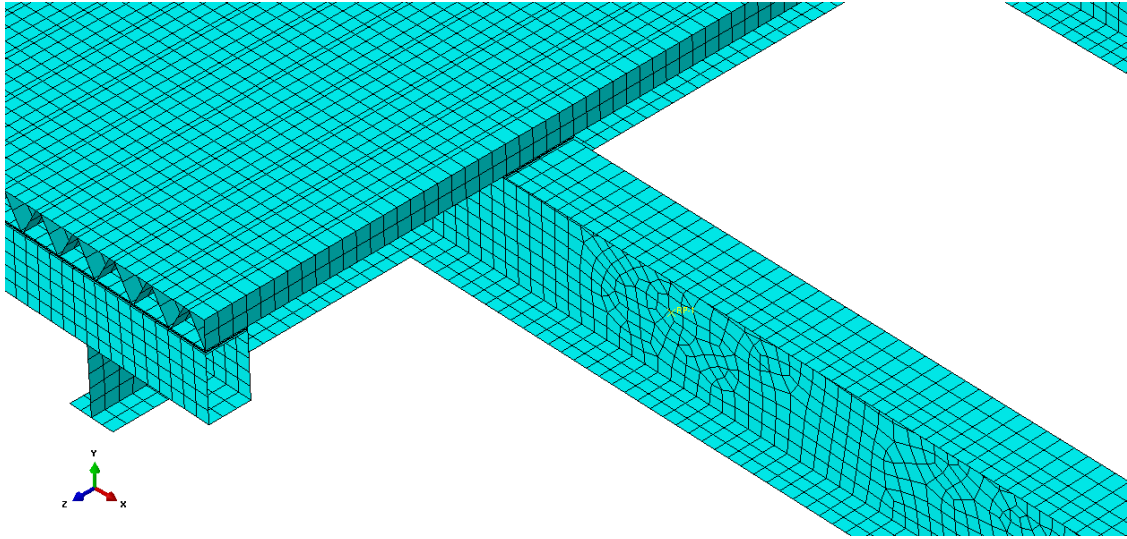
Figure 3-35 Zoomed mesh view when ASSET deck is applied
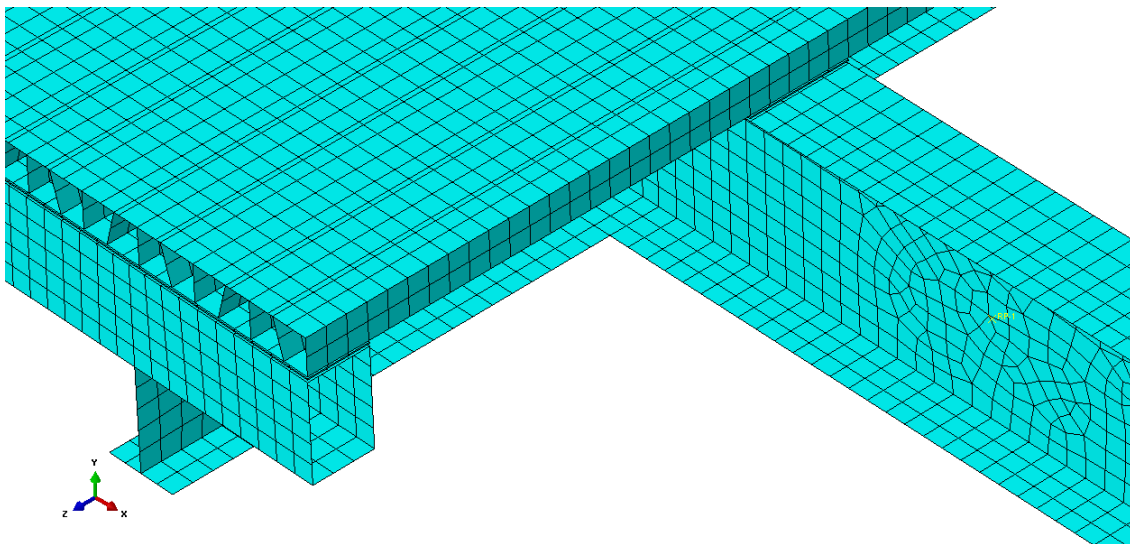


Figure 3-36 Zoomed mesh view when Duraspan deck is applied

### 3.5.6. Approximations

When modelling with shell elements it is of significant importance that the elements are connected to each other in their respective (end) nodes in order to obtain the correct behaviour. In Wilhelminabrug, the main girders are cambered near the ballast and vary in thickness. An approximation regarding dimensions and stiffness was applied during this analysis, since this part of the structure in not of main importance in this study.

# 4. Static Analysis

Chapter 4 presents the static analysis of the bridge. Three type of FRP bridge decks (ASSET, Duraspan and Ecosafe) are incorporated into three type of steel structure configuration. Comparison between each case scenario is evaluated regarding the mass weight, global and local deflection and stresses of the deck and steel structure. In addition, additional investigation is computed for ASSET and Duraspan deck where analytical results provided from finite element modeling are compared with results from experimental data provided through literature research. Last section of the chapter is reserved to present a short summary and discussion of the results.

## 4.1. Self-Weight of FRP decks total structure

It is inevitable that one of the best advantages of using FRP decks in comparison to other traditional materials is the weight reduction of the structure. During the study of upgrading Wilhelminabrug it was shown that the self-weight of FRP decks covering a surface of (16.17x15.15) m of deck is 25.4, 23 and 22 tons respectively for ASSET, Duraspan and Ecosafe. This resulted on a maximum self-weight for the total structure of 86, 84 and 83 tons for respectively, when type 3 configuration (the heaviest) is used. Comparison with the case of steel orthotropic deck solution of 120 tons it is clear the large amount of reduction of self-weight.

Table 4-1 Self-Weight of ECOSAFE deck and total mass of the structure

| ASSET Deck | | |
|---|---|---|
| | | [ton] |
| Deck | | 25.4 |
| Total Structure (Deck+Steel Structure) | Type 1 | 64 |
| | Type 2 | 73 |
| | Type 3 | 86 |

Table 4-2 Self-Weight of Duraspan deck and total mass of the structure

| Duraspan Deck | | |
|---|---|---|
| | | [ton] |
| Deck | | 23 |
| Total Structure (Deck+Steel Structure) | Type 1 | 62 |
| | Type 2 | 70 |
| | Type 3 | 84 |

Table 4-3 Self-Weight of ASSET deck and total mass of the structure

| ECOSAFE Deck | | |
|---|---|---|
| | | [ton] |
| Deck | | 22 |
| Total Structure (Deck+Steel Structure) | Type 1 | 61 |
| | Type 2 | 69 |
| | Type 3 | 83 |

## 4.2. Deflections of the Structure

An important criteria to be met when designing structures with FRP deck and steel girders are the global and local deflection when the bridge is loaded in serviceability limit state (SLS). The maximum deflections occurs in the position where the load is applied, in the middle of the girders. Many researchers have found out that deflections is the governing criteria for most of the cases. The below sections present the deflections (global and local) for the case when three decks are used. The local deflection or the relative deck deflection is calculated as the difference between the deflection of the deck at the point of interest and the corresponding reference girder deflection. In addition, the corresponding values $u_{max}/L$ for the global deflection are given. Unfortunately, guidelines and codes are not yet available to give information for the limiting criteria. Many researchers argue that this limiting deflections should be on the safe side and have to be taken as L/800, a criteria that have been adopted in the design of many bridges.

### 4.2.1. ECOSAFE Deck

Table 4-4 and Table 4-5 present the maximum vertical deflection (U2), global and local respectively, driven from the finite element model when Ecosafe deck is used. Figure 4-1 to Figure 4-3 show the vertical displacement for the three type of superstructure configurations in a deformed shape. Appendix A provides additional information regarding these deflections (graph showing the relations of displacement along the edge of the deck and in the mid-span between the beams).

In the case of global deflection the maximum value of the displacement is 16.6 mm, for type 3 configuration, corresponding to L/840. The minimum value results in type 2 configuration with a value of 14.8 mm corresponding to L/941. The maximum local deflection for the midspan results

111

for type 1 configuration with a value of 3.5 mm where the maximum allowable is set 5 mm (L/800). The maximum local deflection for the cantilever part happens when type 1 configuration is used with a value of 2 mm where the allowable value is set 2.85 mm (L/800). It is clear that all the requirement regarding local and global deflection when Ecosafe deck is used are met.

Table 4-4  Global Deflections of the structure (Ecosafe deck applied)

| Global Deflection - ECOSAFE Deck | | | |
|---|---|---|---|
| | Mid-Span | | |
| | umax  [mm] | span [mm] | 1/L |
| | | | |
| Type-1 | 15.7 | 14000 | 1/891 |
| | | | |
| Type-2 | 14.8 | 14000 | 1/941 |
| | | | |
| Type-3 | 16.6 | 14000 | 1/840 |

Table 4-5  Local Deflections of the structure (Ecosafe deck applied)

| Local Deflection - ECOSAFE Deck | | | | | | |
|---|---|---|---|---|---|---|
| | Mid-Span | | | Cantilever | | |
| | umax  [mm] | span [mm] | L/800 | umax  [mm] | span [mm] | L/800 |
| | | | | | | |
| Type-1 | 3.5 | 4000 | 5 | 2 | 2285 | 2.85 |
| | | | | | | |
| Type-2 | 1.8 | 2000 | 2.5 | 1.3 | 1285 | 1.6 |
| | | | | | | |
| Type-3 | 3 | 4000 | 5 | 1.5 | 2285 | 2.85 |
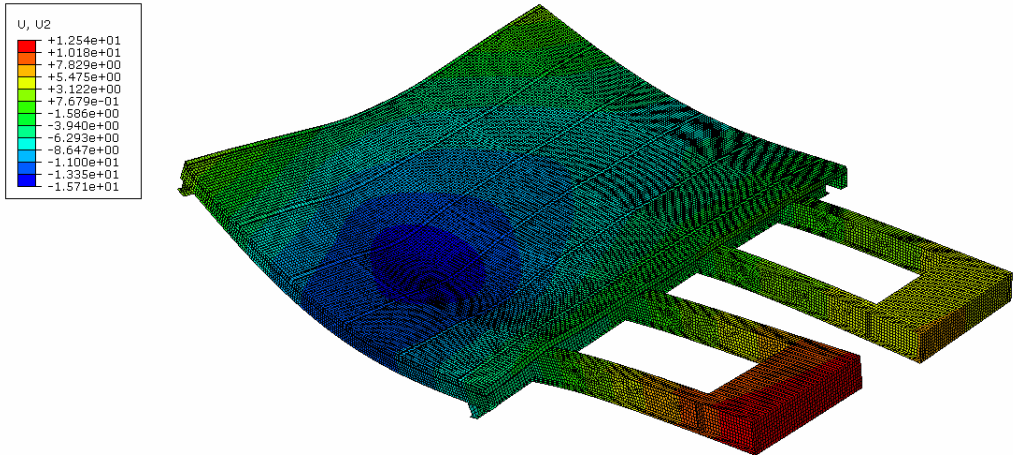
Figure 4-1  Vertical displacement of type 1 configuration (ECOSAFE deck)
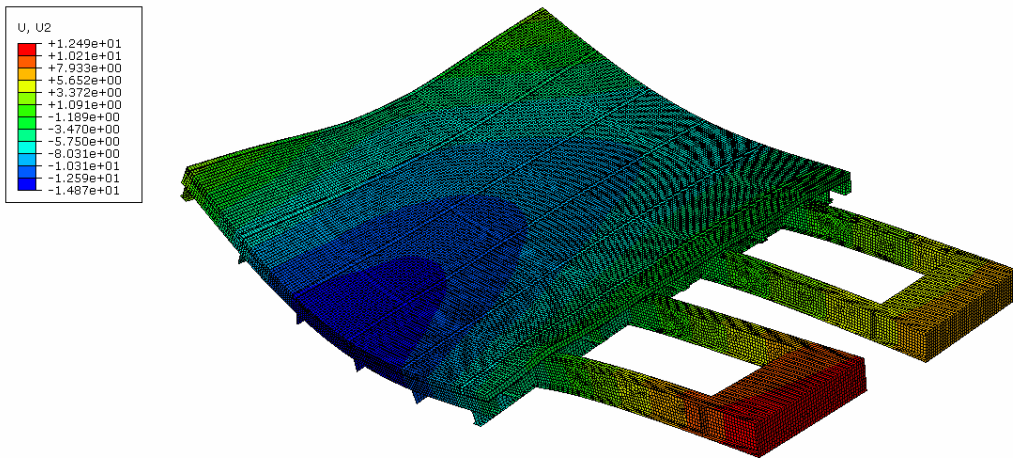


Figure 4-2 Vertical displacement of type 2 configuration (ECOSAFE deck)
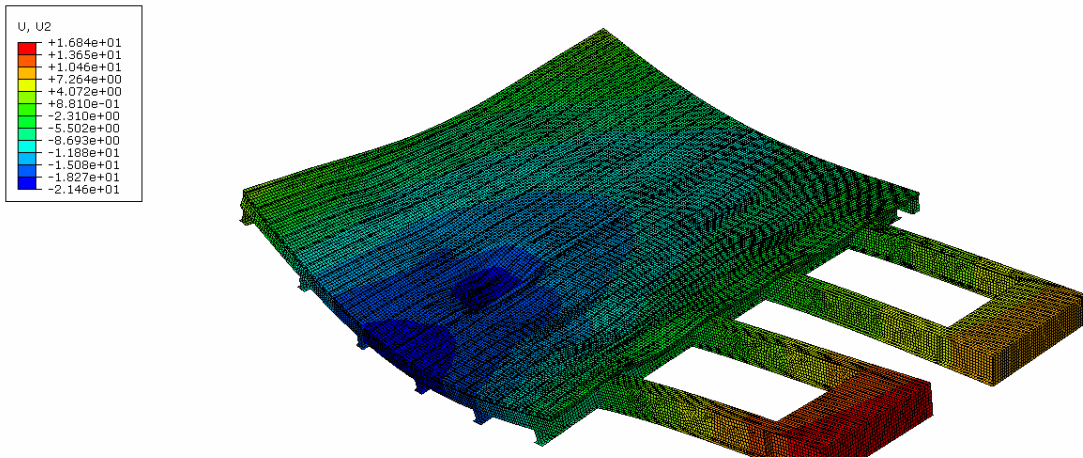


Figure 4-3 Vertical displacement of type 3 configuration (ECOSAFE deck)

### 4.2.2. ASSET Deck

Table 4-6 and 4-7 present the maximum vertical deflections (U2), global and local respectively, driven from the finite element model when ASSET deck is used. Figure 4-4 to Figure 4-7 show the vertical displacement for the three type of superstructure configurations. Appendix A provides additional information regarding these deflections (graph showing the relations of displacement along the edge of the deck and in the mid-span between the beams).

The maximum value of global deflections equals the value of 19.5 mm, for type 1 configuration, corresponding to L/717. The minimum value results when type 2 configuration is used with a value of 16.8 mm corresponding to L/833.

The maximum local deflection for the midspan results for type 1 configuration with a value of 5.2 mm exceeding the maximum allowable set of 5mm (L/800). The other type of configurations do not surpass the limiting value of L/800. Type 2 achieves a value of 92% of the limiting value, while type 3 achieve a value of 62%.

The maximum local deflection for the cantilever part happens when type 3 configuration is used with a value of 2 mm meeting the allowable value of 2.85 (L/800) correspondingly 70%. Moreover, the other types of configuration have resulted with a lower deflection comparing to the limit set of L/800 achieving 17.5% and 94% of the latter, respectively for type 1 and type 3 configuration.

Table 4-6 Global Deflections of the structure (ASSET deck applied)

| Global Deflection -ASSET Deck | | | |
|---|---|---|---|
| | Mid-Span | | |
| | umax [mm] | span [mm] | 1/L |
| | | | |
| Type-1 | 19.5 | 14000 | 1/717 |
| | | | |
| Type-2 | 16.8 | 14000 | 1/833 |
| | | | |
| Type-3 | 18.2 | 14000 | 1/766 |

Table 4-7 Local Deflections of the structure (ASSET deck applied)

| | Mid-Span | | | Cantilever | | |
|---|---|---|---|---|---|---|
| | umax [mm] | span [mm] | L/800 | umax [mm] | span [mm] | L/800 |
| **Local Deflection - ASSET Deck** | | | | | | |
| | | | | | | |
| Type-1 | 5.2 | 4000 | 5 | 1 | 2285 | 2.85 |
| | | | | | | |
| Type-2 | 2.3 | 2000 | 2.5 | 1.5 | 1285 | 1.6 |
| | | | | | | |
| Type-3 | 3.1 | 4000 | 5 | 2 | 2285 | 2.85 |
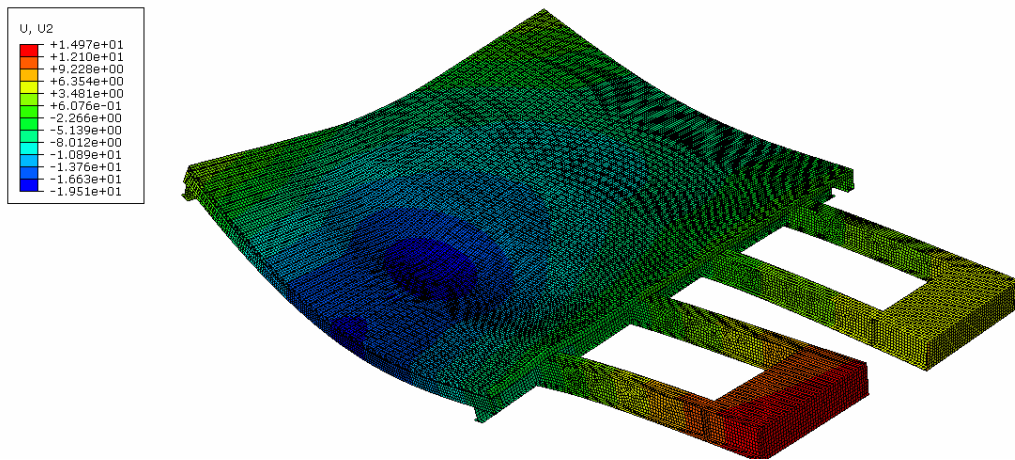


Figure 4-4 Vertical displacement of type 1 configuration (ASSET deck)
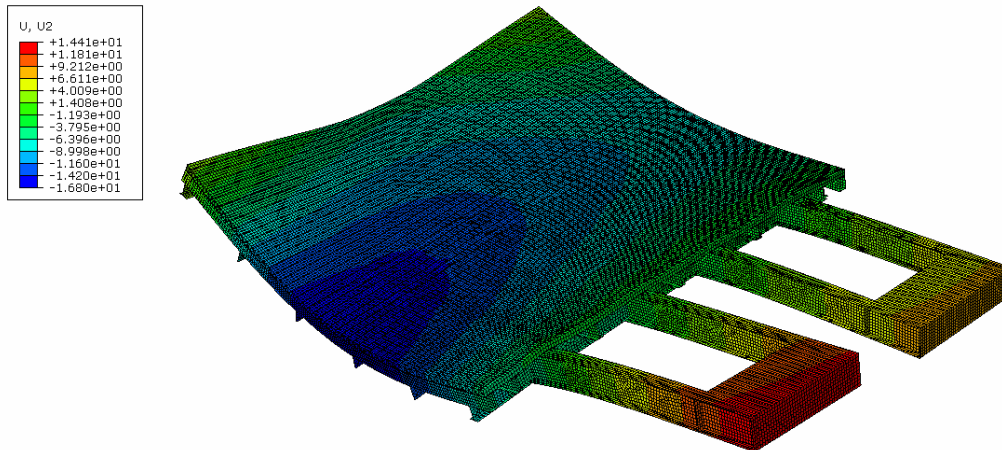
Figure 4-5 Vertical displacement of type 2 configuration (ASSET deck)
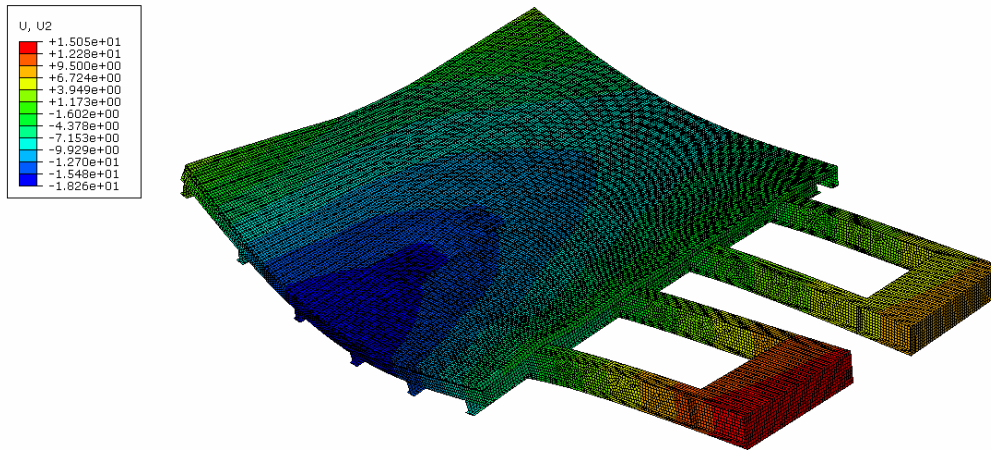


Figure 4-6 Vertical displacement of type 3 configuration (ASSET deck)

Duraspan DeckTable 4-8 and Table 4-9 present the maximum vertical deflection (U2), global and local respectively, driven from the finite element model when Duraspan deck is used. Figure 4-7 and Figure 4-9 show the vertical displacement for the four type of configurations in a deformed shape. Appendix A provides additional information regarding these deflections (graph showing the relations of displacement along the edge of the deck and in the mid-span between the beams).

In the case of global deflection the maximum value of the displacement is 24.3 mm, for type 1 configuration, corresponding to L/575. The minimum value results in type 2 configuration with a value of 18.2 mm corresponding to L/768.

The maximum local deflection for the midspan results for type 1 configuration with a value of 7.5 mm exceeding the maximum allowable is 5 (L/800). The other type of configurations do not surpass the limiting value of L/800. Type 2 achieves a value of 88% of the limiting value, while type 3 achieve a value of 94%.

The maximum local deflection for the cantilever part happens when type 3 configuration is used with a value of 2 mm meeting the allowable value of 2.85 (L/800) correspondingly 70%. However type 2 achieves the limiting value of 1.6 mm (L/800). Type 3 configuration achieves 70% of limiting value.

Table 4-8 Global Deflections of the structure (Duraspan deck applied)

| Global Deflection -Duraspan Deck | | | |
|---|---|---|---|
| | Mid-Span | | |
| | umax [mm] | span [mm] | 1/L |
| | | | |
| Type-1 | 24.3 | 14000 | 1/575 |
| | | | |
| Type-2 | 18.2 | 14000 | 1/768 |
| | | | |
| Type-3 | 21.4 | 14000 | 1/652 |

Table 4-9 Local Deflections of the structure (Duraspan deck applied)

| Local Deflection - Duraspan Deck | | | | | | |
|---|---|---|---|---|---|---|
| | Mid-Span | | | Cantilever | | |
| | umax [mm] | span [mm] | L/800 | umax [mm] | span [mm] | L/800 |
| | | | | | | |
| Type-1 | 7.5 | 4000 | 5 | 1.6 | 2285 | 2.85 |
| | | | | | | |
| Type-2 | 2.2 | 2000 | 2.5 | 1.6 | 1285 | 1.6 |
| | | | | | | |
| Type-3 | 4.7 | 4000 | 5 | 2 | 2285 | 2.85 |
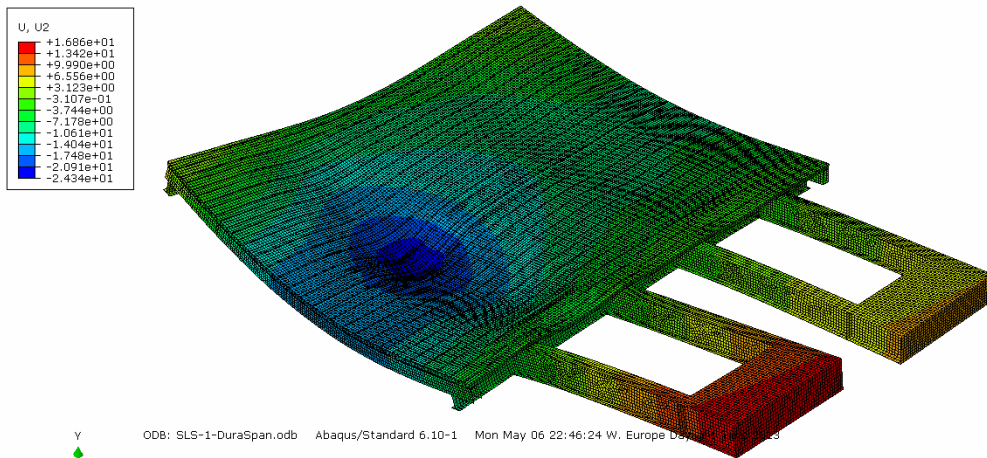


Figure 4-7 Vertical displacement of type 1 configuration (Duraspan deck)
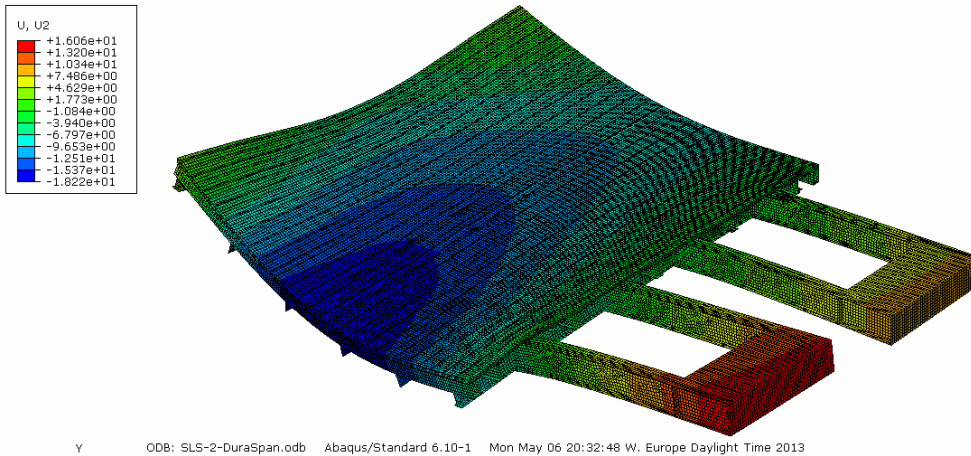
Figure 4-8 Vertical displacement of type 2 configuration (Duraspan deck)
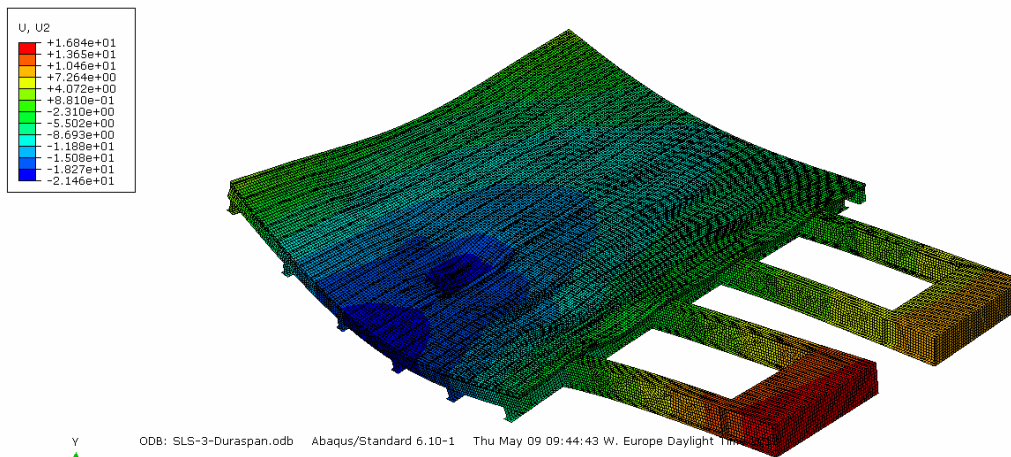


Figure 4-9 Vertical displacement of type 3 configuration (Duraspan deck)

## 4.3. Stresses of the steel structure

### 4.3.1. Ecosafe Deck

When vertical loading is applied in the bridge under ultimate limit state (ULS) the values of stresses are obtained. Table 4-10 show the results of longitudinal stresses for the deck and the steel structure provided by finite element modeling when Ecosafe deck is used for the three types of superstructure configurations. In Appendix B the corresponding figures are plotted. As it is shown the stresses of the Ecosafe deck in each case are very low, with a maximum value of 51 MPa for type 2 configuration and a minimum value of 13.6 MPa for type 3 configuration.

118

Moreover, the stresses in the steel structure in the linear elastic stage have a maximum value of 278 MPa corresponding to a safety value of 1,27[8].

Table 4-10  Stresses of the structure (Ecosafe deck applied)

| | | ECOSAFE Deck | |
|---|---|---|---|
| **Stresses of the structure** | **Type – 1** | Deck | Steel Structure |
| | | [MPa] | [MPa] |
| | | 30 | 250 |
| | | | |
| | **Type – 2** | Deck | Steel Structure |
| | | [MPa] | [MPa] |
| | | 51 | 215 |
| | | | |
| | **Type – 3** | Deck | Steel Structure |
| | | [MPa] | [MPa] |
| | | 20 | 278 |

### 4.3.2.  ASSET Deck

Similar to the previous case of Ecosafe deck, stresses are provided for ultimate limit state (ULS) when ASSET deck is applied for the bridge upgrading. However, driven from the shape of ASSET deck that combined flanges and inclined webs, its behaviour is studied more in depth. It is observed that the forces are mainly transferred through from flanges to the webs by truss action, where compressive and tensile forces happen in the diagonals. The latter is derived due to the triangular configuration of the deck as shown in Figure 4-10. When one of the webs carries tension and the other compression forces, the components of these forces will create force couples in the flanges which will result in local moments and high shear forces between the intersections of diagonals. The moments in the intersections are higher because the moment is a function of the length of the force couple. Thus, peak moments and shear forces result in the intersection between the web and the flange as shown in Figure 4-11.

---

[8] Steel grade S355 is used
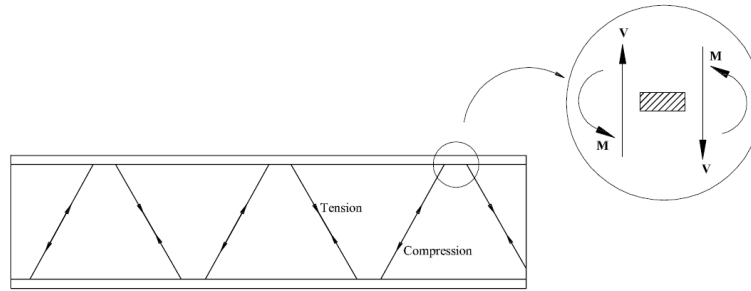
Figure 4-10  Distribution of internal forces in ASSET deck
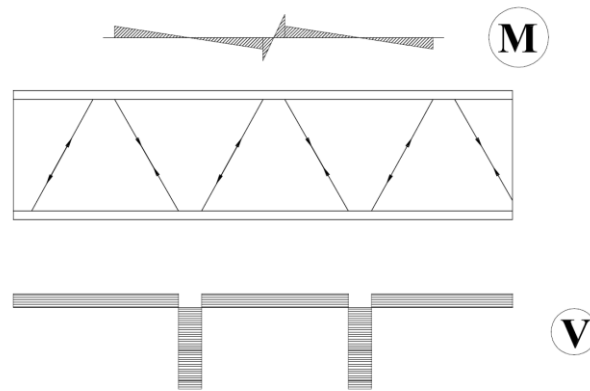


Figure 4-11 Moment and shear distribution in the flanges of ASSET deck

When vertical loading is applied in the bridge under ultimate limit state (ULS) the values of stresses are retrieved.

Table 4-11 show the results of longitudinal stresses for the deck and the steel structure provided by finite element modeling when ASSET deck is used for the four types of configurations. In Appendix B the corresponding figures are plotted. The results show that the stresses of the ASSET deck in each case have a maximum value of 66 MPa for type 3 configuration and a minimum value of 40 MPa for type 2 configuration. Moreover, the stresses in the steel structure

in the linear elastic stage have a maximum value of 282 MPa corresponding to a safety value of 1,25[9].

Table 4-11  Stresses of the structure (ASSET deck applied)

| Stresses of the structure | | | |
|---|---|---|---|
| | **Type – 1** | **ASSET Deck** | |
| | | Deck | Steel Structure |
| | | [MPa] | [MPa] |
| | | 43 | 270 |
| | | | |
| | **Type – 2** | Deck | Steel Structure |
| | | [MPa] | [MPa] |
| | | 40 | 226 |
| | | | |
| | **Type – 3** | Deck | Steel Structure |
| | | [MPa] | [MPa] |
| | | 66 | 282 |

For ASSET deck additional checks are possible due to the information provided from Fiberline. Tensile stresses in longitudinal and transversal direction according to the direction set at Figure 3-11 are compared from the tensile strength as shown in Table 4-12. It is clear that these stresses are lower compared the tensile strength.

Table 4-12 Tensile stresses of Flanges and Webs for ASSET Deck (type 1 and type 2)

| Tensile Stresses - ASSET deck | | | | | | |
|---|---|---|---|---|---|---|
| Property | **Type 1** | | **Type 2** | | **Type 3** | |
| | Flange Plate | Web Plate | Flange Plate | Web Plate | Flange Plate | Web Plate |
| Transverse max Stress [MPa] | 48 | 44.5 | 40 | 10 | 66 | 37.7 |

---

[9] Steel grade S355 is used

| Transverse tensile Stress [MPa] | 240 | 190 | 240 | 190 | 240 | 190 |
|---|---|---|---|---|---|---|
| Safety Factor | **5.0** | **4.3** | **6.0** | **19.0** | **3.6** | **5.0** |
| | | | | | | |
| Longitudinal max Stress [MPa] | 42 | 42.9 | 19.6 | 21.9 | 26 | 66.3 |
| Longitudinal tensile Stress [MPa] | 175 | 210 | 175 | 210 | 175 | 210 |
| Safety Factor | **4.2** | **4.9** | **8.9** | **9.6** | **6.7** | **3.2** |

### 4.3.3. Duraspan Deck

When vertical loading is applied in the bridge under ultimate limit state (ULS) the values of stresses are retrieved. Table 4-13 show the results of stresses (Von Mises) for the deck and the steel structure provided by finite element modeling when Duraspan deck is used for the three types of configurations. In Appendix B the corresponding figures are plotted.

Analogous to ASSET deck, the deck system shear transfer is studied. Due to the trapezoidal shape of Durapsan deck, the in-plane shear force is transferred from one face panel to the other mainly through transverse bending of the cross-sectional web elements, Vierendeel action.

The results show that the stresses of the Duraspan deck have a maximum value of 109 MPa for type 1 configuration and a minimum value of 96 MPa for type 2 configuration. Moreover, the stresses in the steel structure in the linear elastic stage have a maximum value of 300 MPa corresponding to a safety value of 1,18[10].

Tensile stresses in longitudinal and transversal direction are compared from the tensile strength as shown in Table 4-12. It is clear that these stresses are lower compared the tensile strength.

Table 4-13  Stresses of the structure (Duraspan deck applied)

| | | **Duraspan Deck** | |
|---|---|---|---|
| **Stresses of the structure** | **Type – 1** | Deck [MPa] | Steel Structure [MPa] |
| | | 109 | 300 |
| | | | |
| | **Type -2** | Deck [MPa] | Steel Structure [MPa] |

---

[10] Steel grade S355 is used

| | | 96.3 | 241 |
|---|---|---|---|
| **Type – 3** | Deck [MPa] | Steel Structure [MPa] | |
| | 113.5 | 298 | |

Table 4-14 Tensile stresses of Flanges and Webs for Duraspan Deck

| Tensile Stresses - Duraspan deck | | | | | | |
|---|---|---|---|---|---|---|
| Property | Type 1 | | Type 2 | | Type 3 | |
| | Flange Plate | Web Plate | Flange Plate | Web Plate | Flange Plate | Web Plate |
| Transverse max Stress [MPa] | 63 | 62 | 29.7 | 20 | 46.2 | 39 |
| Transverse tensile Stress [MPa] | 147 | 130 | 147 | 130 | 147 | 130 |
| Safety Factor | **2.3** | **2.1** | **4.9** | **6.5** | **3.2** | **3.3** |
| | | | | | | |
| Longitudinal max Stress [MPa] | 109 | 50.2 | 96.3 | 95.2 | 113.5 | 91 |
| Longitudinal tensile Stress [MPa] | 261 | 220 | 261 | 220 | 261 | 220 |
| Safety Factor | **2.4** | **4.4** | **2.7** | **2.3** | **2.3** | **2.4** |

### 4.4. Summary of results and discussion

In this chapter the static analysis of upgrading of Wilhelminabrug with FRP decks was presented. Three types of decks, Ecosafe from Lightweight Structures, ASSET from Fiberline and Duraspan from Martin Marienetta, were used to replace the old wooden deck under four new type of steel structure configurations.

The *total mass* of the structure when Ecosafe deck is applied corresponds to a minimum value of 61 tons for type 1 and a maximum value of 83 tons for type 3. Similarly, the total mass of the structure corresponds to a minimum value of 64 tons for type 1 and a maximum value of 86 tons for type 3 when ASSET deck is applied. Lastly, total mass of the structure corresponds to a minimum value of 62 tons for type 1 and a maximum value of 84 tons for type 3 when Duraspan deck is applied. A comparison of the self-weight of the structures is shown in Figure 4-12.
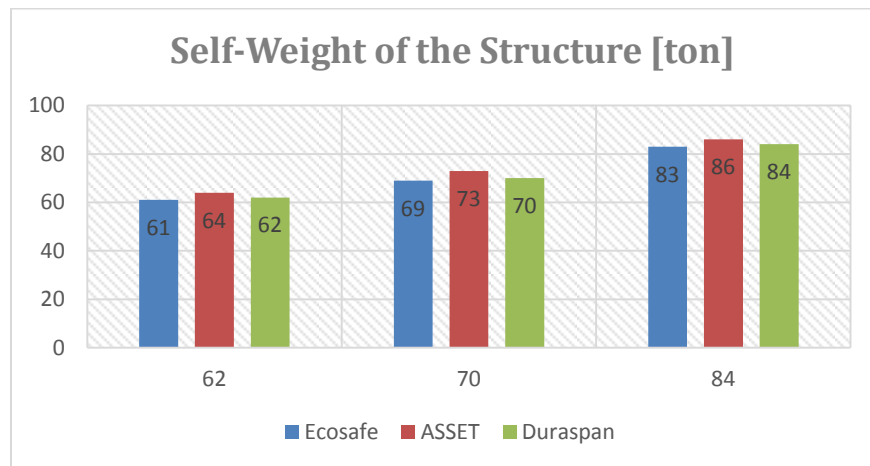


Figure 4-12 Comparison between self-weights

*Stresses* when Ecosafe and ASSET decks are used resulted in a very low values. A comparison of the three deck stresses is shown in Figure 4-13 and Figure 4-15. For Duraspan an ASSET cases the minimum value of the deck is obtained when type 2 configuration is used, while for Ecosafe when steel structure type 3 is used. For Ecosafe deck the maximum superstructure stresses are obtained for configuration 3, while for ASSET and Duraspan it is observed that exist an increase order from type 3 to 1.

Figure 4-13 Comparison between deck stresses
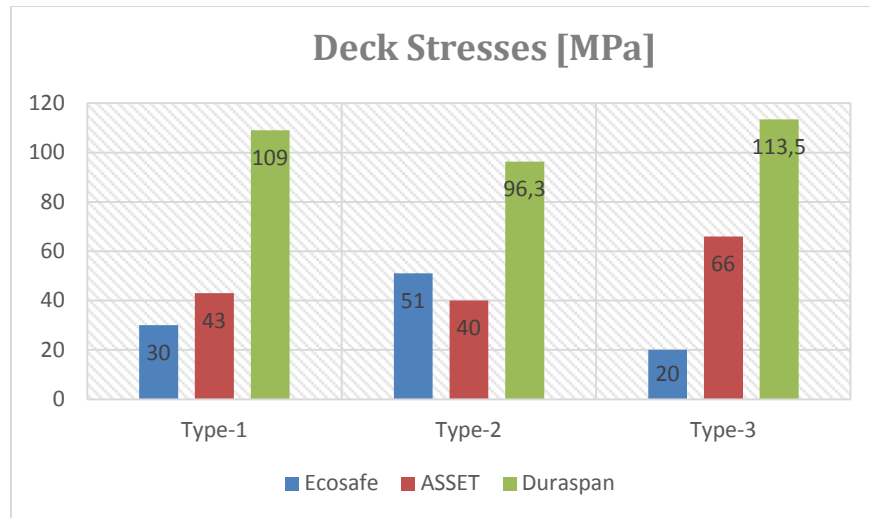


Figure 4-14 Comparison between deck stresses
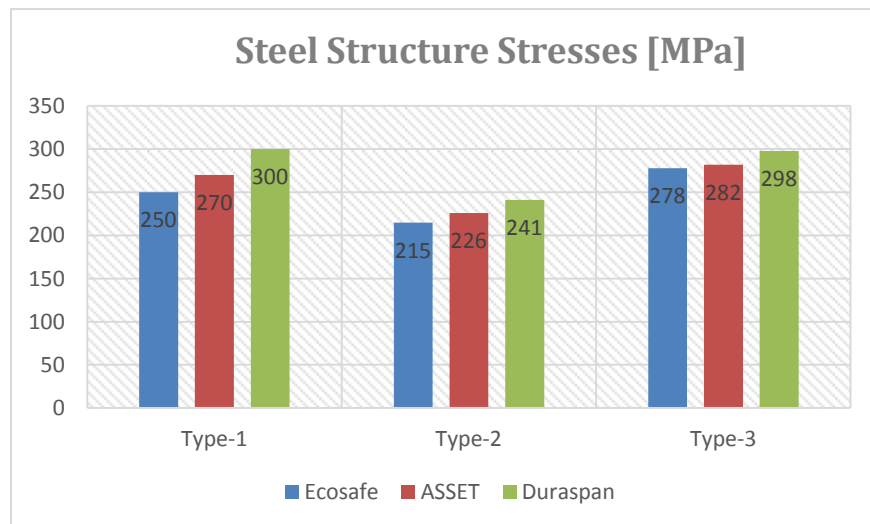


Figure 4-15 Comparison between steel structure stresses

When studying the structure behaviour under service limit state it was observed not all the cases meet the requirements. The maximum *global deflection* when Ecosafe deck is applied correspond to L/840, for ASSET deck corresponds to L/716 and for Duraspan deck corresponds to L/575. Different comparison of the relative deflection ($u/u_{max}$) are displayed in Figure 4-16 to Figure 4-18. When Ecosafe deck is used all type of configurations meet the criteria for local deflection. In case of ASSET and Duraspan deck, only type 1 configuration does not meet the local deflection criteria.
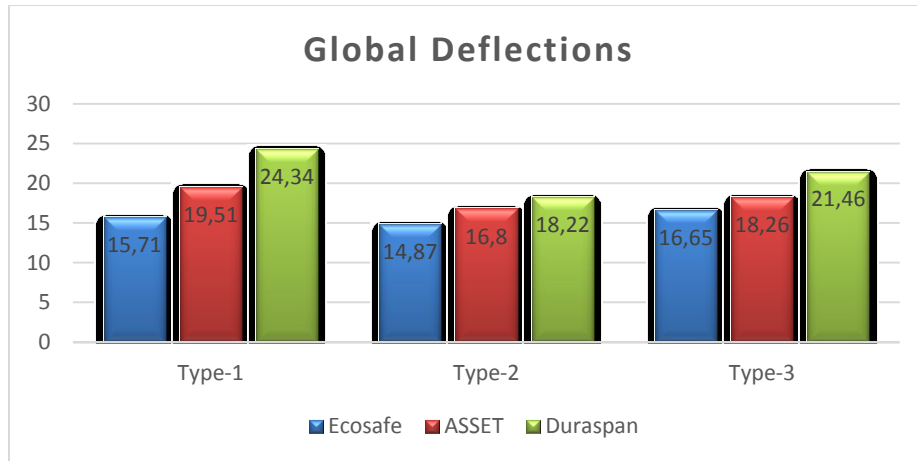
Figure 4-16 Global deflections comparison
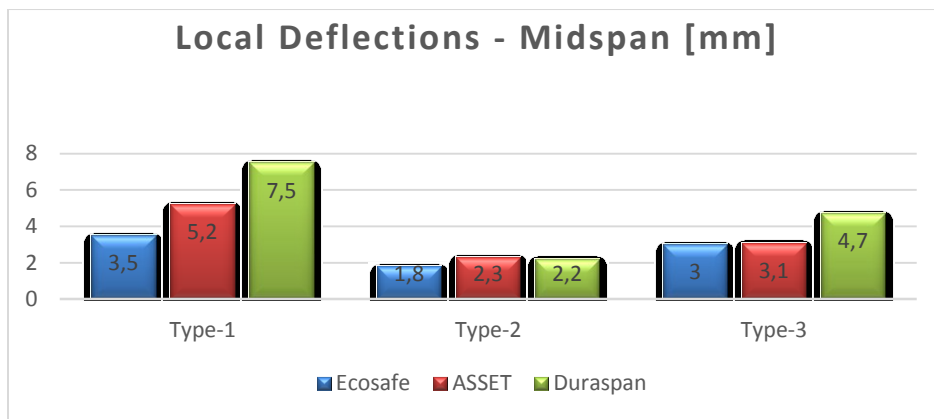


Figure 4-17 Local deflections (midspan) comparison
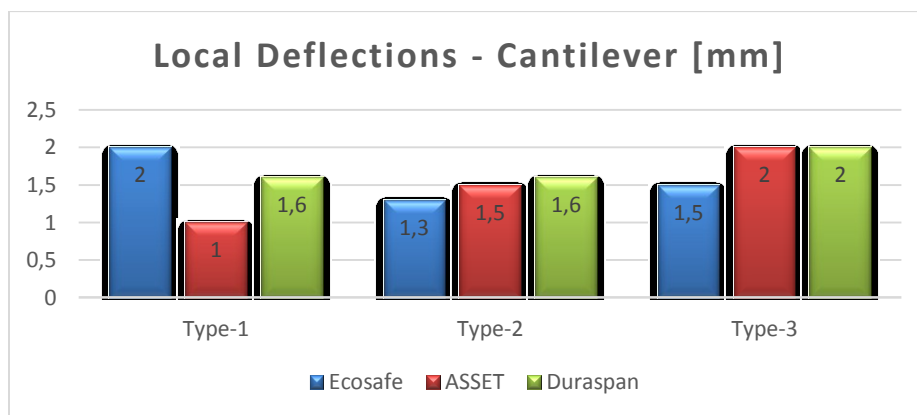


Figure 4-18 Local deflections (cantilever) comparison

It can be concluded that deflection has proven to be the governing criteria in this study. Regarding static stresses and the deflection requirements, type 3 resulted in higher safety factors. Building further to this argument, type 3 configuration own a better grillage system that provides a better global torsional stiffness for the movable bridge, especially in cases when misuse of the mechanical system can occur.

# 5. Composite Action

For conventional concrete to steel girders system in bridge constructions, full composite action is usually preferred and achieved due to the efficiency of the materials used. However, fiber-reinforced polymer (FRP) decks are usually designed in practice for partial or with no composite action. According to (Davalos, Chen, & Qiao, 2013) several limiting factors affect this behaviour as the following:

1- The hollow core configuration of FRP panels and lack of continuous connection at the panel-stringer interface do not allow development of perfect contact and attachment between decks and connections

2- The high modulus ratio between the steel girder and FRP panel (about 30), compared to conventional concrete that is 8-10

3- The practical connection spacing of about 0.6 to 1.2 m for FRP deck, is too large to develop full composite action

A number of design issues related to composite action in FRP deck to girder systems need to be investigated. Among these are: degree of composite action, effective width of the deck and transverse load distribution. These issues will be studied in this chapter for three decks (ASSET, Duraspan and Ecosafe) by means of finite element analysis.

## 5.1. Composite Action

One of the most important issues when studying the hybrid bridges made with steel girders and FRP decks is the degree of the composite action between the deck and the girders. Composite action refers to amount of the degree that horizontal shear forces are transferred between the girder and the deck. When full composite action is revealed 100% of the horizontal force is transferred between the girder and the deck. By contrast, no horizontal shear forces are transferred in a non-composite section. Moreover, partial composite action refers to the situation when a portion of this horizontal shear force is transferred between the deck and the girders. Full composite action is regarded as a plane strain distribution in the composite section, consequently fulfilling the hypothesis of Bernoulli as explained by *Gurtler, 2004* (Figure 2.1).

$$\text{Composite Action:} \quad \int_{0}^{x} \tau \, dx = C_1 + C_2$$
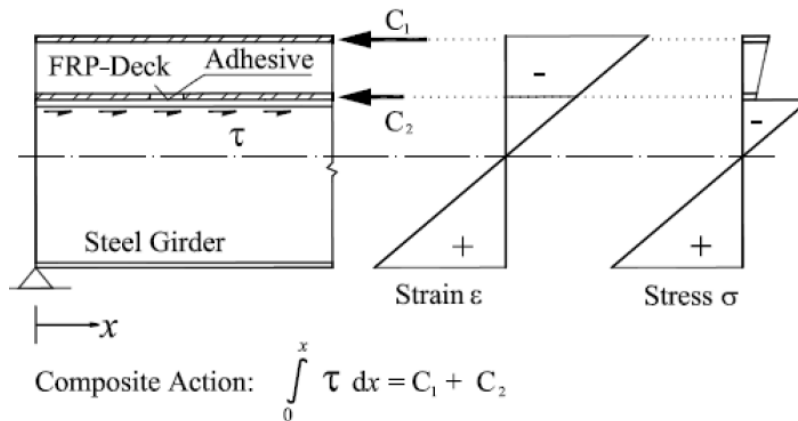
Figure 5-1 Theory of composite action in a composite section (Gurtler, 2004)

Due to the composite action between the steel girder and FRP deck the neutral axis will shift up toward the FRP deck. This behaviour is shown in Figure 5-2 below which presents the shift difference between a simple steel girder and a composite action between steel girder and FRP deck. The shifted neutral axis due to additional FRP deck on top of the steel girder will change the moment of inertia and section modulus of the whole member resulting in the decrease of the



Note: N.A.=Neutral Axis
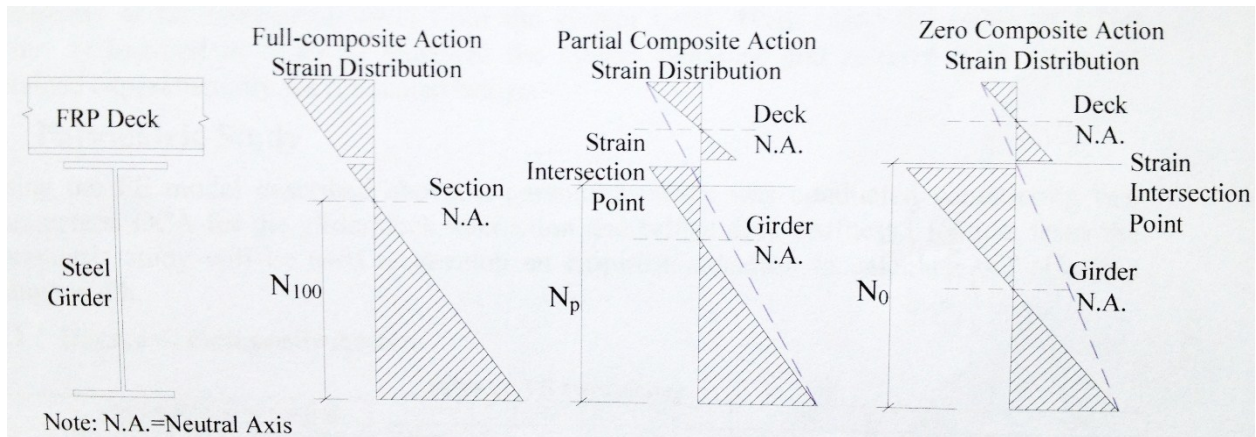
stress in the top flange of the girder.

Figure 5-2 Strain distribution; 100%, partial and 0% composite action (Chen & Davalos, 2012)

Complete adhesive connection between top flange of the stringer and bottom plate of the FRP deck made a smooth intersection of the strain between stringer and FRP deck. The degree to which the FRP deck contributes to the composite action is calculated based on the upward shift of the neutral axis. The shift of the neutral axis is obtained by the results of the analysis in finite

element model for the middle of the span where maximum moment is acting. Section 5.1.1, 5.1.2 and 5.1.3 studies the composite behaviour and the upshift of neutral axis when type 3 configuration is used for the three decks ASSET, Duraspan and Ecosafe respectively.

### 5.1.1. ASSET Deck

The calculated axial strains in the cross-sections at midspan when ASSET deck is applied are
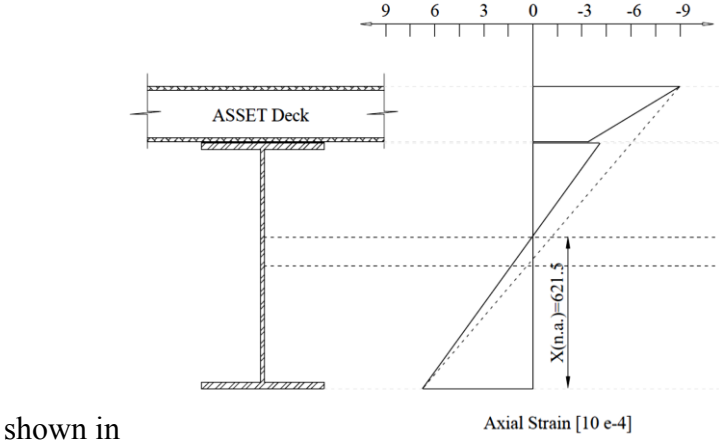


shown in

Figure 5-3 and Figure 5-4 under ULS and SLS loading respectively. Both figures show the neutral axis (N.A.) of the girder being located above the girder's mid-depth, thus indicating some level of composite action between the girder and FRP deck. The upward shift of the neutral axis is calculated 612.5 mm under ULS loading and 625.5 mm under SLS loading, shifting 112.5 mm and 125.5 mm from the mid cross section of the steel girder.
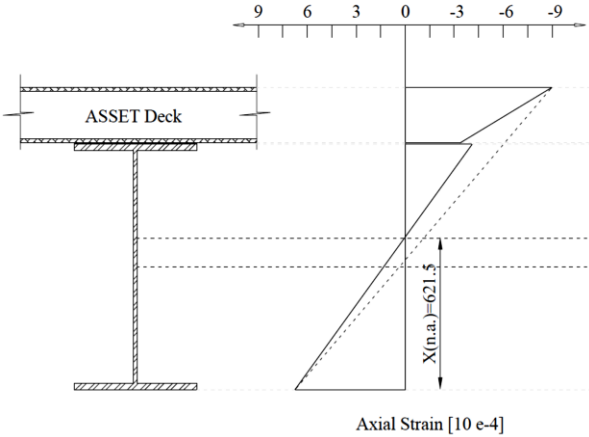


Figure 5-3 Strains at mid-span (cross section 1-1) under ULS loads

130
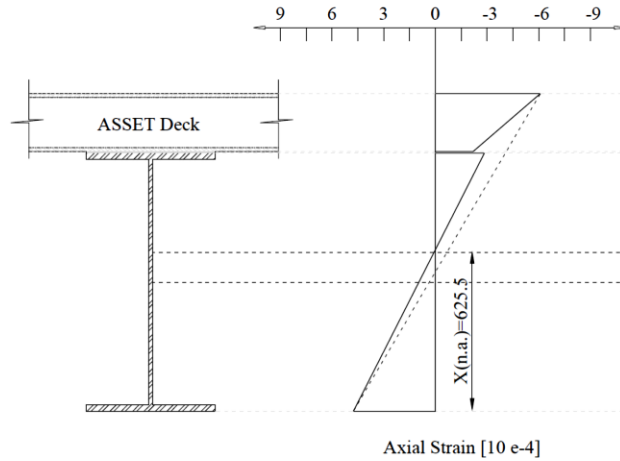
Figure 5-4 Strains at mid-span (cross section 1-1) under SLS loads

## 5.1.2. Duraspan Deck

The calculated axial strains in the cross-sections at midspan when Duraspan deck is applied are shown in Figure 5-5 and Figure 5-6 under ULS and SLS loading respectively. Both figures show the neutral axis of the girder being located above the girder's mid-depth, thus indicating some level of composite action between the girder and FRP deck. In Duraspan deck case the transition between the girder and FRP deck is smoother than for the case of ASSET deck. However the upward shift of neutral axis is lower. The upward shift of the neutral axis is calculated as 608.5 mm for both ULS and SLS loading, shifting 108.5 mm higher from the mid cross section of the steel girder.
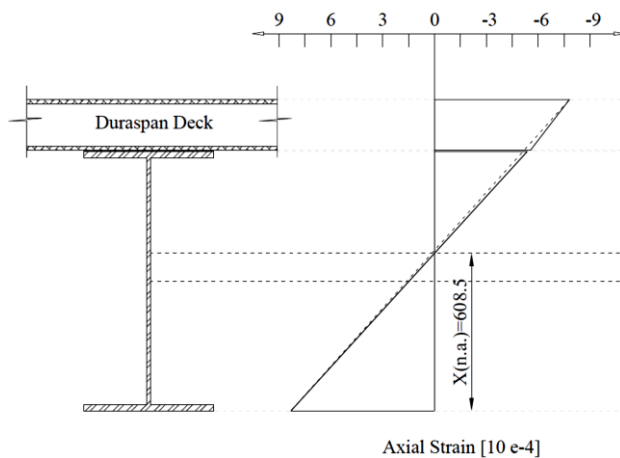


Figure 5-5 Strains at mid-span (cross section 1-1) under ULS loads

131
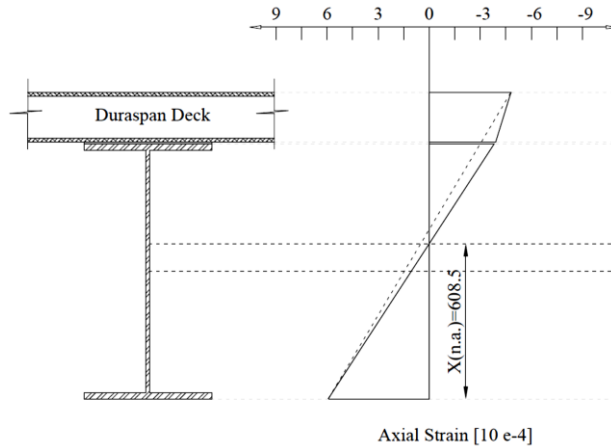
Figure 5-6 Strains at mid-span (cross section 1-1) under SLS loads

### 5.1.3. Ecosafe Deck

The calculated axial strains in the cross-sections at midspan when Ecosafe deck is applied are shown in Figure 5-7 and Figure 5-8 under ULS and SLS loading respectively. Both figures show the neutral axis of the girder being located above the girder's mid-depth, thus indicating some level of composite action between the girder, adhesive and FRP deck. The upward shift of the neutral axis is calculated as 715 mm under ULS loading and 725 mm under SLS loading, shifting 215 mm and 225 mm higher from the mid cross section of the steel girder.
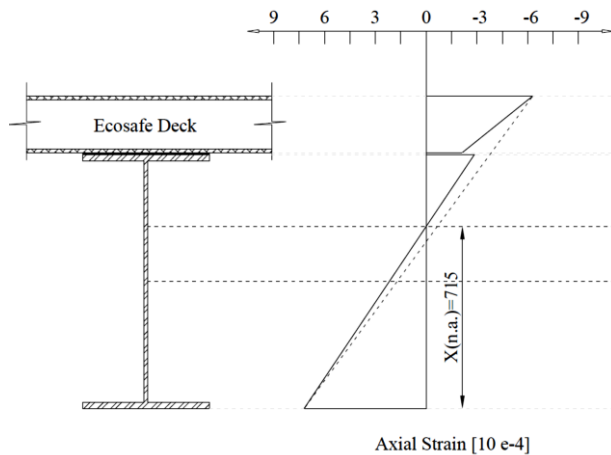


Figure 5-7 Strains at mid-span (cross section 1-1) under ULS loads
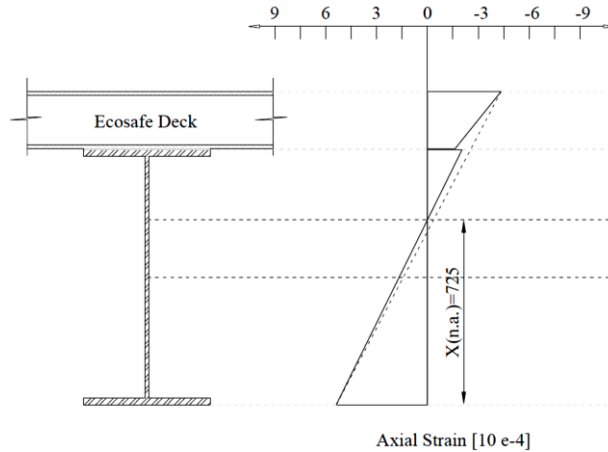
Figure 5-8 Strains at mid-span (cross section 1-1) under SLS loads

## 5.2.Effective width of the deck

In a composite deck-girder system, the effective width of the deck is the portion of the deck assumed to be contributing to the flexural capacity of the longitudinal girder through the development of an assumed uniform longitudinal stress field that serves as an analog for the actual nonlinear stress field across the deck width. Such an approach is adopted as a simplification allowing for the neglect of the actual "shear lag" in the deck plate during flexure. The deck is engaged by providing interfacial continuity between the deck and stringers through the use of adhesive or shear connectors. The width of deck that may be engaged in flexure must be evaluated to optimize the design of the longitudinal girder system. In new construction using FRP decks, many demonstration projects have not relied on composite action between the deck and girders.  Nonetheless, shear connectors and adhesive bonding have been provided in all existing applications, and significant composite action under service loads has been observed during field testing as we have already talked during the literature research.

Based on the upward shift in the calculated steel girder neutral axis location, it is possible to compute the level of assistance the FRP deck (effective width) provides in resisting the internal moments need to equilibrate the loading conditions. Using the approach presented at (Keelor, Luo, Earls, C, & Yulismana, 2004) it is possible to back-calculate the FRP effective compression flange width using standard transformed section properties related to the modular ratio of steel to adhesive or grout (in case of shear studs) and FRP deck. This procedure and the related tables are

133

presented in Appendix E. Moreover, the transverse axial strain distribution is provided to evaluate the effective width. Section 5.2.1, 5.2.2 and 5.2.3 provide the relevant information when ASSET, Duraspan and Ecosafe deck are used.

### 5.2.1. ASSET Deck

The effective width of ASSET deck are calculated when the bridge is loaded under ULS and SLS service by means of finite element analysis. This value is determined approximately 2.8 m (ULS) and 2.9 m (SLS) as shown in Figure 5-9 and Figure 5-10 respectively. Figure 5-11 shows the axial strains measured from finite element modeling. It is clear from the figure that the same result is achieved for the effective width of the flange. In case the whole width of deck would work compositely with the girders this value would be 3.2175 m. This means that in the case of ASSET deck application, approximately 87% of the deck works compositely with the girders.
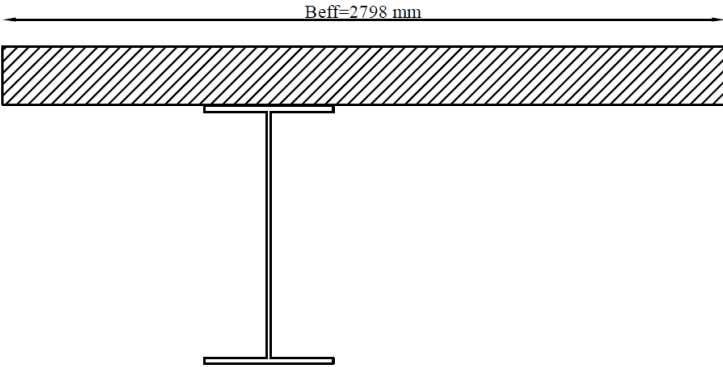


Figure 5-9 Effective width of ASSET deck under ULS loads
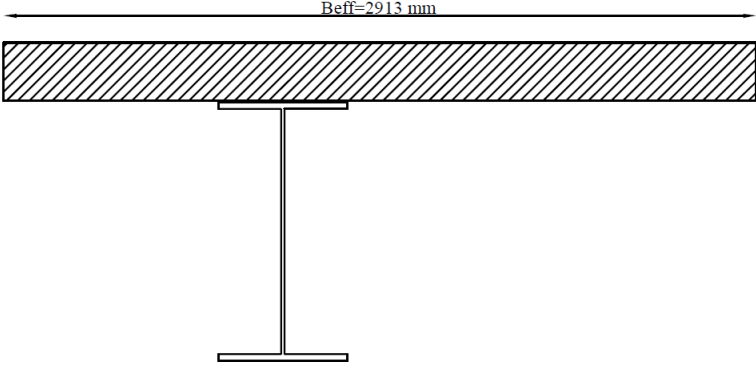


Figure 5-10 Effective width of ASSET deck under SLS loads

134
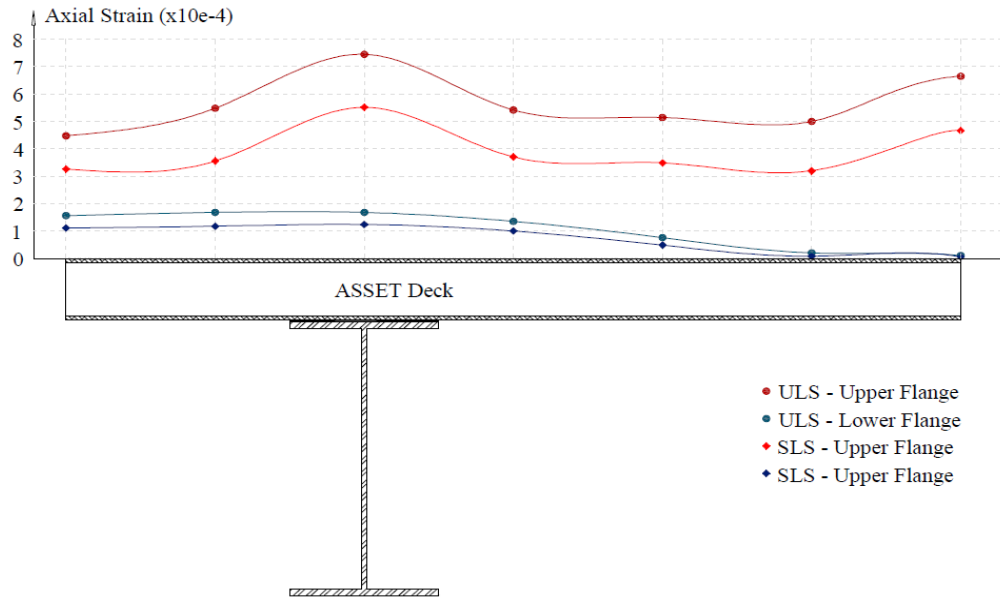
Figure 5-11Effective width: Axial strain and fitted parabolic curves

## 5.2.2. Duraspan Deck

The same procedure as discussed in section 5.2.1 is used in calculating the effective width when Duraspan deck is applied. For both service loadings, ULS and SLS, the effective width is calculated 2.49 m as shown in Figure 5-12 and Figure 5-13. This means that 77% of the deck works compositely with the steel girders.
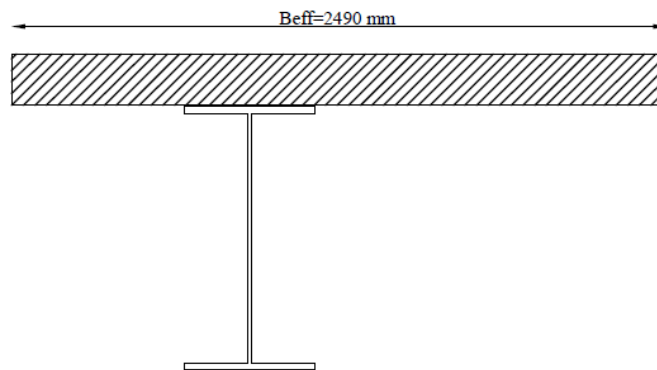


Figure 5-12 Effective width of Duraspan deck under ULS loads

135
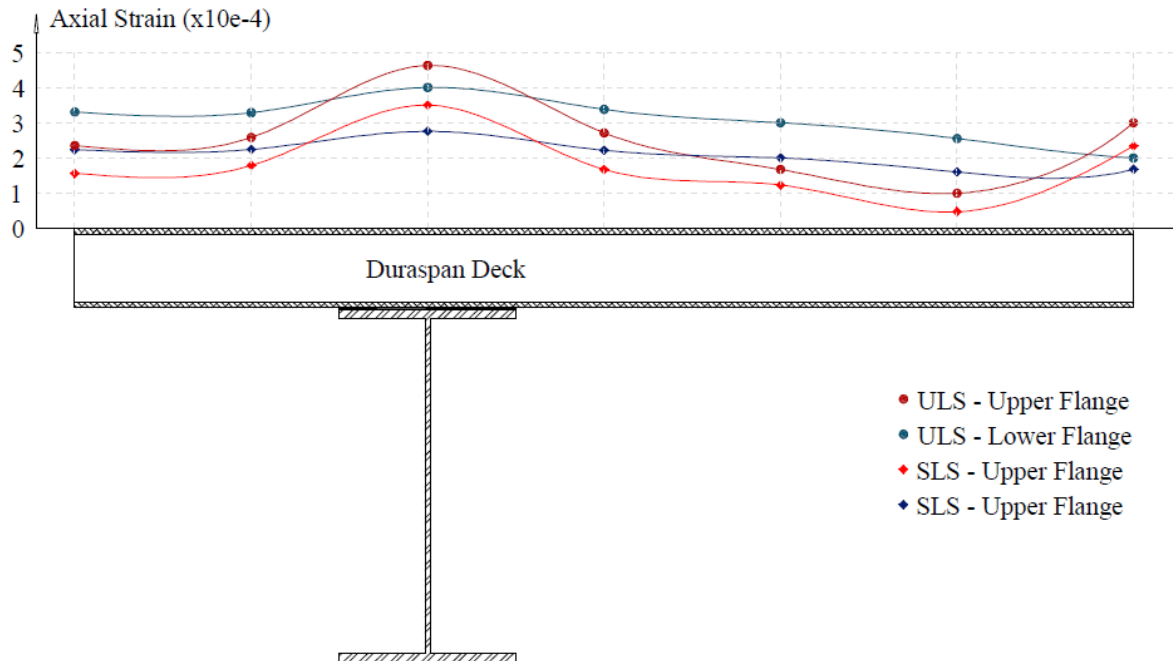
Figure 5-13Effective width: Axial strain and fitted parabolic curves

### 5.2.3. Ecosafe Deck

When Ecosafe deck is applied the neutral axis has a higher upward shift than for the two other decks. As shown in section 5.1.3 the N.A. has a minimum value of 715 mm which means that the deck works 100% compositely with the steel girders (the calculated effective width according to Appendix E has a higher value than 3.1425m). The same results can be seen in Figure 5-14.
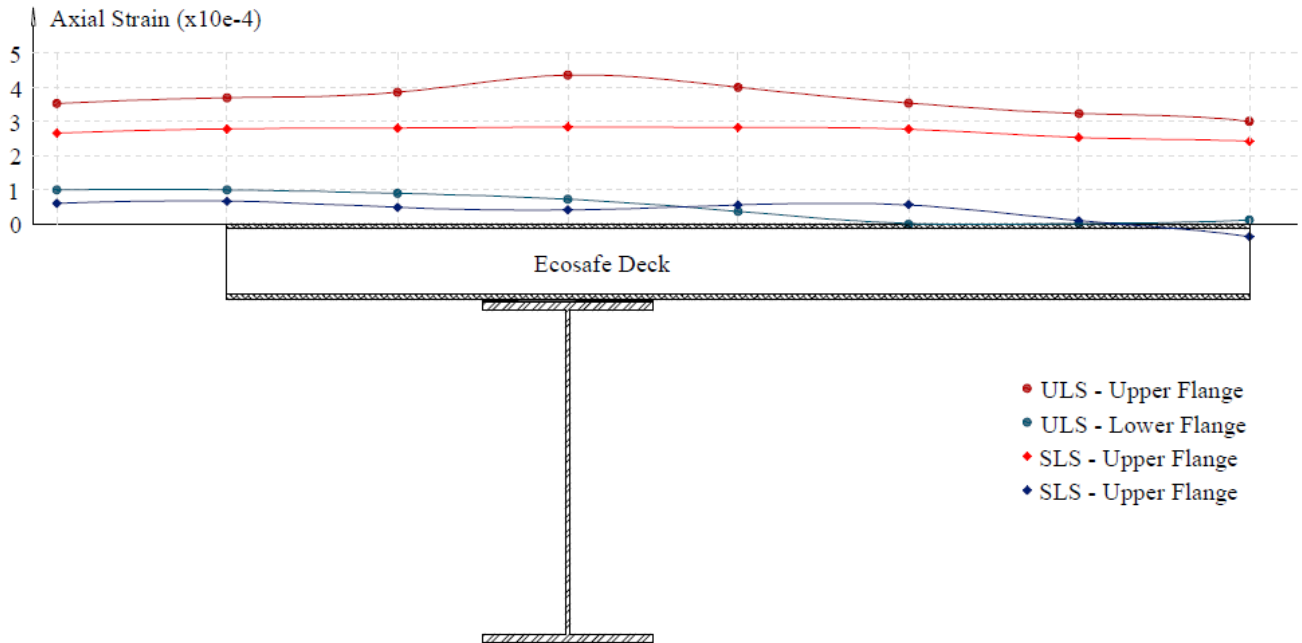
Figure 5-14 Effective width: Axial strain and fitted parabolic curves

## 5.3. Shear Studs Application

Another way to achieve composite action is by joining the FRP deck with the steel girders using shear studs connectors. (Righman J. , 2002) and (Turner, Harries, Petrou, & Rizos, 2002) presented a typical configuration of joining FRP decks with steel girders by means of shear connectors. This is illustrated in Figure 5-15 when Duraspan deck is applied.

In this study the same configuration will be employed for ASSET deck with the only difference that the distribution of shear studs will be 295 mm. This has to do with the center-to-center distance between the inclined webs of the FRP deck, since the shear stud should be placed as shown in Figure 5-15. For each of the decks two case scenarios are studied, when the shear studs distribution spans 305 mm (295 mm in case of ASSET deck) and 610 mm (595 mm in case of ASSET deck).

137
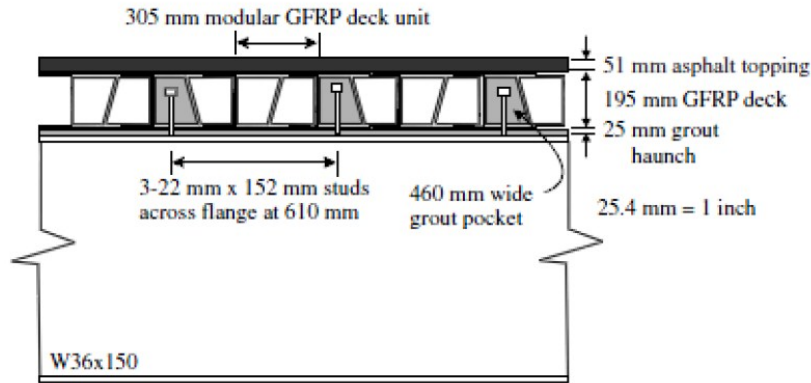
Figure 5-15 Shear stud connection (Turner, Harries, Petrou, & Rizos, 2002)

### 5.3.1. Duraspan Deck

The results retrieved the finite element program when shear studs are used as the steel-to-girder connection are shown in Table 5-1 for the case of Duraspan deck. Comparison of stresses, both steel structure and FRP deck, between the two case scenarios, adhesive bonding and shear studs, are presented. The results show that the stresses of the steel structure when bonded adhesively are lower although they differ only by a low value (2%). Almost the same difference can be observed in case the distribution of shear studs changes from 610 to 305 mm. Regarding the stresses of FRP deck almost the same value can be observed for longitudinal stresses. Contrary, the transverse stresses increase as twice when shear studs are used due to higher stress concentrations provided from shear studs. Appendix F, section 0 present the stresses of the bottom flange of Duraspan deck when shear studs are used.

Appendix D, section 0 shows the measured axial strains under ultimate limit state. For the case scenarios, shear studs spanning 295 and 605 mm, it is observed that the upward shift of neutral axis is 613 and 615 mm respectively. This mean that the effective width of the deck is 2.507 and 2.564 m correspondingly, acting 79 % compositely with the steel girder. The procedure is shown in Appendix E, section 0.

Table 5-1 Stress comparison (Duraspan deck): Adhesive bonding and shear studs

| Duraspan Deck | | | Adhesive | Shear Studs | |
|---|---|---|---|---|---|
| | | | | 610 mm | 305 mm |
| | | | | | |
| Steel Structure | | [Mpa] | 298 | 311 | 304 |
| | | | | | |
| FRP | S11 | [Mpa] | 113 | 116 | 115 |
| | S22 | [Mpa] | 46 | 92 | 84 |

## 5.3.2. ASSET Deck

Similarly to the case of Duraspan deck application, there is a very small difference in values of steel stresses between the case of adhesive bonding and shear studs application. The longitudinal stresses achieve a higher value when shear studs are used, but this increase is more significant when the shear studs span double the center-to-center distance.

Table 5-2 Stress comparison (ASSET deck): Adhesive bonding and shear studs

| ASSET Deck | | | Adhesive | Shear Studs | |
|---|---|---|---|---|---|
| | | | | 595 mm | 295 mm |
| | | | | | |
| Steel Structure | | [Mpa] | 282 | 284 | 283 |
| | | | | | |
| FRP | S11 | [Mpa] | 66 | 105 | 76 |
| | S22 | [Mpa] | 26 | 37 | 37 |

Appendix D, section 0 shows the measured axial strains under ultimate limit state. For both case scenarios, shear studs spanning 295 and 595 mm, it is observed that the upward shift of neutral axis is 626 mm. This mean that the effective width of the deck is 2.82 m, acting 89 % compositely with the steel girder. The procedure is shown in Appendix E, section 0.

Appendix F, section 0 present the stresses of the bottom flange of ASSET deck when shear studs are used. It is observed that the stress distribution when shear studs are applied has more concentrated areas than the case of adhesive bonding.

## 5.4. Load Distribution

The load distribution throughout the bridge deck and the vehicle-induced impact on bridges, have been used worldwide in bridge design, are of primary importance in the design of bridges (Zhang & Cai, 2007). The characteristics of the FRP decks such as mass, stiffness, and damping factor are significantly different from those of the traditional concrete and steel decks, which could result in a different performance of FRP deck bridges from traditional bridges. Lower stresses are achieved by aligning the pultrusion direction of the FRP deck perpendicular to the traffic direction: the load is distributed more effectively to the adjacent girders. Moreover, when the most heavily loaded girder is deflected the neighboring girders will work together in withstanding the forces due to transversal stiffness of the deck in the pultrusion direction.

To investigate the load distribution of Wilhelminabrug through finite element analysis, six passes of vehicle (see Figure 5-16) with center-to-center distance of 1 m are positioned from the beginning of the kerb area to the center width of the deck (since the deck is symmetric only half of it is loaded). The selected load is 300 KN distributed over 4 square surfaces 400x400 mm.
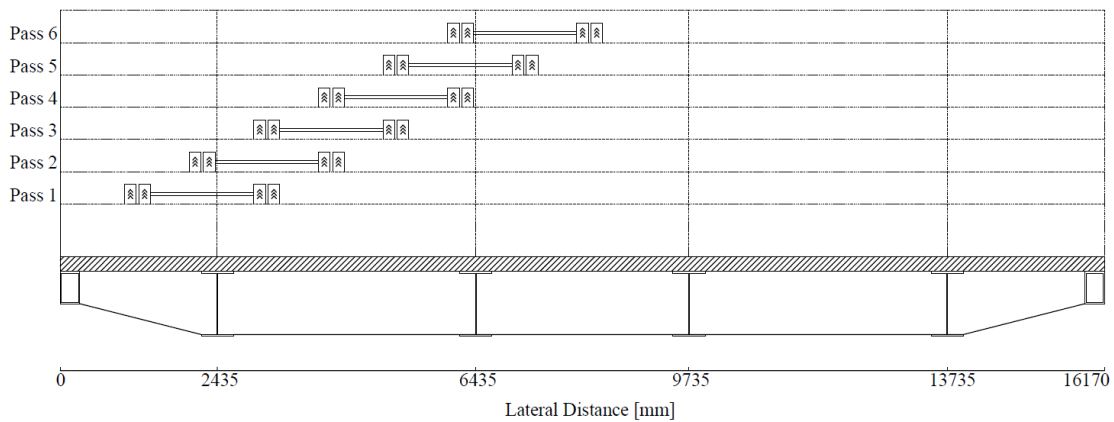


Figure 5-16 Lateral load position

From finite element analysis are measured the stresses of each deck. The lateral distribution factor (LDF) values, according to (Zhang & Cai, 2007), are equal to the actual stress on a particular girder dived by the sum of the stresses n all the girders as:

$$DF_i = \frac{\sigma_{girder-i}}{\sum_{j=1}^{6} \sigma_{girder-j}}$$

(Zhang & Cai, 2007) investigated the lateral distribution of hybrid bridge and compared the values of strain gages of field work with finite element models of bridge, both with composite and non-composite action. It was concluded that FEM software are reliable in such studies.

### 5.4.1. ASSET Deck

For each position of loading (1-6) the distribution factors are calculated and plotted as shown in Figure 5-17. The calculated values are presented in Appendix F, section G from Table G-1 to Table G-3 for each of three decks. In addition, the stress distribution is plotted in the graph as shown in Figure 5-18. As it can be observed the maximum value of LDF for interior girder is achieved for the girder number 2[11] under load position 1, with the value 0.2843. The minimum value is obtained under the same loading condition for girder number 4, with the value 0.141. Regarding the exterior girders, the maximum and minimum values are 0.1582 and 0.079 respectively for girder 1 and 6 under load position 1.
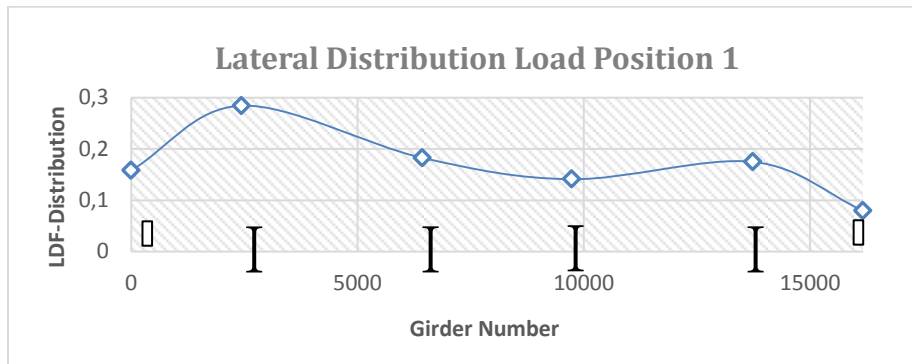


(a)
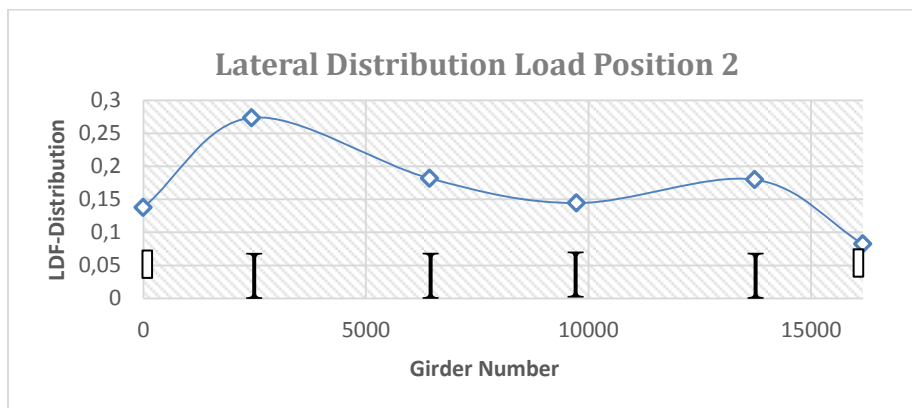


(b)

---

[11] Numbering is selected from left to right.
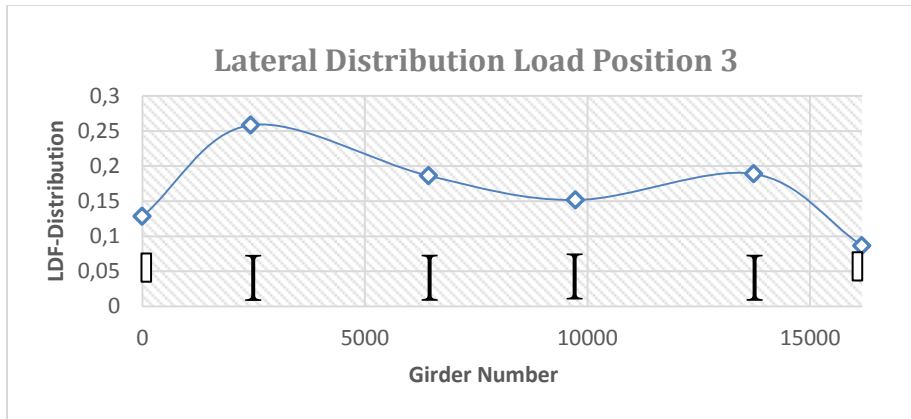
(c)
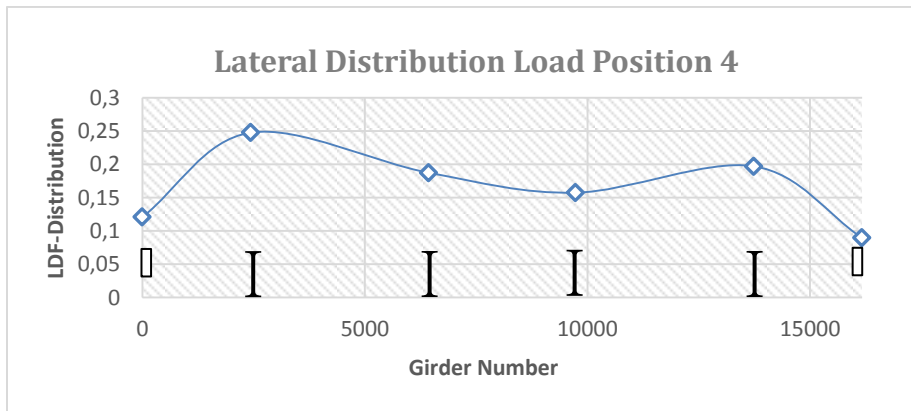


(d)
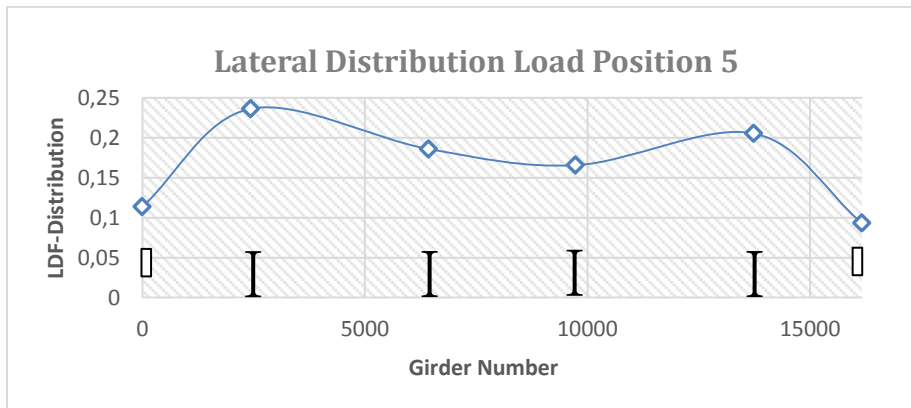


(e)
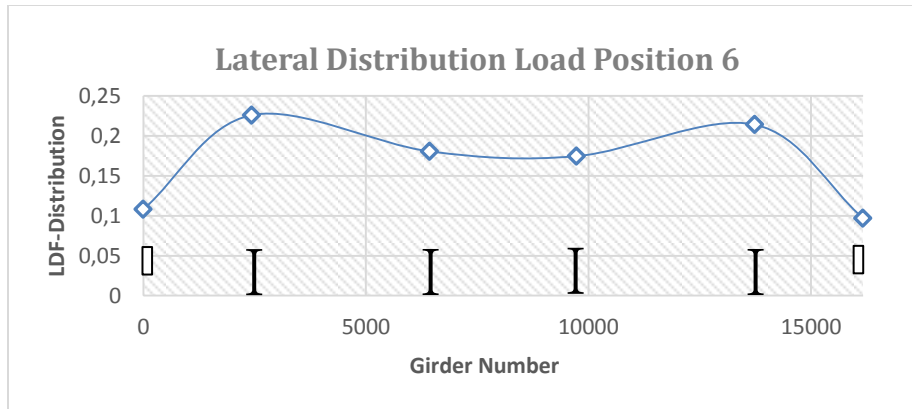
(f)

Figure 5-17 Load distribution results when ASSET deck is applied
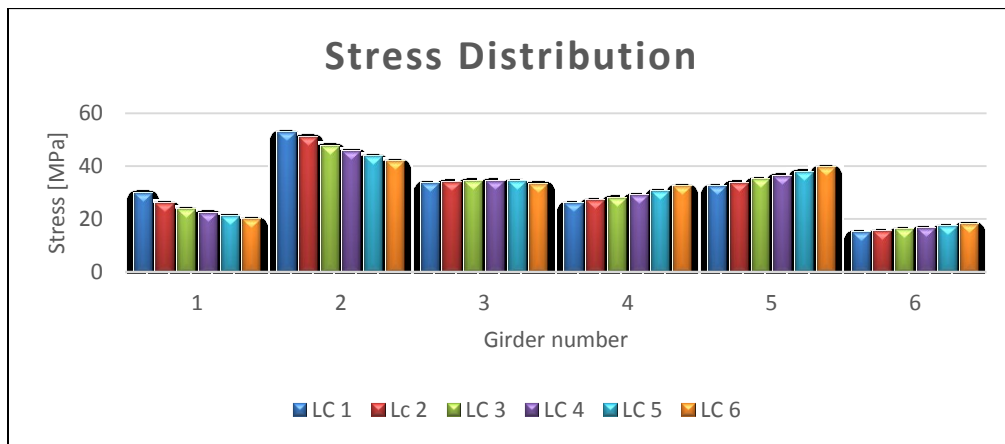


Figure 5-18 Stress distribution when ASSET deck is applied[12]

---

[12] LC- Load Case

### 5.4.2. Duraspan Deck

For each position of loading (1-6) the distribution factors are calculated and plotted as shown in Figure 5-19. In addition the stress distribution is plotted in the graph as shown in Figure 5-20. As it can be observed the maximum value of LDF for interior girder is obtained for the girder number 2 under load position 1, with the value 0.2825. The minimum value is found under the same loading condition for girder number 4, with the value 0.1374. Regarding the exterior girders, the maximum and minimum values are 0.1542 and 0.077 respectively for girder 1 and 6 under load condition 1.
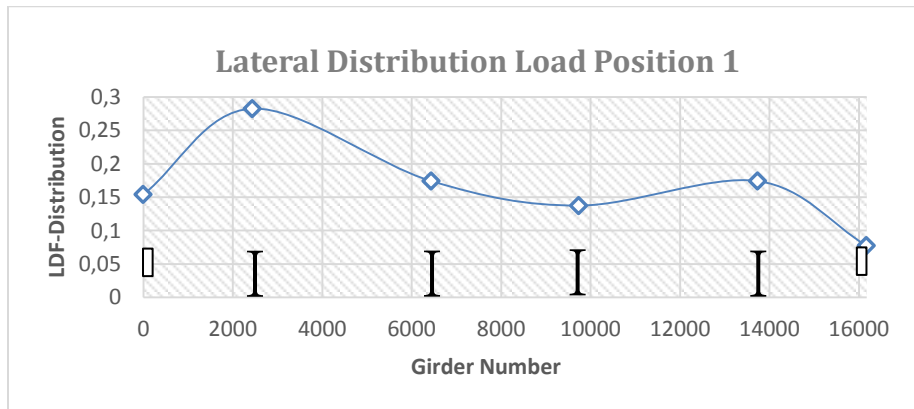


(a)
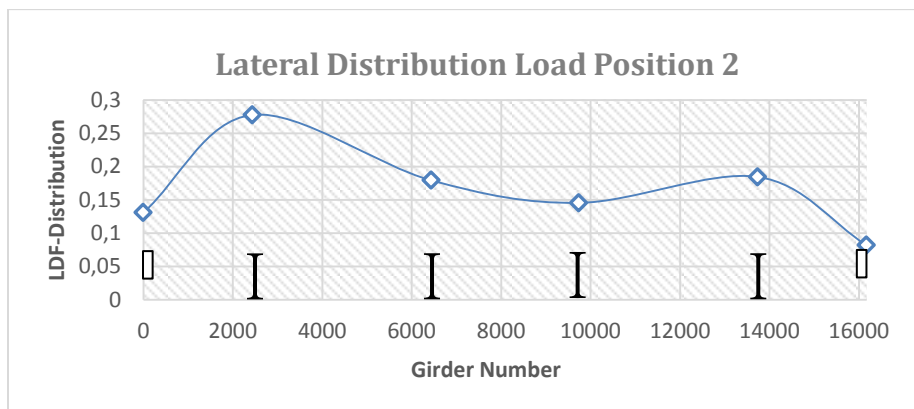


(b)
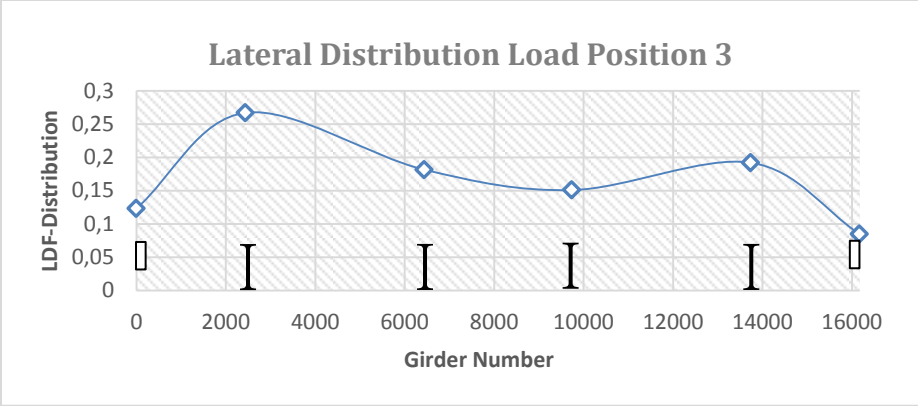
(c)
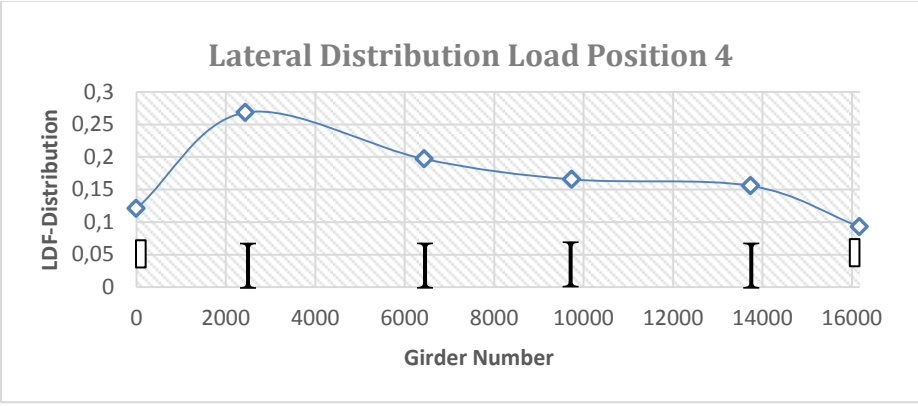


(d)
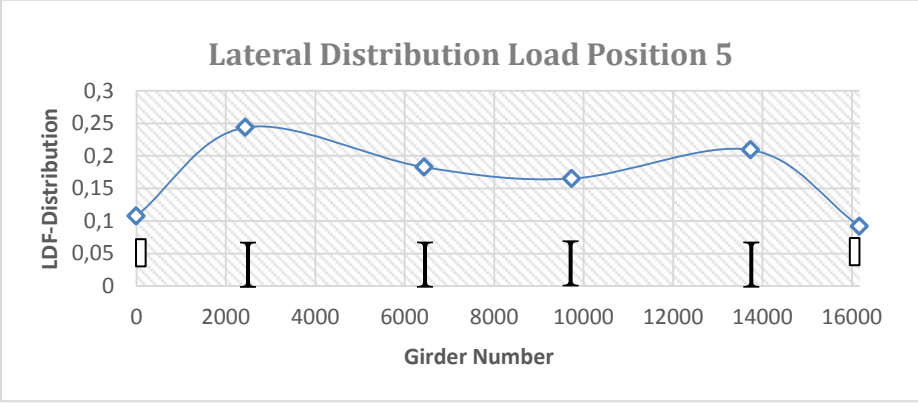


(e)
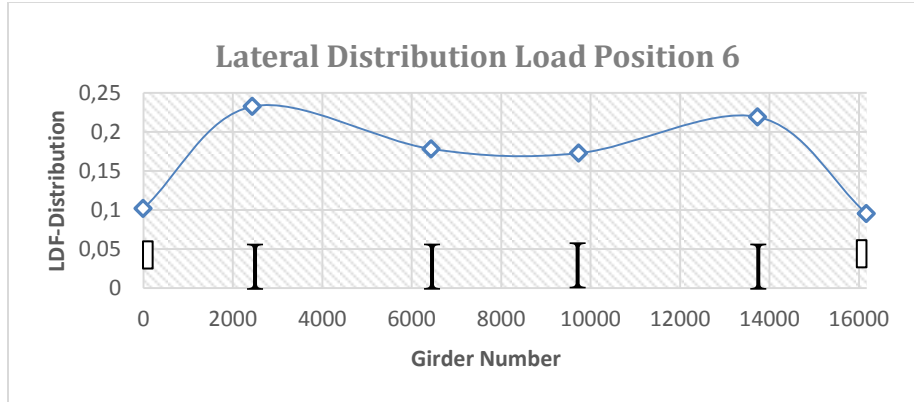
(f)

Figure 5-19 Load distribution results when ASSET deck is applied
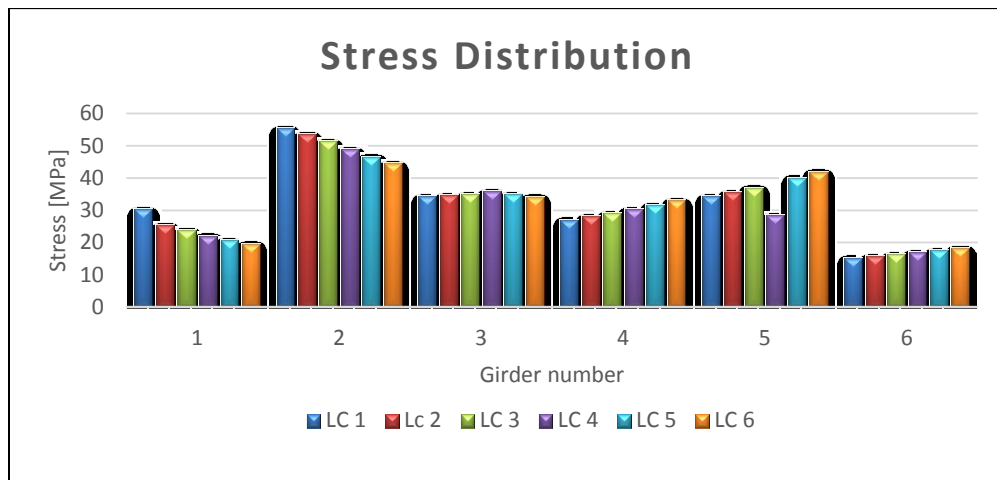


Figure 5-20 Stress distribution when ASSET deck is applied

### 5.4.3. Ecosafe Deck

For each position of loading (1-6) the distribution factors are calculated and plotted as shown in Figure 5-21. In addition the stress distribution is plotted in the graph as shown in Figure 5-22. As it can be observed the maximum value of LDF for interior girder is achieved for the girder number 2 under load position 1, with the value 0.2706. The minimum value is obtained under the same loading condition for girder number 4, with the value 0.1445. Regarding the exterior girders, the maximum and minimum values are 0.1517 and 0.081 respectively for girder 1 and 6 under load condition 1.

146
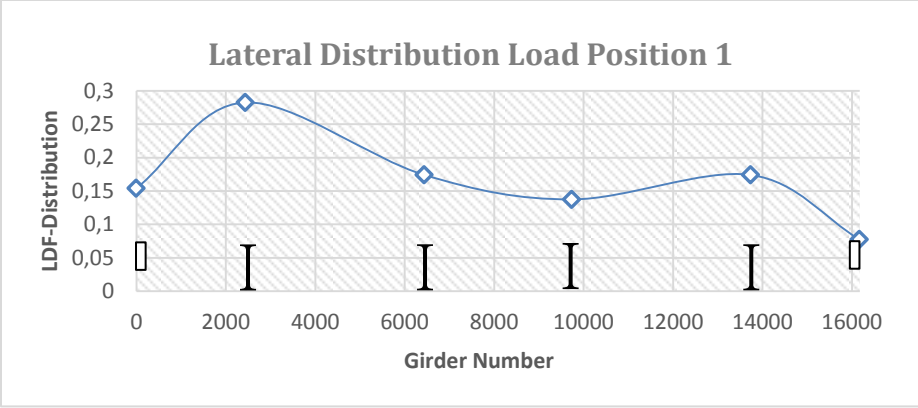
(a)
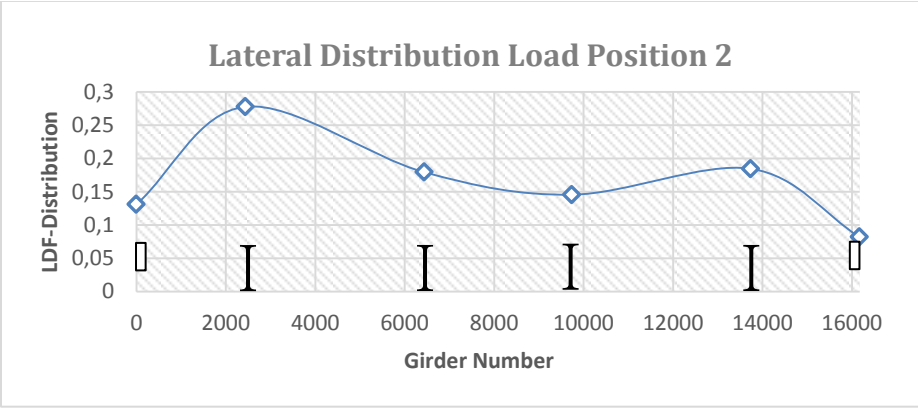


(b)
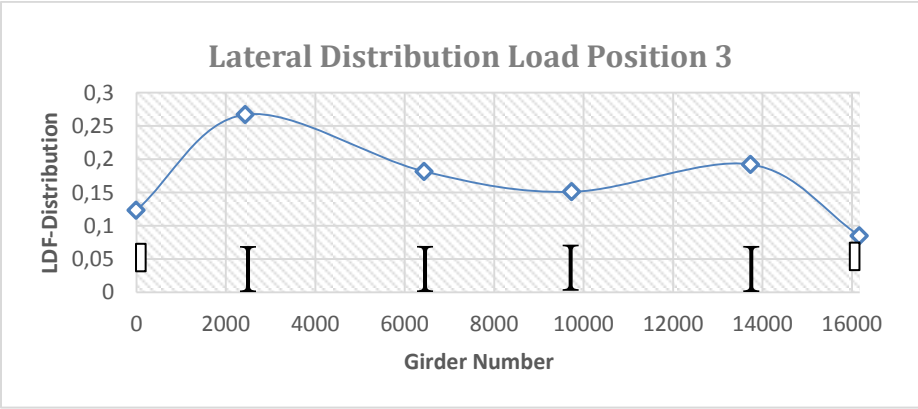


(c)
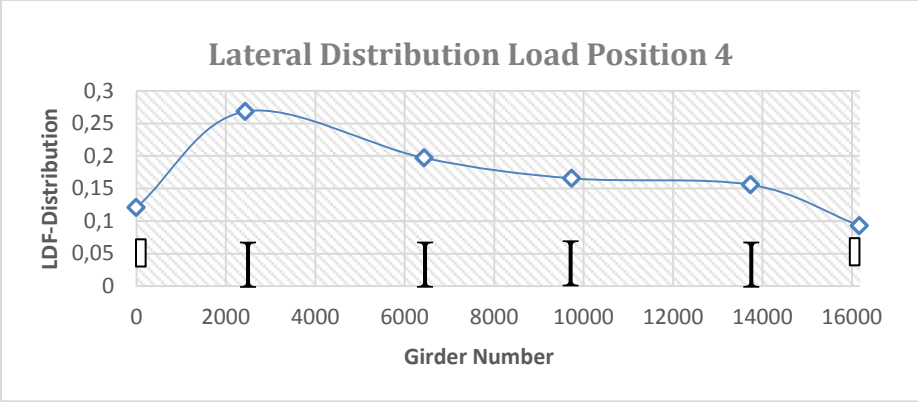
(d)
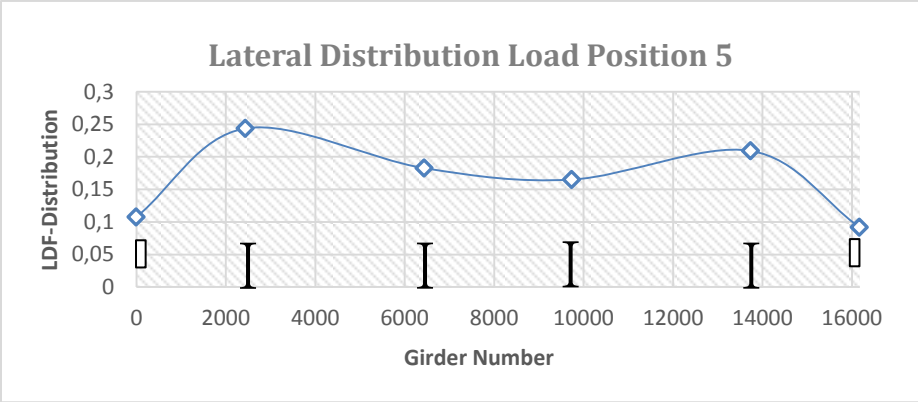


(e)
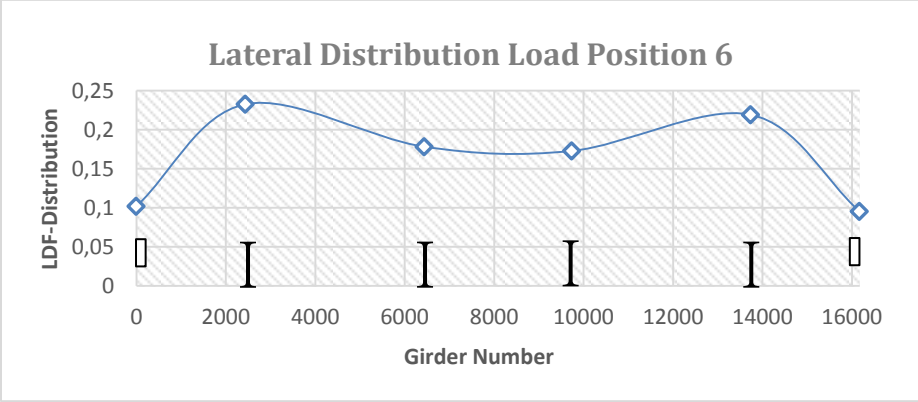


(f)

Figure 5-21 Load distribution results when ASSET deck is applied
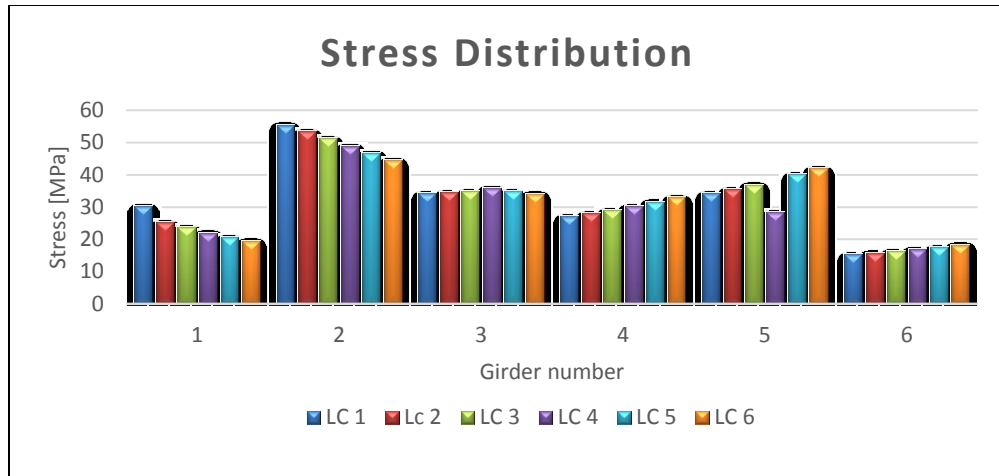
Figure 5-22 Stress distribution when ASSET deck is applied

## 5.5.Summary of results and discussion

*The composite action* level of the bonded connection deck-girder was verified using the strain distribution which was calculated from FEM analysis. Prediction of the composite girders behavior assumed composite action between all components of the cross-sections for both deck systems. As the numerical studies showed, the adhesively-bonded joints between bridge decks and steel girders were sufficiently stiff and resistant to guarantee composite action between the top steel flanges and lower deck face panels at all load levels up to failure. The upward shift under ultimate limit state equals the value of 612.5 mm, 608.5 mm and 715 mm respectively when ASSET, Duraspan and Ecosafe deck are used as shown in Figure 5-23. At ULS the panels in case of Ecosafe and ASSET deck showed decrease participation in composite behaviour. Contrary, in case of Duraspan deck almost the same behaviour as at SLS was observed.

*The effective width* of the FRP decks was calculated based on the upward shift of the neutral axis of steel girder and based on the axial strain distribution. Consistent with the much higher in-plane shear stiffness of the FRP decks it was possible to observe the decrease in participation in composite action. According to the findings, Ecosafe deck fully participated as top chord over the whole width; ASSET deck participated 87% and Duraspan 77%.

149
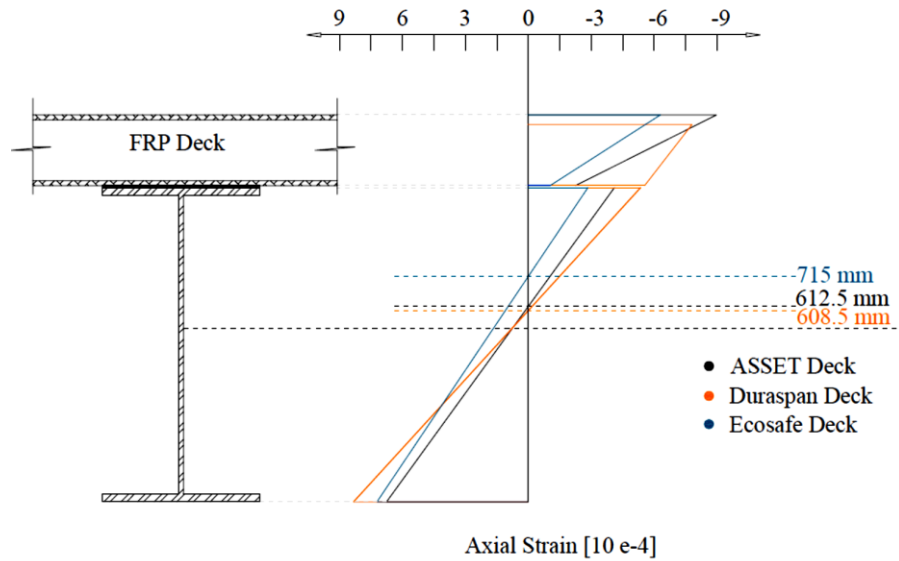
Figure 5-23 Comparison of axial strain distributions in the mid-span cross-section at ULS

*Shear studs connections* was investigated as another way to achieve composite behavior between FRP decks and steel girders. It was observed that a very small difference could be spotted in the upward shift of neutral axis. Moreover, the superstructure stresses were almost identical. The longitudinal stresses remain the same while the transverse stresses differs almost significantly. However, it can concluded that in case of adhesive bonding a smoother transition of stresses in the deck could be detected.

Lastly, *the lateral distribution* of the FRP decks was investigated and the maximum and minimum respective values are plotted from Table 5-3 to Table 5-5. A comparison of the lateral distribution factor along the width of the deck is shown in Figure 5-24. It can be concluded that the maximum LDF is obtained when ASSET deck is used and minimum value of LDF when Ecosafe deck is used.

Table 5-3 Maximum and minimum values of lateral distribution factor

|  | ASSET | | Duraspan | | Ecosafe | |
|---|---|---|---|---|---|---|
|  | Interior | Exterior | Interior | Exterior | Interior | Exterior |
| Max. DF | 0.2843 | 0.1528 | 0.2825 | 0.1542 | 0.2706 | 0.1517 |
| Min. DF | 0.141 | 0.079 | 0.1374 | 0.077 | 0.1445 | 0.081 |

150

Table 5-4 Maximum load distribution factor for three decks
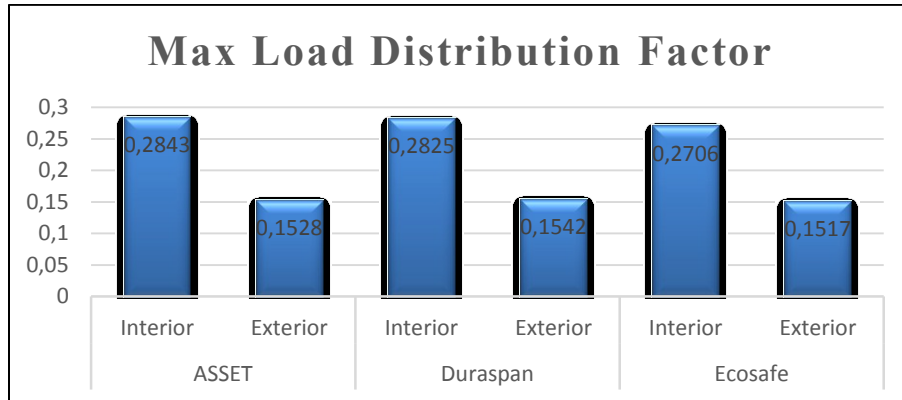


Table 5-5 Minimum load distribution factor for three decks
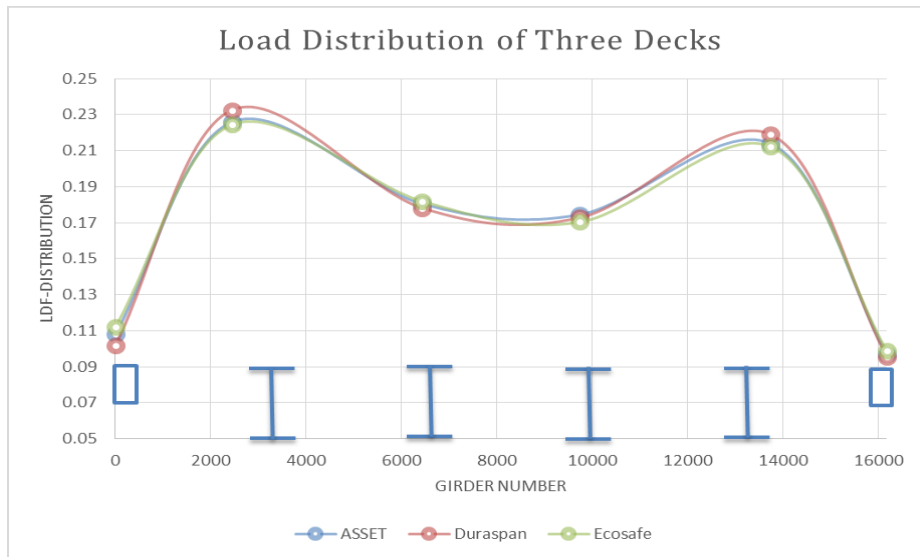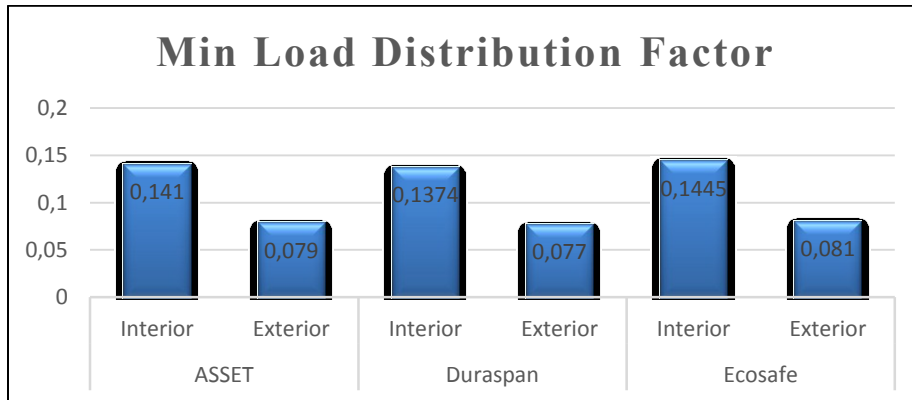




Figure 5-24 Comparison of LDF for the three decks under load position 6

151

# 6. Fatigue Assessment

This chapter is dedicated to the fatigue assessment of Wilhelminabrug. Eurocode and the national Dutch code will be used as guidance to check the fatigue requirement for the superstructure and the deck.

## 6.1. What is fatigue?

It is a well-known fact that if the maximum load acting on a structure becomes higher than its material yield strength limit, a failure is assumed in the structure. However, in a structure that undergoes fluctuating loads, even if they are well below the material elastic limit, a failure can be expected after many loading cycles. The latter situation, which is a result of accumulated damages in the material, is known as fatigue failure, the mechanism whereby the cracks grow in a structure (Kolstein, 2007). In other words, static loading of a ductile material which increases from zero to a maximum, will cause large deformations and failure of the structure occurs after a single load application with large plastic deformation. Whereas, when the same material is repeatedly loaded to stresses occurring below the elastic limit, fatigue failure may happen after several hundred or million cycles of load application without any large plastic deformation.

## 6.2. Fatigue loading

As mentioned before, structures that are subjected to fatigue loading, experience fluctuated loads during their lifetime. Generally, the stress history of such structures varies constantly. However, the simplest stress history that can be assumed for a structure is a constant amplitude cyclic stress, as illustrated in Figure 6-1. This type of loading is usually experienced by the specimens tested in the laboratories as it doesn't require advanced testing equipment. A constant amplitude loaded structure, is subjected to a maximum stress ($\sigma_{max}$) and a minimum stress ($\sigma_{min}$). Thus, the stress range and the mean stress can be expressed as:

$$\Delta\sigma = \sigma_{max} - \sigma_{min}$$

$$\sigma_{mean} = \frac{\sigma_{max} + \sigma_{min}}{2}$$

Stress amplitude ($\sigma_{amp}$) is defined as half of the stress range, and hence it can be calculated as follows:

$$\sigma_a = \frac{\sigma_{max} - \sigma_{min}}{2}$$

Stress ratio, which implicitly represents the loading type, is defined as the ratio of the minimum to maximum stress:

$$R = \frac{\sigma_{min}}{\sigma_{max}}$$
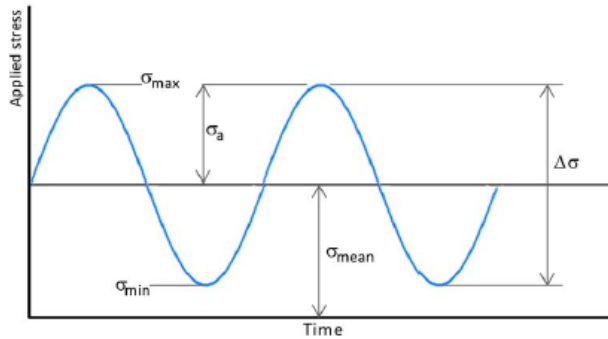


Figure 6-1 Constant amplitude loading
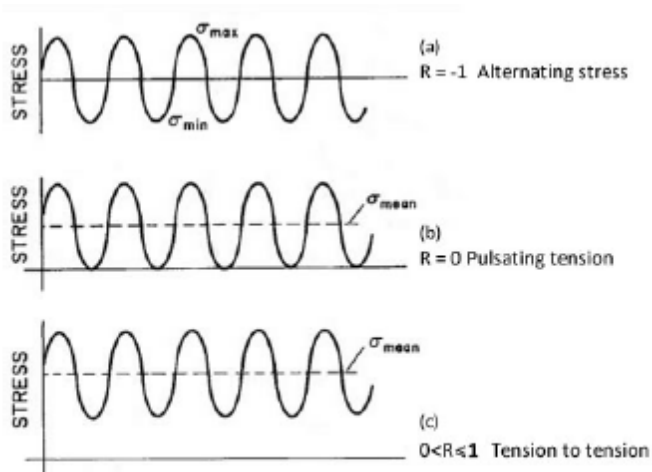


Figure 6-2 Different stress ratios for various loadings

As shown in Figure 6-2, R = -1 is followed by reversing the stress state from a compressive stress to an equal tensile stress, while $0 \le R \le 1$ corresponds to any fluctuation of stress from a minimum tensile to a maximum tensile load.

(a) *Variable amplitude loading*     (b) *Typical representation of a stress histogram*
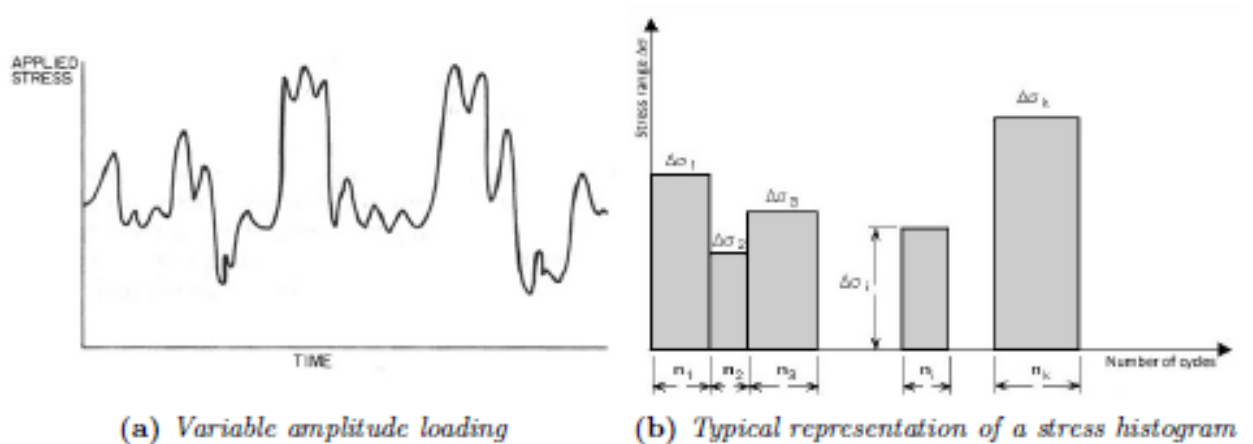
Figure 6-3 Variable amplitude loading and stress histogram as a simplification method of variable amplitude loaded structures

In general, the fatigue life depends mainly on the stress range ($\Delta\sigma$) so that a higher stress range would result in a lower fatigue life. Nevertheless, the constant amplitude loading is not a realistic loading pattern for real structures such as bridges, buildings or offshore platforms. The mentioned structures experience random sequence load histories through their life time. This loading pattern is called variable amplitude loading and cannot be represented by an analytical model. Figure 6-3 (a) shows an example of a variable amplitude loading which may be experienced by a structure. For such loadings, a stress histogram is usually used to simplify the problem. A stress histogram is a chart of separate blocks that defines the number of cycles that a constant stress range is repeated during the life time of the structure, see Figure 6-3 (b).

### 6.3. Nominal stress method

According to Eurocode the nominal stress method is sufficient to assess the fatigue life and the method is widely used. One major advantage with this method is the simplicity of how to determine the stresses for which the fatigue analysis was performed. The nominal stress method uses the nominal stress range, which corresponds directly to the applied load. Basically the method can be performed in two steps; calculation of stress in critical section and the determination of detail category from tables provided by codes and guidelines.

The detail category depends on which type of connection and what kind of load the member is experiencing, see Figure 3.4 for example of detail categories. The value of the detail category

154

corresponds to the value of stress variation that the connection can experience and fail due to fatigue after 2 million load cycles.

| Detail category | Constructional detail | | Description | Requirements |
|---|---|---|---|---|
| 36 | | | 13) Butt welds made from one side only. | 13) Without backing strip. |
| 71 | size effect for t>25mm: $k_s=(25/t)^{0.2}$ | (13) | 13) Butt welds made from one side only when full penetration checked by appropriate NDT. | |
| 71 | size effect for t>25mm: $k_s=(25/t)^{0.2}$ | (14) (15) >10mm ≤1/4 | With backing strip: 14) Transverse splice. 15) Transverse butt weld tapered in width or thickness with a slope ≤ ¼. Also valid for curved plates. | Details 14) and 15): Fillet welds attaching the backing strip to terminate ≥ 10 mm from the edges of the stressed plate. Tack welds inside the shape of butt welds. |

Figure 6-4 Example of detail category (EN 1993-1-9, 2005)

The detail categories are based on test results from a number of specimens with the identical connection type, which have been loaded until failure with varying stress variation. The resulting relation between stress variation (S) and number of cycles (N) before failure build the S-N curve, which can be seen in Figure 6-5.
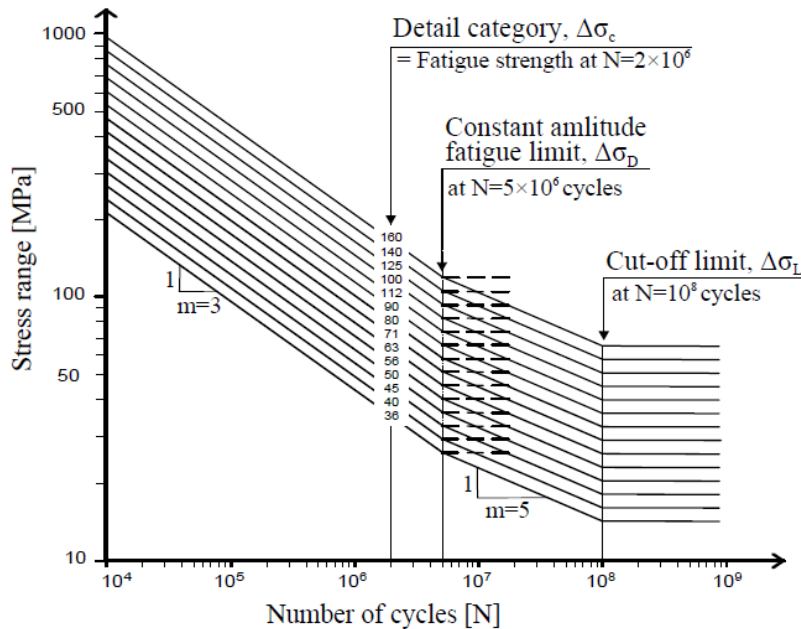


Figure 6-5 S-N curves of steel for normal stress range (EN 1993-1-9, 2005)

155

In Eurocode, EN 1993-1-9, fatigue strength for construction details in steel structures is given by the graph show in Figure 6-5. For normal stress induced fatigue failure modes the characteristics of the S-N relation is defined by the stress value corresponding to failure after 5 million cycles ($\Delta\sigma_D$) and 100 million cycles ($\Delta\sigma_L$). For various detail categories, these values are given as empirical determined values, along with the value $\Delta\sigma_C$ which corresponds to failure after 2 million cycles of constant amplitude. The lower stress limit, corresponding to 100 million cycles, is a "cut-off limit", i.e. cycles with stress range below this limit does not affect the fatigue. The values of the characteristic limits are established from the construction details corresponding $\Delta\sigma_C$ -value as given in equations below.

$$\Delta\sigma_D = \left(\frac{2}{5}\right)^{1/3} \Delta\sigma_C$$

$$\Delta\sigma_L = \left(\frac{5}{100}\right)^{1/5} \Delta\sigma_D$$

These limits are used when identifying on which slope of the S-N relation the stress ranges obtained from the stress cycle counting methods are acting. With the help of the S-N relations given in Figure 6-5 it is possible to establish the amount of cycles until failure for each identified stress range. The S-N relations for steel construction details with normal stress as the governing failure stress can be expressed in equation below.

$$\Delta\sigma_R^m N_R = \Delta\sigma_C^m 5x10^6 \qquad \text{with } m = 3 \text{ for } N \leq 5\cdot10^6$$

$$\Delta\sigma_R^m N_R = \Delta\sigma_C^m 5x10^6 \qquad \text{with } m = 5 \text{ for } 5\cdot10^6 \leq N \leq 10^8$$

The S-N relation should also include partial factors for the fatigue load model and fatigue strength, $\gamma_{Ff}$ and $\gamma_{Mf}$ where;

$\gamma_{Ff}$ is partial factor for equivalent constant amplitude stress ranges

$\gamma_{Mf}$ partial factor for fatigue strength

When these partial factors are introduced the expressions given in above change to:

$$N_{Ri} = 2x10^6 \left(\frac{\Delta\sigma_C/\gamma_{Mf}}{\gamma_{Ff}\Delta\sigma_i}\right)^3 \qquad \text{if} \quad \gamma_{Mf}\Delta\sigma_i \geq \frac{\Delta\sigma_D}{\gamma_{Mf}}$$

$$N_{Ri} = 5x10^6 \left(\frac{\Delta\sigma_C/\gamma_{Mf}}{\gamma_{Ff}\Delta\sigma_i}\right)^5 \qquad \text{if} \quad \frac{\Delta\sigma_L}{\gamma_{Mf}} \leq \gamma_{Mf}\Delta\sigma_i < \frac{\Delta\sigma_D}{\gamma_{Mf}}$$

$$N_{Ri} = \infty \qquad \text{if} \quad \gamma_{Mf}\Delta\sigma_i < \frac{\Delta\sigma_L}{\gamma_{Mf}}$$

Where

$N_{Ri}$ is the number of cycles until failure with the current stress range $\Delta\sigma_i$ ,

$\Delta\sigma_i$ is the current stress range.

The total damage can be linearly summarized according to equation above. The criterion to be fulfilled is according to Palmgren-Miner's rule stating that the sum of all damages should be less than, or equal to, one.

$$D_{tot} = \sum D_i = \sum \frac{n_i}{N_i}$$

Where

$n_i$ is the number of cycles,

$N_i$ is the expected capacity in number of cycles until failure,

$D_i$ is the damage ratio.

### 6.4. Calculation of pressure device in the ballast

The pressure devise serves as a mechanism which applies a force in the ballast in order to avoid tensile stresses at the supports in case of movable bridges (see Figure 6-6). This force should be found by taking into account the worst situation including loadings from self-weight, wind and dynamic factors. The resulting stresses in the support should have a magnitude of 50-80 kN. The calculation is computing using standard Excel sheets provided by Iv-Infra Amsterdam. This procedure is presented in Appendix H and the resulting value of the force is 431 kN. This value should will be used for the successive fatigue check.
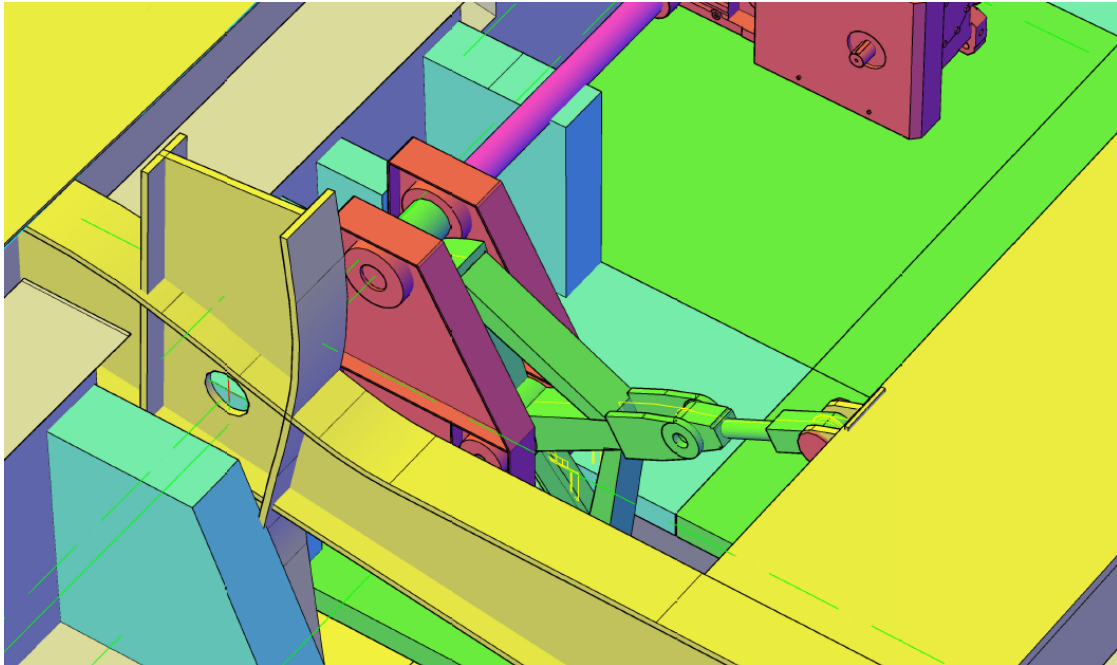
Figure 6-6 Pressure device

## 6.5. Fatigue check of ASSET Deck

As already discussed in the literature review the Eurocodes do not provide guidelines to assess the fatigue life of FRP decks. Contrary, the Dutch National Code (CUR-Aanbeveling 96, 2003) provides recommendation and guidelines to assess the fatigue life of FRP structures. According to the latter, Figure 6-7; Figure 6-8 and Table 6-1 show the fatigue load models.
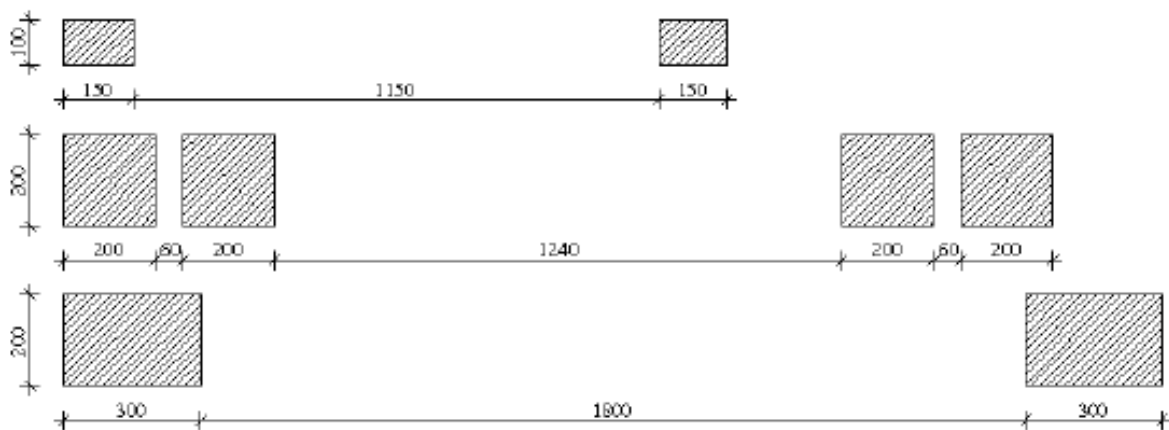


Figuur VI.1: Asconfiguraties en afmetingen wielprenten t.b.v. berekening levensduur VVK brugdek

Figure 6-7 Fatigue load models – Wheel prints (NEN6788, 1995)

158
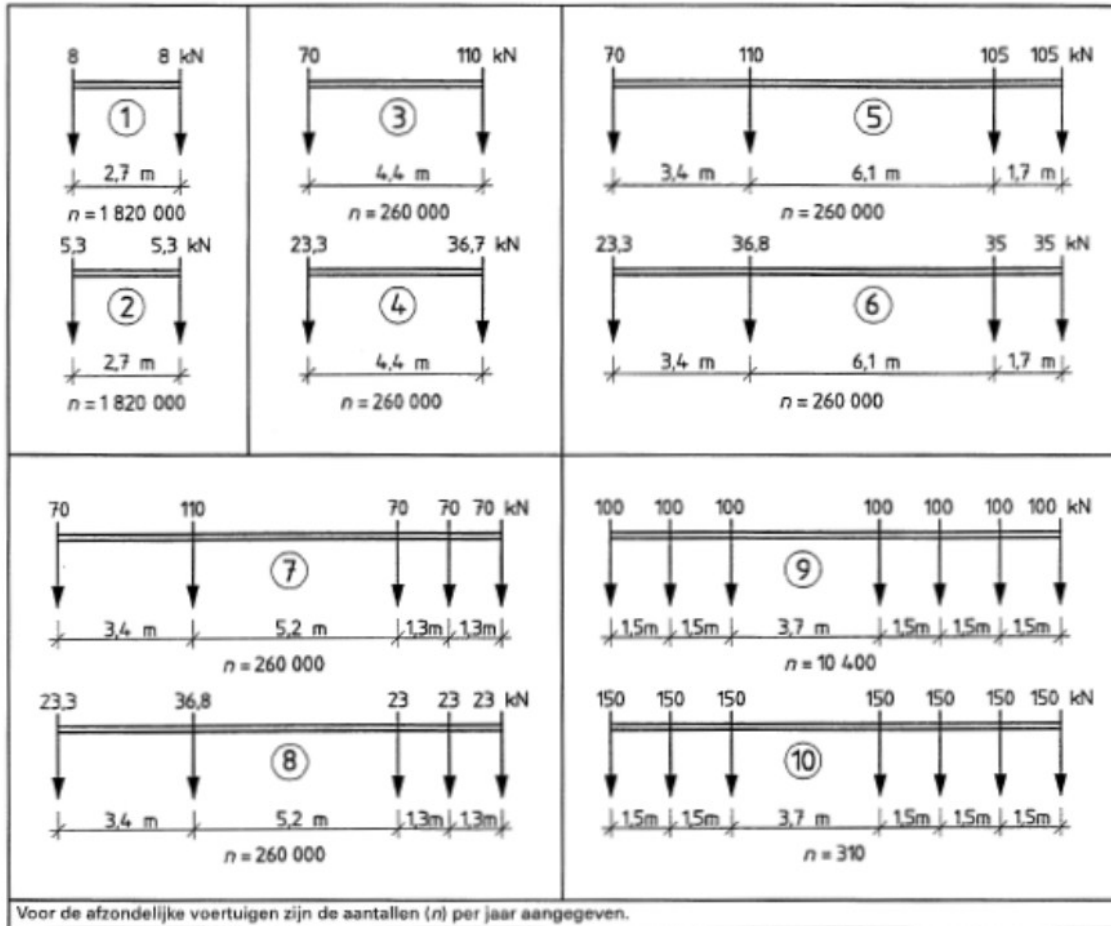
Figure 6-8 Fatigue load models (NEN6788, 1995)

Table 6-1 Fatigue load models (NEN6788, 1995)

| Nr. (figuur 19.2) | Asdruk (kN) | Elke asdruk verdeeld over | Wielprent (mm) |
|---|---|---|---|
| 1 | 8,0 | 2 wielen | 150 x 100 |
| 2 | 5,3 | 2 wielen | 150 x 100 |
| 3 | 110 | 4 wielen | 200 x 200 |
| 4 | 36,7 | 4 wielen | 200 x 200 |
| 5 | 105,0 | 2 wielen | 300 x 200 |
| 6 | 35,0 | 2 wielen | 300 x 200 |
| 7 | 70,0 | 2 wielen | 300 x 200 |
| 8 | 23,0 | 2 wielen | 300 x 200 |
| 9 | 100,0 | 4 wielen | 200 x 200 |
| 10 | 150,0 | 4 wielen | 200 x 200 |

Tabel VI.1: Maten en belastingen wielprenten t.b.v. berekening vermoeiing

159
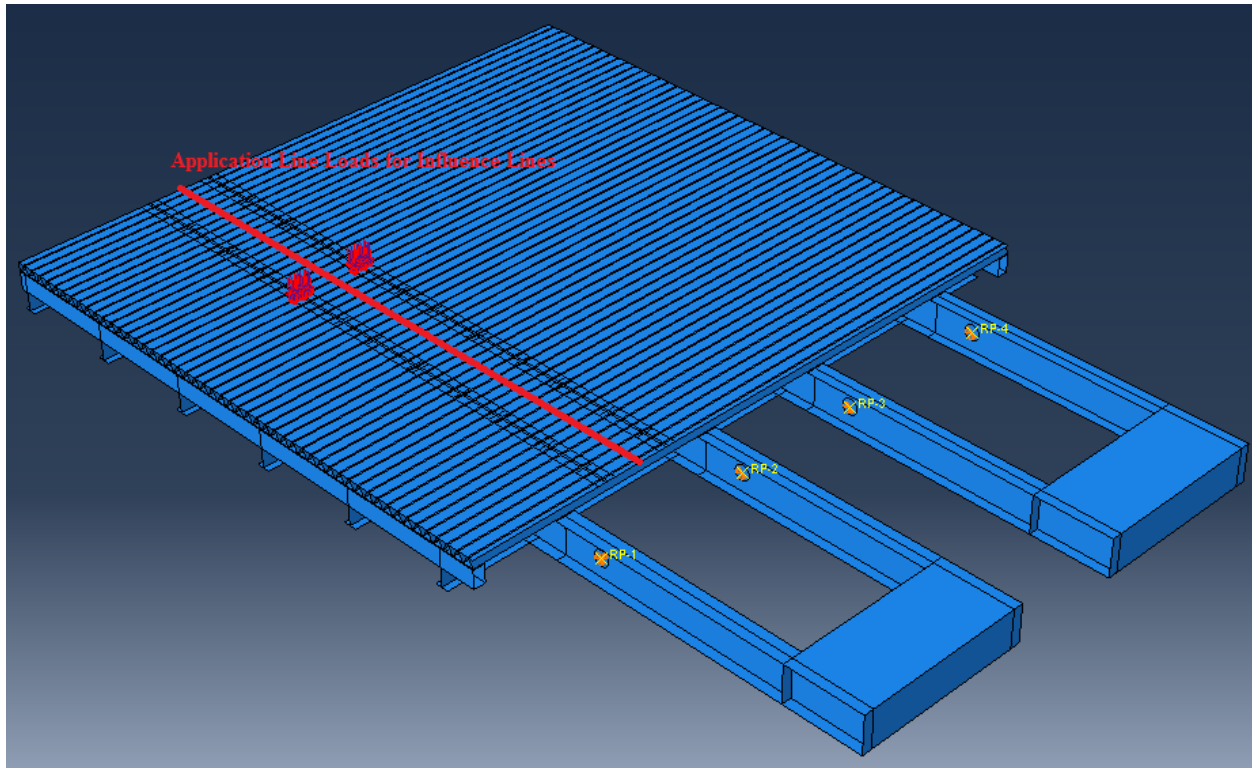
Figure 6-9 Direction of loadings to create the influence lines for FLM 9&10
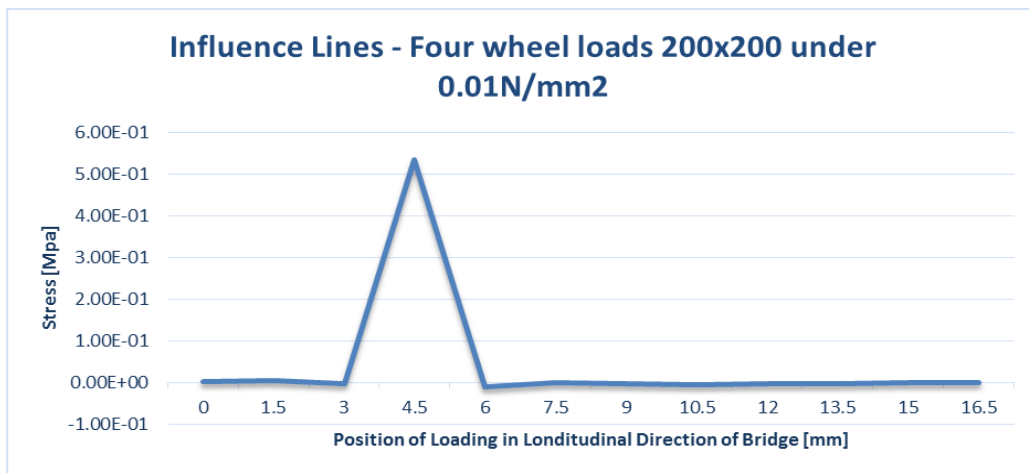


Figure 6-10 Influence Lines of one axle with four loads 0.01 N/mm$^2$ under wheel prints according to FLM 9&10

As the results of influence line show, the influence of 1 axle passing the bridge can be considered 3 m. However, as already discussed, the wheel loads generate a local effect when stresses are considered and this is less than three meters influence. The latter implies that the step used for passing 1 axle load, which equals 1.5 m, is too large to provide an accurate overview of the

160

influence lines. If a more detailed influence line should be aimed for by providing shorter step of axle loading, would require very much time and powerful computer tools. However, since there is only one peak stress we may address the latter issue by providing a more accurate influence line in local regions, where the maximum peak stress occurs. The results of this calculation is shown in Figure 6-11.
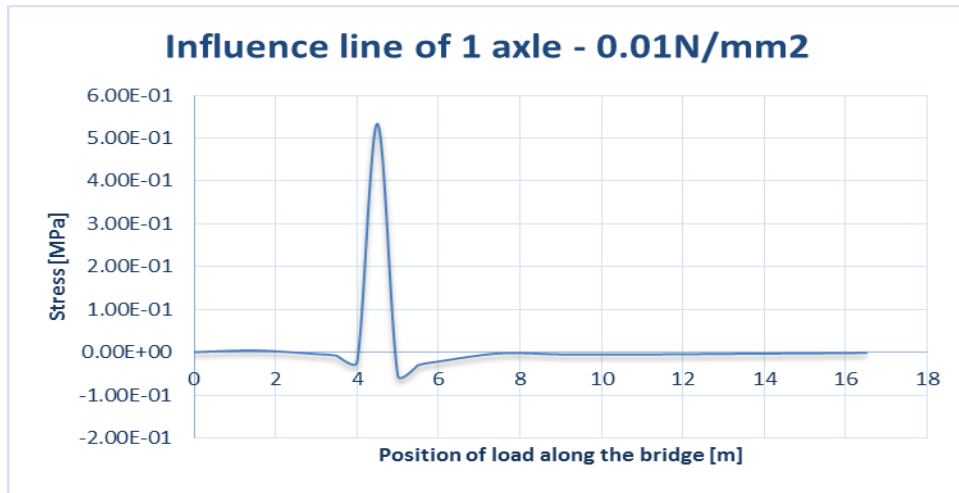


Figure 6-11 Influence line – more detailed

For each axle load of the fatigue load models there is only one peak stress since the span between the axles exceeds the minimum distance of impact; we can conclude that for each load model will be influencing cycles equaling the amount of how many axle loads are applied. For instance, when Fatigue Load Model 9 or 10 are used, one cycle of the vehicle passing the total bridge will give 7 stress cycle ranges to be used for fatigue calculation. Each of the stress can be computed by multiplying the peak stress by the amount of the characteristic load that the axle offers. The same procedure is used for other fatigue load models.

According to (CUR-Aanbeveling 96, 2003) the fatigue damage is calculated with the following formula:

$$D = \sum_{i=1}^{m} \frac{n_i}{N_i} = \frac{n_1}{N_1} + \frac{n_2}{N_2} + \ldots + \frac{n_m}{N_m} \leq 1$$

Where,

$n_i$ is the number of cycles,

161

$N_i$ is the expected capacity in number of cycles until failure,

$D_i$ is the damage ratio

In order to calculate the capacity in number of cycles until failure $N_i$ the following equation are used

$$\sigma_{gem} \geq 0; \ N_f = \left( \frac{\sigma_{t,u,d} - \sigma_{gem}}{\sigma_{amp}} \right)^k$$

$$\sigma_{gem} \leq 0; \ N_f = \left( \frac{\sigma_{t,u,d}\left[1 - \frac{\sigma_{gem}}{\sigma_{c,u,d}}\right]}{\sigma_{amp}} \right)^k$$

$$\sigma_{gem} = \frac{\sigma_{max} + \sigma_{min}}{2}$$

$$\sigma_{amp} = \frac{\sigma_{max} - \sigma_{min}}{2}$$

Where;

$\sigma_{t,u,d}$ is the tensile strength of the flanges, $\sigma_{t,u,k} / \gamma_m$

$\sigma_{c,u,d}$ is compressive strength of the flanges, $\sigma_{c,u,k} / \gamma_m$

$k = 8$ (glass/polyester)

$\gamma_m = \gamma_{m1} \times \gamma_{m2}$

$\gamma_{m1}$ – is the partial factor due to uncertainties in obtaining material properties, and equals 1.35

$\gamma_{m2}$ – is the partial factor that takes into account the production method and equals 1.1

$\gamma_m = \gamma_{m1} \times \gamma_{m2} = 1.35 \times 1.1 = 1.485$ --> $\sigma_{t,u,d} = 121$ MPA

Making use of the above equations, Table 6-2 shows the damage ratio of each of the fatigue load models. When movable bridges are designed for fatigue assessment, despite the ten fatigue load models caused from moving vehicles, an additional stress range should be calculated taking into account the motion of the bridge when opening and closing occurs. The calculated values of the

162

moments are for each different angles of degrees when the deck is in motion are presented in Appendix H.

Table 6-2 Fatigue check of ASSET Deck

| | LM-1 | LM-2 | LM-3 | LM-4 | LM-5 | LM-6 | LM-7 | LM-8 | LM-9 | LM-10 | Open-Close |
|---|---|---|---|---|---|---|---|---|---|---|---|
| | | | | | Fatigue check of ASSET Deck | | | | | | |
| $\sigma_{max}$ | 4.392 | 2.9 | 29.99 | 12.25 | 48.2 | 16 | 32 | 13.7 | 33.4 | 50.1 | 18.8 |
| $\sigma_{min}$ | -0.015 | -0.01 | -0.367 | -0.1225 | -0.375 | -0.125 | -0.25 | -0.1 | -3.34 | -5.02 | 7.68 |
| $\sigma_{amp}$ | 2.2035 | 1.455 | 15.1785 | 6.18625 | 24.2875 | 8.0625 | 16.125 | 6.9 | 18.37 | 27.56 | 5.56 |
| $\sigma_{gem}$ | 2.1885 | 1.445 | 14.8115 | 6.06375 | 23.9125 | 7.9375 | 15.875 | 6.8 | 15.03 | 22.54 | 13.24 |
| $N_{f,I\ [xe9]}$ | 54.0147 | 82.3127 | 7.00982 | 18.6133 | 4.00607 | 14.0493 | 6.5324 | 16.5812 | 5.78008 | 3.58019 | 19.41906475 |
| $n_{i/year}$ | 1820000 | 1820000 | 260000 | 260000 | 260000 | 260000 | 260000 | 260000 | 10400 | 310 | 10000 |
| $n_i/N_{f,i}$ | 0.06739 | 0.04422 | 0.06068 | 0.02284 | 0.17731 | 0.05056 | 0.22289 | 0.08781 | 0.01259 | 0.00061 | 0.000514958 |

From Table 6-2 we can conclude that the bridge is safe since:

$$D = 0.75$$

## 6.6.Fatigue check of Steel Superstructure

The fatigue check of the main steel girders will be analyzed with the λ-method according to (EN-1991-2, 2003), (EN 1993-1-9, 2005) and (EN 1993-2, 2006). According to the latter fatigue load model 3 will be used. This model consists of four axles, each of them having two identical wheels. The geometry is shown in Figure 6-12. The weight of each axle is equal to 120 kN, and the contact surface of each wheel is a square 0.4x 0.4 m. Influence lines are created by shifting load model 3 from the start to the bridge end (see Figure 6-13and Figure 6-14) in order to simulate one cycle of loading. Stresses were measured for each new location of the axle load and then imported to create the influence lines. It was observed that the maximum stress range is achieved in the point shown in Figure 6-15 and the latter is used to create the influence lines as shown in Figure 6-16.
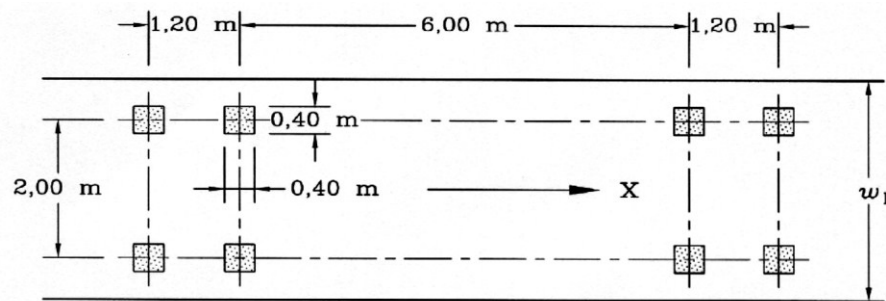


**Key**
$w_l$ : Lane width
X : Bridge longitudinal axis

Figure 6-12 Fatigue Load Model 3 (EN-1991-2, 2003)
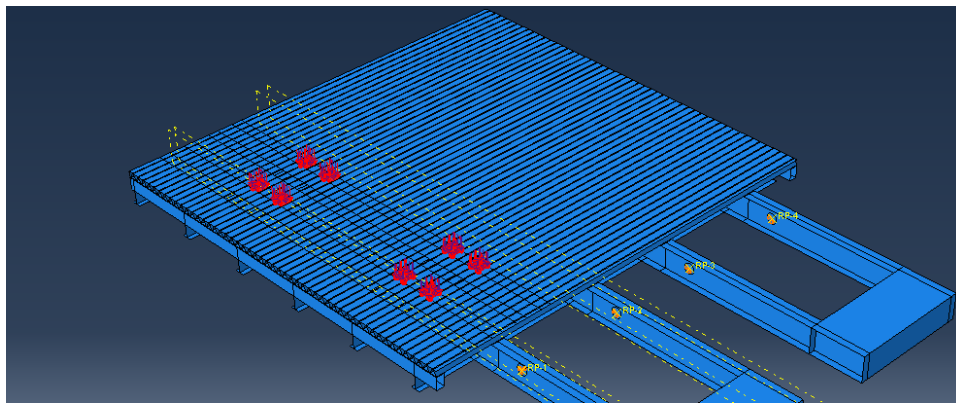


Figure 6-13 Application of Fatigue Load Model 3
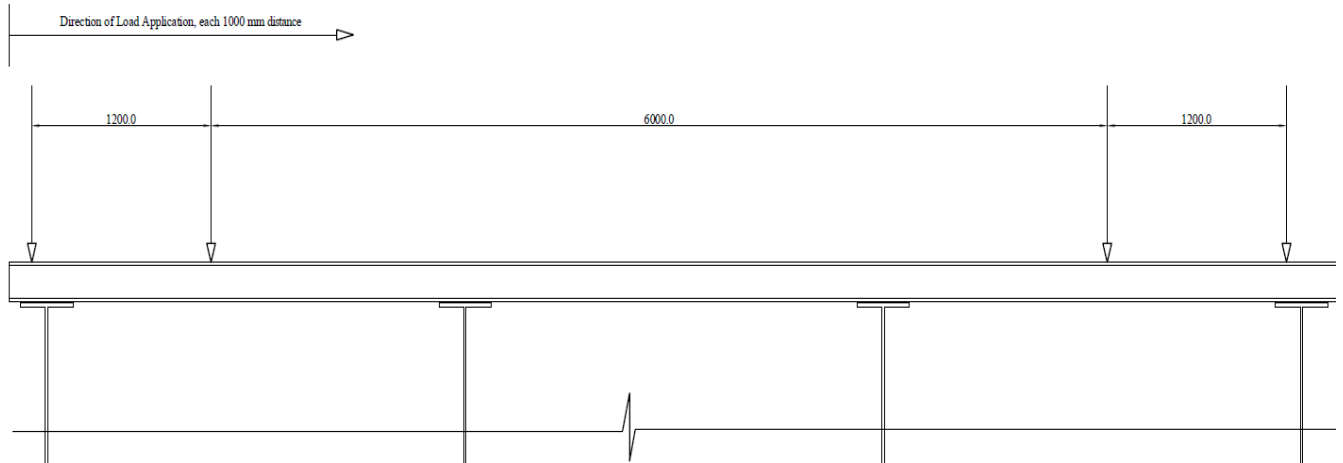
Figure 6-14 Application of Fatigue Load Model 3 to create influence lines
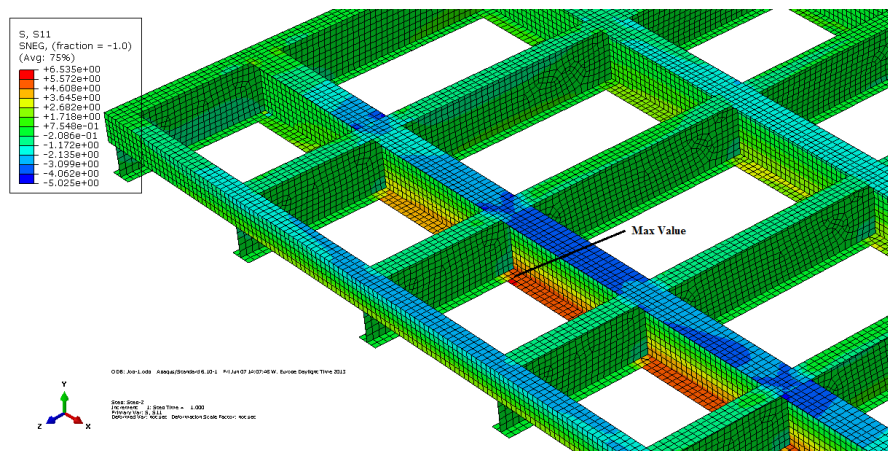


Figure 6-15 Position of maximum stress
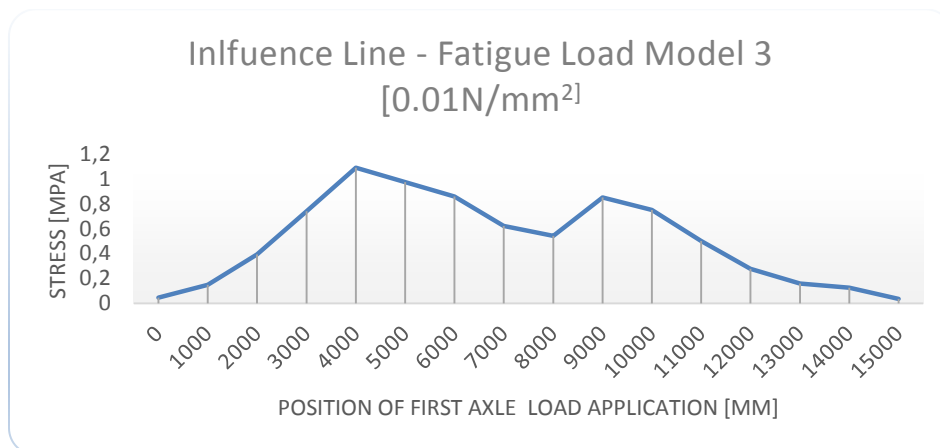


Figure 6-16 Influence Lines of Steel Girder – Fatigue Load model 3

166

The simplified fatigue assessment (λ-coefficient method) shall be carried out according to (EN 1993-1-9, 2005). For steel bridges the safety verification shall be carried out by ensuring that the following condition is satisfied

$$\gamma_{Ff}\lambda\Phi_2\Delta\sigma_E \leq \frac{\Delta\sigma_c}{\gamma_{Mf}}$$

Where:

$\lambda$ is the damage equivalence factor for fatigue which takes account of the service traffic on the bridge and the span of the member

$\Phi_2$ is the dynamic factor

$\Delta\sigma_E$ is the stress range due to the Load Model 3 being placed in the most unfavorable position for the element under consideration

$\Delta\sigma_c$ is the reference value of the fatigue strength

$\gamma_{Mf}$ is the partial safety factor for fatigue strength

- Damage equivalence factors λ for road bridges

The damage equivalence factor λ for road bridges with a span up to 100 m should be determined as follows:

$$\lambda = \lambda 1 \times \lambda 2 \times \lambda 3 \times \lambda 4 \qquad\qquad \text{but } \lambda \leq \lambda_{max} \quad \text{where,}$$

$\lambda_1$ is the factor for the damage effect of traffic and depends on the length of the critical influence line or area;

$\lambda_2$ is the factor for the traffic volume;

$\lambda_3$ is the factor for the design life of the bridge;

$\lambda_4$ is the factor for the traffic on other lanes;

$\lambda_{max}$ is the maximum λ-value taking account of the fatigue limit

The factor $\lambda_{max}$ should be obtained from the relevant fatigue stress spectra shown in Figure 6-17. For the span equaling 16.16 m this value equals

$$\lambda_{max} = 2.058$$
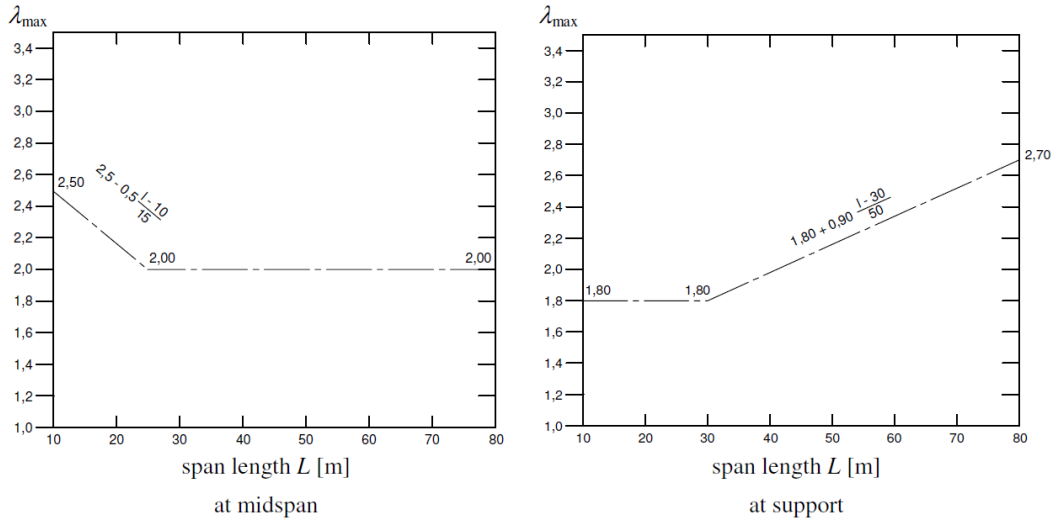


Figure 6-17 $\lambda_{max}$ for moments for road bridges (EN 1993-2, 2006)

In determining $\lambda_1$ the critical length of the influence line or area may be taken as the span length for simply supported spans. From Figure 6-18 this value equals, $\lambda_1 = 2.486$.
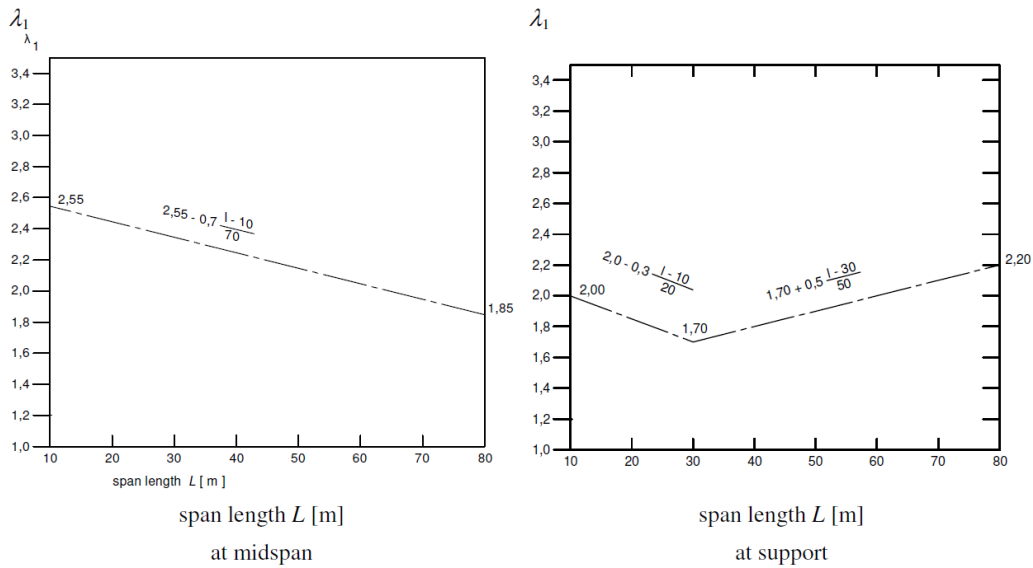


Figure 6-18 $\lambda_1$ for moments for road bridges (EN 1993-2, 2006)

Since $\lambda_1 \geq \lambda_{max}$ it is no longer needed to calculate the values of $\lambda_2$; $\lambda_3$; and $\lambda_4$ which have a value more than 1. Finally,

$$\lambda = 2.058$$

- Partial factors for fatigue verifications

The partial factor for fatigue loads shall be taken as $\gamma_{Ff}$. The use of $\gamma_{Ff} = 1,0$ is recommended. The partial factor for fatigue resistance shall be taken as $\gamma_{Mf}$. The values are given in Table 6-3 of EN 1993-1-9 which is shown below. Considering Safe Life and High consequence of failure the partial factor is taken $\gamma_{Mf}$=1.35.

Table 6-3 Safety factors (EN 1993-1-9, 2005)

| Assessment method | Consequence of failure | |
|---|---|---|
| | Low consequence | High consequence |
| Damage tolerant | 1,00 | 1,15 |
| Safe life | 1,15 | 1,35 |

- Stress range due to the Load Model 3

The reference stress range $\Delta\sigma_p$ for determining the damage effects of the stress range spectrum should be obtained from:

$$\Delta\sigma_p = |\sigma_{p,max} - \sigma_{p,min}|$$

The maximum stress $\sigma_{P,max}$ and the minimum stress $\sigma_{P,min}$ should be determined by evaluating influence areas.

$$\Delta\sigma_p = 37.5 \text{ Mpa}$$

When the balancing force is applied in the ballast as discussed before the stress range is differs very slight with

$$\Delta\sigma_p = 41 \text{ Mpa}$$

The damage effects of the stress range spectrum may be represented by the damage equivalent stress range related to $2 \times 10^6$ cycles:

169

$$\Delta \sigma_{E2} = \lambda \Phi_2 \Delta \sigma_p$$

where $\lambda$ is the damage equivalence factor as defined before;

$\Phi_2$ is the damage equivalent impact factor.

For road bridges $\Phi 2$ may be taken as equal to 1,0, as it is included in the fatigue load model.

The size effect due to thickness or other dimensional effects should be taken into account for the representative detail category. The fatigue strength then is given by:

$$\Delta\sigma_c = ks \text{ x } \Delta\sigma_{\text{detail category}} = 1 \text{ x } \Delta\sigma_{\text{detail category}}$$

Where: $ks = \left(\frac{25}{t}\right)^{0.2}$, t-thickness of plate

Since the thickness t = 25 mm the value of $k_s$=1.

The fatigue assessment is checked with the following equation;

$$\gamma_{Ff}\lambda\Phi_2\Delta\sigma_E \leq \frac{\Delta\sigma_{detail\ category}}{\gamma_{Mf}}$$

$$\Delta\sigma_{detail\ category} = 41 \times 1.35 \times 1 \times 1 \times 2.058 = 114 \text{ N/mm}^2$$

The minimum detail category suggested from the fatigue analysis should be $\Delta\sigma$ =114 N/mm$^2$ which may be considered a high detail category. To improve this fatigue damage flange thicknesses of main girders can be chosen thicker. However, if the safety factor is taken 1, for low consequence of failure and damage tolerant, instead of 1.35 the minimum detail category to provide a lifetime of the bridge 100 years is detail 84. On the other hand, the simplified λ-method may be considered a conservative method in fatigue checking. Other conclusion may be drawn when the cumulative damage model is used to check the fatigue lifetime of the superstructure of the bridge due to the more accurate results that are provided. Moreover, it should be pointed out that in case of movable bridges the safety factors used do not take into account the moving motion (closings and openings during working time of the bridge) which may own considered influence.

## 6.7. Discussion of results

The chapter investigates the fatigue analysis of upgrading Wilhelminabrug when ASSET deck is applied as deck replacement. The chapter first introduces the concept of fatigue and the methods used to assess the fatigue life. Under the recommendations and guidelines of (CUR-Aanbeveling 96, 2003), Dutch National Code, the fatigue assessment of ASSET deck for 100 years is estimated using the damage equivalent method. Furthermore, the minimum detail category of the steel superstructure is predicted using λ-method according to Eurocodes.

As a conclusion, the value of the FRP deck damage under fatigue loadings for 100 years is estimated less than 1. Nevertheless, it is worthy to mention that the environmental effects, such as for example creep, are not taken into account from the safety factors. In addition, the steel superstructure requires a very high detail category to survive fatigue for 100 years. This implies that the self-weight of the steel superstructure is considered lower and should be increased to accommodate lower fatigue details for the bridge. However, the λ-method may be considered too conservative to assess the real fatigue life and does not take into account the openings and closing during the lifetime of movable bridges.

# 7. Temperature Loading

The objectives of this study are to determine thermal deflections of a FRP deck subjected to temperature difference through finite element modeling.

All structures are subjected to varying structural responses under thermal changes including bridges that are subjected to high temperature difference on deck slab. Therefore it is necessary to understand and include the thermal effects in the structural design (Vinson, 1999). Through years several authors have investigated the difference in temperature in composite bridge structures, however (Kennedy & Soliman, 1997) appeared to be the most realistic and simple concept confirmed by field test measurements (See Figure 7-1). Moreover, the calculation of thermal stresses and displacements based on a linear-uniform variation became much simpler for bridges.
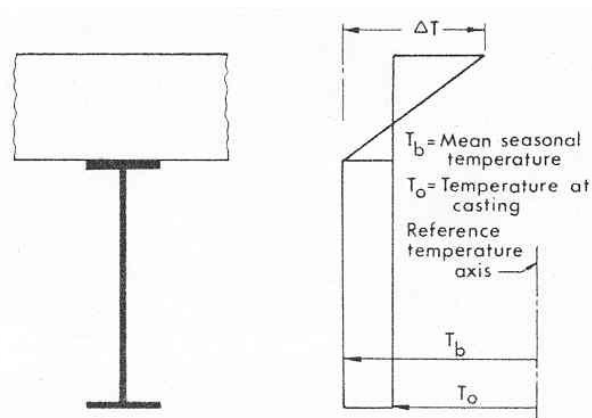


Figure 7-1 Linear-Uniform Vertical Temperature Distribution; $\Delta T$ =Temperature Differential (Kennedy & Soliman, 1997)

(Dutta, Kwon, & Lopez-Anido, 2003) performed outdoor tests with sun exposure on FRP bridge decks to monitor temperature rise and fall on FRP bridge deck on both top and bottom surfaces during summer months and he concluded that the difference between the temperature on top and bottom can be 73° F with respectively 150° F and 77° F on top and bottom surface. Moreover, it was evaluated the fatigue performance of FRP bridge decks under high and low temperatures (four million simulated wheel load cycles at low temperature, -30°C (-22°F), and another four million cycles at high temperature, 50°C (122°F)). Progressive degradation in stiffness was observed with load cycling under two extreme temperatures, -30°C (-22°F) and 50°C (122°F) and

the stiffness of FRP bridge decks under wheel loads was more susceptible to two extreme temperature changes than to ten million cumulative load cycles. (Laosiriphong, 2004) performed laboratory tests and field investigation on composite bridge structures with FRP deck. It was concluded that the deflections in FRP deck exhibits a hogging effect when the temperature of top surface is higher than the bottom and vice versa. Furthermore, it was concluded that the FRP deck deflection did not depend primarily on the temperature of top or bottom surface individually, but on the temperature difference between the top and bottom surfaces and while increasing the magnitude of the latter the deflection will increase too. Additionally, it was observed a good correlation between the experimental tests and finite element modeling (Laosiriphong, 2004) and (Nelson, 2005).

This chapter studies the temperature effect on the displacement of the composite bridge. According to NEN 6788 (A.6) three different load cases are investigated under service limit state, as shown in Figure 7-2.
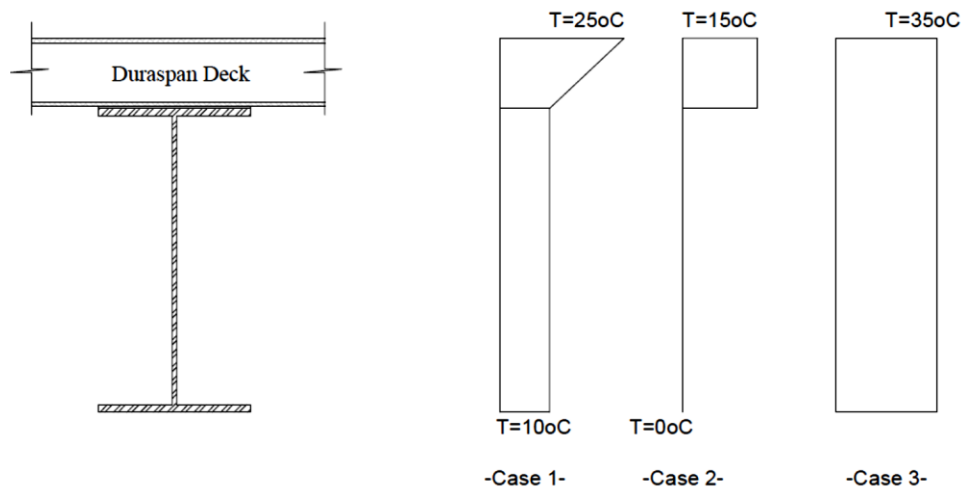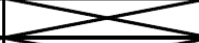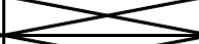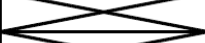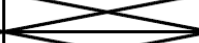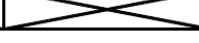


Figure 7-2 Temperature load cases

Due to limited availability of the data properties for the FRP decks, only Duraspan deck will be studied for this particular loading case. The specific properties are retrieved from experimental data and shown in Table 7-1 and Table 7-2 and are used to conduct the finite element analysis with Abaqus software under temperature loadings shown in Figure 7-2.

Table 7-1 Duraspan Deck Properties (Bai, 2011)

| DuraSpan slab | |
|---|---|
| Property | Value |
| Mass fraction | 61% (fiber) |
| Volume fraction | 52% (fiber) |
| Density | 1870 kg/m$^3$ |
| Specific heat capacity | 1170 J/kg-K |
| Thermal conductivity | 0.35 W/m-K |

Table 7-2 Coefficient of thermal expansion from testing results (Nelson, 2005)

| | | Strain Gage | LVDT | PI Gage |
|---|---|---|---|---|
| | | (in/in/degree F) x 10^-6 | | |
| Lateral | 766 | 7.3 | 8.0 | 7.4 |
| | 500 | 9.0 | 7.2 | 7.7 |
| Longitudinal | 766 | 4.4 | 4.6 | |
| | 500 | 5.1 | 5.2 | |
| Steel | | 5.8 | | |
| Carbon | | -0.6 | | |
| Polymer Concrete 1 | | 17.8 | | |
| Polymer Concrete 2 | | 15.5 | | |

The results are shown for temperature loading and self-weight only. Figure 7-3 to Figure 7-5 show the deformed shape of the FRP deck under load cases 1-3 respectively. In two cuts of the deck cross section, as presented in Figure 7-3 and Figure 7-7, are plotted the vertical displacement across the transverse direction of the bridge while in Figure 7-6 are shown the horizontal deflections. The horizontal deflections have a maximum value of 6.8 mm. As the graphs in Figure 7-8 to Figure 7-10 demonstrate, the maximum vertical deflection for cut A-A is 1.2 mm and for cut B-B 0.6 mm. Considering a vertical deflection limit of 5 mm we can conclude that the vertical deflections under temperature differences meet the requirements. The horizontal deflections may be accommodated and prevented using bearings systems.
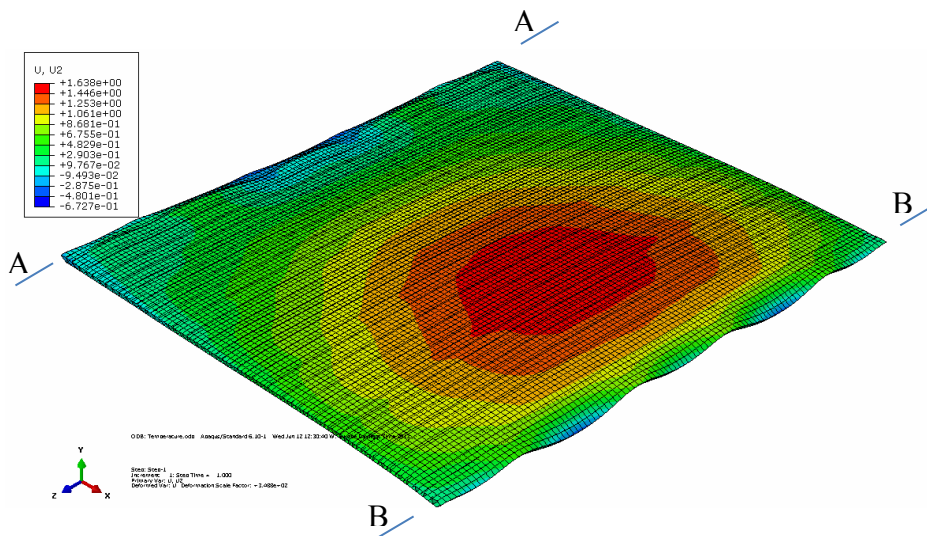
Figure 7-3 Vertical displacement [mm] of deformed deck under temperature load case 1
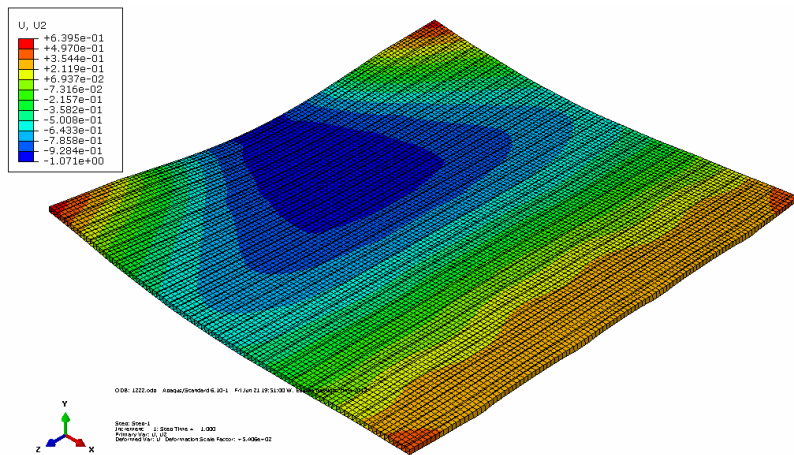


Figure 7-4 Vertical displacement [mm] of deformed deck under temperature load case 2
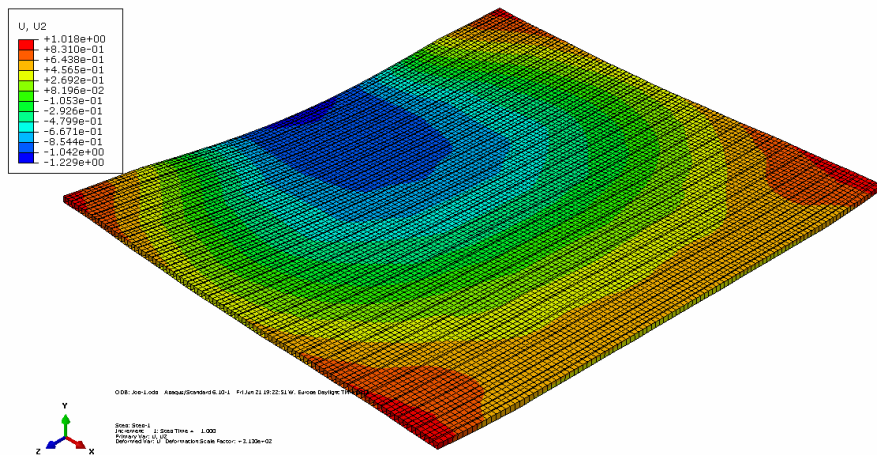


Figure 7-5 Vertical displacement [mm] of deformed deck under temperature load case 3

175
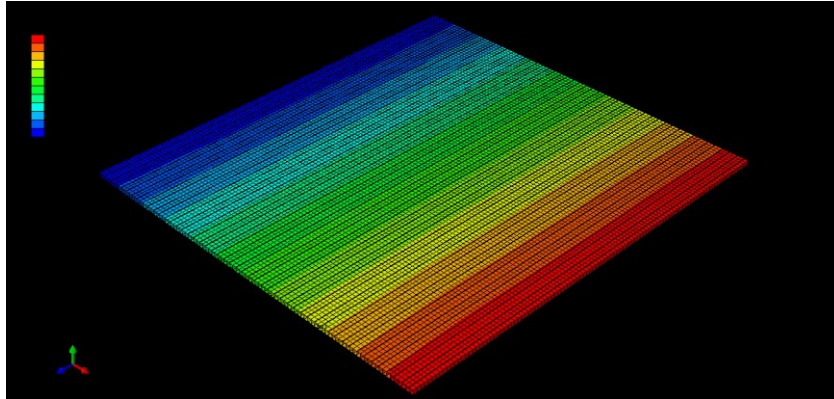
Figure 7-6 Horizontal displacement under load case 3
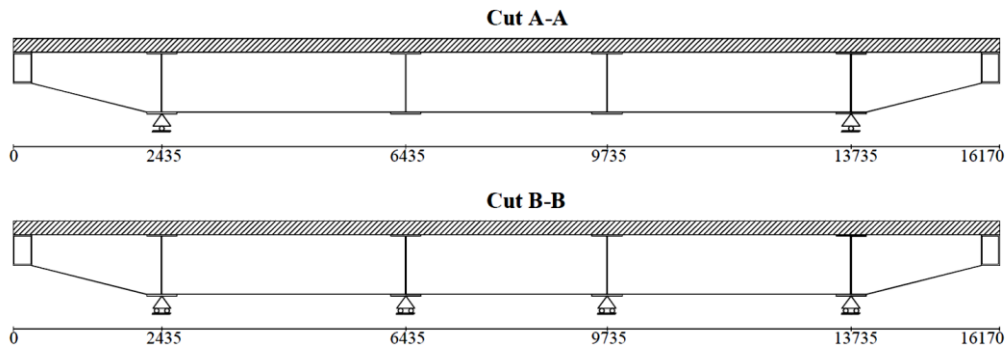


Figure 7-7 Cut A-A and B-B according to Figure 7-3
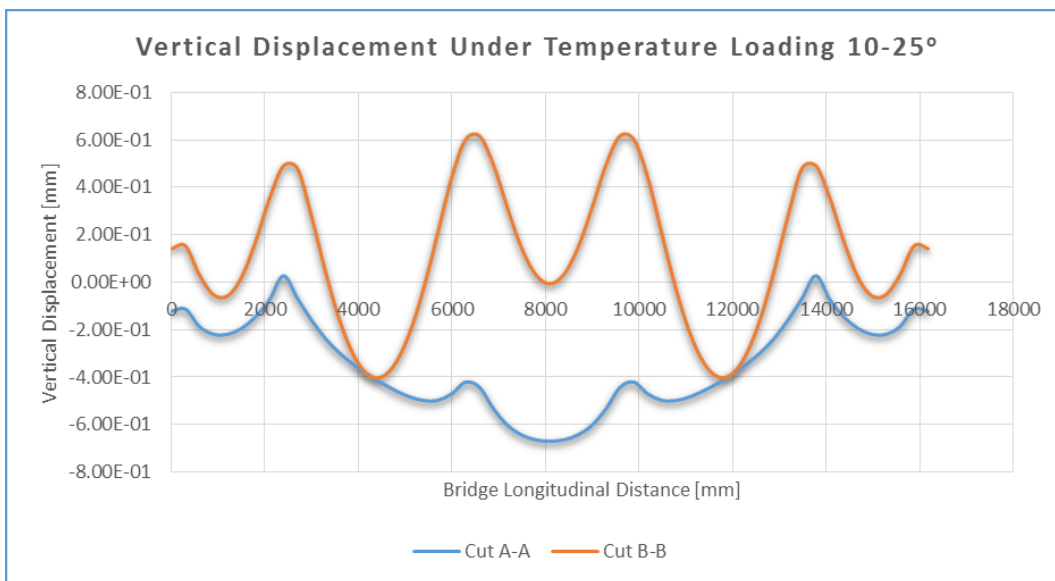


Figure 7-8 Plotted vertical displacement [mm] of Duraspan deck under temperature load case 1

176
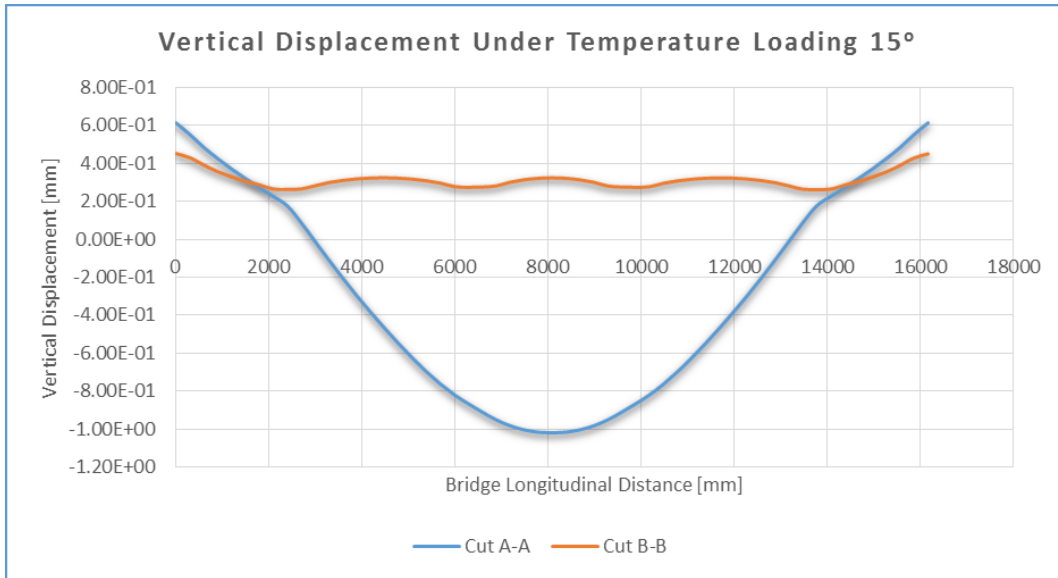
Figure 7-9 Plotted vertical displacement [mm] of Duraspan deck under temperature load case 2
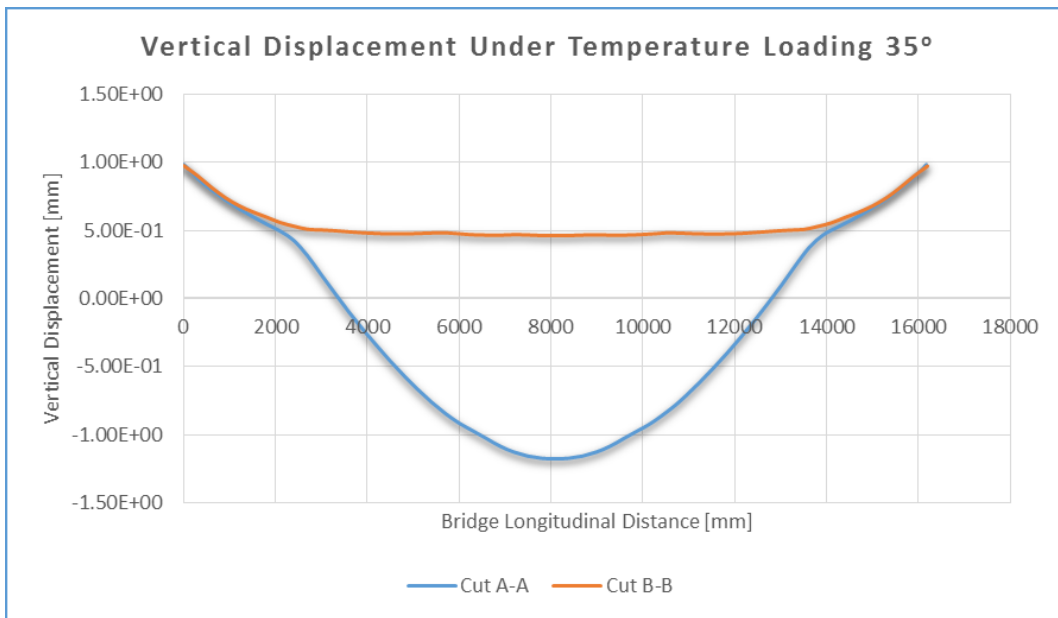


Figure 7-10 Plotted vertical displacement [mm] of Duraspan deck under temperature load case 3

# 8. Parametric Study

In this chapter is presented the parametric study illustrating the effect of the flange thickness of Ecosafe deck. During the static analysis is was shown that the Ecosafe deck met the requirements of stresses and deflections with high safety factor, especially for the stresses. This implies the possibility of decreasing the dimensions of flange thickness.

Ecosafe deck offers the advantage of the possibility to choose between variable dimensions of flange thickness and height when composing the deck configuration. In this study, the flange thickness is chosen 15.6 mm (control model) with a height of the deck 215 mm. To further understand the influence of flange thickness in the behaviour of Ecosafe deck a small parameter study will be held in this part of the research. Four case studies with different flange thickness will be analyzed based on finite element studies, specifically with flange thickness 9.6 mm; 11.6mm and 13.6 mm besides the control model as shown in Figure 8-1.
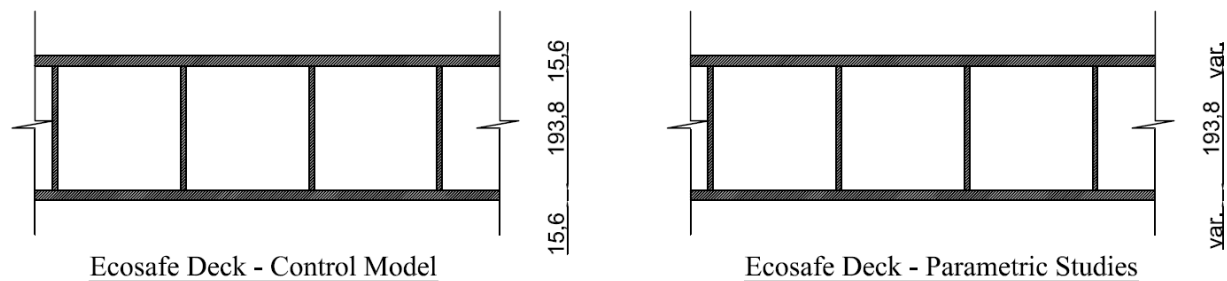


Figure 8-1 Ecosafe variable dimensions for parametric study

The results are gathered for different properties such as stresses deflections and shift of neutral axis. Table 8-1 shows the results of longitudinal (S11) and transverse (S22) stresses, von Mises stresses the shift of neutral axis and the longitudinal stresses of the steel superstructure. Figure 8-2 presents the graph comparison of the deck stresses while Figure 8-3 shows the global deflection of the bridge for all four case studies.

As the results illustrate, the influence of such parameter is relatively small for thickness 11.6 and 13.6 mm, while a decrease of bearing capacity if observed when the flange thickness is 9.6 mm. The shift of neutral axis differs approximately with 10 % for an increase in flange thickness of 2 mm. However each of the results shows that the deck acts compositely 100 %. Moreover, the difference in global deflection between the four case studies is very small.

178

Considering the results obtained, we may conclude that the flange thickness could have been chosen less than 15.6 mm and the deck stresses and deflection could meet the requirements.

Table 8-1 Comparison of different properties for different flange thickness

|  |  | Flange thickness [mm] | | | |
|---|---|---|---|---|---|
|  |  | 9.6 | 11.6 | 13.6 | 15.6 |
| S11 | [Mpa] | 19 | 15.41 | 14 | 13.5 |
| S22 | [Mpa] | 23 | 19.25 | 18.5 | 13.5 |
| Mises | [Mpa] | 45 | 37 | 34 | 20 |
| N.A. | [mm] | 705 | 715 | 721 | 736 |
| Steel S11 | [Mpa] | 284 | 282 | 280 | 278 |
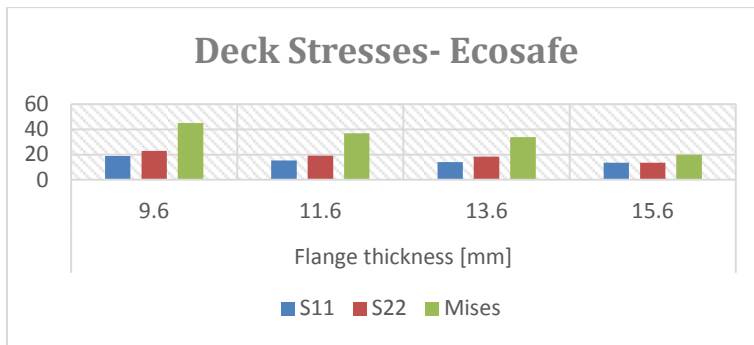


Figure 8-2 Comparison of stress values for different flange thickness
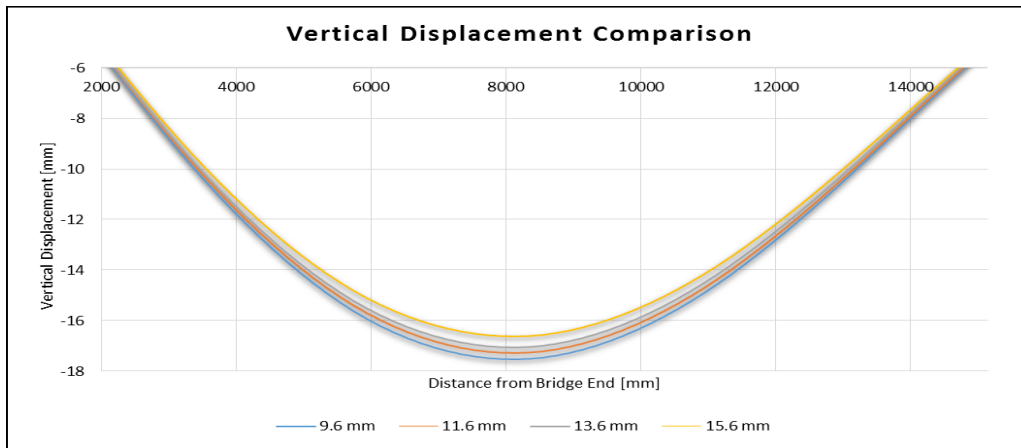


Figure 8-3Comparison of global deflections for different flange thickness

## 9. Conclusions

The aim of the thesis seeks to address some technical needs and questions to advance FRP deck application in bridge engineering. The aspects considered in this research are: static analysis, composite behaviour, lateral distribution and fatigue life assessment through the development of finite element modeling using the Abaqus software. Based on the result of this study the following conclusion has been attained:

- **Self-weight of Structure**

FRP decks provide a lightweight solution for replacement of old bridge decks and new-build. For a square surface of deck 15.15x16.17 m the self-weight of three FRP deck is revealed between 23-25 tons correspondingly to an average of 84 tons for the total structure. In addition, this lightweight nature of the material when used for bridge deck application may allow for easy installation and very quick assembly.

- **Deflections of the Structure**

Deflection (a serviceability limit state) governs the design, as opposed to strength (an ultimate limit state). In this thesis the limitation of L/800 is used as a requirement, which may be too conservative according to some sources (literature study). However in this case study this requirement is met when Ecosafe and ASSET deck are applied (type three steel configuration), while in case of Duraspan deck the vertical deflections indicate the level of L/650.

- **Stresses of the Structure**

On the basis of the results of this research, it can be concluded that stresses of FRP decks are spread locally where the wheels of vehicles are positioned. The results show that when Ecosafe deck and ASSET deck are applied the deck stresses are very low. In case of Duraspan these stresses are considerably higher although they meet the requirements.

Configuration of the geometry of the deck is crucial since it influences the performance of the deck. ASSET deck exhibits a truss action when transferring the forces, while Duraspan deck Vierendeel action. Concentrated forces and stresses are obtained in the intersections between the webs and the girders, which might be critical for the bearing capacity of the deck. To obtain

more detailed data on the local effects on the ASSET and Duraspan profile, a more complex, layered solid element model is recommended.

- **Composite Action and Lateral Distribution**

Prediction of the composite girders behavior assumed composite action between all components of the cross-sections for both deck systems. As the numerical studies showed, the adhesively-bonded joints between bridge decks and steel girders were sufficiently stiff and resistant to guarantee composite action between the top steel flanges and lower deck face panels at all load levels up to ultimate limit state. The upward shift under ultimate limit state equals the value of 112.5 mm, 108.5 mm and 215 mm, which is approximately 11.2%, 10.8% and 21.5% of the girder height respectively when ASSET, Duraspan and Ecosafe deck. Since the neutral axis is not in the middle of the beam and the beam is symmetric section, the FRP deck does act compositely with the steel beams to some extent and hence assist the steel girders in resisting applied moments. The possible deck contribution depends mainly on the in-plane deck stiffness in the longitudinal direction of the bridge axis. Apart from the composite behaviour, the investigation implies that aligning the pultrusion direction of the FRP deck to the traffic direction can results in load distribution which spread effectively to adjacent girders. Almost the same behaviour is observed when applying the three FRP decks.

- **Effective Width**

FRP decks acting compositely with underlying main steel girders exhibit an effective width. When Ecosafe deck is applied at ultimate limit state condition the effective width result 100% of the beam spacing for interior girders, while ASSET and Duraspan exhibit 87% and 77% respectively. Further study and research is recommended to obtain the precise coefficients with actual FRP material properties, the knowledge of which can increase the load bearing capacity of the hybrid bridge.

- **Shear Stud Application**

Shear studs represents an alternative joining technique for which composite action may be opted. On the basis of the results when the span of shear studs is selected 305 mm (Duraspan) or 295 mm (ASSET), it can be concluded that the same stress levels are achieved in the deck although

stress concentration areas are more spotted. Such joining method, however, may need improvement for the procedure of drilling and fastening the flanges of the FRP deck and steel girders.

- **Fatigue Assessment**

The fatigue assessment for the FRP deck is checked using the cumulative damage method while for the steel superstructure fatigue life is analyzed using the simplified $\lambda$-method. Results demonstrate that the FRP deck can survive the fatigue loading under life expectancy of 100 years with a unity check of 0.72. For the steel superstructure the results suggest a high minimum detail category (114 $N/mm^2$). To reduce this value the flanges of the steel main girders should be increased. In case of movable bridge the simplified $\lambda$-method does not take into account the openings and closing of the bridge during its lifetime which concludes that such method may be conservative and incapable of estimating accurate results. The damage cumulative method is advised to perform the fatigue assessment.

- **Temperature Loading**

From finite element analysis under temperature loading it is shown that the maximum vertical deflection in the lateral axis between the supports is lower than the minimum requirement set. Complete calculation considering the time behaviour and more detailed modeling of the adhesive is recommended to provide a more realistic overview.

Based on the findings of the investigation of the upgrading of Wilhelminabrug and literature study we may conclude that FRP bridge decking systems offer a potential alternative for deck replacement in old (movable) bridges. The study shows a reduction in self-weight of the deck and total structure and the requirements are met both under SLS and ULS. However, based on the findings of fatigue assessment the self-weight of the superstructure should be increased to accommodate lower fatigue detail categories. The composite action between the GFRP bridge decks and steel girders increases the stiffness and the resistance and reduces the deflections of the composite girders considerably. Nevertheless, the FRP deck acceptance into bridge engineering industry is quite low. Contributing issues are costs, structural performance, code specifications or guidelines and durability. Before it is fully accepted as practical construction

material, more projects involving FRP hybrid bridges are still need to verify the long-term cost savings and in service durability of the structure.

## 10.Further Research

FRP composites can be successfully used as structural elements, but they are still far from being accepted as a construction material equal to traditional materials. More projects involving FRP composites, especially those involving material-adapted concepts, still needed to verify their long-term cost-saving and in-service durability.

The recommended areas of future research, mainly through experimental studies and field investigation, presented in this section address several aspects of FRP bridge deck to overcome any reluctance to adopt FRP deck into mainstream application as an every-day alternative for common bridge design. Further research provides a greater scope in playing an important role in future bridge constructions, and such approach may have more influence when comparing different traditional material to FRP bridge deck.

**Life Cycle Cost (LCC) Analysis**

High initial cost is the first concern that hinders the use of FRP bridge deck systems. This cost is considerably higher than typically quoted for the new construction or replacement of a deck with conventional materials. According to sources, the initial higher cost is compensated from the maintenance cost. To help FRP deck get widely accepted in the civil engineering field, advances in technology of production quantities and manufacturing in order to reduce the high initial project costs is greatly needed. LCC effectiveness optimum design must also be performed by considering durability and damage accumulation induced by environmental effects.

**Design Guidelines and Codes**

Works on such standardization of design practices and/or acceptance criteria are said to have been carried away for many years, but standards codes and complete guidelines are still far from introducing. There is uncertainty in defining the deflection limits in existing design guidelines for FRP composites construction. For the time being, FRP bridge deck designers quantify deck performance in terms of criteria developed for conventional materials. Different authors have implemented as design criteria for deflection the limits L/450; L/600 and L/800. To further justify each of the above argument, future research should focus on static deflection or dynamic motion due to vehicular traffic and the development of partial safety factors for steel/FRP composite girders. One problem of the aforementioned issues may originate from the vast variety

that FRP decks are released in the market. As a start, manufactures may produce their own design guidelines which can get accepted by authorities and used by designers.

**Research on investigation and evaluation the durability of the FRP bridge deck system**.

The majority of sources according to literature study are very optimistic about the long-term durability of FRP materials and predict lower life-cycle costs for constructions made of them. Nevertheless, it is not possible to justify the claims, because only a limited number of relevant projects have been built and their lifetime does not exceed 40 years.

Rates of material degradation over time and damage accumulation induced by combined mechanical loads and environmental effects, such as moisture and UV light exposure should be monitored by extensive visual and nondestructive evaluation in a long-term basis. Durability characteristics should be measured in regard to material property changes due to seasonal temperature variations. Deck fire retardant and fire mitigation measures are additional important topics that needs further investigation. Since such research can be carried out only by means of accelerated laboratory tests, the groundwork of test standards is of immediate relevance.

**Fatigue behavior of FRP bridge deck system**.

One of the main gaps of knowledge that became increasingly apparent deals with understanding the fatigue cracking and damaging of FRP decking systems. General fatigue curves of the pultruded material based on the number of cycles to failure given a nominal stress needs to be developed in a broader sense. Parametric study can be carried out on material and geometry based on fatigue performance, and can be correlated to develop design criteria. In this way, guidance can be provided to the designer and provide less uncertainty for adoption of these materials.

Another area of potential research that would be of benefit include the propagation of the deck deflection during fatigue loading, which may not be directly related to the strength of the deck, but needs to be further studied and monitored in the field.

**Adhesives and mechanical connections**

Since panels are typically connected in the field to make full decks, the connections in terms of structural as well as overlay integrity need to be further understood which requires additional

investigation. Although fundamental studies have been conducted regarding adhesive joints, there are still some missing research such as the influence of different adhesive materials and depths on load bearing capacity. In addition, moisture effects and creep behaviour need further investigation. On the other hand, although mechanical faster as a traditional method to join two different materials have been studied, additional research should be conducted regarding the procedure of drilling and fastening in order to provide rapid installation so the time efficiency of FRP deck should be exploited as much as possible.

**Finite Element Modeling**

The finite element technique can be an extremely powerful tool and should be expanded to optimize multiple laboratory tests or even field investigation data. To allow for sufficiently generalized descriptions of service life, credible durability simulations of FRP bridge decks must be created and must be able to predict the combined effects of mechanical loads and service environments. These simulations must be developed from reliable descriptions of material degradation mechanisms and their interactions and must be validated over a wide range of conditions, at both the component and structural levels.

# Bibliography

AASHTO. (2008). *Guide Specifications for Design of FRP pedestrian Bridges.* Washington DC: American Association of State Highway and Transport.

Abaqus CAE. (2010). *Abaqus 6.10 CAE documentation.*

ALE. (n.d.). *Advanced Lightweight Engineering*. Retrieved December 8, 2012, from Advanced Lightweight Engineering: www.ale.nl

Alnahhal, W., & Chiewanichakorn, M. (2006). Temporal Thermal Behavior and Damage Simulations of FRP Deck. *JOURNAL OF BRIDGE ENGINEERING*, 452-464.

Bai, Y. (2011). *Fiber Reinforced Polymer Composites under Elevated and High Temperatures.* Lausanne: EPFL.

Bank, L. C. (2006). *Composites for Construction: Structural Design with FRP Materials.* New Jersey: John Wiley & Sons.

Bedford. (2010, July). *Bedford Reinforced.* Retrieved December 9, 2012, from Bedford Reinforced: www.redfordreinforced.com

Brown, D., & Berman, J. (2010). Fatigue and Strength Evaluation of Two Glass Fiber-Reinforced Polymer Bridge Decks. *Journal of Bridge Engineering*, 290-301.

Burgueno, Seible, Karbhari, Davol, & Zhao. (1999). *Manufactoring and Construction Support Dcument for the Kings Stormwarter Channel Bridge.* San Diego: University of California.

Busel, J. (2012). *FRP Composite Products Udes in Accelerated Bridge Construction.* Austin: American Composites Manufacturers Association.

Camata, G., & Shing, B. (2005). Evaluation of gfrp honeycomb beams for the O'fallon Park Bridge. *Journal of Composites for Construction*, 545-555.

Cassity, P., Richards, D., & Gillespie, J. (2002). Compositely Acting FRP deck and Girder System. *Structural Engineering International*, 71-75.

Cassity, P., Richards, D., & Gillispie, J. (2002). Compositely Acting FRP deck and Girder System. *Structural Engineering International*, 71-75.

Chan, T. H., & Li, Z. X. (2001). Fatigue analysis and life prediction of bridges with structural health monitoring data -- Part II: application. *International Journal of Fatigue*, 55-64.

Chen, A., & Davalos, J. (2012). Effect of degrees of composite action on effecive flange of FRP sandwich bridge deck. *Journal of Bridge Engineering, ASCE*.

Chiewanichakorn, M., & Aref, A. J. (2007). Dynamic and fatigue response of a truss bridge with fiber reinforced polymer deck. *International Journal of Fatigue*, 1475-1489.

Corporation, S. (2003). *Strongwell Corporation.* Retrieved December 9, 2012, from http://www.strongwell.com/PDFfiles/Extren/EXTREN%20DWB%20Design%20Guide.pdf

Costanos, A. (2000). *Analysis and Redesign of a Fiber Reinforced Plastic Design Deck.* North Carolina State University.

Craing, J., & Sweet, T. (2005). *FRP Bridge Decks.* New York.

CUR-Aanbeveling 96. (2003). *VEZELVERSTERKTE KUNSTSTOFFEN IN CIVIELE DRAAGCONSTRUCTIES.* Civieltechnisch Centrum Uitvoering Research en Regelgeving.

Davalos, J., Chen, a., & Qiao, P. (2013). *FRP Deck and Steel Girder Bridge Systems: Analysis and Design.* CRC Press 2013.

Dutta, P. K., Kwon, S.-C., & Lopez-Anido, R. (2003). *Fatigue Performance Evaluation of FRP Composite Bridge Deck Prototypes under High and Low Temperatures.* Washington, D.C.: Transportation Research Board.

Dutta, P., Lopez-Anido, R., Kwon, S., & Durell, G. (2003). *FATIGUE EVALUATION OF MULTIPLE FIBER-REINFORCED POLYMER BRIDGE DECK SYSTEMS OVER EXISTING GIRDERS PHASE 2 REPORT.* US Army Cold Regions Research and Engineering Laboratory.

EN 1991-2, E. (2003). *Eurocode 1: Actions on structures - part 2: Traffic loads on bridges.*

EN 1993-1-9. (2005). *Design of steel structures, Part 1-9: Fatigue.* Brussels.

EN 1993-2. (2006). *Design of steel structures - Part 2: Steel Bridges.* Brussels.

EN-1991-2. (2003). *Eurocode 1: Actions on Structures – Part 2: Traffic loads on bridges.*

EUROCOMP. (1996). *Eurocomp Design Code and Handbook.* Halcrow Polymerics Ltd.

FHWA, U. D. (n.d.). *Federal Highway Administration*. Retrieved December 7, 2012, from Fiber Reinforced Polymer Composite Bridge Technology: http://www.fhwa.dot.gov/bridge/frp/deck04.cfm

Fiberline. (n.d.). *Fiberline Composites.* Retrieved December 9, 2012, from www.fiberline.com

Gleason, A., & Dusicka, P. (2012). *STRENGTH AND FATIGUE OF THREE GLASS FIBER REINFORCED COMPOSITE BRIDGE DECKS WITH MECHANICAL DECK TO STRINGER CONNECTIONS.* Portland State University.

Gurtler, H. (2004). *Composite Action of FRP Bridge Decks Adhesively bonded to Steel Main Girders.* Lausanne: ÉCOLE POLYTECHNIQUE FÉDÉRALE DE LAUSANNE.

Hamrick, C. (2012). A green double-leaf: Portland bridge better for environment with FRP deck. *FRP Bridge Decks*, 46-51.

Harries, K. A., & J.Moses. (2007). Replacing a composite rc bridge deck with an frp deck - the effect on superstructure stresses.

Hoffard, T., & Malvar, j. (2005). *Fiber-Reinforced Polymer Composites in Bridges: A State-of-the-Art Report.* Port Hueneme: Naval Facilities Engineering Service Center.

Jiang, X., Kolstein, M., & Bijlaard, F. (2013). Study on mechanical behaviors of FRP-to-steel adhesively-bonded joint under tensile loading. *Composite Structures*, 192-201.

Keelor, D., Luo, Y., Earls, C, & Yulismana, W. (2004). Service Load Effective Compression Flange Width in Fiber Polymer Deck Systems Acting Compositely with Steel Girders. *Composite for Construction*, 289-297.

Keller, & Schollmayer. (2004, June). Plate bending behavior of a pultruded GFRP bridge deck system. *Composite Structures*, 285-295.

Keller, T. (2000). *Use of fibre reinforced polymers in bridge construction.*

Keller, T. (2003). *Use of Fibre Reinforced Polymers in Bridge Construction.* Multi Science Publishing Company.

Keller, T., & Gurtler, H. (2004). In-plane compression and shear performance of FRP bridge decks acting as top chord of bridge girders. *Composite Structures*, 151-162.

Keller, T., & Gurtler, H. (2005). Composite action and adhesive bond between FRP bridge decks and main girders. *Journal of Composites for Construction*, 360-368.

Keller, T., & Gurtler, H. (2006). In-plane tensile performance of a cellular FRP bridge deck acting as top chord of continuous bridge girders. *Composite Structures*, 130-140.

Keller, T., & T., V. (2005a). Adhesively bonded lap joints from pultruded GFRP profiles. part i: Stress-strain analysis and failure modes. *Composites part B: Engineering*, 331-340.

Keller, T., & Vallee, T. (2005a331-340). Adhesively bonded lap joints from pultruded GFRP profiles. *Composites*.

Keller, T., & Vallee, T. (2005b). Adhesively bonded lap joints from pultruded GFRP profiles. Part ii: Joint strength prediction. *Composites Part B: Engineering*, 341-350.

Keller, Th; Gurtler, H. (2004). Performance of Adhesively Bonded FRP deck and Steel Bridge Girders. *ACMBS*.

Kendall, D. (2008). The busines case for composites in construction. *Reinforced Plastics*, 20-28.

Kennedy, J. B., & Soliman, M. H. (1997). Temperature Distribution in Composite Bridges. *Journal of Structural Engineering*.

*KEROCK*. (n.d.). Retrieved December 12, 2012, from Industries and Export Limited: www.kemrock.com

Knippers, J., & Gabler, M. (2006). New Design Concepts for Advanced Composite Bridges- The Friedberg Bridge Germany.

Knippers, J., & Gabler, M. (2008). The FRP road bridge in Friedberg Germany –new approaches to a holistic and aesthetic design. *Fourth International Conference on FRP Composites in Civil Engineering (CICE2008)*.

Kolstein, M. (2007). *Fatigue.* Delft University of Technology.

Laosiriphong, K. (2004). *Theoretical and Experimental Analysis of FRP Bridge Decks under Thermal Loads.* Morgantown, West Virginia: West Virginia University.

Liu, Z. (2007). *Testing and Analysis of a Fiber-Reinforced Polymer (FRP) Bridge Deck.* Blacksburg, VA: Virginia Polytechnic Institute and State University.

M.H.Kolstein. (2008). *Fibre Reinforced Polymer (FRP) Structures.*

Majumdar, P. (2008). *Strength and Life Prediction of FRP Composite Bridge Deck.* Blacksburg: Virginia Polytechnic Institute and State University.

Mara, V. (2011). *Fibre reinforcedpolymer bridge decks.* Gotheburg: Chalmers University of Technology.

Mara, V., & Al-Emrani, M. (2012). UPGRADING OF AN EXISTING CONCRETE-STEEL BRIDGE USING FIBRE REINFORCED POLYMER DECK- A FEASIBILITY STUDY.

Mara, V., & Haghani, R. (2012). UPGRADING BRIDGES WITH FIBRE REINFORCED POLYMER DECKS – A SUSTAINABLE SOLUTION. *Conference on Civil Engineering Infrastructure Based on Polymer Composites.* Krakow: CECOM.

MMM Group, M. G. (2011). *DECK OPTIONS ANALYSIS REPORT: Johnson Street Bridge Replacement.* MMM Group.

Montley, D., Castanos, A., & Klang, E. (n.d.). Effects of diagonal webs in FRP bridge decks.

NCHRP, N. C. (2006). *Field Inspection of In-Service FRP Bridge Decks.* WASHINGTON, D.C: National Cooperative Highway Research program.

Nelson, J. L. (2005). *Behavior of GFRP Bridge Decks for Highway Bridges.* Raleigh, NC: North Carolina State University.

NEN6788. (1995). *Het ontwerpen van stalen bruggen.* Nederlands Normalisitatie-institut.

Park, K.-T., Hwang, Y.-K., Lee, Y.-H., & Jung, J. (2007). Experimental Study on Durability Comparison of the GFRP Decks by Resin Types. *KSCE Journal of Civil Engineering*, 261-267.

Potyrała, P. B. (2011, June). Use of Fibre Reinforced Polymers in Bridge Construction. State of the. Barcelona, Spain.

Righman, J. (2002). *Development of an innovative connection for frp bridge decks to steel girders.*

Righman, J. (2002). *DEVELOPMENT OF AN INNOVATIVE CONNECTION FOR FRP BRIDGE DECKS TO STEEL GIRDERS.* West Virginia: West Virginia University.

Sams, K. M. (2005). Broadway Bridge: An Ideal Application for FRP Bridge Decks. *FRP INTERNATIONAL*.

Smith, C. (2001). Environmental Testing on Pultruded Structural Shapes. *Composites*.

Stankiewicz, B. (2012). Composite GFRP Deck for Bridge Structures. *Steel Structures and Bridges 2012*, 423-427.

*Tap Plastics*. (n.d.). Retrieved December 8, 2012, from Tap Plastics: www.tapplastics.com

*The RC*. (n.d.). Retrieved December 8, 2012, from The RC: www.the-rc.com

Turner, M., Harries, A., Petrou, M., & Rizos, D. (2002). In situ structural evaluation of a gfrp bridge deck system. *Composite Structures*, 157-165.

Vinson, J. R. (1999). *Behavior of Sanwich Structures.* CRC Press.

Vovesnýa, M., & Rottera, T. (2012). GFRP bridge deck panel. *Procedia Engineering*, 492- 497.

*Wikipedia*. (2012, January 30). Retrieved from Wikipedia.

Winkelman, T. (2002). *FIBERGLASS REINFORCED POLYMER COMPOSITE BRIDGE DECK CONSTRUCTION IN ILLINOIS.* Illinois: Illinois Department of Transportation.

ZellComp. (n.d.). *ZellComp*. Retrieved 01 30, 2012, from www.zellcomp.com: http://www.zellcomp.com/highway_bridge_instal.html

Zetteberg, & Astrom. (2001). On design of joints between composite profiles for bridge deck applications. *Composite Structures*, 83-91.

Zhang, Y., & Cai, C. (2007). Load distribution and dynamic response of multi-girder bridges with FRP decks. *Engineering Structures*, 1676–1689.

Zhou, A., & Keller, T. (2005). Joining techniques for fiber reinforced polymer composite bridge deck systems. *Composite Structures*, 336-345.

## A. Appendix – Local and Global Deflections

This section presents the global and local deflection of the bridge deck. Two cuts of the FRP deck will be presented as shown in Figure A-1.
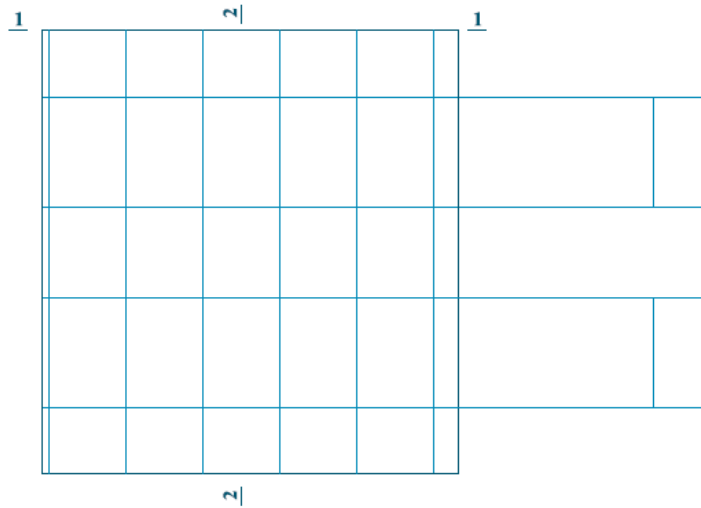


Figure A-1 Cut 1-1 and 2-2 of the bridge deck
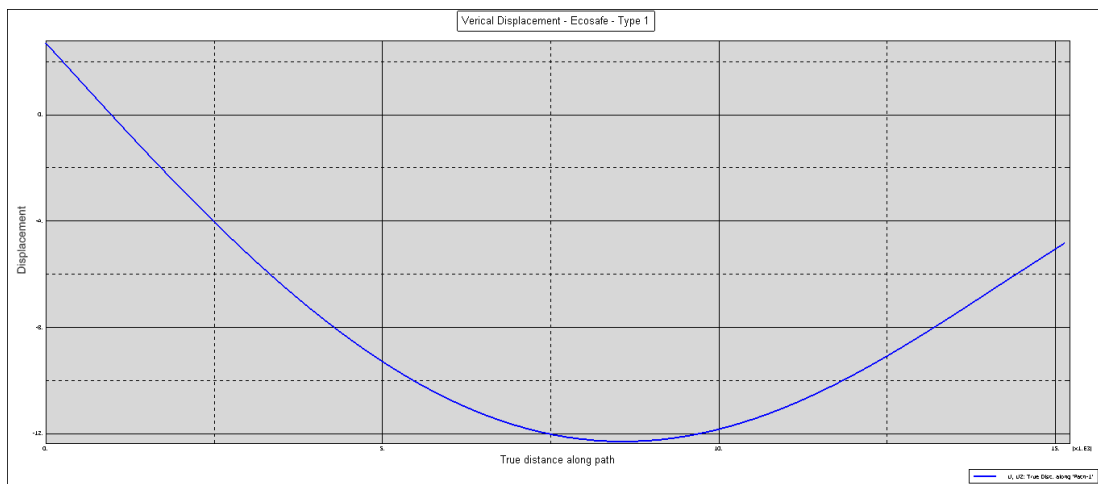


Figure A-2 Cut '1-1'of Ecosafe deck – type 1 configuration
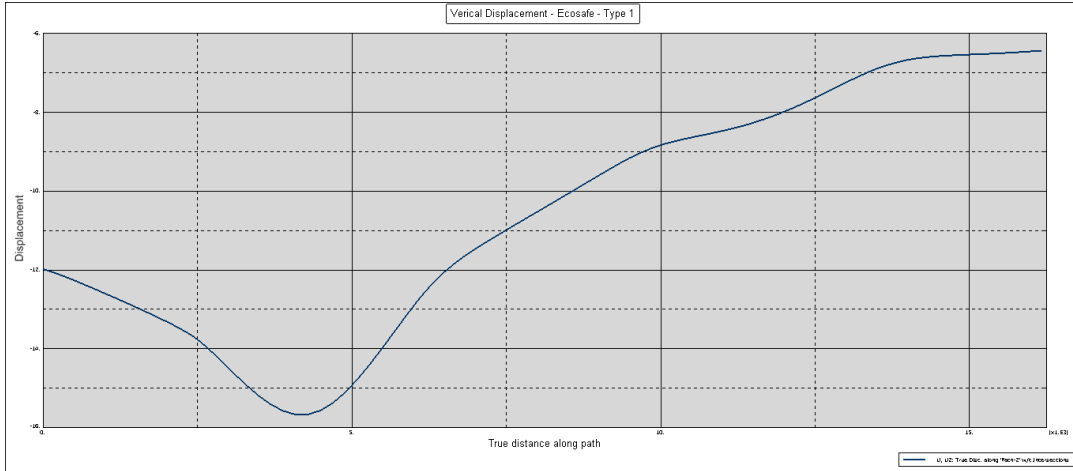
Figure A-3 Cut '2-2'of Ecosafe deck – type 1 configuration
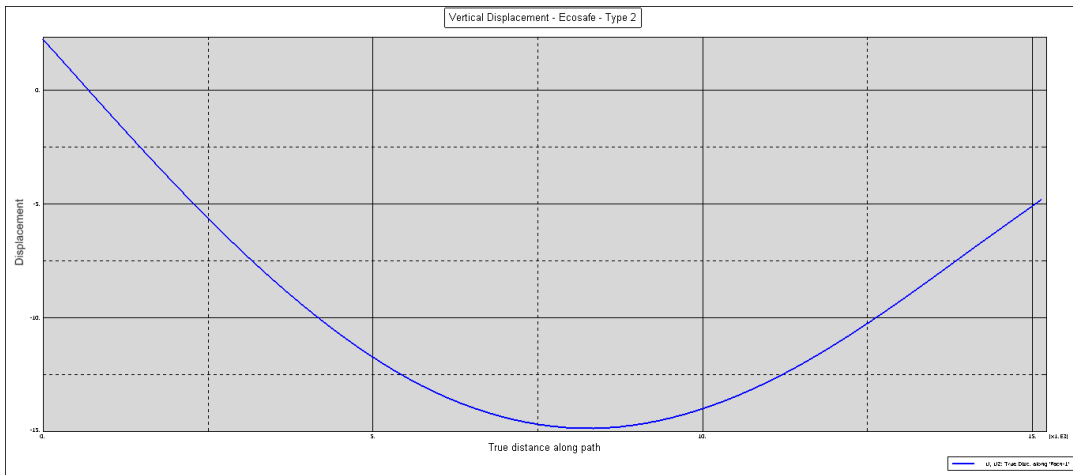


Figure A-4 Cut '1-1'of Ecosafe deck – type 2 configuration
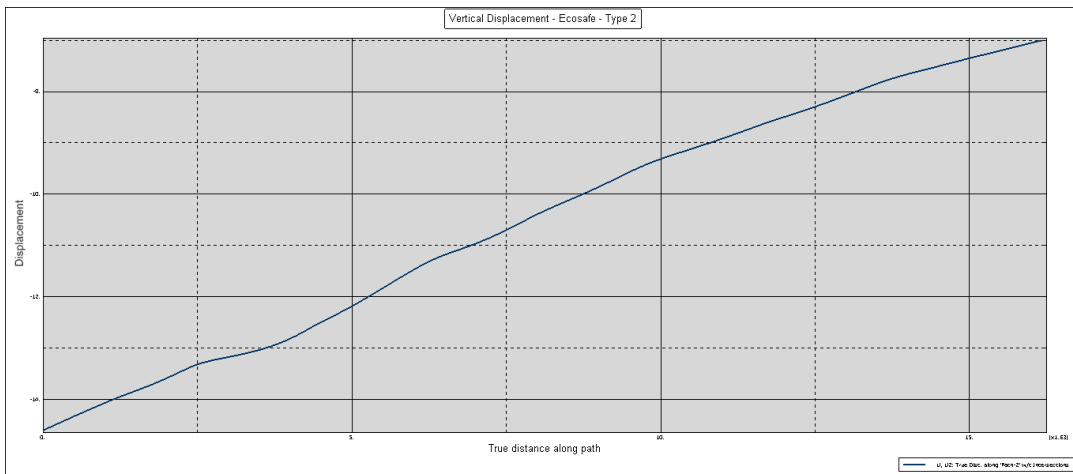


Figure A-5 Cut '2-2'of Ecosafe deck – type 2 configuration

195
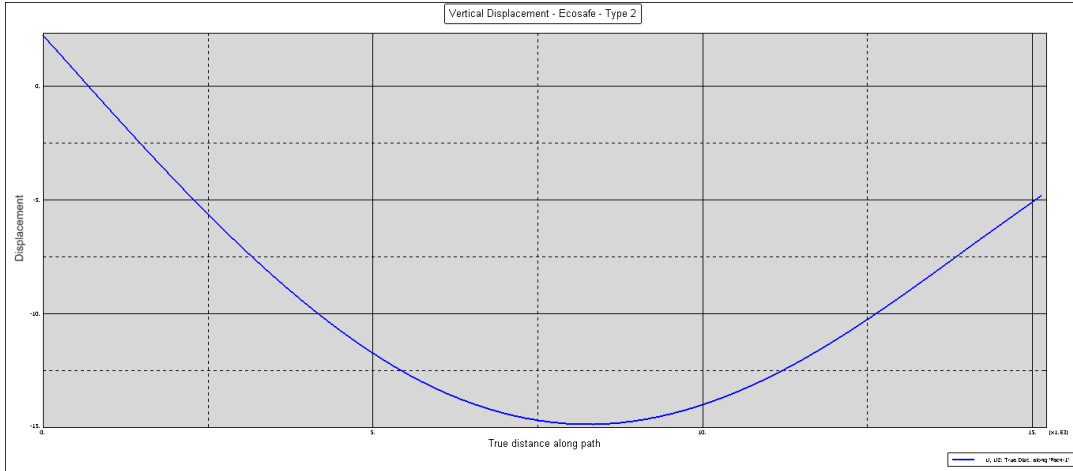
Figure A-6 Cut '1-1'of Ecosafe deck – type 3 configuration
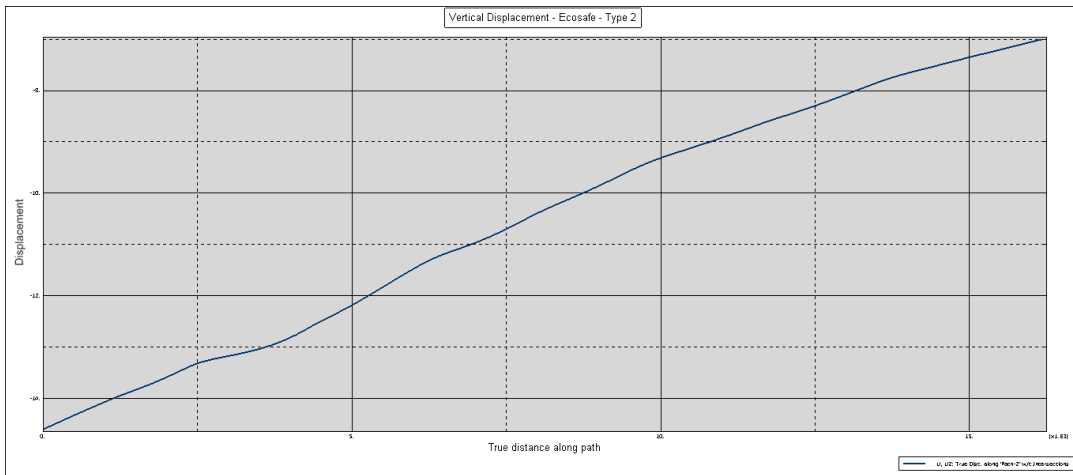


Figure A-7 Cut '2-2'of Ecosafe deck – type 3 configuration
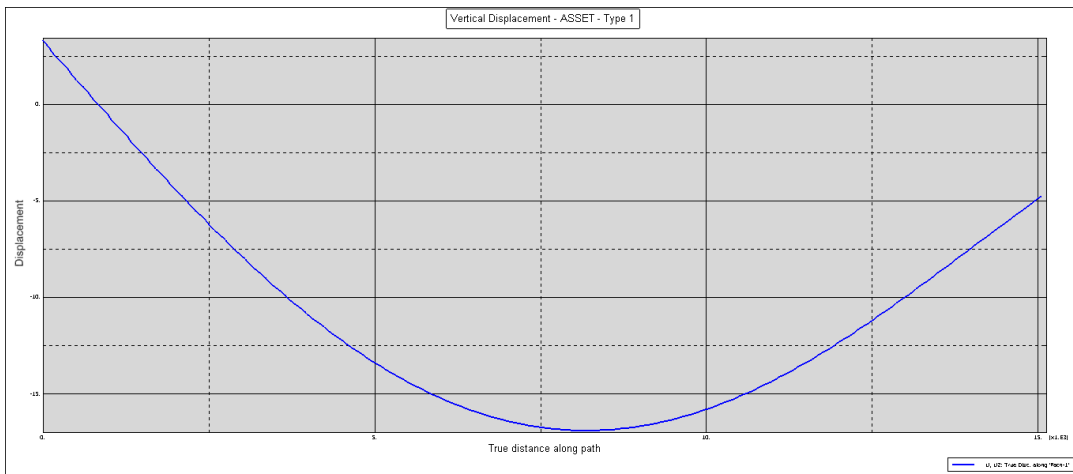


Figure A-8 Cut '1-1'of ASSET deck – type 1 configuration
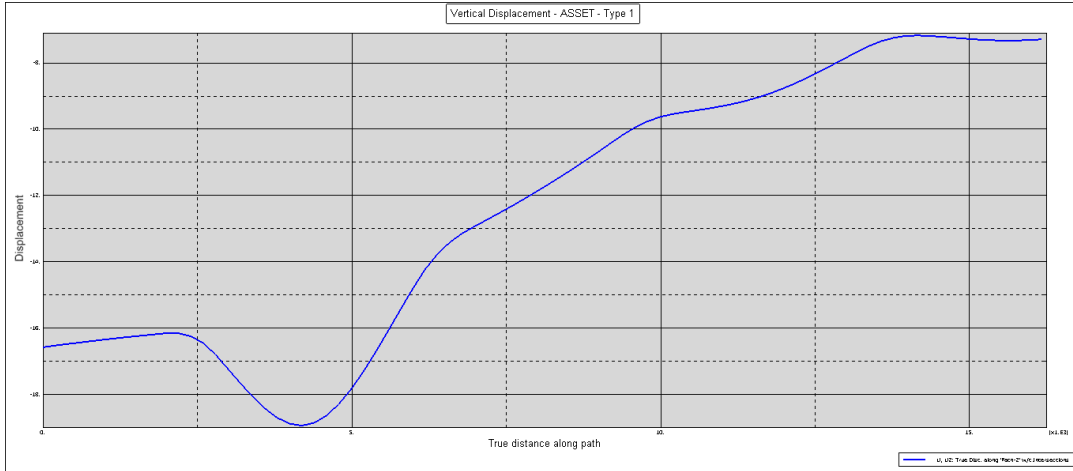
Figure A-9 Cut '2-2'of ASSET deck – type 1 configuration
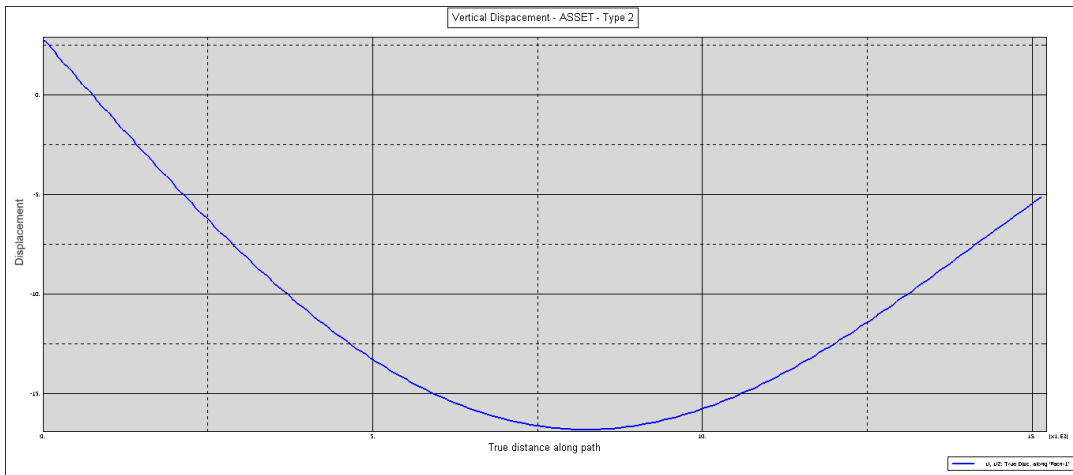


Figure A-10 Cut '1-1'of ASSET deck – type 2 configuration
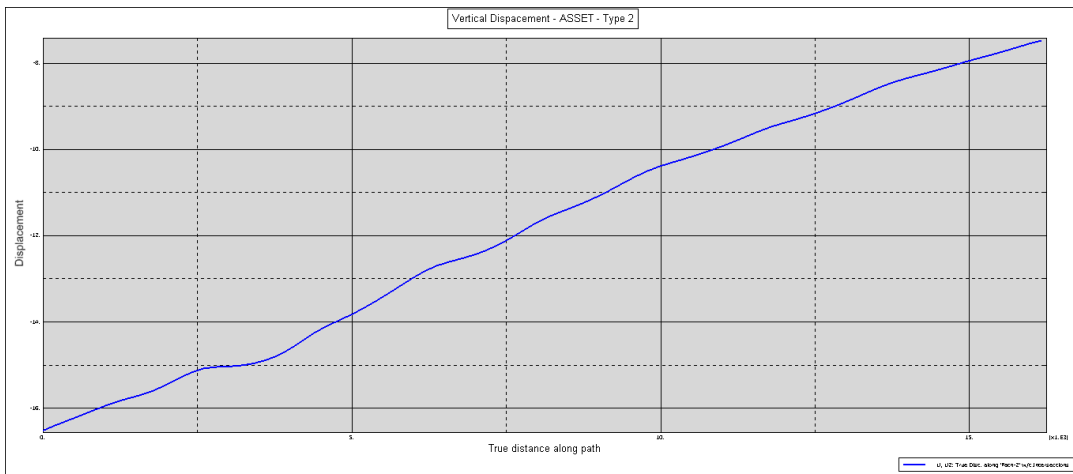


Figure A-11 Cut '2-2'of ASSET deck – type 2 configuration

197
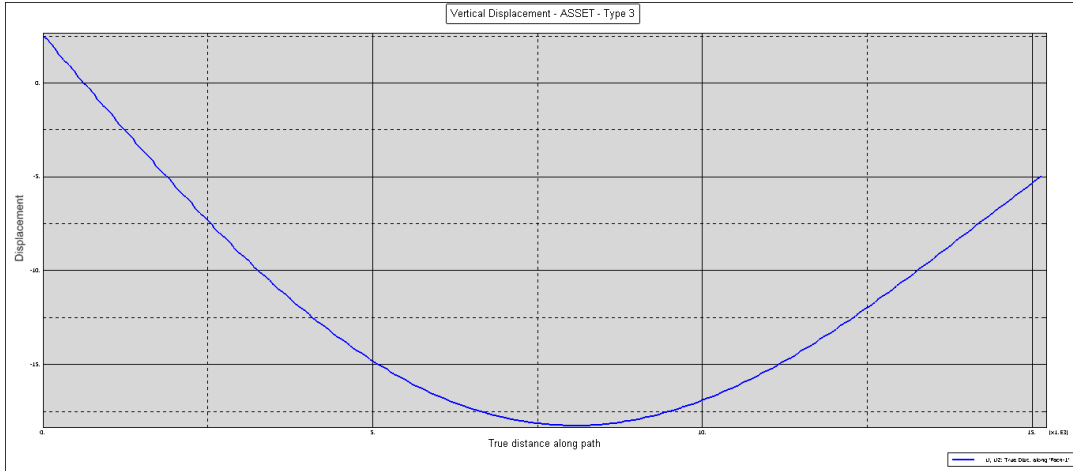
Figure A-12 Cut '1-1'of ASSET deck – type 3 configuration
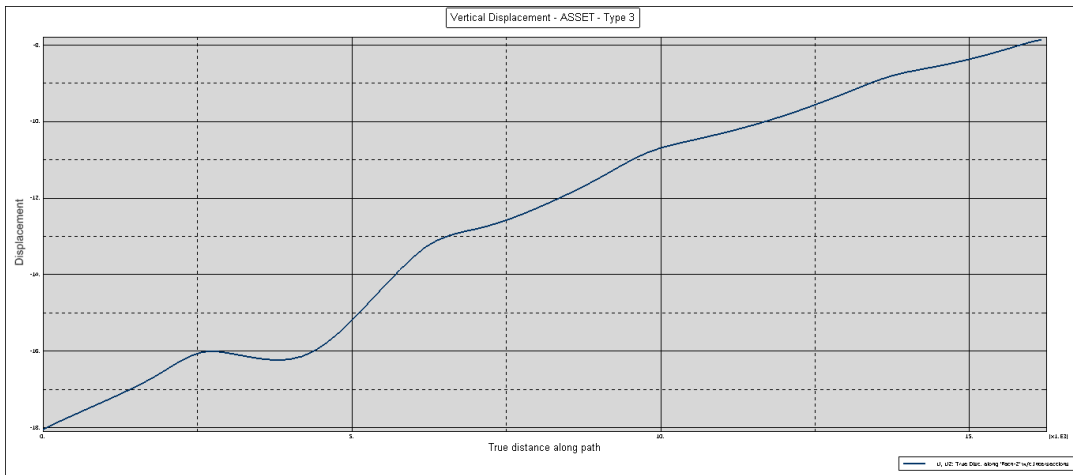


Figure A-13 Cut '2-2'of ASSET deck – type 3 configuration
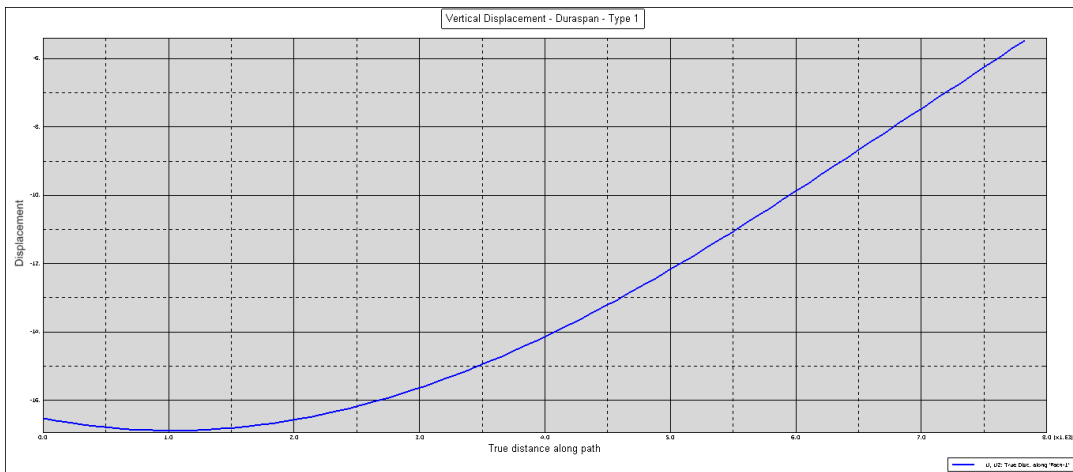


Figure A-14 Cut '1-1'of Duraspan deck – type 1 configuration

198
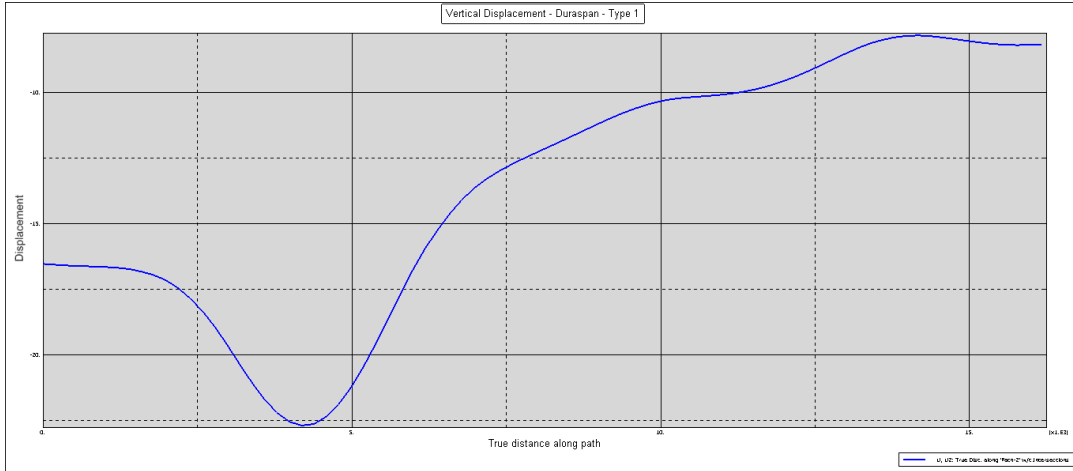
Figure A-15 Cut '2-2'of Duraspan deck – type 1 configuration
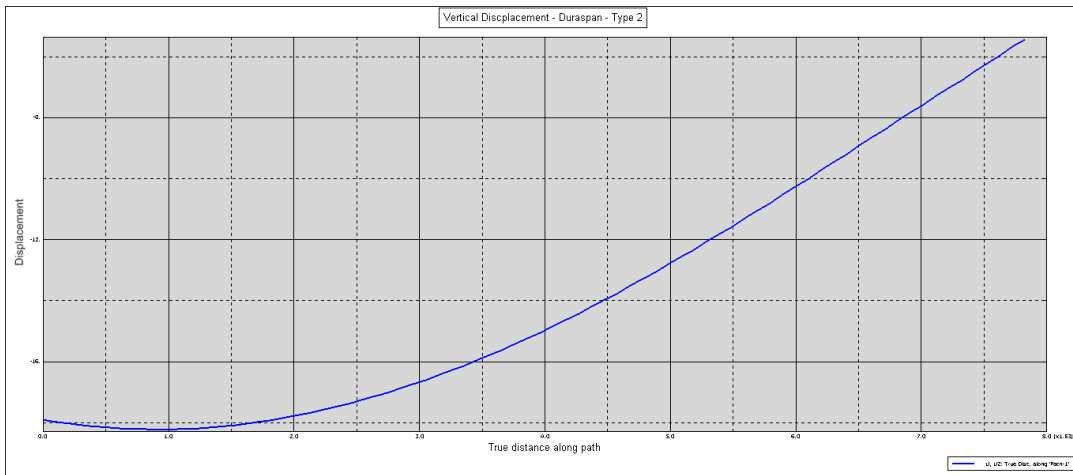


Figure A-16 Cut '1-1'of Duraspan deck – type 2 configuration
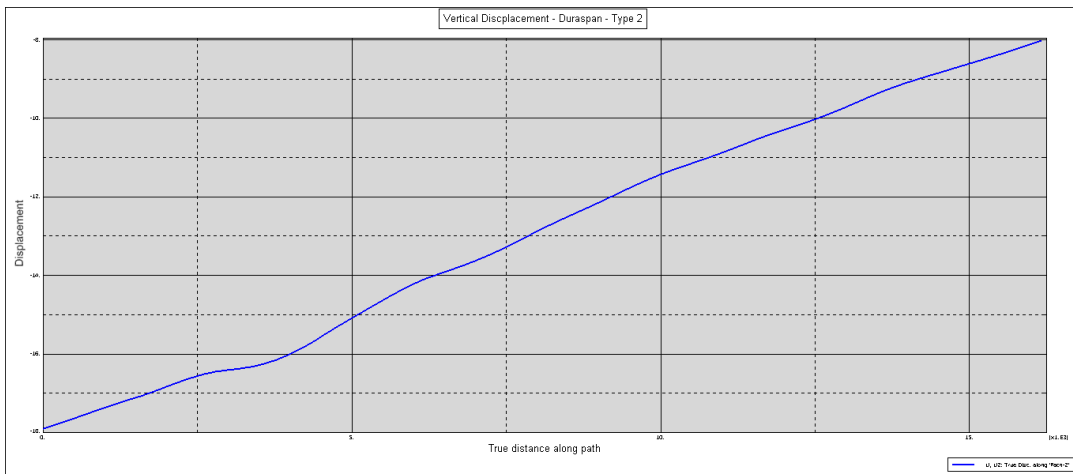


Figure A-17 Cut '2-2'of Duraspan deck – type 2 configuration

199
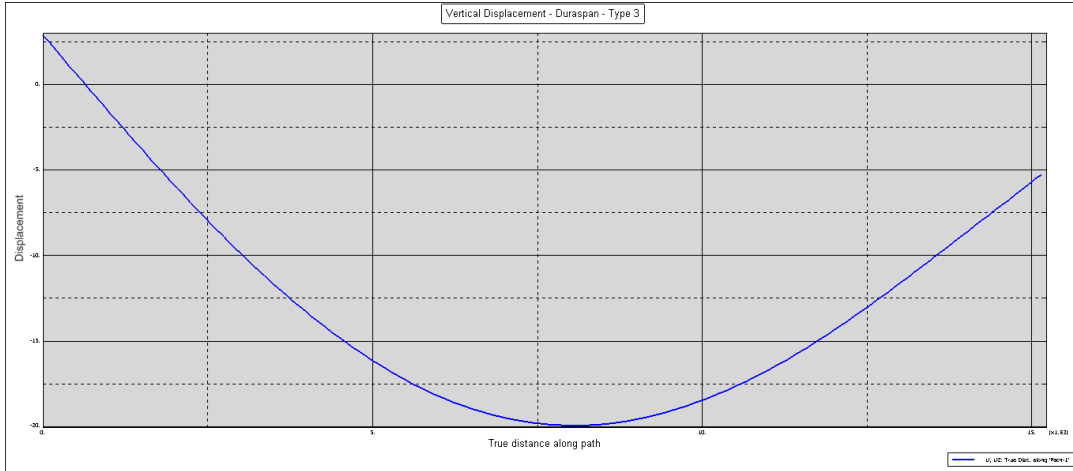
Figure A-18 Cut '1-1'of Duraspan deck – type 3 configuration
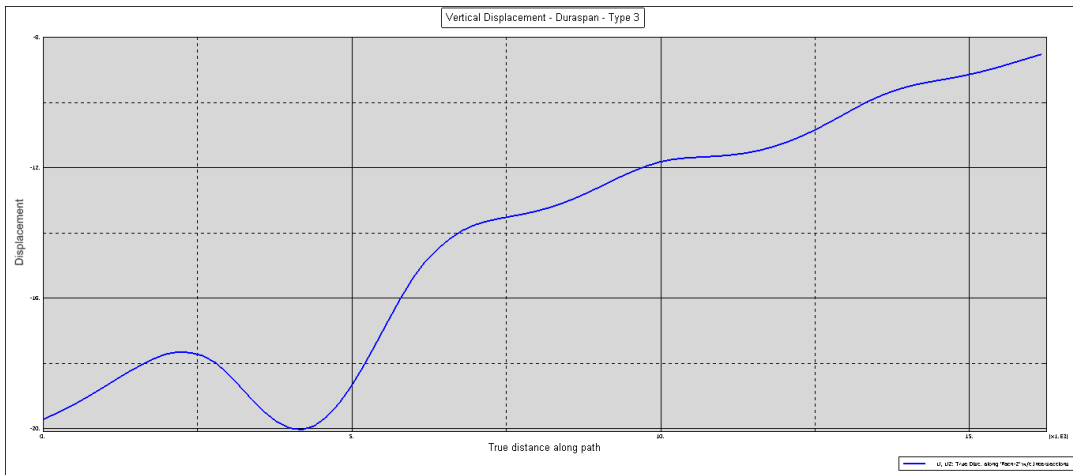


Figure A-19 Cut '2-2'of Duraspan deck – type 3 configuration

# B. Appendix – Stresses of the Deck and Steel Structure

Ecosafe Deck – Type 1 Configuration
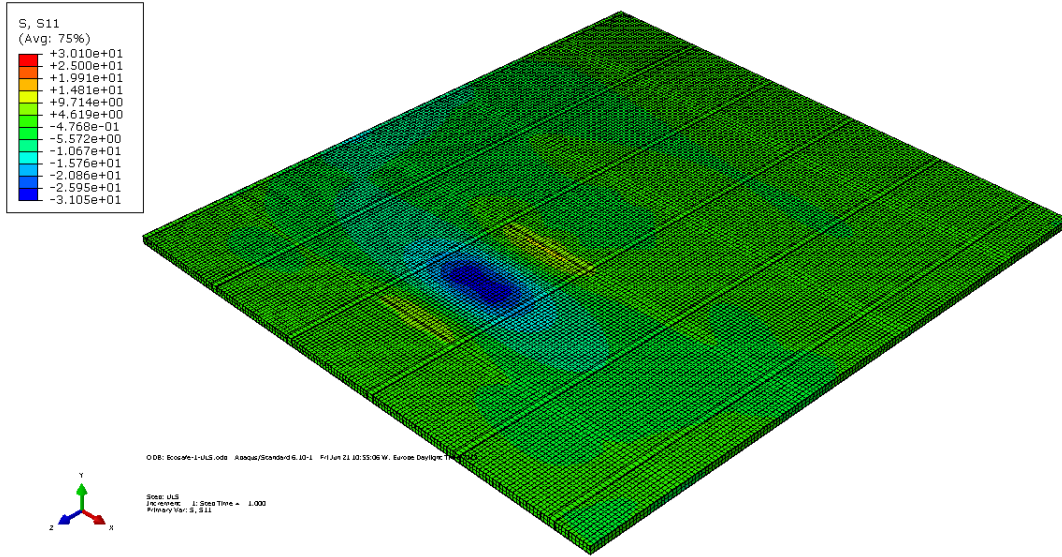


Figure B-1 Stresses of FRP deck - type 1 configuration (Ecosafe)
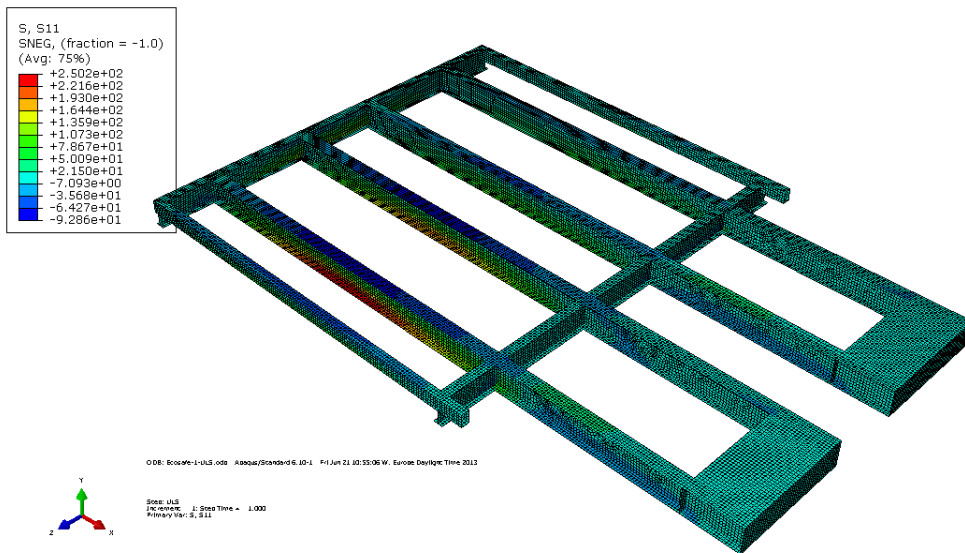


Figure B-2  Stresses of steel structure - type 1 configuration (Ecosafe)

Ecosafe Deck – Type 2 Configuration
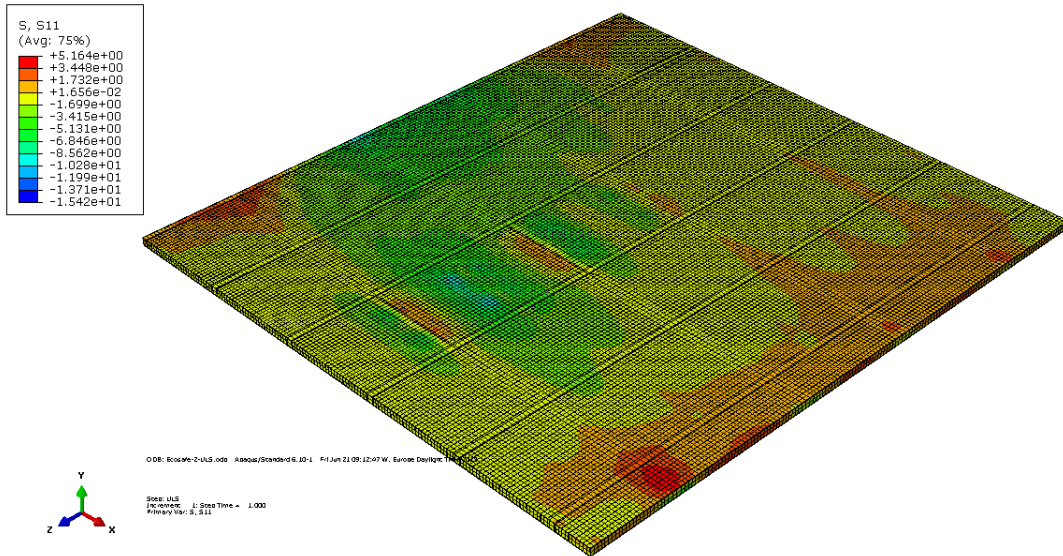


Figure B-3 Stresses of FRP deck - type 2 configuration (Ecosafe)
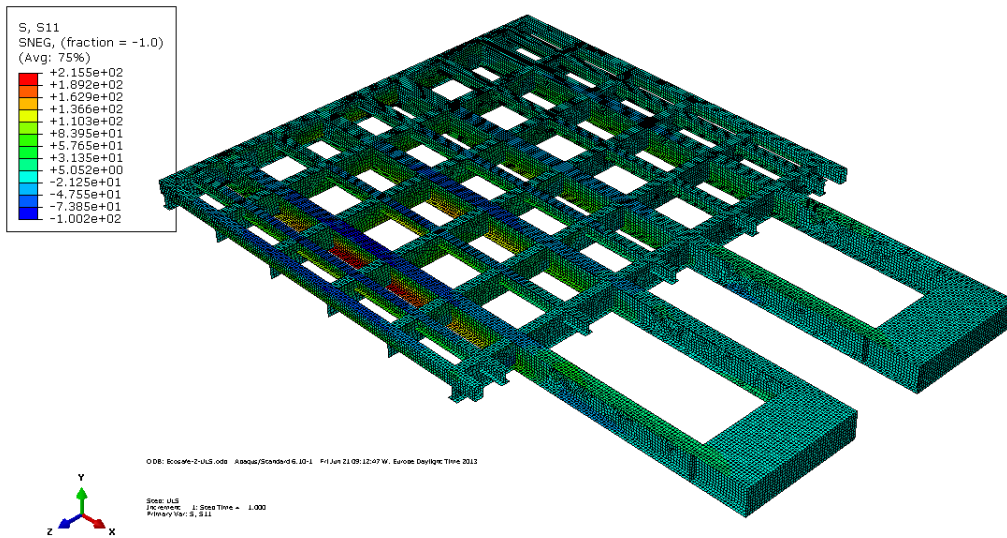


Figure B-4  Stresses of steel structure - type 2 configuration (Ecosafe)

Ecosafe Deck – Type 3 Configuration
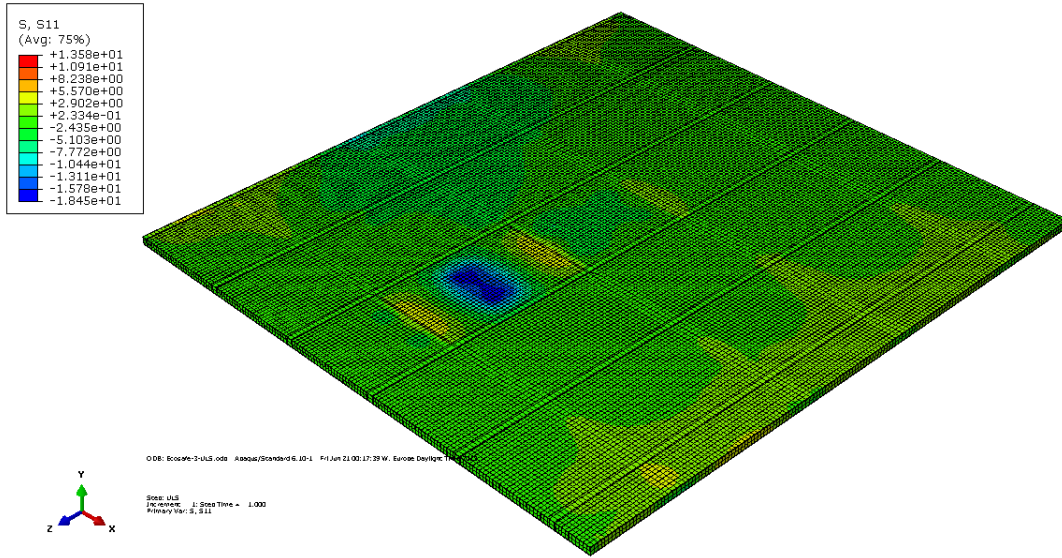


Figure B-5 Stresses of FRP deck - type 3 configuration (Ecosafe)
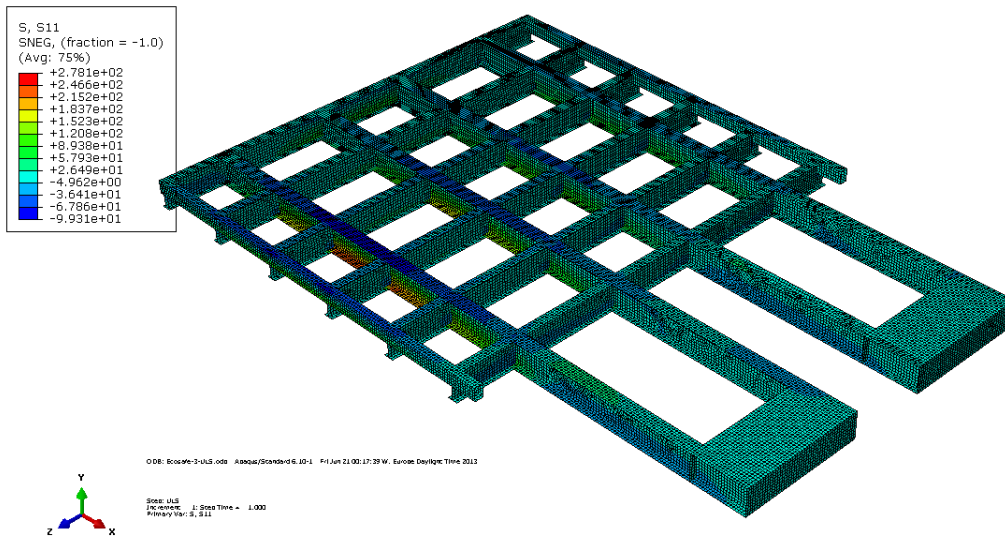


Figure B-6  Stresses of steel structure - type 3 configuration (Ecosafe)

ASSET Deck – Type 1 Configuration
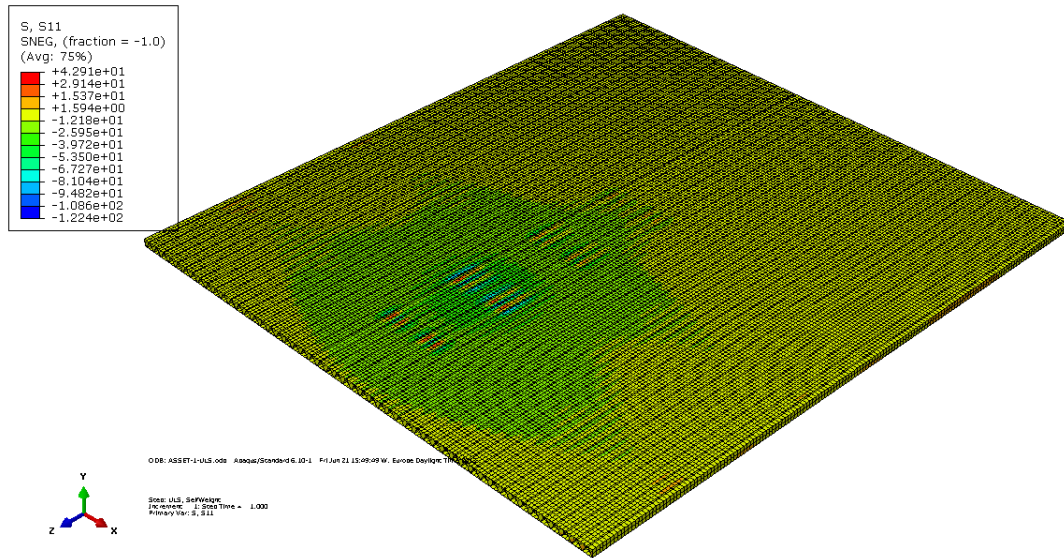


Figure B-7 Stresses of FRP deck - type 1 configuration (ASSET)
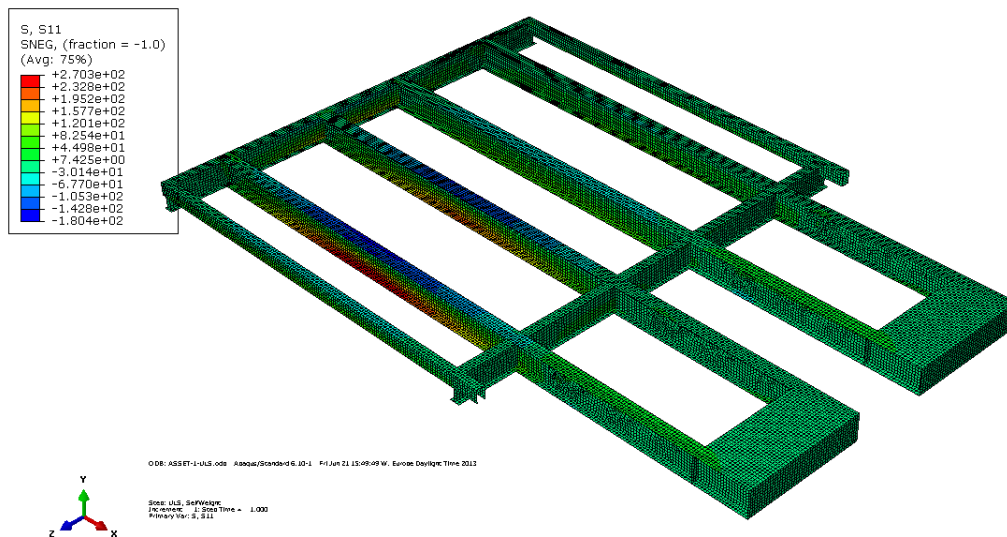


Figure B-8  Stresses of steel structure - type 1 configuration (ASSET)

ASSET Deck – Type 2 Configuration
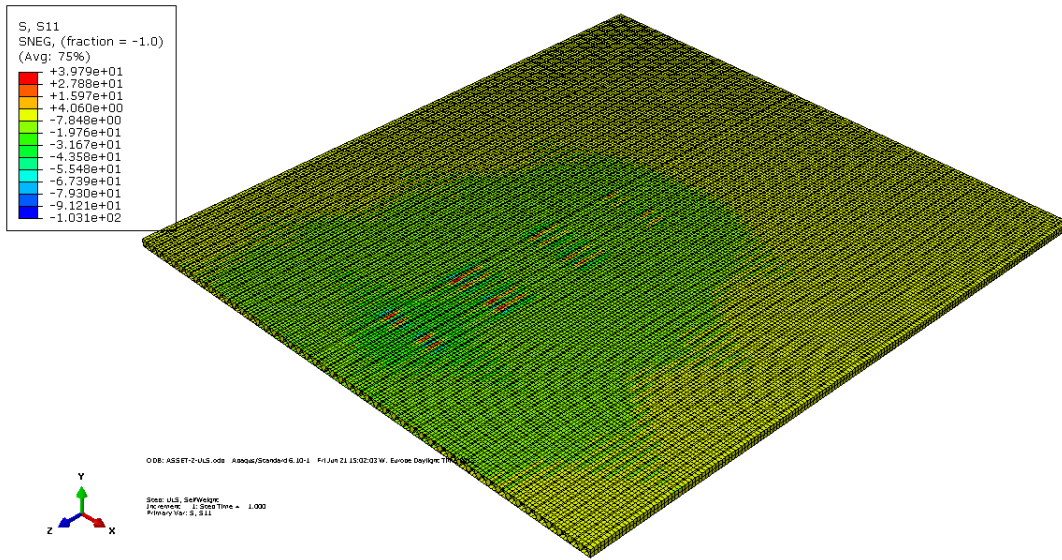


Figure B-9 Stresses of FRP deck - type 2 configuration (ASSET)
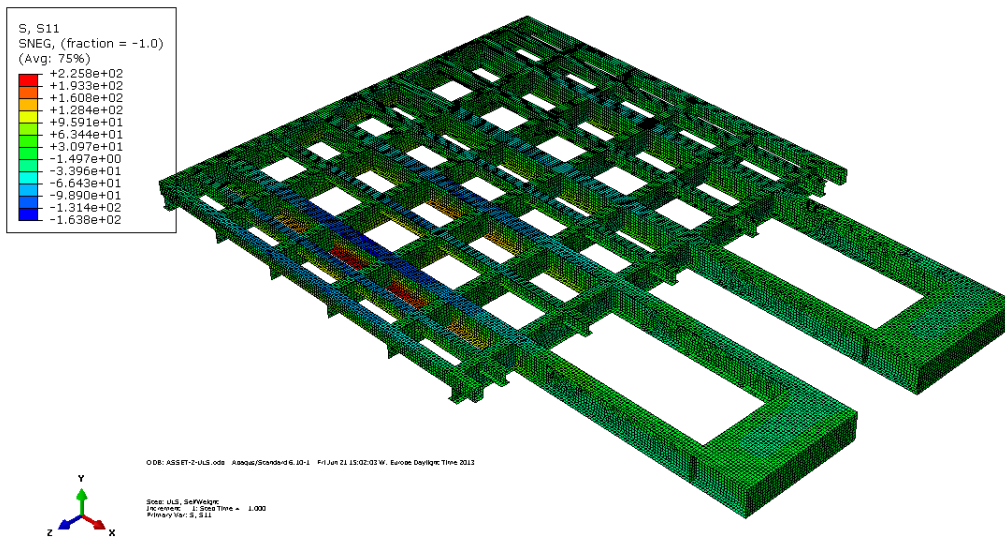


Figure B-10  Stresses of steel structure - type 2 configuration (ASSET)

ASSET Deck – Type 3 Configuration
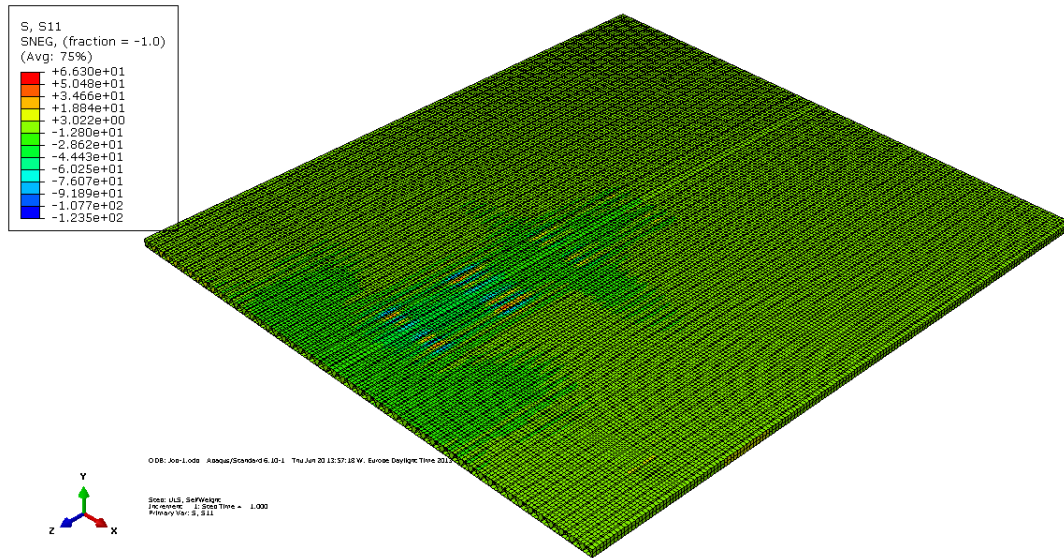


Figure B-11 Stresses of FRP deck - type 3 configuration (ASSET)
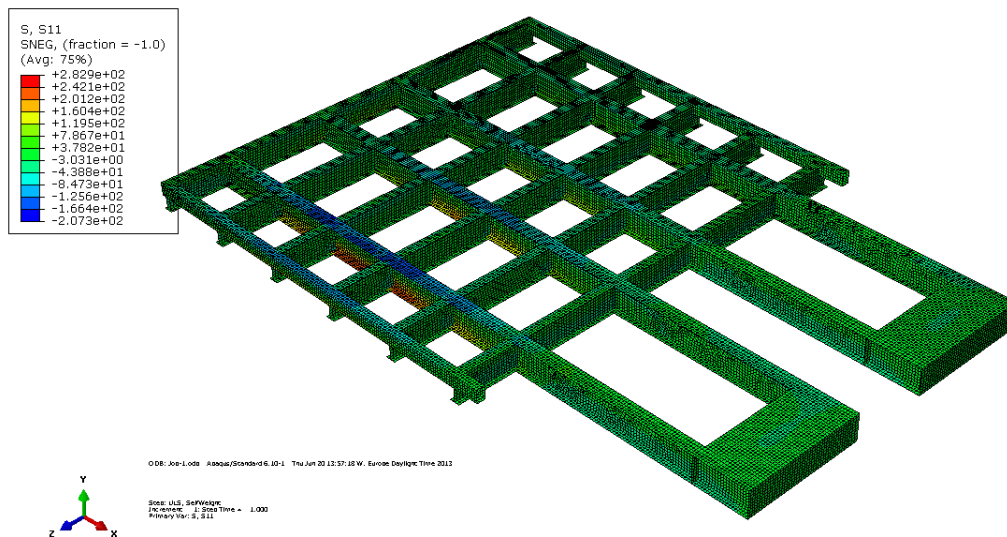


Figure B-12  Stresses of steel structure - type 3 configuration (ASSET)

Duraspan Deck – Type 1 Configuration
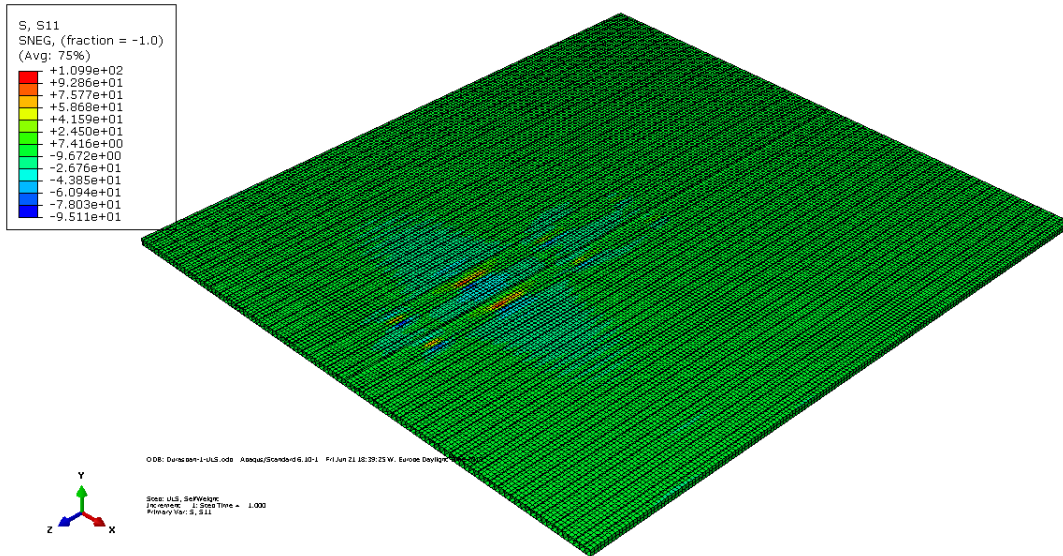


Figure B-13 Stresses of FRP deck - type 1 configuration (Duraspan)
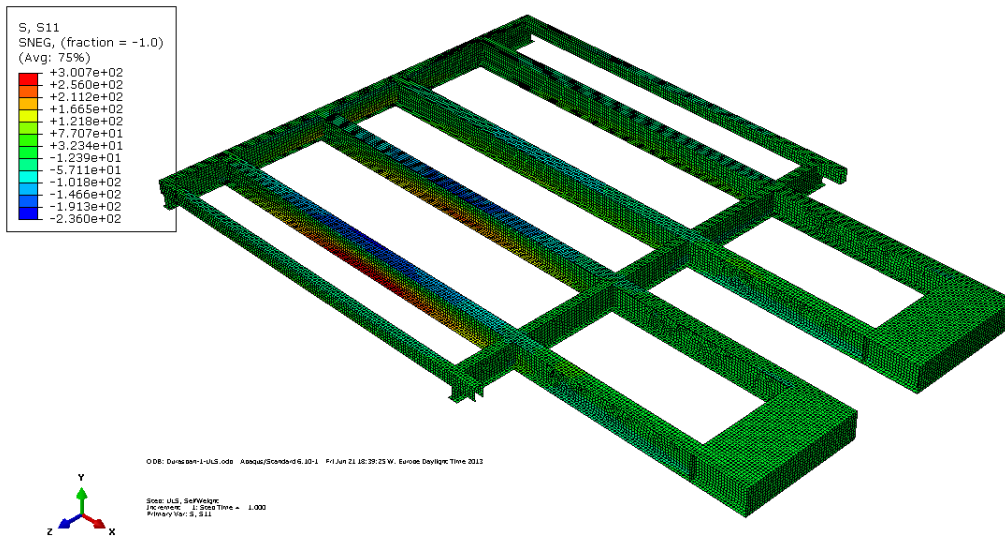


Figure B-14  Stresses of steel structure - type 1 configuration (Duraspan)

Duraspan Deck – Type 2 Configuration
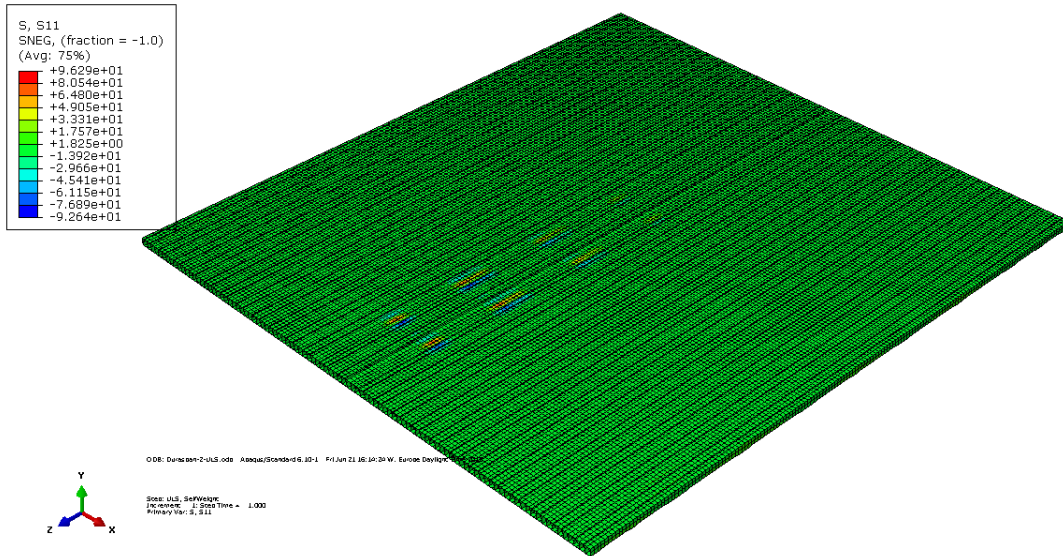


Figure B-15 Stresses of FRP deck - type 2 configuration (Duraspan)
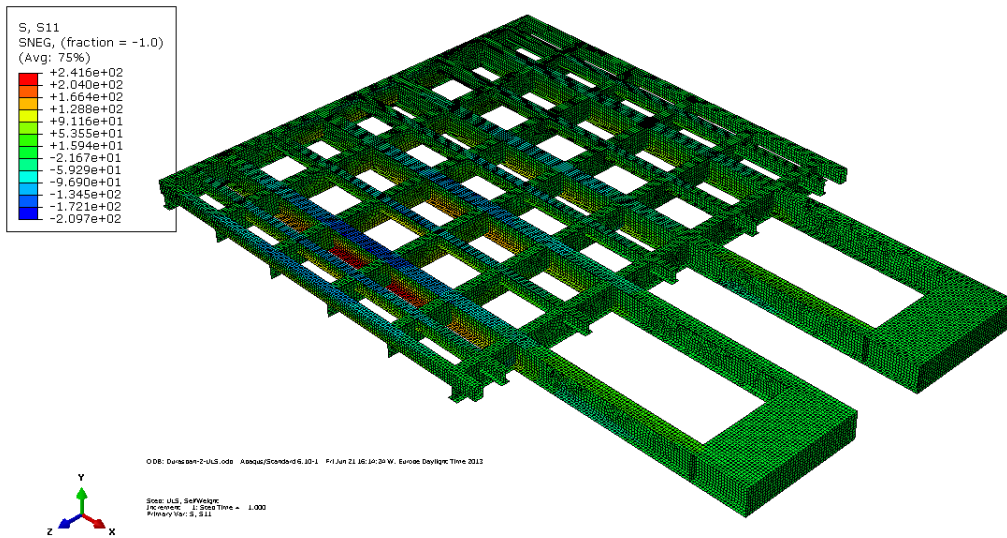


Figure B-16  Stresses of steel structure - type 2 configuration (Duraspan)

Duraspan Deck – Type 3 Configuration
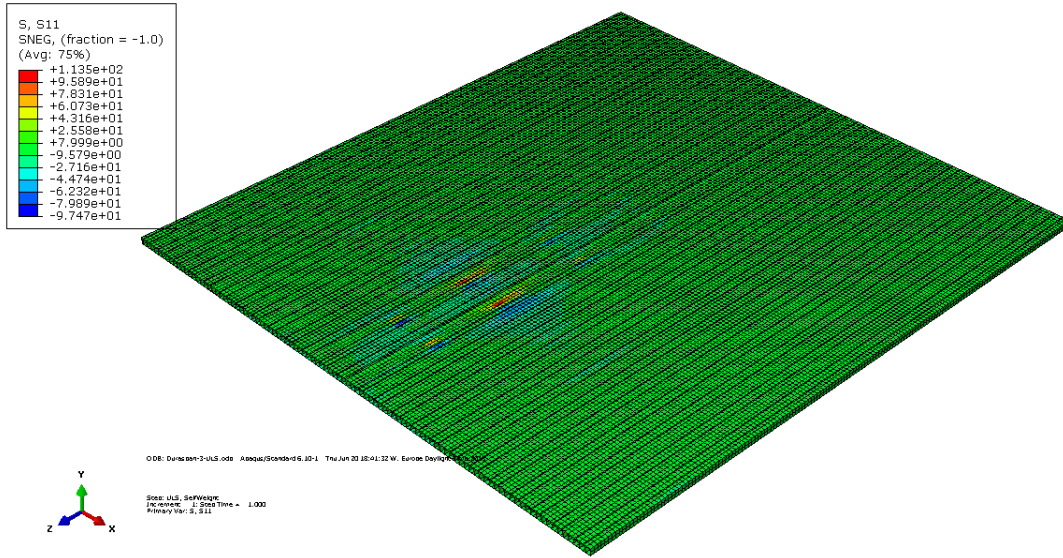


Figure B-17 Stresses of FRP deck - type 3 configuration (Duraspan)
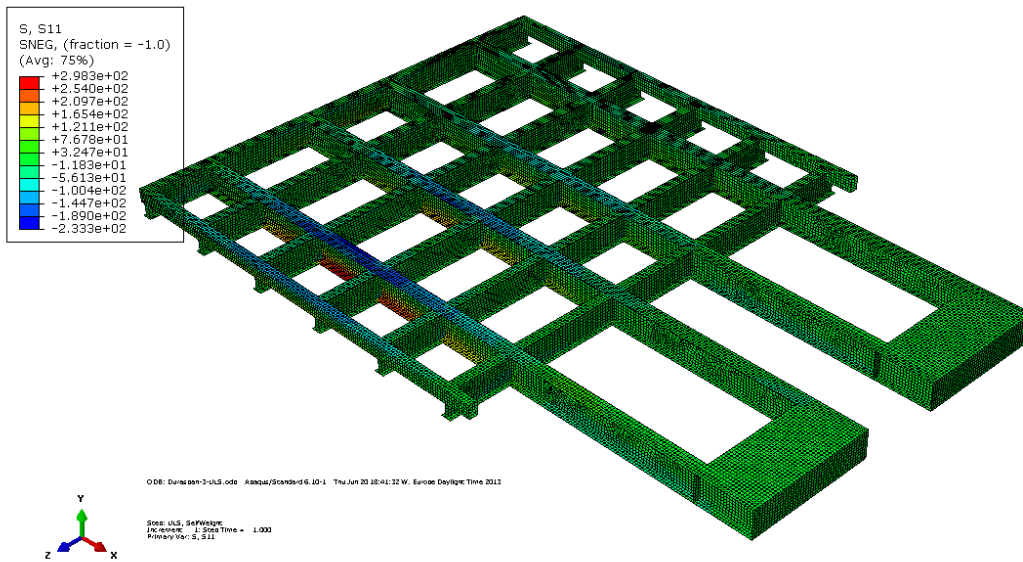


Figure B-18  Stresses of steel structure - type 3 configuration (Duraspan)

## C. Appendix – Shear and tensile stresses of the adhesive

In this appendix are shown the shear and tensile stresses of the adhesive for the three FRP decks when steel configuration 3 is applied (See Figure C-1 to Figure C-6). A comparison between each deck is shown in Table C-1. These values are lower to the failure values of the Epoxy and Polyurethane SikaDur adhesives tested by Keller, T. and T. Vallée, 2005, shown in Table C-2.

Table C-1 Shear and tensile stresses of the adhesive for three FRP decks[13]

|  |  | Ecosafe | | ASSET | | Duraspan | |
|---|---|---|---|---|---|---|---|
|  |  | Tension | Compression | Tension | Compression | Tension | Compression |
|  |  | [Mpa] | | [Mpa] | | [Mpa] | |
| Shear Stress | S22 | 1.3 | -2.6 | 4.4 | -5.4 | 7 | -6.6 |
| Tensile Stress | S13 | 0.67 | -0.5 | 1.2 | -1 | 0.77 | -0.75 |
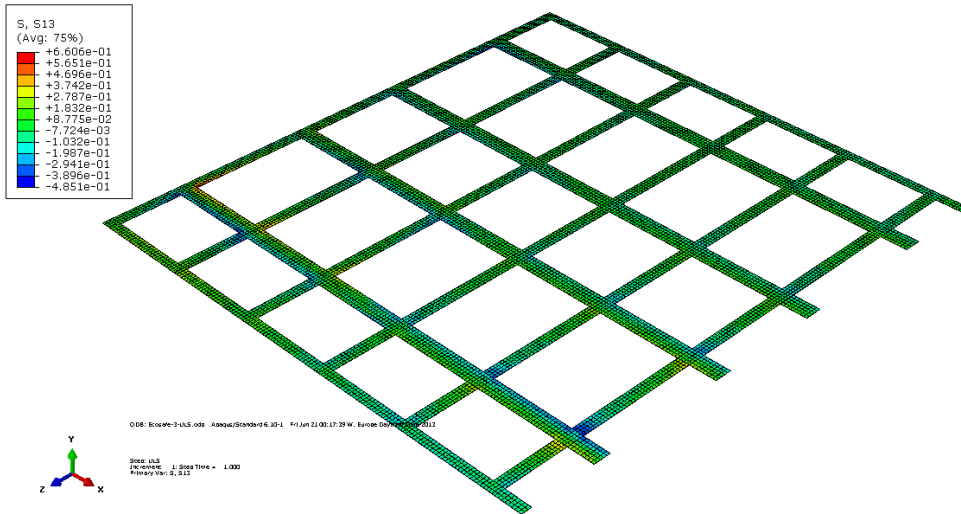


Figure C-1 Shear stresses S13 of Adhesive (Ecosafe deck applied)

---

[13] 1-longitudinal direction, 2-transverse direction, 3-upward direction
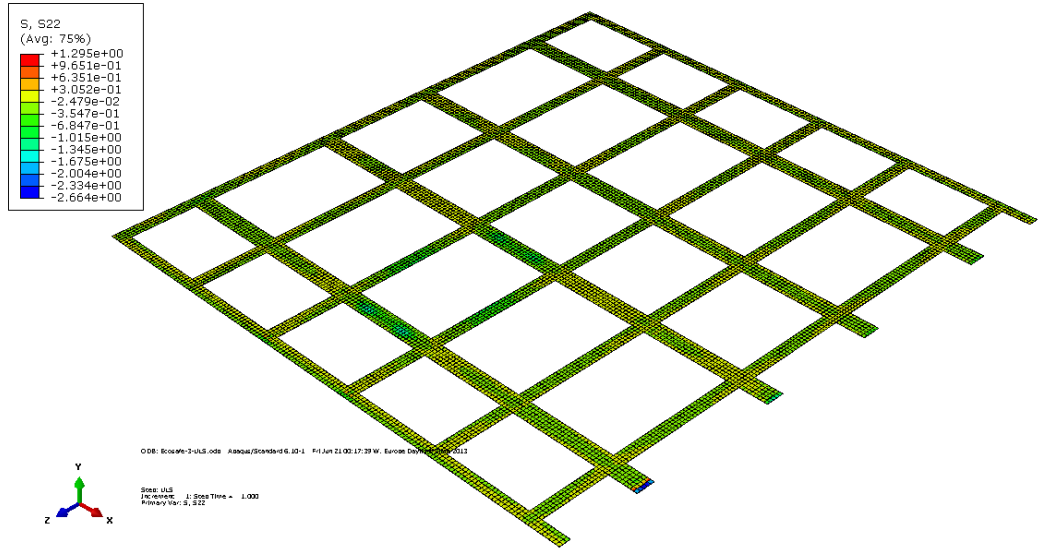
Figure C-2 Tensile stresses S22 of Adhesive (Ecosafe deck applied)
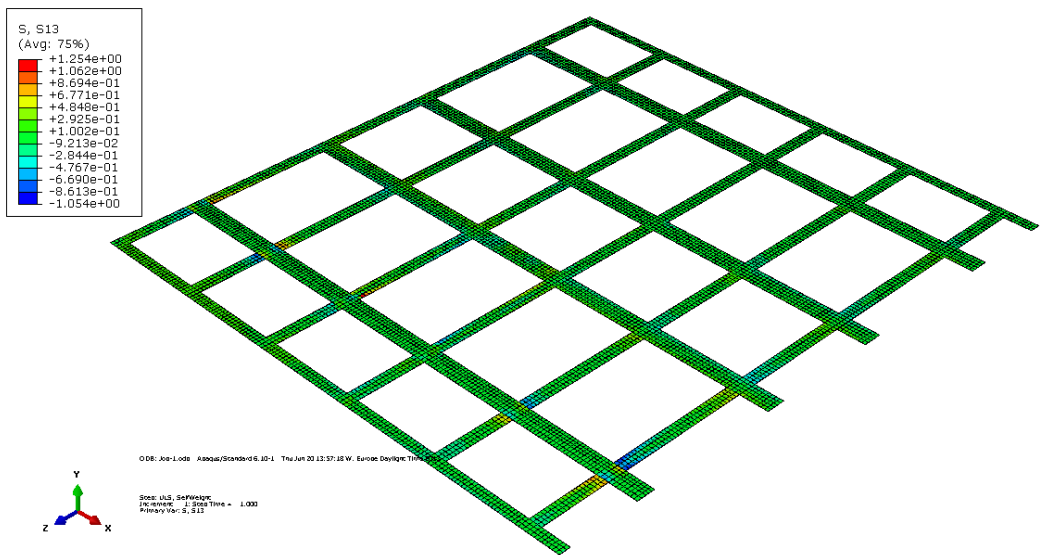


Figure C-3 Shear stresses S13 of Adhesive (ASSET deck applied)

211
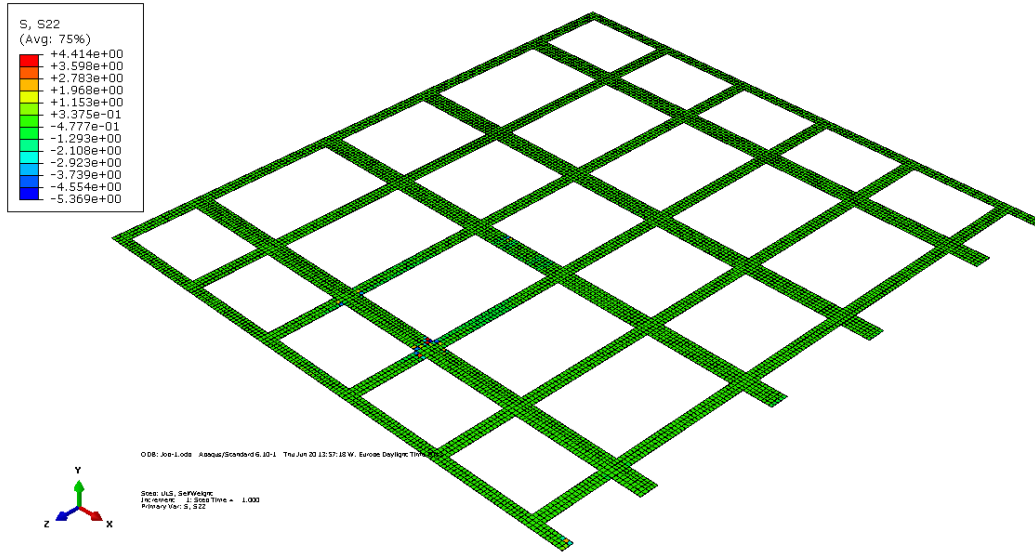
Figure C-4 Tensile stresses S22 of Adhesive (ASSET deck applied)
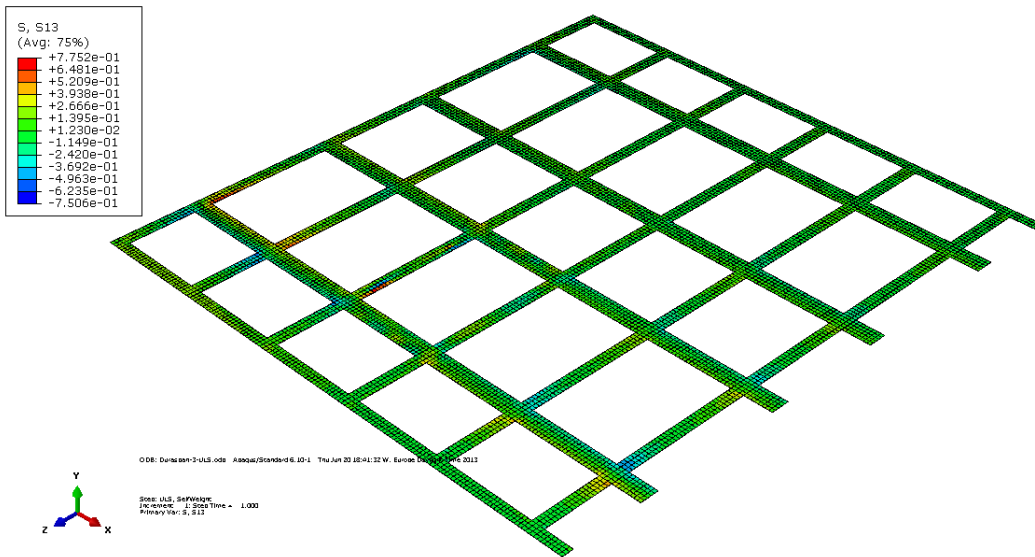


Figure C-5 Shear stresses S13 of Adhesive (Duraspan deck applied)

212
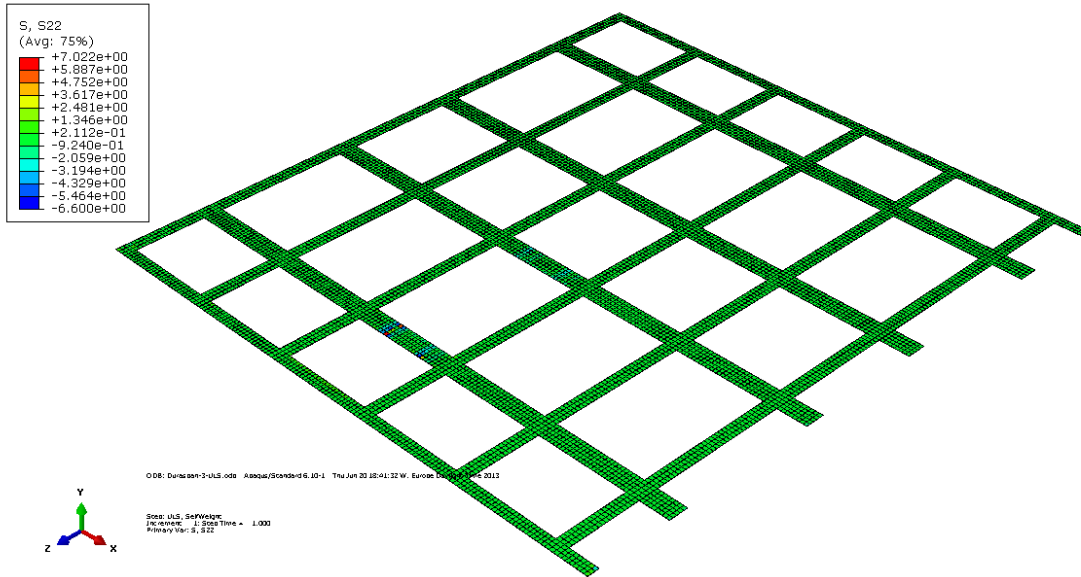
Figure C-6 Tensile stresses S22 of Adhesive (Duraspan deck applied)

Table C-2 Tensile and compression properties of epoxy and polyurethane adhesives (Keller, T. and T. Vallée, 2005)

| Adhesive | Loading | Nominal Stress (MPa) | Strain (%) | E-modulus (MPa) |
|---|---|---|---|---|
| SikaDur 330 epoxy | Tension (ISO 527) (5 specimens) | 38.1 ± 2.1 (failure) | 1.0 ± 0.1 (failure) | 4550 ± 140 |
| | Compression ASTM 694 (5 sp.) | -80.7 ± 2.6 (maximum) | -3.7 ± 0.1 (maximum) | 3050 ± 33 |
| SikaForce 7851 Polyurethane | Tension (ISO 527) (5 specimens) | 18.4 ± 1.0 (failure) | 37.1 ± 1.5 (failure) | 571 ± 56 |
| | Compression ASTM 694 (5 sp.) | -85.6 ± 2.5 (at -60% strain) | -60 (experiments stopped) | 371 ± 37 |

## D. Appendix – Axial Strains

Appendix D presents respectively the data taken from ABAQUS showing the axial strain for the case adhesive bonding and shear studs are used.

**Adhesive Bonding**
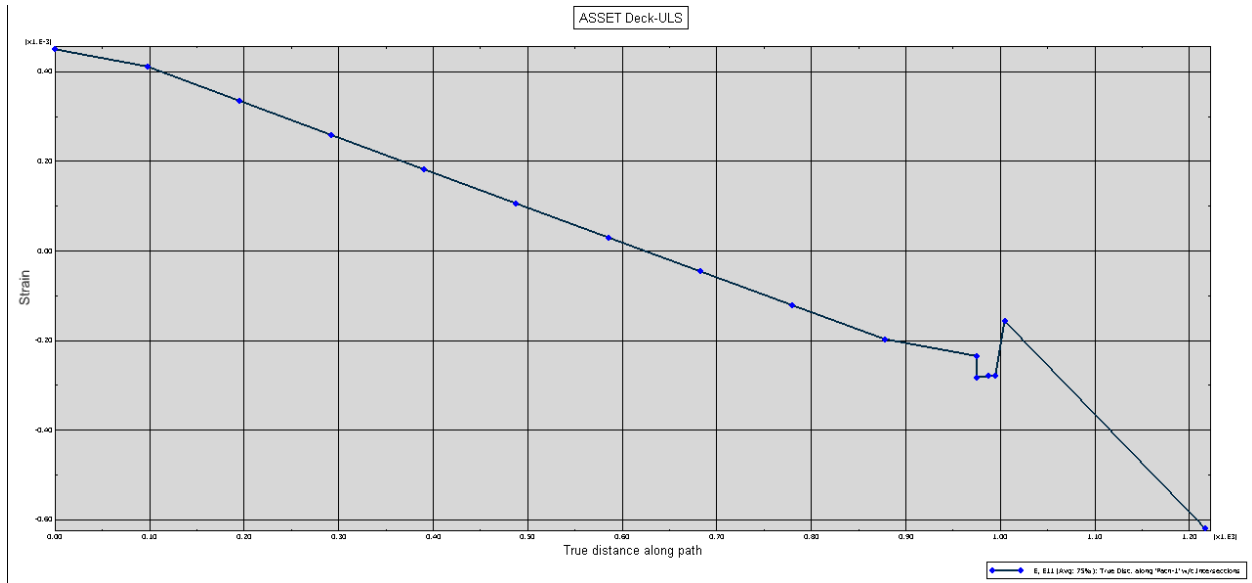


Figure D-1 Axial strain under ULS loading (ASSET Deck)
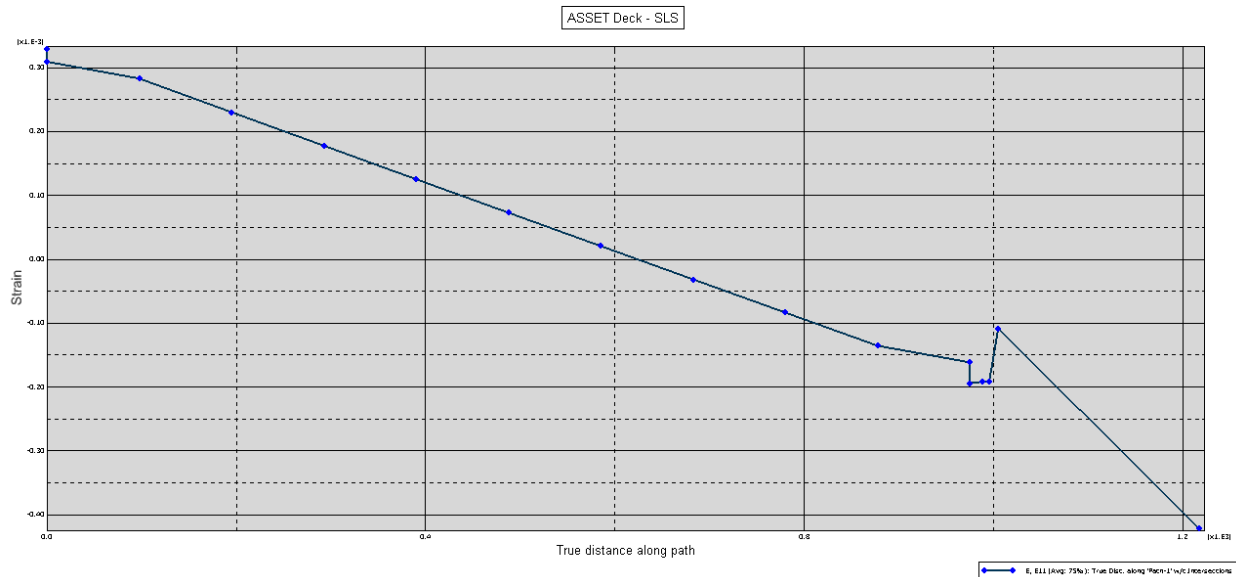


Figure D-2 Axial strain under SLS loading (ASSET Deck)
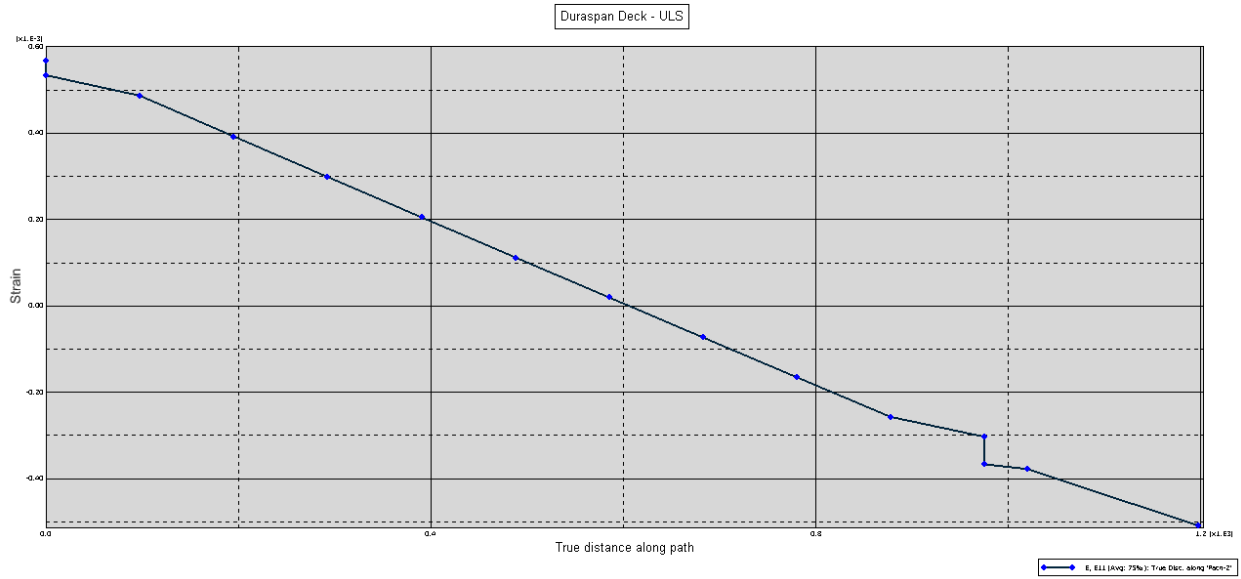
Figure D-3 Axial strain under ULS loading (Duraspan Deck)
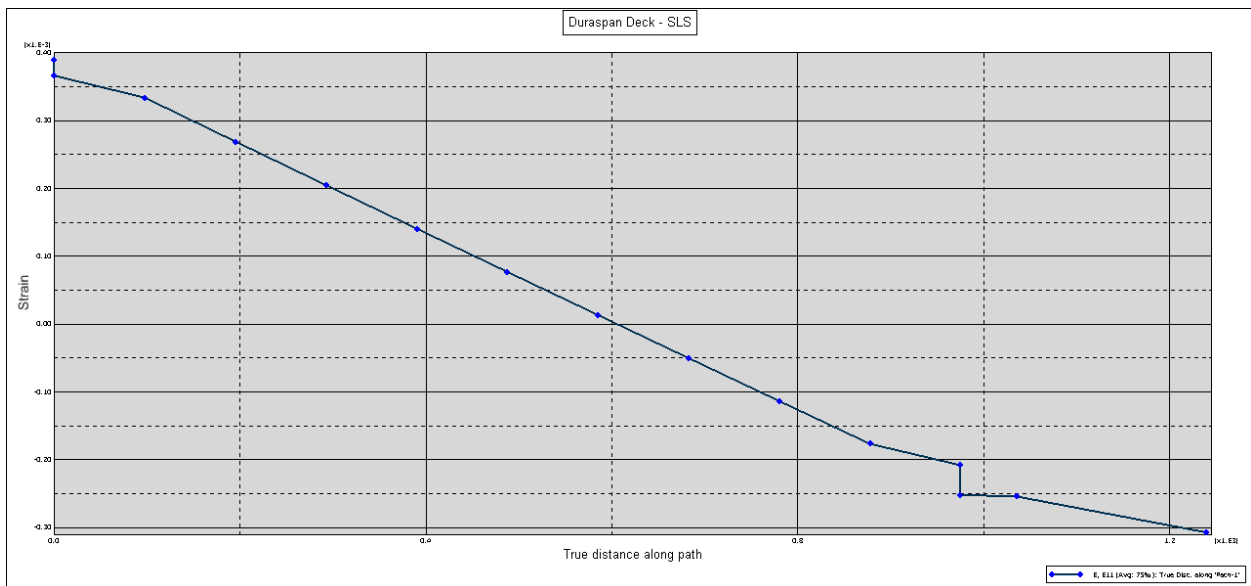


Figure D-4 Axial strain under SLS loading (Duraspan Deck)

**Shear Studs**
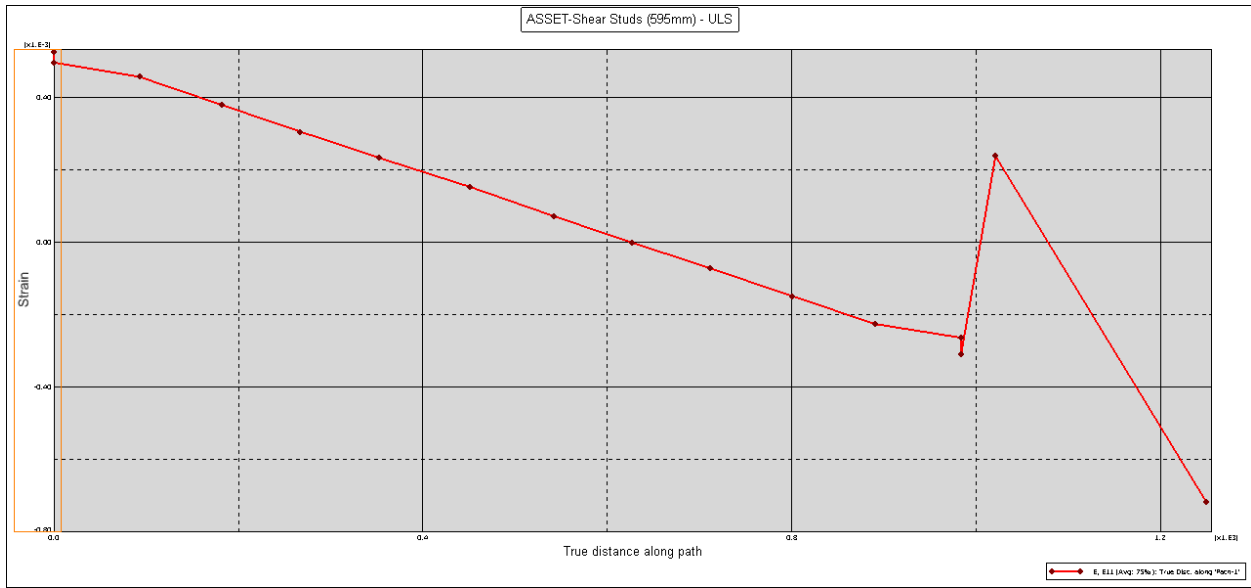


Figure D-5 Axial strain under ULS of ASSET deck (shear studs – 595mm)
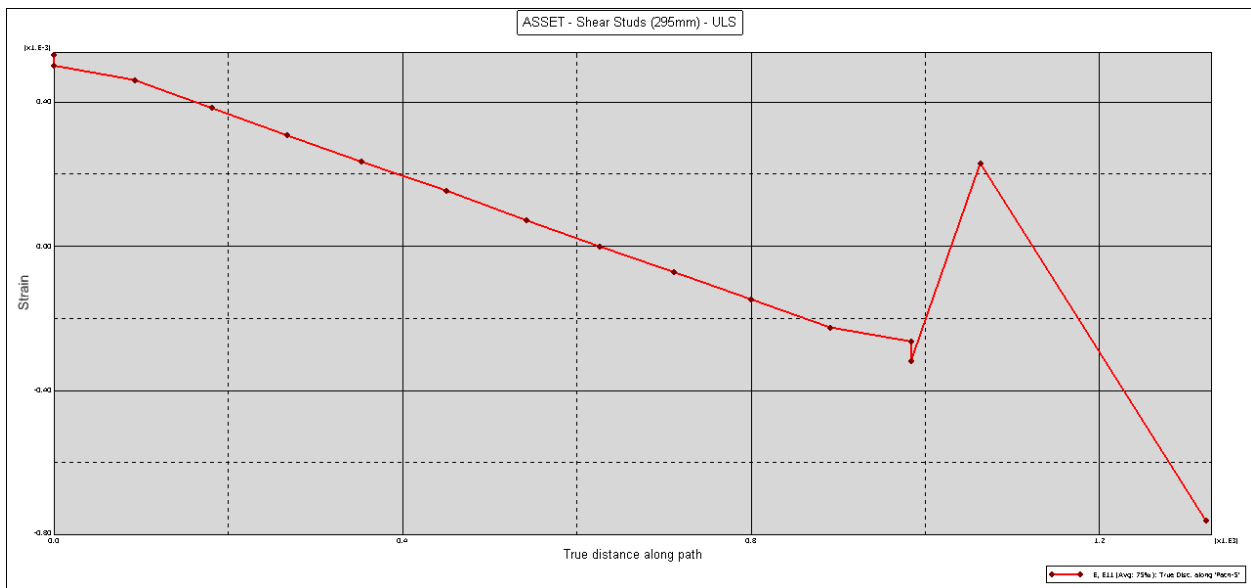


Figure D-6 Axial strain under ULS of ASSET deck (shear studs – 295mm)
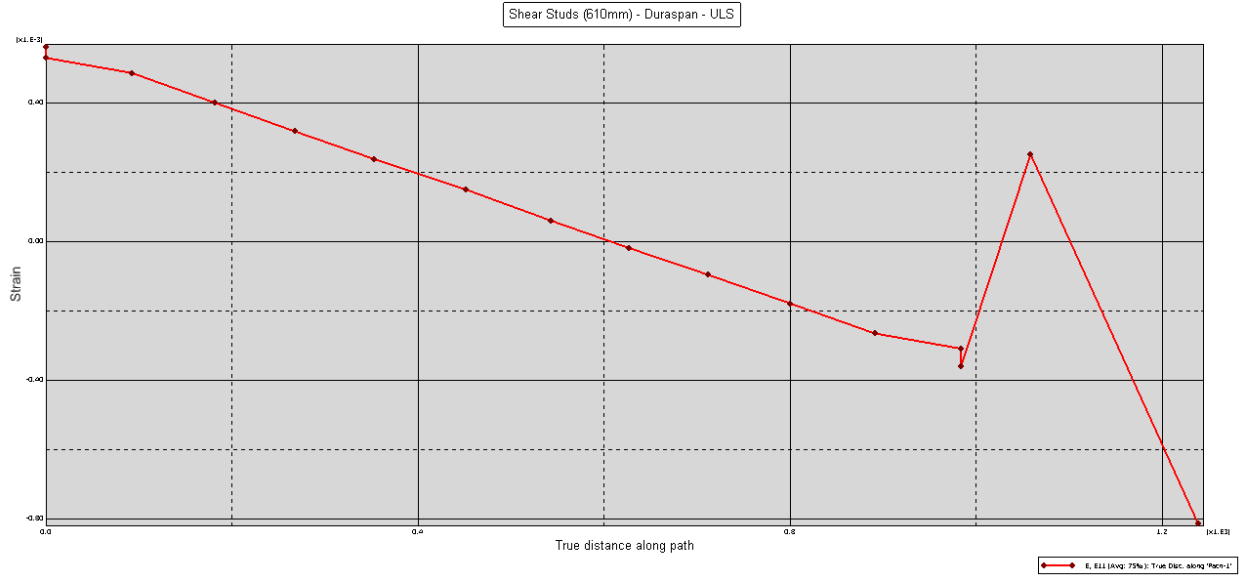
Figure D-7 Axial strain under ULS of Duraspan deck (shear studs – 610mm)
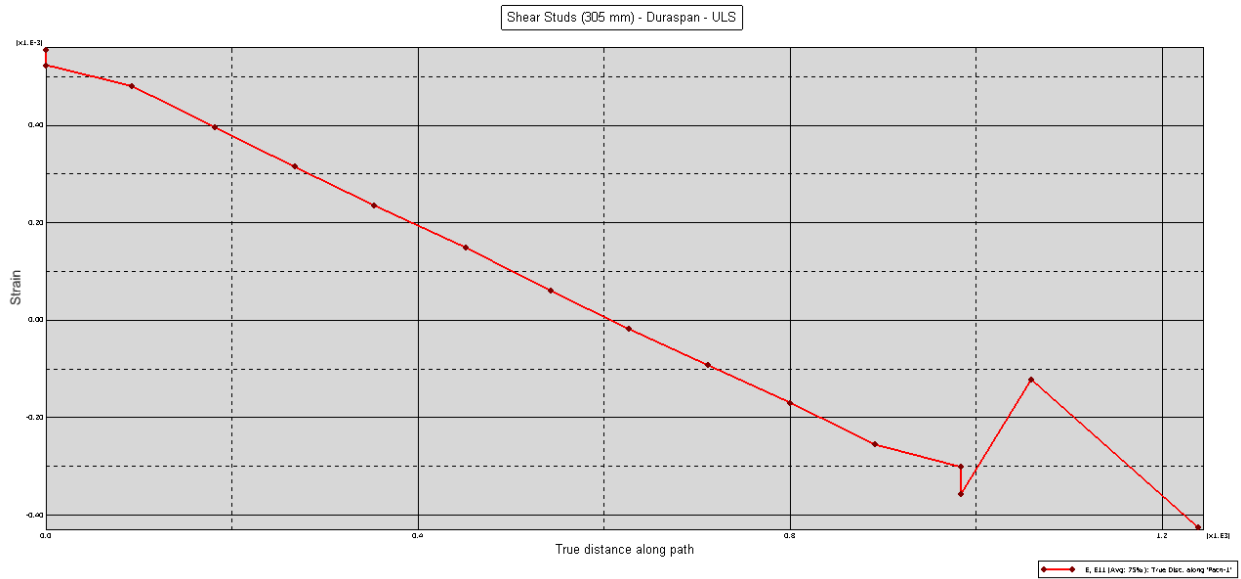


Figure D-8 Axial strain under ULS of Duraspan deck (shear studs – 305mm)

## E. Appendix – Calculation of effective width
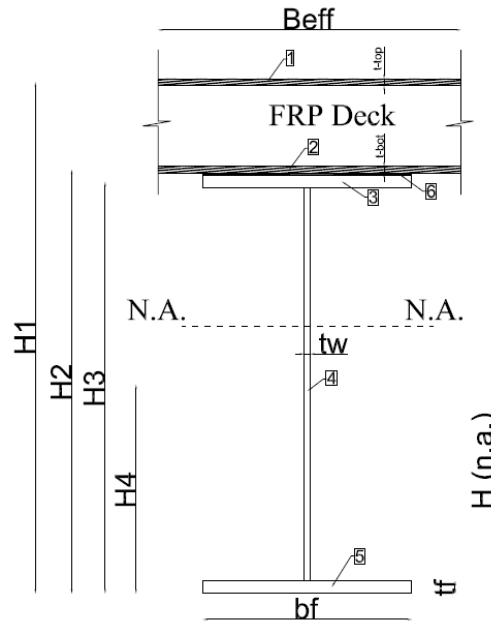


Figure E-1 Calculation of effective width

The calculation of the effective width follows from the following equation according to (Keelor, Luo, Earls, C, & Yulismana, 2004);

$$\left( \sum_{i=1}^{6} Ai \right) H_{N.A.} = \sum_{i=1}^{6} Ai \times Hi$$

$$A_1 = b_{eff} \times t_{top}$$

$$A_2 = b_{eff} \times t_{bot}$$

$$A_3 = b_f \times t_f$$

$$A_4 = (H - 2t_f) \times t_w$$

$$A_5 = b_f \times t_f$$

$$A_6 = b_{adh} \times t_{adh}$$

Here are presented the calculation of effective width when adhesive bonding or shear studs are used to join the FRP deck with steel girders.

**Adhesive bonding**

Table E-1 Calculation of effective width for ASSET Deck (ULS Loading)

| Calculation of effective width (ULS loading) - ASSET Deck | | | | | | | | | | |
|---|---|---|---|---|---|---|---|---|---|---|
| $t_d$ | $t_{top}=t_{bot}$ | $t_{adh}$ | $t_f$ | $b_f$ | $t_w$ | H | $H_{N.A.}$ | $E_s$ | $E_{FRP}$ | $E_{adh}$ |
| [mm] | [mm] | [mm] | [mm] | [mm] | [mm] | [mm] | [mm] | [Mpa] | [Mpa] | [Mpa] |
| 225 | 15.6 | 6 | 25 | 500 | 15 | 1000 | 621.5 | 210000 | 23000 | 3400 |
| | | | | | | | | | | |
| Y1 | [mm] | 1223.2 | | A1 | [mm2] | $b_{eff}*t_{top}/N_1$ | | | $N_1=E_s/E_{FRP}$ | 9.13 |
| Y2 | [mm] | 1013.8 | | A2 | [mm2] | $b_{eff}*t_{bot}/N_1$ | | | $N_2=E_s/E_{adh}$ | 61.76 |
| Y3 | [mm] | 987.5 | | A3 | [mm2] | 12500 | | | | |
| Y4 | [mm] | 500 | | A4 | [mm2] | 14250 | | | | |
| Y5 | [mm] | 12.5 | | A5 | [mm2] | 12500 | | | $b_{eff}$ | 2797 |
| Y6 | [mm] | 1003 | | A6 | [mm2] | 48.57 | | | | |
| $(A1+A2+A3+A4+A5+A6)*H_{N.A.}=\Sigma(A_i*Y_i)$ | | | | | | | | | | |

Table E-2 Calculation of effective width for Duraspan Deck (ULS Loading)

| Calculation of effective width (ULS loading) - Duraspan Deck | | | | | | | | | | |
|---|---|---|---|---|---|---|---|---|---|---|
| $t_d$ | $t_{top}=t_{bot}$ | $t_{adh}$ | $t_f$ | $b_f$ | $t_w$ | H | $H_{N.A.}$ | $E_s$ | $E_{FRP}$ | $E_{adh}$ |
| [mm] | [mm] | [mm] | [mm] | [mm] | [mm] | [mm] | [mm] | [Mpa] | [Mpa] | [Mpa] |
| 195 | 17 | 6 | 25 | 500 | 15 | 1000 | 608.5 | 210000 | 21240 | 3400 |
| | | | | | | | | | | |
| Y1 | [mm] | 1192.5 | | A1 | [mm2] | $b_{eff}*t_{top}/N_1$ | | | $N_1=E_s/E_{FRP}$ | 9.887 |
| Y2 | [mm] | 1014.5 | | A2 | [mm2] | $b_{eff}*t_{bot}/N_1$ | | | $N_2=E_s/E_{adh}$ | 61.76 |
| Y3 | [mm] | 987.5 | | A3 | [mm2] | 12500 | | | | |
| Y4 | [mm] | 500 | | A4 | [mm2] | 14250 | | | | |
| Y5 | [mm] | 12.5 | | A5 | [mm2] | 12500 | | | $b_{eff}$ | 2491 |
| Y6 | [mm] | 1003 | | A6 | [mm2] | 48.57 | | | | |
| $(A1+A2+A3+A4+A5+A6)*H_{N.A.}=\Sigma(A_i*Y_i)$ | | | | | | | | | | |

Table E-3 Calculation of effective width for Ecosafe Deck (ULS Loading)

| Calculation of effective width (ULS loading) - Ecosafe Deck | | | | | | | | | | |
|---|---|---|---|---|---|---|---|---|---|---|
| $t_d$ | $t_{top}=t_{bot}$ | $t_{adh}$ | $t_f$ | $b_f$ | $t_w$ | H | $H_{N.A.}$ | $E_s$ | $E_{FRP}$ | $E_{adh}$ |
| [mm] | [mm] | [mm] | [mm] | [mm] | [mm] | [mm] | [mm] | [Mpa] | [Mpa] | [Mpa] |
| 225 | 15.6 | 6 | 25 | 500 | 15 | 1000 | 715 | 210000 | 17257 | 3400 |

| | | | | | | | | |
|---|---|---|---|---|---|---|---|---|
| Y1 | [mm] | 1223.2 | A1 | [mm2] | $b_{eff}*t_{top}/N_1$ | | $N_1=E_s/E_{FRP}$ | 12.17 |
| Y2 | [mm] | 1013.8 | A2 | [mm2] | $b_{eff}*t_{bot}/N_1$ | | $N_2=E_s/E_{adh}$ | 61.76 |
| Y3 | [mm] | 987.5 | A3 | [mm2] | 12500 | | | |
| Y4 | [mm] | 500 | A4 | [mm2] | 14250 | | | |
| Y5 | [mm] | 12.5 | A5 | [mm2] | 12500 | | $b_{eff}$ | 8144 |
| Y6 | [mm] | 1003 | A6 | [mm2] | 48.57 | | | |

$(A1+A2+A3+A4+A5+A6)*H_{N.A.}=\Sigma(A_i*Y_i)$

**Shear Studs**

Table E-4 Calculation of effective width for ASSET Deck with shear studs (295 mm) (ULS Loading)

| Calculation of effective width (ULS loading) - ASSET Deck with shear studs (295mm) | | | | | | | | | | |
|---|---|---|---|---|---|---|---|---|---|---|
| $t_d$ | $t_{top}=t_{bot}$ | $t_{adh}$ | $t_f$ | $b_f$ | $t_w$ | H | $H_{N.A.}$ | $E_s$ | $E_{FRP}$ | $E_{grout}$ |
| [mm] | [mm] | [mm] | [mm] | [mm] | [mm] | [mm] | [mm] | [Mpa] | [Mpa] | [Mpa] |
| 225 | 15.6 | 6 | 25 | 500 | 15 | 1000 | 626 | 210000 | 23000 | 37000 |

| | | | | | | | | |
|---|---|---|---|---|---|---|---|---|
| Y1 | [mm] | 1223.2 | A1 | [mm2] | $b_{eff}*t_{top}/N_1$ | | $N_1=E_s/E_{FRP}$ | 9.13 |
| Y2 | [mm] | 1013.8 | A2 | [mm2] | $b_{eff}*t_{bot}/N_1$ | | $N_2=E_s/E_{adh}$ | 5.676 |
| Y3 | [mm] | 987.5 | A3 | [mm2] | 12500 | | | |
| Y4 | [mm] | 500 | A4 | [mm2] | 14250 | | | |
| Y5 | [mm] | 12.5 | A5 | [mm2] | 12500 | | $b_{eff}$ | 2820 |
| Y6 | [mm] | 1003 | A6 | [mm2] | 528.57 | | | |

$(A1+A2+A3+A4+A5+A6)*H_{N.A.}=\Sigma(A_i*Y_i)$

Table E-5 Calculation of effective width for Duraspan Deck with shear studs (305 mm) (ULS Loading)

| Calculation of effective width (ULS loading) - Duraspan Deck with shear studs (305mm) | | | | | | | | | | |
|---|---|---|---|---|---|---|---|---|---|---|
| $t_d$ | $t_{top}=t_{bot}$ | $t_{adh}$ | $t_f$ | $b_f$ | $t_w$ | H | $H_{N.A.}$ | $E_s$ | $E_{FRP}$ | $E_{adh}$ |
| [mm] | [mm] | [mm] | [mm] | [mm] | [mm] | [mm] | [mm] | [Mpa] | [Mpa] | [Mpa] |
| 195 | 17 | 6 | 25 | 500 | 15 | 1000 | 615 | 210000 | 21240 | 37000 |
| | | | | | | | | | | |
| Y1 | [mm] | 1192.5 | | A1 | [mm2] | $b_{eff}*t_{top}/N_1$ | | | $N_1=E_s/E_{FRP}$ | 9.887 |
| Y2 | [mm] | 1014.5 | | A2 | [mm2] | $b_{eff}*t_{bot}/N_1$ | | | $N_2=E_s/E_{adh}$ | 5.676 |
| Y3 | [mm] | 987.5 | | A3 | [mm2] | 12500 | | | | |
| Y4 | [mm] | 500 | | A4 | [mm2] | 14250 | | | | |
| Y5 | [mm] | 12.5 | | A5 | [mm2] | 12500 | | | $b_{eff}$ | 2565 |
| Y6 | [mm] | 1003 | | A6 | [mm2] | 528.57 | | | | |
| $(A1+A2+A3+A4+A5+A6)*H_{N.A.}=\Sigma(A_i*Y_i)$ | | | | | | | | | | |

## F. Appendix – FRP deck stresses when shear studs are applied

**ASSET Deck**
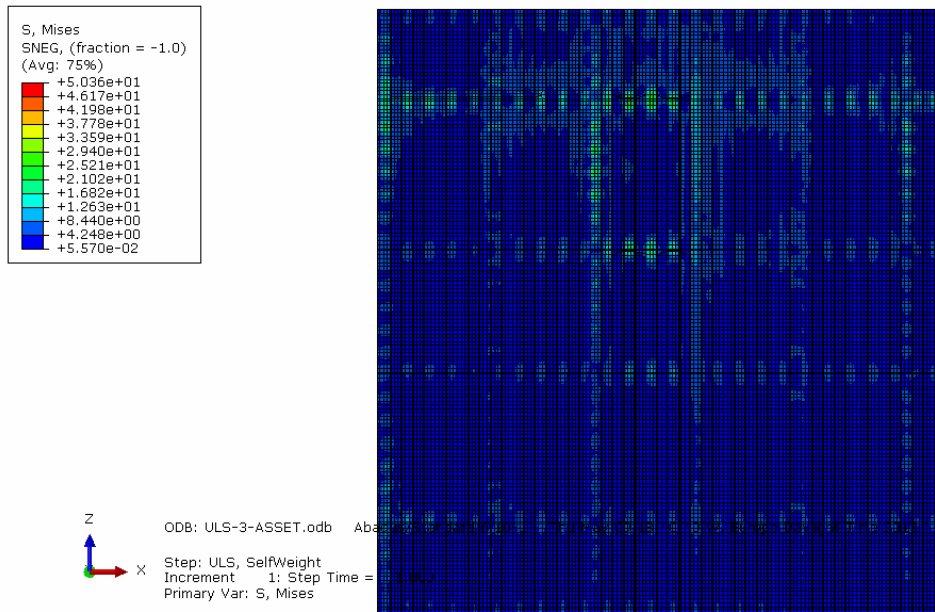


Figure F-1 Von Mises stresses of bottom flange of ASSET deck when shear studs span 595 mm
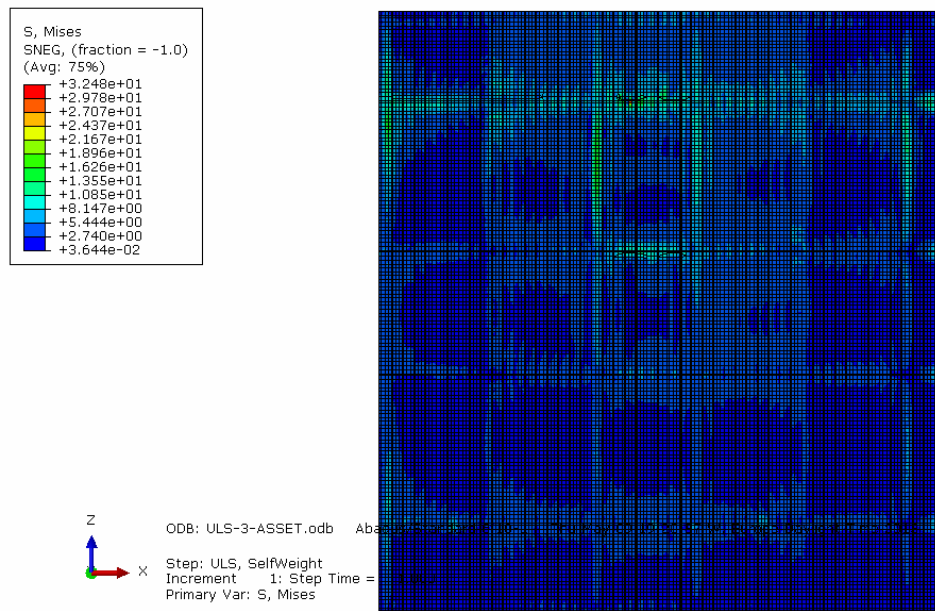


Figure F-2 Von Mises stresses of bottom flange of ASSET deck when shear studs span 295 mm

**Duraspan Deck**
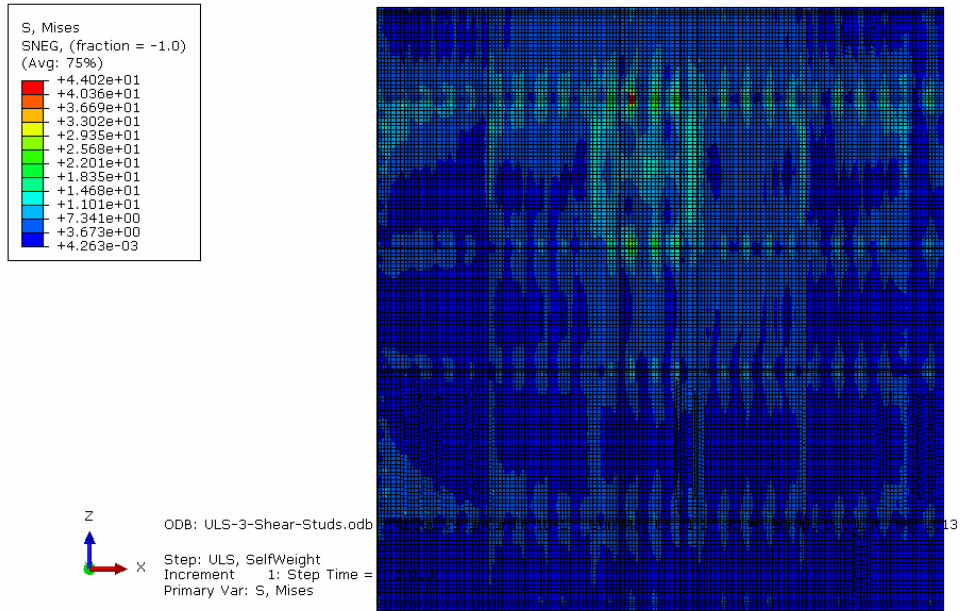


Figure F-3 Von Mises stresses of bottom flange of Duraspan deck when shear studs span 610 mm
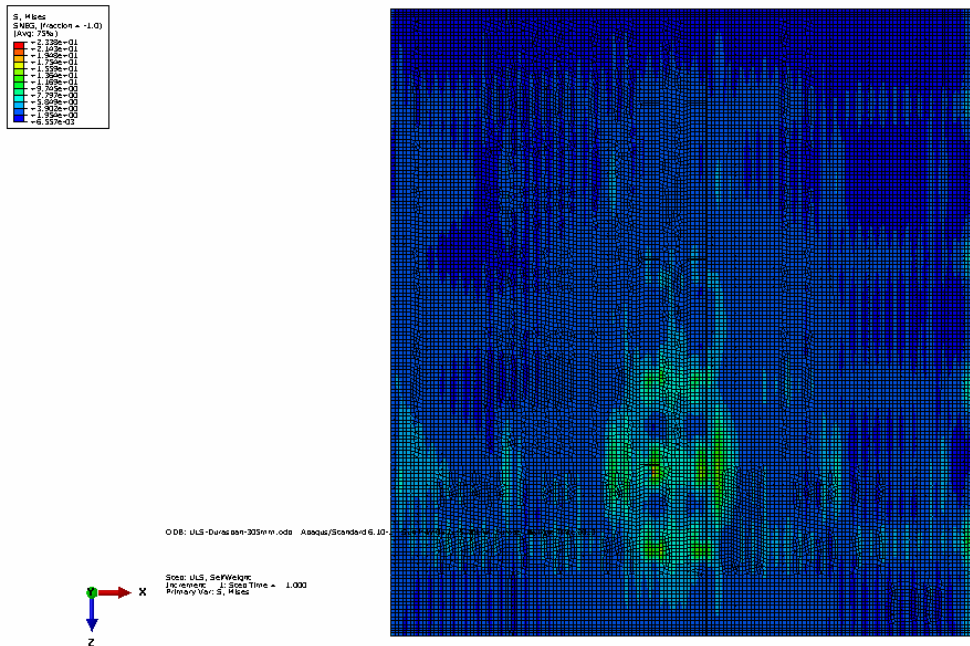


Figure F-4 Von Mises stresses of bottom flange of Duraspan deck when shear studs span 610 mm

# G. Appendix – Lateral Distribution Factor

Table G-1 Load distribution factor when ASSET deck is applied

| Load Case | Girder Position | Stress [MPa] | LDF |
|---|---|---|---|
| | ASSET Deck | | |
| | | | |
| 1 | 0 | 30 | 0.158261 |
| | 2435 | 52.7 | 0.284312 |
| | 6435 | 33.58 | 0.182639 |
| | 9735 | 26 | 0.14109 |
| | 13735 | 32.4 | 0.17487 |
| | 16170 | 14.88 | 0.079773 |
| 2 | 0 | 25.8 | 0.137931 |
| | 2435 | 51.2 | 0.273724 |
| | 6435 | 34 | 0.18177 |
| | 9735 | 27 | 0.144346 |
| | 13735 | 33.65 | 0.179898 |
| | 16170 | 15.4 | 0.082331 |
| 3 | 0 | 23.7 | 0.128358 |
| | 2435 | 47.7 | 0.258341 |
| | 6435 | 34.36 | 0.186092 |
| | 9735 | 28 | 0.151646 |
| | 13735 | 34.88 | 0.188908 |
| | 16170 | 16 | 0.086655 |
| 4 | 0 | 22.25 | 0.120825 |
| | 2435 | 45.6 | 0.247624 |
| | 6435 | 34.5 | 0.187347 |
| | 9735 | 29 | 0.15748 |
| | 13735 | 36.3 | 0.197122 |
| | 16170 | 16.5 | 0.089601 |
| 5 | 0 | 21 | 0.113778 |
| | 2435 | 43.6 | 0.236225 |
| | 6435 | 34.3 | 0.185837 |
| | 9735 | 30.57 | 0.165628 |
| | 13735 | 37.9 | 0.205342 |
| | 16170 | 17.2 | 0.09319 |
| 6 | 0 | 20 | 0.108079 |
| | 2435 | 41.8 | 0.225885 |
| | 6435 | 33.4 | 0.180492 |
| | 9735 | 32.3 | 0.174547 |
| | 13735 | 39.6 | 0.213996 |
| | 16170 | 17.95 | 0.097001 |

Table G-2 Load distribution factor when Duraspan deck is applied

| Duraspan Deck | | | |
|---|---|---|---|
| Load Case | Girder Position | Stress [MPa] | LDF |
| | | | |
| 1 | 0 | 30.3 | 0.154277 |
| | 2435 | 55.5 | 0.282587 |
| | 6435 | 34.2 | 0.174134 |
| | 9735 | 27 | 0.137475 |
| | 13735 | 34.2 | 0.174134 |
| | 16170 | 15.2 | 0.077393 |
| 2 | 0 | 25.2 | 0.131004 |
| | 2435 | 53.41 | 0.277656 |
| | 6435 | 34.5 | 0.179351 |
| | 9735 | 28 | 0.14556 |
| | 13735 | 35.5 | 0.18455 |
| | 16170 | 15.75 | 0.081878 |
| 3 | 0 | 23.7 | 0.123373 |
| | 2435 | 51.3 | 0.267048 |
| | 6435 | 34.88 | 0.181572 |
| | 9735 | 29 | 0.150963 |
| | 13735 | 36.9 | 0.192087 |
| | 16170 | 16.32 | 0.084956 |
| 4 | 0 | 22 | 0.120766 |
| | 2435 | 48.87 | 0.268266 |
| | 6435 | 35.87 | 0.196904 |
| | 9735 | 30.16 | 0.16556 |
| | 13735 | 28.36 | 0.155679 |
| | 16170 | 16.91 | 0.092825 |
| 5 | 0 | 20.6 | 0.107718 |
| | 2435 | 46.59 | 0.243621 |
| | 6435 | 34.92 | 0.182598 |
| | 9735 | 31.57 | 0.165081 |
| | 13735 | 40 | 0.209161 |
| | 16170 | 17.56 | 0.091822 |
| 6 | 0 | 19.52 | 0.101985 |
| | 2435 | 44.51 | 0.23255 |
| | 6435 | 34.1 | 0.178161 |
| | 9735 | 33.07 | 0.17278 |
| | 13735 | 41.94 | 0.219122 |
| | 16170 | 18.26 | 0.095402 |

Table G-3 Load distribution factor when Ecosafe deck is applied

| Ecosafe Deck | | | |
|---|---|---|---|
| Load Case | Girder Position | Stress [MPa] | LDF |
| | | | |
| 1 | 0 | 32.5 | 0.151763 |
| | 2435 | 57.95 | 0.270605 |
| | 6435 | 38.1 | 0.177913 |
| | 9735 | 30.95 | 0.144525 |
| | 13735 | 37.25 | 0.173943 |
| | 16170 | 17.4 | 0.081251 |
| 2 | 0 | 28.7 | 0.137111 |
| | 2435 | 55.39 | 0.264619 |
| | 6435 | 38.35 | 0.183212 |
| | 9735 | 31.53 | 0.150631 |
| | 13735 | 37.4 | 0.178674 |
| | 16170 | 17.95 | 0.085754 |
| 3 | 0 | 26.92 | 0.128681 |
| | 2435 | 52.78 | 0.252294 |
| | 6435 | 38.6 | 0.184512 |
| | 9735 | 32.78 | 0.156692 |
| | 13735 | 39.6 | 0.189293 |
| | 16170 | 18.52 | 0.088528 |
| 4 | 0 | 25.43 | 0.122702 |
| | 2435 | 50.39 | 0.243136 |
| | 6435 | 38.62 | 0.186345 |
| | 9735 | 32.83 | 0.158408 |
| | 13735 | 40.87 | 0.197201 |
| | 16170 | 19.11 | 0.092207 |
| 5 | 0 | 24.2 | 0.117021 |
| | 2435 | 48.27 | 0.233414 |
| | 6435 | 38.35 | 0.185445 |
| | 9735 | 33.93 | 0.164072 |
| | 13735 | 42.31 | 0.204594 |
| | 16170 | 19.74 | 0.095455 |
| 6 | 0 | 23.17 | 0.112182 |
| | 2435 | 46.35 | 0.224412 |
| | 6435 | 37.57 | 0.181902 |
| | 9735 | 35.19 | 0.170379 |
| | 13735 | 43.85 | 0.212308 |
| | 16170 | 20.41 | 0.098819 |

# H. Appendix - Calculation of ballast and moments during opening and closing procedure

Table H-1 Calculation of ballast weight

**Project** : Wilhelminabrug Zaanstad

**Onderdeel** : Evenwichtsberekening

Iv-Infra
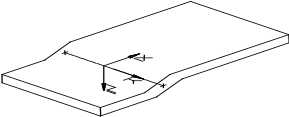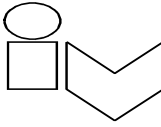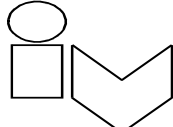
| Omschrijving | Lengte (x) [mm] | Breedte (y) [mm] | Hoogte (z) [mm] | s.m. [kg/mm³] | Aantal [st.] | Massa [kg] | X [mm] | Z [mm] | $M_{dicht}$ 0° [kgm] | $M_{open}$ 90° [kgm] | Ip [kgm²] |
|---|---|---|---|---|---|---|---|---|---|---|---|
| **Val** | | | | | | | | | | | |
| Slijtlaag (rijweg) | 15,923 | 16,200 | 8 | 2.5 E-6 | 1 | 5,159 kg | 9,277 | -1,080 | 47,861 | -5,572 | 559,023 |
| Kunststof dek | 15,923 | 16,200 | 225 | 4.0 E-7 | 1 | 23,000 kg | 9,277 | -960 | 213,371 | -22,069 | 2,486,670 |
| Middenhoofdligger - lijfplaat onder dek | 15,220 | 15 | 950 | 7.9 E-6 | 2 | 3,405 kg | 9,277 | -322 | 31,589 | -1,096 | 359,393 |
| - onderflens onder dek | 15,220 | 500 | 25 | 7.9 E-6 | 2 | 2,987 kg | 9,277 | -322 | 27,710 | -962 | 315,032 |
| Buitenhoofdligger - lijfplaat onder dek | 15,220 | 15 | 950 | 7.9 E-6 | 2 | 3,405 kg | 9,277 | -322 | 31,589 | -1,096 | 359,393 |
| - onderflens onder dek | 15,220 | 500 | 25 | 7.9 E-6 | 4 | 5,974 kg | 9,277 | -322 | 55,419 | -1,924 | 630,065 |
| Randkoker - (rechts en links) - koker 350x150x6 | 15,130 | 17 | 350 | 7.9 E-6 | 2 | 1,388 kg | 9,277 | -921 | 12,880 | -1,279 | 147,170 |
| Achterhar rijweg - lijf | 12 | 16,200 | 950 | 7.9 E-6 | 2 | 2,899 kg | 1,910 | -221 | 5,538 | -641 | 10,937 |
| Achterhar rijweg - flens | 350 | 16,200 | 25 | 7.9 E-6 | 2 | 2,225 kg | 1,910 | -221 | 4,251 | -492 | 8,250 |
| Dwarsdrager 1 rijweg - lijf | 12 | 11,050 | 950 | 7.9 E-6 | 1 | 989 kg | 4,910 | -322 | 4,855 | -318 | 24,017 |
| Dwarsdrager 1 rijweg - flens | 350 | 11,050 | 25 | 7.9 E-6 | 2 | 1,518 kg | 4,910 | -322 | 7,453 | -489 | 36,769 |
| Dwarsdrager 1 rijweg - lijf | 12 | 2,575 | 300 | 7.9 E-6 | 2 | 146 kg | 4,910 | -322 | 715 | -47 | 3,525 |
| Dwarsdrager 1 rijweg - flens | 350 | 11,050 | 25 | 7.9 E-6 | 4 | 3,036 kg | 4,910 | -322 | 14,907 | -978 | 73,538 |
| Dwarsdrager 2 rijweg - lijf | 12 | 11,050 | 950 | 7.9 E-6 | 1 | 989 kg | 7,910 | -322 | 7,822 | -318 | 62,048 |
| Dwarsdrager 2 rijweg - flens | 350 | 11,050 | 25 | 7.9 E-6 | 2 | 1,518 kg | 7,910 | -322 | 12,007 | -489 | 95,151 |
| Dwarsdrager 2 rijweg - lijf | 12 | 2,575 | 300 | 7.9 E-6 | 2 | 146 kg | 7,910 | -322 | 1,151 | -47 | 9,122 |
| Dwarsdrager 2 rijweg - flens | 350 | 11,050 | 25 | 7.9 E-6 | 4 | 3,036 kg | 7,910 | -322 | 24,015 | -978 | 190,302 |
| Dwarsdrager 3 rijweg - lijf | 12 | 11,050 | 950 | 7.9 E-6 | 1 | 989 kg | 10,910 | -322 | 10,789 | -318 | 117,880 |
| Dwarsdrager 3 rijweg - flens | 350 | 11,050 | 25 | 7.9 E-6 | 2 | 1,518 kg | 10,910 | -322 | 16,561 | -489 | 180,857 |
| Dwarsdrager 3 rijweg - lijf | 12 | 2,575 | 300 | 7.9 E-6 | 2 | 146 kg | 10,910 | -322 | 1,588 | -47 | 17,339 |
| Dwarsdrager 3 rijweg - flens | 350 | 11,050 | 25 | 7.9 E-6 | 4 | 3,036 kg | 10,910 | -322 | 33,123 | -978 | 361,714 |
| Dwarsdrager 4 rijweg - lijf | 12 | 11,050 | 950 | 7.9 E-6 | 1 | 989 kg | 13,910 | -322 | 13,755 | -318 | 191,510 |
| Dwarsdrager 4 rijweg - flens | 350 | 11,050 | 25 | 7.9 E-6 | 2 | 1,518 kg | 13,910 | -322 | 21,115 | -489 | 293,887 |
| Dwarsdrager 4 rijweg - lijf | 12 | 2,575 | 300 | 7.9 E-6 | 2 | 146 kg | 13,910 | -322 | 2,024 | -47 | 28,176 |
| Dwarsdrager 4 rijweg - flens | 350 | 11,050 | 25 | 7.9 E-6 | 4 | 3,036 kg | 13,910 | -322 | 42,231 | -978 | 587,773 |
| Voorhar rijweg - lijf | 12 | 16,200 | 950 | 7.9 E-6 | 1 | 1,450 kg | 16,910 | -221 | 24,515 | -320 | 414,730 |
| Voorhar rijweg - flens | 350 | 16,200 | 25 | 7.9 E-6 | 2 | 2,225 kg | 16,910 | -221 | 37,633 | -492 | 636,502 |
| Onvoorzien (5% van bovenstaande) | | | | | | 3,844 kg | 9,277 | 0 | 35,657 | 0 | 330,791 |
| staart lijf | 4,800 | 50 | 1,200 | 7.9 E-6 | 2 | 4,522 kg | -1,025 | 170 | -4,635 | 769 | 14,105 |
| staart onderflens | 4,800 | 500 | 40 | 7.9 E-6 | 2 | 1,507 kg | -1,025 | 640 | -1,545 | 965 | 5,095 |
| staart bovenflens | 4,800 | 500 | 40 | 7.9 E-6 | 2 | 1,507 kg | -1,025 | -400 | -1,545 | -603 | 4,719 |
| Buis | 762 | 1,000 | 20 | 7.9 E-6 | 2 | 732 kg | 0 | 0 | 0 | 0 | 35 |
| Draaias | 470 | 1,300 | 470 | 7.9 E-6 | 2 | 3,541 kg | 0 | 0 | 0 | 0 | 130 |
| **Ballastkist (Huid)** | | | | | | | | | | | |
| voorplaat | 40 | 11,300 | 1,400 | 7.9 E-6 | 1 | 4,967 kg | -3,424 | 399 | -17,009 | 1,982 | 59,840 |
| achterplaat | 40 | 11,300 | 1,400 | 7.9 E-6 | 1 | 4,967 kg | -5,444 | 476 | -27,043 | 2,365 | 149,159 |
| bovenplaat | 1,700 | 11,300 | 40 | 7.9 E-6 | 1 | 6,032 kg | -4,335 | -245 | -26,148 | -1,478 | 115,169 |
| onderplaat | 1,700 | 11,300 | 40 | 7.9 E-6 | 1 | 6,032 kg | -4,533 | 1,121 | -27,343 | 6,762 | 132,978 |
| **Subtotaal Val:** | | | | | | **114,524 kg** | | | **636,856** | **-32,508** | **9,012,796** |
| **Ballast Val** | | | | | | | | | | | |
| stalen ballast | 1,650 | 11,000 | 545 | 7.0 E-6 | 1 | 69,206 kg | -4,334 | 806 | -299,941 | 55,756 | 1,362,275 |
| lood | 1,650 | 11,000 | 40 | 1.1 E-5 | 0 | 0 kg | -4,334 | 600 | 0 | 0 | 0 |
| **Subtotaal Ballast :** | | | | | | **69,206 kg** | | | **-299,941** | **55,756** | **1,362,275** |

**Verzamelstaat val:**

| | Massa | X | Z | $M_{dicht}$ | $M_{open}$ | Ip |
|---|---|---|---|---|---|---|
| **Totaal val** (excl. Ballast): | 114,524 kg | 5,561 | -284 | 636,856 | -32,508 | 9,012,796 |
| **Ballast** (vast en regel): | 69,206 kg | -4,334 | 806 | -299,941 | 55,756 | 1,362,275 |
| **Totaal val** (incl. ballast): | 183,730 kg | 1834 | 127 | 336,916 | 23,248 | 10,375,071 |

| | | | | 3,369 kNm | 232 kNm | |
|---|---|---|---|---|---|---|
| Oplegdruk gesloten stand | 19,924 kg | 16,910 | | 336,916 | 0 | <= Bij 0.0° |
| Kracht op voorhar in open stand **84°** | 3,450 kg | 16,910 | | 35,217 | 23,120 | <= Bij 84.0° |
| | | | | Openingshoek is : | **84°** | |

Table H-2 Calculation of moments in the bridge during opening and closing procedure

(a)

| Onderwerp: | : Bruggen Wilhelminasluis |
| Onderdeel: | Representatieve statische belastingen op beweegbaar deel |
| | Wind, overgewicht, variabel dekgewicht en tapwrijving |

| | | Wind | Openend | | | | Wind | Sluitend | | | | Gewicht | |
|---|---|---|---|---|---|---|---|---|---|---|---|---|---|
| $\phi$ | h brug | $C_t$ | $P_{w;rep}$ | $M_{w;rep}$ | $P_{w;rep}$ | $M_{w;rep}$ | $C_t$ | $P_{w;rep}$ | $M_{w;rep}$ | $P_{w;rep}$ | $M_{w;rep}$ | $M_{og;rep}$ | $M_{veg;rep}$ |
| (°) | (m) | - | (N/m²) | (kNm) | (N/m²) | (kNm) | - | (N/m²) | (kNm) | (N/m²) | (kNm) | (kNm) | (kNm) |
| | | | 13,7 m/s2 | | 15,8 m/s2 | | | 13,7 m/s2 | | 15,8 m/s2 | | var. | + / - |
| 0 | 4,0 | -0,40 | -100 | -239 | -133 | -318 | 0,40 | 100 | 239 | 133 | 318 | 423 | 119 |
| 0,5 | 4,1 | -0,41 | -105 | -250 | -140 | -333 | 0,40 | 102 | 242 | 135 | 322 | 423 | 119 |
| 1 | 4,3 | -0,43 | -110 | -262 | -146 | -349 | 0,40 | 103 | 246 | 137 | 327 | 423 | 119 |
| 2 | 4,6 | -0,45 | -120 | -287 | -160 | -382 | 0,40 | 106 | 253 | 141 | 337 | 422 | 119 |
| 3 | 4,9 | -0,48 | -131 | -312 | -174 | -415 | 0,40 | 109 | 260 | 145 | 346 | 422 | 119 |
| 4 | 5,2 | -0,51 | -141 | -337 | -188 | -449 | 0,40 | 112 | 266 | 149 | 354 | 422 | 119 |
| 6,1 | 5,8 | -0,56 | -164 | -392 | -219 | -522 | 0,40 | 117 | 279 | 155 | 371 | 420 | 119 |
| 8,2 | 6,4 | -0,62 | -188 | -449 | -250 | -597 | 0,40 | 122 | 290 | 162 | 386 | 418 | 118 |
| 10,3 | 7,0 | -0,67 | -212 | -507 | -283 | -674 | 0,40 | 126 | 300 | 168 | 399 | 416 | 117 |
| 12,4 | 7,6 | -0,73 | -237 | -566 | -316 | -753 | 0,40 | 130 | 310 | 173 | 412 | 413 | 116 |
| 14,5 | 8,3 | -0,79 | -263 | -627 | -349 | -833 | 0,40 | 134 | 319 | 178 | 424 | 409 | 115 |
| 16,6 | 8,9 | -0,84 | -289 | -688 | -384 | -915 | 0,40 | 137 | 327 | 182 | 435 | 405 | 114 |
| 18,7 | 9,4 | -0,90 | -315 | -751 | -419 | -999 | 0,40 | 140 | 334 | 186 | 445 | 400 | 113 |
| 20,8 | 10,0 | -0,95 | -342 | -815 | -454 | -1084 | 0,41 | 148 | 353 | 197 | 470 | 395 | 111 |
| 22,9 | 10,6 | -1,01 | -369 | -879 | -490 | -1169 | 0,45 | 164 | 392 | 219 | 522 | 389 | 110 |
| 25 | 11,2 | -1,07 | -396 | -944 | -527 | -1256 | 0,49 | 181 | 432 | 241 | 574 | 383 | 108 |
| 27,1 | 11,7 | -1,12 | -424 | -1010 | -564 | -1344 | 0,52 | 198 | 472 | 263 | 628 | 376 | 106 |
| 29,2 | 12,3 | -1,18 | -452 | -1077 | -601 | -1432 | 0,56 | 215 | 513 | 286 | 682 | 369 | 104 |
| 31,3 | 12,8 | -1,20 | -466 | -1112 | -620 | -1479 | 0,60 | 232 | 554 | 309 | 737 | 361 | 102 |
| 33,4 | 13,3 | -1,20 | -472 | -1126 | -628 | -1498 | 0,63 | 250 | 596 | 332 | 792 | 353 | 100 |
| 35,5 | 13,8 | -1,20 | -478 | -1140 | -636 | -1516 | 0,67 | 267 | 638 | 356 | 848 | 344 | 97 |
| 37,6 | 14,3 | -1,20 | -484 | -1153 | -643 | -1534 | 0,71 | 285 | 680 | 379 | 905 | 335 | 94 |
| 39,7 | 14,8 | -1,20 | -489 | -1165 | -650 | -1550 | 0,74 | 303 | 723 | 403 | 962 | 325 | 92 |
| 41,8 | 15,2 | -1,20 | -493 | -1177 | -656 | -1565 | 0,78 | 321 | 766 | 427 | 1019 | 315 | 89 |
| 43,9 | 15,7 | -1,20 | -498 | -1187 | -662 | -1579 | 0,82 | 339 | 810 | 452 | 1077 | 305 | 86 |
| 46 | 16,1 | -1,20 | -502 | -1197 | -668 | -1593 | 0,86 | 358 | 853 | 476 | 1135 | 294 | 83 |
| 48,1 | 16,5 | -1,20 | -506 | -1207 | -673 | -1605 | 0,89 | 376 | 897 | 500 | 1193 | 282 | 80 |
| 50,2 | 16,9 | -1,20 | -510 | -1216 | -678 | -1617 | 0,93 | 394 | 941 | 525 | 1251 | 271 | 76 |
| 52,3 | 17,3 | -1,20 | -513 | -1224 | -683 | -1628 | 0,97 | 413 | 984 | 549 | 1309 | 259 | 73 |
| 54,4 | 17,6 | -1,20 | -516 | -1232 | -687 | -1638 | 1,00 | 431 | 1028 | 574 | 1368 | 246 | 69 |
| 56,5 | 17,9 | -1,20 | -519 | -1239 | -691 | -1648 | 1,04 | 450 | 1072 | 598 | 1426 | 233 | 66 |
| 58,6 | 18,2 | -1,20 | -522 | -1245 | -695 | -1656 | 1,08 | 468 | 1116 | 623 | 1485 | 220 | 62 |
| 60,7 | 18,5 | -1,20 | -525 | -1251 | -698 | -1664 | 1,10 | 482 | 1150 | 641 | 1529 | 207 | 58 |
| 62,8 | 18,8 | -1,20 | -527 | -1257 | -701 | -1672 | 1,11 | 487 | 1162 | 648 | 1546 | 193 | 55 |
| 64,9 | 19,1 | -1,20 | -529 | -1262 | -704 | -1679 | 1,12 | 492 | 1174 | 655 | 1562 | 179 | 51 |
| 67 | 19,3 | -1,20 | -531 | -1267 | -706 | -1685 | 1,12 | 497 | 1186 | 661 | 1577 | 165 | 47 |
| 69,1 | 19,5 | -1,20 | -533 | -1271 | -709 | -1690 | 1,13 | 502 | 1197 | 668 | 1592 | 151 | 43 |
| 71,2 | 19,7 | -1,20 | -534 | -1274 | -711 | -1695 | 1,14 | 506 | 1208 | 674 | 1607 | 136 | 38 |
| 73,3 | 19,8 | -1,20 | -536 | -1278 | -713 | -1699 | 1,14 | 511 | 1218 | 680 | 1620 | 121 | 34 |
| 75,4 | 20,0 | -1,20 | -537 | -1280 | -714 | -1703 | 1,15 | 515 | 1228 | 685 | 1634 | 107 | 30 |
| 77,5 | 20,1 | -1,20 | -538 | -1283 | -715 | -1706 | 1,16 | 519 | 1238 | 690 | 1647 | 91 | 26 |
| 79,6 | 20,2 | -1,20 | -539 | -1284 | -716 | -1708 | 1,17 | 523 | 1247 | 696 | 1659 | 76 | 22 |
| 81,7 | 20,3 | -1,20 | -539 | -1286 | -717 | -1710 | 1,17 | 527 | 1256 | 701 | 1671 | 61 | 17 |
| 83,8 | 20,3 | -1,20 | -540 | -1287 | -718 | -1711 | 1,18 | 530 | 1264 | 705 | 1682 | 46 | 13 |
| 84 | 20,3 | -1,20 | -540 | -1287 | -718 | -1711 | 1,18 | 531 | 1265 | 706 | 1683 | 44 | 12 |

Wind:
$C_{dim}$ = 0,95
$\phi w$ = 1,15
lengte/breedte val = 0,97    $C_t$ = -1,2    (bij brug 90° open, wind op onderzijde val)
windgebied = II    $Z_0$ = 0,2 m
niet-beschikbaarheid per jaar = 2 dagen    $U_R$ = 13,7 m/s    in beweging
niet-beschikbaarheid per jaar = 0,5 dagen    $U_R$ = 15,8 m/s    vasthouden in elke stand
Overige belastingen:    $M_{wr;rep}$ = 14 kNm    (tapwrijving, in elke stand van de brug)
$M_{veg;rep}$ = 119 kNm    (in elke openingsstand van de brug, positief of negatief)
$M_{og;rep}$ = 423 kNm    (maximaal in gesloten stand, neemt af met openingshoek brug)

(b)

| $\phi$ (°) | $\alpha$ (°) | x (mm) | $\beta$ (°) | $\varepsilon$ (°) | I (-) | P-Bo (mm) | Q-B (mm) | P-Q (mm) | $\lambda$ (°) | S (-) getal | arm (mm) drijfstang | $\omega_{val}$ (rad/s) | $I_2$ (kgm²) |
|---|---|---|---|---|---|---|---|---|---|---|---|---|---|
| 0 | 64 | 2962 | 84 | 170 | 0,1369 | 3648 | 2280 | 3346 | 5 | 2968 | 300 | 0,0098 | 0,0323 |
| 0,5 | 63 | 2946 | 87 | 164 | 0,2029 | 3929 | 2469 | 3586 | 8 | 2960 | 473 | 0,0145 | 0,0710 |
| 1 | 63 | 2929 | 89 | 160 | 0,2449 | 4154 | 2606 | 3768 | 10 | 2951 | 594 | 0,0175 | 0,1034 |
| 2 | 62 | 2895 | 92 | 153 | 0,3019 | 4546 | 2820 | 4069 | 15 | 2934 | 776 | 0,0216 | 0,1572 |
| 3 | 61 | 2861 | 96 | 148 | 0,3417 | 4907 | 2990 | 4332 | 18 | 2917 | 914 | 0,0244 | 0,2014 |
| 4 | 60 | 2827 | 98 | 143 | 0,3722 | 5260 | 3135 | 4579 | 22 | 2900 | 1027 | 0,0266 | 0,2388 |
| 6,1 | 58 | 2755 | 104 | 135 | 0,4187 | 6018 | 3386 | 5097 | 29 | 2864 | 1213 | 0,0300 | 0,3023 |
| 8,2 | 56 | 2683 | 108 | 128 | 0,4512 | 6851 | 3587 | 5668 | 31 | 2828 | 1352 | 0,0323 | 0,3511 |
| 10,3 | 54 | 2611 | 113 | 122 | 0,4751 | 7828 | 3750 | 6366 | 27 | 2792 | 1460 | 0,0340 | 0,3893 |
| 12,4 | 52 | 2539 | 117 | 116 | 0,4931 | 9043 | 3883 | 7292 | 22 | 2756 | 1542 | 0,0353 | 0,4192 |
| 14,5 | 49 | 2467 | 122 | 111 | 0,5065 | 10667 | 3989 | 8623 | 17 | 2720 | 1606 | 0,0362 | 0,4424 |
| 16,6 | 47 | 2395 | 126 | 106 | 0,5165 | 13042 | 4071 | 10710 | 12 | 2684 | 1653 | 0,0370 | 0,4600 |
| 18,7 | 45 | 2323 | 130 | 102 | 0,5235 | 17013 | 4131 | 14406 | 6 | 2648 | 1686 | 0,0375 | 0,4726 |
| 20,8 | 43 | 2252 | 134 | 97 | 0,5281 | 25375 | 4171 | 22512 | 0 | 2613 | 1708 | 0,0378 | 0,4809 |
| 22,9 | 41 | 2181 | 138 | 93 | 0,5305 | 56273 | 4192 | 53182 | -7 | 2577 | 1719 | 0,0380 | 0,4853 |
| 25 | 39 | 2111 | 142 | 89 | 0,5309 | -138834 | 4196 | 142123 | -88 | 2542 | 1721 | 0,0380 | 0,4861 |
| 27,1 | 37 | 2042 | 146 | 85 | 0,5296 | -27004 | 4184 | 30457 | -83 | 2508 | 1715 | 0,0379 | 0,4836 |
| 29,2 | 35 | 1974 | 150 | 82 | 0,5266 | -13510 | 4158 | 17092 | -78 | 2474 | 1703 | 0,0377 | 0,4782 |
| 31,3 | 33 | 1907 | 154 | 78 | 0,5221 | -8203 | 4119 | 11881 | -73 | 2440 | 1684 | 0,0374 | 0,4701 |
| 33,4 | 31 | 1842 | 158 | 75 | 0,5162 | -5341 | 4069 | 9084 | -70 | 2408 | 1660 | 0,0369 | 0,4595 |
| 35,5 | 28 | 1778 | 162 | 71 | 0,5090 | -3539 | 4009 | 7317 | -66 | 2376 | 1632 | 0,0364 | 0,4467 |
| 37,6 | 26 | 1717 | 166 | 68 | 0,5006 | -2293 | 3941 | 6082 | -64 | 2345 | 1601 | 0,0358 | 0,4321 |
| 39,7 | 24 | 1657 | 170 | 66 | 0,4911 | -1379 | 3868 | 5157 | -62 | 2315 | 1567 | 0,0351 | 0,4159 |
| 41,8 | 22 | 1601 | 174 | 63 | 0,4807 | -680 | 3790 | 4428 | -61 | 2287 | 1532 | 0,0344 | 0,3985 |
| 43,9 | 20 | 1547 | 179 | 60 | 0,4696 | -129 | 3711 | 3833 | -60 | 2260 | 1495 | 0,0336 | 0,3803 |
| 46 | 18 | 1497 | 183 | 58 | 0,4581 | 314 | 3632 | 3335 | -60 | 2235 | 1459 | 0,0328 | 0,3619 |
| 48,1 | 16 | 1451 | 188 | 56 | 0,4464 | 676 | 3556 | 2911 | -60 | 2212 | 1423 | 0,0319 | 0,3436 |
| 50,2 | 14 | 1410 | 193 | 54 | 0,4349 | 973 | 3483 | 2548 | -61 | 2192 | 1390 | 0,0311 | 0,3261 |
| 52,3 | 12 | 1373 | 198 | 52 | 0,4239 | 1219 | 3417 | 2236 | -63 | 2173 | 1359 | 0,0303 | 0,3099 |
| 54,4 | 10 | 1341 | 203 | 51 | 0,4139 | 1423 | 3358 | 1969 | -66 | 2157 | 1331 | 0,0296 | 0,2954 |
| 56,5 | 7 | 1315 | 208 | 49 | 0,4053 | 1591 | 3310 | 1745 | -70 | 2144 | 1308 | 0,0290 | 0,2833 |
| 58,6 | 5 | 1295 | 213 | 49 | 0,3986 | 1728 | 3273 | 1560 | -76 | 2134 | 1290 | 0,0285 | 0,2740 |
| 60,7 | 3 | 1282 | 218 | 48 | 0,3942 | 1840 | 3249 | 1416 | -82 | 2128 | 1278 | 0,0282 | 0,2679 |
| 62,8 | 1 | 1275 | 224 | 48 | 0,3925 | 1929 | 3240 | 1312 | -90 | 2124 | 1271 | 0,0281 | 0,2657 |
| 64,9 | -1 | 1274 | 229 | 48 | 0,3940 | 1998 | 3248 | 1251 | -98 | 2124 | 1271 | 0,0282 | 0,2677 |
| 67 | -3 | 1281 | 234 | 48 | 0,3990 | 2050 | 3275 | 1232 | -107 | 2127 | 1277 | 0,0285 | 0,2745 |
| 69,1 | -5 | 1294 | 239 | 48 | 0,4078 | 2088 | 3324 | 1259 | -117 | 2134 | 1290 | 0,0292 | 0,2867 |
| 71,2 | -7 | 1313 | 245 | 49 | 0,4208 | 2112 | 3398 | 1330 | -126 | 2143 | 1307 | 0,0301 | 0,3053 |
| 73,3 | -9 | 1339 | 249 | 51 | 0,4382 | 2126 | 3504 | 1448 | -134 | 2156 | 1330 | 0,0314 | 0,3311 |
| 75,4 | -11 | 1370 | 254 | 52 | 0,4604 | 2131 | 3648 | 1616 | -141 | 2172 | 1357 | 0,0329 | 0,3656 |
| 77,5 | -14 | 1407 | 259 | 54 | 0,4878 | 2129 | 3843 | 1842 | -148 | 2190 | 1387 | 0,0349 | 0,4103 |
| 79,6 | -16 | 1448 | 263 | 56 | 0,5207 | 2120 | 4106 | 2143 | -154 | 2211 | 1421 | 0,0373 | 0,4674 |
| 81,7 | -18 | 1494 | 267 | 58 | 0,5595 | 2107 | 4469 | 2545 | -159 | 2234 | 1456 | 0,0400 | 0,5399 |
| 83,8 | -20 | 1543 | 270 | 60 | 0,6051 | 2090 | 4984 | 3101 | -164 | 2258 | 1492 | 0,0433 | 0,6313 |
| 84 | -20 | 1548 | 271 | 60 | 0,6098 | 2088 | 5044 | 3165 | -164 | 2261 | 1496 | 0,0436 | 0,6412 |

Krukdrijfstangmechanisme:

| aantal = | 2 | stuks | | $\omega_{kruk}$ = | 0,072 | rad/s | nom. hoeksnelh. krukarm |
|---|---|---|---|---|---|---|---|
| a = | 1722 | mm | lengte krukarm | $n_{motor}$ = | 1476 | omw/min | nom. toerental motor |
| b = | 1252 | mm | lengte drijfstang - niet opgezet | $i_{overbr.}$ = | 2160 | - | $n_{elektromotor}$ / $n_{krukarm}$ |
| c = | 3242 | mm | lengte achterarm, loopt horizontaal | $I_{val}$ = | 8047993 | kgm² | massatraagheid val |
| ha = | 865 | mm | hor. afstand drpnt val - drpnt krukw. | | | | |
| va = | 1768 | mm | vert. afstand drpnt val - drpnt krukw. | | | | |
| va = | 1968 | mm | vert. afstand drpnt val - drpnt krukw. | | | | |
| $\alpha$ = | 63,9 | ° | indien brug gesloten | | | | |
| $\Delta\beta$ = | 186,9 | ° | doorlopen krukhoek bij openen / sluiten van de brug | | | | |

(c)
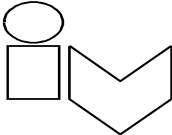
| Onderwerp: | **: Bruggen Wilhelminasluis** |
|---|---|
| Toetsing: | **Uiterste grenstoestand vermoeiing overbrenging** |
| Situatie: | **7. Eenparig bewegen** |
| Rekenwaarde: | $M_{s;d}$ |

| | Openend moment op val | | | | | Sluitend moment op val | | | | |
|---|---|---|---|---|---|---|---|---|---|---|
| | | | | $M_{motoras}$ | | | | | $M_{motoras}$ | |
| $\phi$ | $M_{w;brug}$ | $M_{o;ls;brug}$ | $M_{tot;brug}$ | $M_{s;d}$ | $F_{drijfst}$ | $M_{w;brug}$ | $M_{o;ls;brug}$ | $M_{tot;brug}$ | $M_{s;d}$ | $F_{drijfst}$ |
| (°) | kNm | kNm | kNm | Nm | kN | kNm | kNm | kNm | Nm | kN |
| 0 | -84 | 192 | 109 | 8 | 28 | 84 | 667 | 751 | 53 | 191 |
| 0,5 | -88 | 192 | 105 | 11 | 25 | 85 | 667 | 752 | 78 | 179 |
| 1 | -92 | 192 | 101 | 13 | 23 | 86 | 667 | 753 | 95 | 172 |
| 2 | -100 | 192 | 92 | 14 | 20 | 89 | 667 | 755 | 117 | 163 |
| 3 | -109 | 192 | 83 | 15 | 17 | 91 | 666 | 757 | 133 | 157 |
| 4 | -118 | 192 | 74 | 14 | 15 | 93 | 666 | 759 | 145 | 153 |
| 6,1 | -137 | 191 | 54 | 12 | 10 | 98 | 663 | 761 | 164 | 146 |
| 8,2 | -157 | 190 | 33 | 8 | 6 | 102 | 660 | 762 | 177 | 141 |
| 10,3 | -177 | 189 | 12 | 3 | 2 | 105 | 657 | 762 | 186 | 138 |
| 12,4 | -198 | 188 | -10 | 3 | 2 | 108 | 652 | 760 | 193 | 135 |
| 14,5 | -219 | 186 | -33 | 9 | 6 | 112 | 646 | 758 | 197 | 133 |
| 16,6 | -241 | 184 | -57 | 15 | 10 | 114 | 640 | 754 | 200 | 131 |
| 18,7 | -263 | 181 | -81 | 22 | 14 | 117 | 633 | 750 | 202 | 129 |
| 20,8 | -285 | 179 | -106 | 29 | 18 | 124 | 625 | 748 | 203 | 129 |
| 22,9 | -308 | 176 | -132 | 36 | 23 | 137 | 616 | 753 | 205 | 129 |
| 25 | -331 | 173 | -158 | 43 | 27 | 151 | 606 | 757 | 207 | 130 |
| 27,1 | -354 | 170 | -184 | 50 | 32 | 165 | 596 | 761 | 207 | 130 |
| 29,2 | -377 | 166 | -211 | 57 | 36 | 179 | 584 | 764 | 207 | 131 |
| 31,3 | -389 | 162 | -227 | 61 | 39 | 194 | 572 | 766 | 206 | 132 |
| 33,4 | -394 | 158 | -236 | 63 | 41 | 208 | 560 | 768 | 204 | 133 |
| 35,5 | -399 | 154 | -245 | 64 | 43 | 223 | 546 | 769 | 201 | 133 |
| 37,6 | -404 | 149 | -255 | 66 | 44 | 238 | 532 | 770 | 198 | 134 |
| 39,7 | -408 | 144 | -264 | 67 | 46 | 253 | 517 | 770 | 195 | 134 |
| 41,8 | -412 | 139 | -273 | 67 | 48 | 268 | 502 | 770 | 190 | 134 |
| 43,9 | -416 | 134 | -282 | 68 | 49 | 283 | 485 | 769 | 186 | 134 |
| 46 | -419 | 129 | -290 | 68 | 51 | 299 | 469 | 767 | 181 | 134 |
| 48,1 | -422 | 123 | -299 | 69 | 52 | 314 | 451 | 765 | 176 | 133 |
| 50,2 | -425 | 117 | -308 | 69 | 54 | 329 | 433 | 762 | 170 | 133 |
| 52,3 | -428 | 111 | -317 | 69 | 55 | 345 | 414 | 759 | 165 | 132 |
| 54,4 | -431 | 105 | -326 | 69 | 56 | 360 | 395 | 755 | 161 | 130 |
| 56,5 | -434 | 99 | -335 | 70 | 58 | 375 | 376 | 751 | 157 | 129 |
| 58,6 | -436 | 92 | -344 | 70 | 59 | 391 | 356 | 746 | 153 | 128 |
| 60,7 | -438 | 86 | -352 | 71 | 60 | 402 | 335 | 737 | 149 | 126 |
| 62,8 | -440 | 79 | -361 | 73 | 62 | 407 | 314 | 721 | 145 | 124 |
| 64,9 | -442 | 72 | -370 | 75 | 64 | 411 | 293 | 704 | 143 | 121 |
| 67 | -443 | 65 | -378 | 78 | 66 | 415 | 271 | 686 | 141 | 119 |
| 69,1 | -445 | 58 | -387 | 81 | 68 | 419 | 249 | 668 | 140 | 117 |
| 71,2 | -446 | 51 | -395 | 86 | 71 | 423 | 226 | 649 | 140 | 116 |
| 73,3 | -447 | 43 | -404 | 91 | 74 | 426 | 204 | 630 | 142 | 115 |
| 75,4 | -448 | 36 | -412 | 98 | 78 | 430 | 181 | 611 | 145 | 115 |
| 77,5 | -449 | 29 | -420 | 105 | 82 | 433 | 157 | 591 | 148 | 115 |
| 79,6 | -450 | 21 | -428 | 115 | 87 | 437 | 134 | 571 | 153 | 116 |
| 81,7 | -450 | 13 | -437 | 126 | 93 | 440 | 111 | 550 | 158 | 117 |
| 83,8 | -450 | 6 | -444 | 138 | 100 | 443 | 87 | 530 | 165 | 119 |
| 84 | -450 | 5 | -445 | 140 | 101 | 443 | 85 | 528 | 165 | 119 |
| | | | Maximum: | 140 | 101 | | | Maximum: | 207 | 191 |

| Factoren: | $y$ = 0,25 | $g_w$ = 1,4 | $g_o$ = 1,2 | $\eta$ = 0,9 |
|---|---|---|---|---|

(d)

| Onderwerp: | **: Bruggen Wilhelminasluis** |
|---|---|
| Toetsing: | **Uiterste grenstoestand vermoeiing overbrenging** |
| Situatie: | **Maximale rekenwaarde van koppel op motoras** |
| Rekenwaarde: | $M_{s;d}+M_{s;max;d}$ |

| | | Openend moment val | | | | | | Sluitend moment op val | | | | | |
|---|---|---|---|---|---|---|---|---|---|---|---|---|---|
| | | $M_{val}$ | | | $M_{motoras}$ | | | $M_{val}$ | | | $M_{motoras}$ | | |
| $\phi$ | $\omega$ | $M_{w;brug}$ | $M_{o;ls;brug}$ | $M_{tot;brug}$ | $M_{s;d}$ | $M_{s;d}+M_{s;max;d}$ | $F_{drijfst}$ | $M_{w;brug}$ | $M_{o;ls;brug}$ | $M_{tot;brug}$ | $M_{s;d}$ | $M_{s;d}+M_{s;max;d}$ | $F_{drijfst}$ |
| (°) | (rad/s) | kNm | kNm | kNm | Nm | Nm | kN | kNm | kNm | kNm | Nm | Nm | kN |
| 0 | 15,5 | -84 | 192 | 109 | 8 | 377 | 1360 | 84 | 667 | 751 | 54 | 423 | 1526 |
| 0,5 | 37,5 | -88 | 192 | 105 | 11 | 558 | 1277 | 85 | 667 | 752 | 80 | 627 | 1434 |
| 1 | 54,3 | -92 | 192 | 101 | 13 | 674 | 1224 | 86 | 667 | 753 | 96 | 757 | 1376 |
| 2 | 81,8 | -100 | 192 | 92 | 15 | 829 | 1155 | 89 | 667 | 755 | 119 | 934 | 1301 |
| 3 | 105,2 | -109 | 192 | 83 | 15 | 937 | 1107 | 91 | 666 | 757 | 135 | 1057 | 1249 |
| 4 | 126,3 | -118 | 192 | 74 | 14 | 1019 | 1071 | 93 | 666 | 759 | 148 | 1152 | 1211 |
| 6,1 | 154,6 | -137 | 191 | 54 | 12 | 1142 | 1017 | 98 | 663 | 761 | 167 | 1296 | 1154 |
| 8,2 | 154,6 | -157 | 190 | 33 | 8 | 1225 | 979 | 102 | 660 | 762 | 180 | 1397 | 1116 |
| 10,3 | 154,6 | -177 | 189 | 12 | 3 | 1285 | 951 | 105 | 657 | 762 | 189 | 1471 | 1089 |
| 12,4 | 154,6 | -198 | 188 | -10 | 3 | 1333 | 934 | 108 | 652 | 760 | 196 | 1526 | 1069 |
| 14,5 | 154,6 | -219 | 186 | -33 | 9 | 1376 | 925 | 112 | 646 | 758 | 201 | 1568 | 1054 |
| 16,6 | 154,6 | -241 | 184 | -57 | 15 | 1409 | 921 | 114 | 640 | 754 | 204 | 1597 | 1044 |
| 18,7 | 154,6 | -263 | 181 | -81 | 22 | 1435 | 919 | 117 | 633 | 750 | 205 | 1618 | 1036 |
| 20,8 | 154,6 | -285 | 179 | -106 | 29 | 1454 | 920 | 124 | 625 | 748 | 207 | 1632 | 1032 |
| 22,9 | 154,6 | -308 | 176 | -132 | 37 | 1468 | 922 | 137 | 616 | 753 | 209 | 1640 | 1031 |
| 25 | 154,6 | -331 | 173 | -158 | 44 | 1476 | 927 | 151 | 606 | 757 | 210 | 1643 | 1031 |
| 27,1 | 154,6 | -354 | 170 | -184 | 51 | 1480 | 932 | 165 | 596 | 761 | 211 | 1640 | 1033 |
| 29,2 | 154,6 | -377 | 166 | -211 | 58 | 1479 | 938 | 179 | 584 | 764 | 210 | 1631 | 1035 |
| 31,3 | 154,6 | -389 | 162 | -227 | 62 | 1471 | 944 | 194 | 572 | 766 | 209 | 1618 | 1038 |
| 33,4 | 154,6 | -394 | 158 | -236 | 64 | 1457 | 948 | 208 | 560 | 768 | 207 | 1600 | 1041 |
| 35,5 | 154,6 | -399 | 154 | -245 | 65 | 1439 | 952 | 223 | 546 | 769 | 205 | 1578 | 1044 |
| 37,6 | 154,6 | -404 | 149 | -255 | 67 | 1417 | 956 | 238 | 532 | 770 | 202 | 1552 | 1047 |
| 39,7 | 154,6 | -408 | 144 | -264 | 68 | 1393 | 960 | 253 | 517 | 770 | 198 | 1523 | 1050 |
| 41,8 | 154,6 | -412 | 139 | -273 | 69 | 1366 | 963 | 268 | 502 | 770 | 194 | 1491 | 1051 |
| 43,9 | 154,6 | -416 | 134 | -282 | 69 | 1336 | 966 | 283 | 485 | 769 | 189 | 1456 | 1052 |
| 46 | 154,6 | -419 | 129 | -290 | 70 | 1306 | 967 | 299 | 469 | 767 | 184 | 1420 | 1051 |
| 48,1 | 154,6 | -422 | 123 | -299 | 70 | 1274 | 967 | 314 | 451 | 765 | 179 | 1383 | 1050 |
| 50,2 | 154,6 | -425 | 117 | -308 | 70 | 1244 | 967 | 329 | 433 | 762 | 173 | 1347 | 1047 |
| 52,3 | 154,6 | -428 | 111 | -317 | 70 | 1214 | 965 | 345 | 414 | 759 | 168 | 1312 | 1043 |
| 54,4 | 154,6 | -431 | 105 | -326 | 71 | 1187 | 963 | 360 | 395 | 755 | 164 | 1280 | 1039 |
| 56,5 | 154,6 | -434 | 99 | -335 | 71 | 1165 | 962 | 375 | 376 | 751 | 159 | 1253 | 1034 |
| 58,6 | 154,6 | -436 | 92 | -344 | 72 | 1147 | 960 | 391 | 356 | 746 | 156 | 1231 | 1031 |
| 60,7 | 154,6 | -438 | 86 | -352 | 73 | 1136 | 960 | 402 | 335 | 737 | 152 | 1216 | 1028 |
| 62,8 | 154,6 | -440 | 79 | -361 | 74 | 1133 | 963 | 407 | 314 | 721 | 148 | 1207 | 1026 |
| 64,9 | 154,6 | -442 | 72 | -370 | 76 | 1139 | 968 | 411 | 293 | 704 | 145 | 1208 | 1027 |
| 67 | 154,6 | -443 | 65 | -378 | 79 | 1155 | 977 | 415 | 271 | 686 | 143 | 1220 | 1032 |
| 69,1 | 154,6 | -445 | 58 | -387 | 83 | 1183 | 991 | 419 | 249 | 668 | 142 | 1243 | 1041 |
| 71,2 | 154,6 | -446 | 51 | -395 | 87 | 1222 | 1010 | 423 | 226 | 649 | 143 | 1278 | 1057 |
| 73,3 | 154,6 | -447 | 43 | -404 | 93 | 1275 | 1036 | 426 | 204 | 630 | 144 | 1327 | 1078 |
| 75,4 | 139,4 | -448 | 36 | -412 | 99 | 1342 | 1068 | 430 | 181 | 611 | 147 | 1389 | 1106 |
| 77,5 | 106,0 | -449 | 29 | -420 | 107 | 1423 | 1108 | 433 | 157 | 591 | 151 | 1467 | 1142 |
| 79,6 | 74,5 | -450 | 21 | -428 | 117 | 1522 | 1157 | 437 | 134 | 571 | 155 | 1560 | 1186 |
| 81,7 | 45,2 | -450 | 13 | -437 | 128 | 1638 | 1215 | 440 | 111 | 550 | 161 | 1671 | 1240 |
| 83,8 | 17,9 | -450 | 6 | -444 | 141 | 1773 | 1284 | 443 | 87 | 530 | 168 | 1800 | 1303 |
| 84 | 15,5 | -450 | 5 | -445 | 142 | 1787 | 1291 | 443 | 85 | 528 | 168 | 1814 | 1310 |
| | | | | **Maximum:** | | 1787 | 1360 | | | **Maximum:** | | 1814 | 1526 |

$C_1 = 151{,}52$ Nm/rad rotatiestijfheid overbrenging teruggerekend naar de motoras

$\omega = 15{,}46$ rad/s hoeksnelheid motor op kruipsnelheid bij eindstanden

$\omega = 154{,}6$ rad/s hoeksnelheid motor op nominale snelheid

$\beta = 18{,}45$ ° doorlopen krukhoek bij versnellen/ vertragen

Factoren:  y = 0,25  $g_w$ = 1,4  $g_o$ = 1,2  $\eta$ = 0,885

(e)
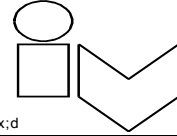
| Onderwerp: | : **Bruggen Wilhelminasluis** |
|---|---|
| Toetsing: | **<u>Uiterste grenstoestand vermoeiing overbrenging</u>** |
| Situatie: | **8.  Begin openen vanuit gesloten stand** |
| Rekenwaarde: | $M_{s;d}+e*M_{a;d} + 0.9*\sqrt{\{(e * M_{a;d})^2 + g_o^2 * w^2*C_1*I_2\}}$        L        $M_{s;d}+M_{s;max;d}$ |

| $\phi$ (°) | $M_{s;d}$ Nm | $I_2$ (kgm$^2$) | $\varepsilon$ - | $\omega$ (rad/s) | $M_{a;d}$ Nm | $M_{motoras}$ Nm | $M_{s;d}+M_{s;max;d}$ Nm | $F_{drijfst}$ kN |
|---|---|---|---|---|---|---|---|---|
| 0 | 54 | 0,0323 | 0,0326 | 15,5 | 20 | 91 | 423 | 329 |

| | **Maximum:** | **91** | **423** | **329** |
|---|---|---|---|---|

| $C_1$ = | 151,52 | Nm/rad | rotatiestijfheid overbrenging teruggerekend naar de motoras |
|---|---|---|---|
| $\omega$ = | 15,46 | rad/s | hoeksnelheid motor op kruipsnelheid |
| $\omega$ = | 154,6 | rad/s | hoeksnelheid motor op nominale snelheid |
| $I_1$ = | 1,15 | kgm$^2$ | massatraagheidsmoment motoras |
| $C_1$ = | 151,52 | kgm$^3$ | rotatiestijfheid overbrenging |
| $d\omega/dt$ = | 13,9 | rad/s$^2$ | hoekversnelling/-vertraging elektromotor |

| Factoren: | y  = 0,25 | $g_w$ = 1,4 | $g_o$ = 1,2 | $\eta$ = 0,885 |
|---|---|---|---|---|
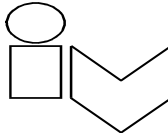
(f)

| Onderwerp: | **: Bruggen Wilhelminasluis** |
| Toetsing: | **Uiterste grenstoestand vermoeiing overbrenging** |
| Situatie: | **9. Aanvang versnellen/vertragen in open stand** |
| Rekenwaarde: | $\phi_a * \varepsilon * (M_{s;d} + M_{a;d}) + (1 - \phi_a * \varepsilon) * M_{s;d}$     L     $M_{s;d} + M_{s;max;d}$ |

|  |  |  | **Openend moment val** | | | | | **Sluitend moment op val** | | | | |
|---|---|---|---|---|---|---|---|---|---|---|---|---|
| $\phi$ | $I_2$ | $\varepsilon$ | $M_{s;d}$ | $M_{a;d}$ | $M_{motoras}$ | $M_{s;d}+M_{s;max;d}$ | $F_{drijfst}$ | $M_{s;d}$ | $M_{a;d}$ | $M_{motoras}$ | $M_{s;d}+M_{s;max;d}$ | $F_{drijfst}$ |
| (°) | (kgm²) | - | Nm | Nm | Nm | Nm | kN | Nm | Nm | Nm | Nm | kN |
| | | | | | | | | | | | | |
| | | | | | Tussenstanden zijn voor vermoeiing niet maatgevend | | | | | | | |
| 84 | 0,6412 | 0,4010 | 142 | 31 | 166 | 1787 | 120 | 168 | 31 | 192 | 1814 | 139 |

| | | | **Maximum:** | 166 | 1787 | 120 | | **Maximum:** | 192 | 1814 | 139 |
|---|---|---|---|---|---|---|---|---|---|---|---|

| $C_1$ = | 151,52 | Nm/rad | rotatiestijfheid overbrenging teruggerekend naar de motoras |
|---|---|---|---|
| $\omega$ = | 15,46 | rad/s | hoeksnelheid motor op kruipsnelheid |
| $\omega$ = | 154,6 | rad/s | hoeksnelheid motor op nominale snelheid |
| $I_1$ = | 1,15 | kgm² | massatraagheidsmoment motoras |
| $C_1$ = | 151,52 | kgm³ | rotatiestijfheid overbrenging |
| $d\omega/dt$ = | 13,9 | rad/s² | hoekversnelling/-vertraging elektromotor |

| Factoren: | y = 0,25 | $g_w$ = 1,4 | $g_o$ = 1,2 | $\eta$ = 0,885 | $\phi_a$ = 1,9 |
|---|---|---|---|---|---|

(g)

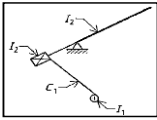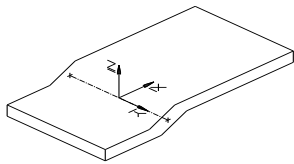| | φ | Moment |
|---|---|---|
| | (°) | kNm |
| Start opening | 0 | 1292 |
| | 0 | 751 |
| | 0,5 | 752 |
| | 1 | 753 |
| | 2 | 755 |
| | 3 | 757 |
| | 4 | 759 |
| | 6,1 | 761 |
| | 8,2 | 762 |
| | 10,3 | 762 |
| | 12,4 | 760 |
| | 14,5 | 758 |
| | 16,6 | 754 |
| | 18,7 | 750 |
| | 20,8 | 748 |
| | 22,9 | 753 |
| | 25 | 757 |
| | 27,1 | 761 |
| | 29,2 | 764 |
| | 31,3 | 766 |
| | 33,4 | 768 |
| | 35,5 | 769 |
| | 37,6 | 770 |
| Opening | 39,7 | 770 |
| | 41,8 | 770 |
| | 43,9 | 769 |
| | 46 | 767 |
| | 48,1 | 765 |
| | 50,2 | 762 |
| | 52,3 | 759 |
| | 54,4 | 755 |
| | 56,5 | 751 |
| | 58,6 | 746 |
| | 60,7 | 737 |
| | 62,8 | 721 |
| | 64,9 | 704 |
| | 67 | 686 |
| | 69,1 | 668 |
| | 71,2 | 649 |
| | 73,3 | 630 |
| | 75,4 | 611 |
| | 77,5 | 591 |
| | 79,6 | 571 |
| | 81,7 | 550 |
| | 83,8 | 530 |
| | 84 | 528 |
| Start Closing | 84 | 612 |



Angle Motion 0-84
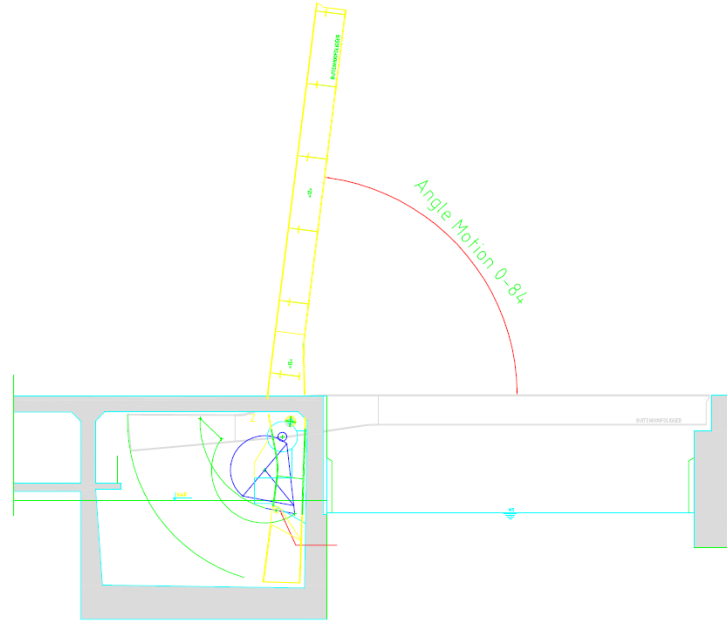
# Table H-3 Calculation of needed force in the ballast

## (a)

---

Project : Bruggen Wilhelminasluis

Onderdeel : Gegevens beweegbaar deel

---

**Brugbeweging:** Openen

| | | |
|---|---|---|
| Totale draaitijd (openen / sluiten): | 60 s | 60.000 s (berekend) |
| Kruiptijd (aan *begin* van de beweging): | 3 s | 1.1111 s 0 naar $\omega_{kruip}$ |
| Versnellingstijd: | 10 s | van $\omega_{kruip}$ naar $\omega_{nom}$. |
| Eenparige snelheid | 34 s | |
| Vertragingstijd: | 10 s | |
| Kruiptijd (aan *eind* van de beweging): | 3 s | |

| | | |
|---|---|---|
| Kruipsnelheid in % van max. snelheid: | 10% | |
| Maximale vertragingstijd bij **noodstop**: | 6 s | 3sec bij $A_{val}$<125m² óf 6sec bij $A_{val}$≥125m² |
| Stijfheid overbrenging $C_1$ | 152 Nm/rad | |
| Massatraagheid aandrijving: $I_1$ | 1.15E+00 kgm² | |
| Massatraagheid val: $I_2$ | 8.05E+06 kgm² | inclusief ballast |
| Maximale openingshoek brug | 84 ° | |

**Windbelasting:**

| | | | |
|---|---|---|---|
| Lengte dek vanaf draaipunt: | L : | 17.23 m | |
| Lengte dek (windvangend) | $L_{dek}$ : | 15.66 m | |
| Breedte dek (windvangend): | $B_{dek}$ : | 16.2 m | $A_{val}$: 254 m² |
| Statisch moment voor wind: | S : | 2385 m³ | $x_S$: 9.4 m |
| Hoogte bk. dek boven draaipunt: | | 0.889 m | |
| Hoogte bk. dek boven maaiveld: | | 3.969 m | |

| | | |
|---|---|---|
| Windgebied (I, II of III): | II | |
| Ruw heidslengte $Z_0$ : | 0.2 m | |

*- Beweging*

| | | |
|---|---|---|
| Niet-beschikbaarheid per jaar: | 2 dagen | |
| $U_R$ op 10 m hoogte - beweging: | 13.7 m/s | (Tabel 3, NEN6786:2001, blz93) |
| Windbelasting $P_{wind;rep}$ : | -540 N/m² | maximaal, bij brug 90° open, wind op onderzijde val |
| Koppel $M_{wind;rep}$: | -1287 kNm | |

*- Vasthouden:*

| | | |
|---|---|---|
| Niet-beschikbaarheid per jaar: | 0.5 dag | |
| $U_R$ op 10 m hoogte - vasthouden: | 15.8 m/s | |
| Windbelasting $P_{wind;rep}$ : | -718 N/m² | maximaal, bij brug 90° open, wind op onderzijde val |
| Koppel $M_{wind;rep}$: | -1711 kNm | |

**Overige belastingen:**

Variabel dekgewicht

| | | |
|---|---|---|
| $P_{veg:rep}$ (pos. of neg.): | 50 N/m² | stalen dek |
| $M_{veg:rep}$ : | 119 kNm | in gesloten stand van de brug, positief of negatief |

Overgewicht

| | | |
|---|---|---|
| Afstand vooropleggingen-draaipunt: | 16.91 m | |
| Brug gesloten: t.p.v. vooropleggingen: | 25 kN | |
| $P_{og:rep}$ : | 177 N/m² | |
| $M_{og:rep}$ : | 423 kNm | |

| | | |
|---|---|---|
| Brug 90 graden geopend: t.p.v. vooropleg | 5 kN | |
| $P_{og:rep}$ : | 35 N/m² | |
| $M_{og:rep}$ : | 9 kNm | |

| | | |
|---|---|---|
| Wrijvingsdiameter draaiassen: | 0.43 m | |
| Wrijvingscoëfficiënt draailagers $\mu_f$ : | 0.02 | |
| Totale vertikale lagerbelasting: | 1620 kN | (gewicht rep.) |
| $M_{wr;rep}$ : | 14 kNm | in elke openingsstand van de brug |

(b)

## Elektromotor (geregelde snelheid)

| | Instelling/capaciteit | Berekend | | |
|---|---|---|---|---|
| Nominaal toerental: | 1476 | | | |
| Toerental bij kruipsnelheid: | 147.6 | | | |
| Nominaal koppel: | 194 | 219 | Nm | Gemiddelde uit: Overschr. Toegek. Motorkoppel |
| Kipkoppel: nominaal koppel x 2.1 | 408 | 390 | Nm | Maximum uit: Overschr. Grensmotorkoppel |
| Nominaal motorvermogen: | 30 | 30 | kW | Gemiddelde uit: Overschr. Toegek. Motorkoppel |

Nominale hoeksnelheid motor $\omega_{nom}$ = 154.57 rad/s
Hoeksnelheid motor bij kruipen $\omega_{kruip}$ = 15.46 rad/s
Versnellen / vertragen motoras: $d\omega/dt$ = 13.91 rad/s² van kruipsnelheid naar nominale snelheid en v.v.
Totaal aantal rotaties door brugbeweging: 7048 rad
Totaal aantal rotaties motor bij openen / sluiten: 7048 rad

## Blokkenrem

Instelling/capaciteit
vlgns §9.8.6.1 incl. $\gamma_m$=1.1 Berekend

| | | | | |
|---|---|---|---|---|
| Remkoppel bij noodstop (=$M_{br;rep}$): | 382.41 Nm | 348 | Nm | Maximum uit: Overschr. noodstop-remkoppel |
| Remkoppel bij vasthouden op wind: | 656.33 Nm | 597 | Nm | Maximum uit: Overschr. vasthoud-remkoppel |
| Noodstop op blokkenrem: | $d\omega/dt$ = 25.8 rad/s² | | | van nominale snelheid naar 0 in 6 sec |

## Overberenging:

Berekend maximaal moment (maximum uit: overbelasten overbrenging)

| | | | | | | |
|---|---|---|---|---|---|---|
| 1. Overbrenging twk: | $n_{in}/n_{uit}$ = 219 | 285.9 | kNm | 476.45 VOBB | 0.70 rad/s | |
| 2. Aantal tanden aandrijvend tandwiel: | 16 | m | 20 | Dstc | 320 mm | |
| Aantal tanden aangedr. tandwiel: | 42 | | 20 | | 840 mm | |
| $n_{in}/n_{uit}$ = | 2.625 | 750.4 | kNm | centrale as en rondsel 1 | | |
| 3. Aantal tanden rondsel 1: | 16 | m | 25 | Dstc | 400 mm | 1.06 m/s |
| Aantal tanden tandwiel 1: | 60 | | 25 | | 1500 mm | 2.58 m/s |
| $n_{in}/n_{uit}$ = | 3.750 | 2814 | kNm | tandwiel 1 / rondsel | 0.1878 | |
| 4. Aantal tanden rondsel 2: | 1 | | | | | |
| Aantal tanden krukwiel: | 1 | | | | | |
| $n_{in}/n_{uit}$ = | 1.000 | 2814 | kNm | krukas | | |
| Totale overbrenging:$n_{motor}/n_{krukwiel}$ = | **2160** 2160.4 | | | O V | | |
| | | Omtrekskracht (rep): | 2501 | 497 kN | | |

Rendementsfactor overbrenging $\eta$ = 0.885
Dynamische vergrotingsfactoren
Door terugslag na remmen/vertragen $\phi_{br}$ = 1.5 Er wordt bij remmen een speling of buffer doorlopen
Voor aanvang versnellen/vertragen $\phi_a$ = 1.9

## Krukdrijfstangmechanisme:

aantal = 2 stuks (Wordt alleen gebruikt bij $F_{drijfstang}$)
Verdeling 67 % op 1 kant
a = 1721.5 mm
b = 1252 mm
c = 3242 mm
ha = 865 mm
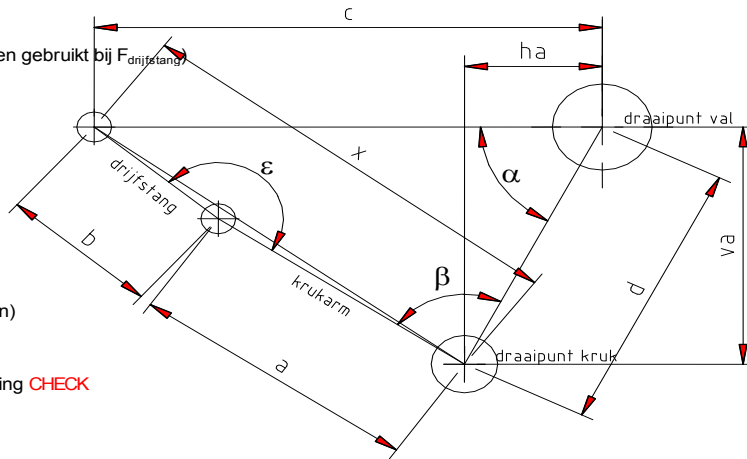va = 1768 mm
d = 1968 mm
$\alpha$ = 63.9 °
x = 2962 mm
$\Delta x$ = 11.1 mm (Bij opzetten)

$M_B$= Nm Voorspanning CHECK



Bewegingswerk – schematisch

$\Delta\beta$ = 186.9 ° doorlopen krukhoek bij openen/sluiten
$\Delta\beta$ = 18.45 ° doorlopen krukhoek bij versnellen/vertragen
$\omega_{kruk}$ = 0.072 rad/s nom. hoeksnelheid krukarm

(c)

<table>
<tr><td>Project</td><td>: Bruggen Wilhelminasluis</td><td></td></tr>
<tr><td>Onderdeel</td><td>: Overzicht rekenwaarden van momenten, krachten en vermogens</td><td></td></tr>
</table>

**Uiterste grenstoestand: overbelasten overbrenging**                                                                                                                1

| Situatie | $M_{toetsing}$ [Nm] | | $M_{s;d}+M_{s;max;d}$ [Nm] | Maatgevend [Nm] | $F_{drijfstang}$ [kN] |
|---|---|---|---|---|---|
| 1. Vasthouden in elke stand | 964 | | - | 964 | 696 |
| 2. Begin openen vanuit gesloten stand | 128 | ^ | 543 | 128 | 463 |
| 3. Aanvang versn./vertr. vanuit open of tussenstand | 572 | ^ | 2599 | 572 | 413 |
| 4. Invallen van remkoppel op volle snelheid | 551 | ^ | 2537 | 551 | 398 |
| 5. Terugslag na remmen | 1113 | ^ | 2537 | 1113 | 804 |
| 6. Doorlopen van een verende buffer | 1303 | | - | 1303 | 941 |
| Aandrukken op opleggingen | nvt | | | | |
| | | | **Rekenwaarde :** | **1303** | **941** |

**Uiterste grenstoestand: vermoeiing overbrenging**

| Situatie | $M_{toetsing}$ [Nm] | | $M_{s;d}+M_{s;max;d}$ [Nm] | Maatgevend [Nm] | $F_{drijfstang}$ [kN] |
|---|---|---|---|---|---|
| 7. Eenparig bewegen | 207 | | - | 207 | 119 |
| 8. Begin openen vanuit gesloten stand | 91 | ^ | 423 | 91 | 329 |
| 9. Aanvang versnellen/vertragen in open stand | 192 | ^ | 1814 | 192 | 139 |
| Invallen van remkoppel | nvt | | | | |
| Terugslag na remmen | nvt | | | | |
| Aandrukken op opleggingen | nvt | | | | |
| | | | **Rekenwaarde :** | **207** | **329** |

**Bruikbaarheidsgrenstoestand: overschrijden grensmotorkoppel**

| Situatie | $M_{motoras}$ | | $P_{motoras}$ | | $F_{drijfstang}$ | |
|---|---|---|---|---|---|---|
| | maximaal [Nm] | gemiddeld [Nm] | maximaal [kW] | gemiddeld [kW] | maximaal [kN] | gemiddeld [kN] |
| 10. Eenparig bewegen | 374 | 250 | 44 | 33 | 270 | 199 |
| 11. Versnellen / vertragen | 390 | 280 | 48 | 37 | 257 | 196 |
| Aandrukken op opleggingen | | | | | | |
| **Maxima:** | **390** | **280** | **48** | **37** | **270** | **199** |

**Bruikbaarheidsgrenstoestand: overschrijden toegekend motorkoppel**

| Situatie | $M_{motoras}$ | | $P_{motoras}$ | | $F_{drijfstang}$ | |
|---|---|---|---|---|---|---|
| | maximaal [Nm] | gemiddeld [Nm] | maximaal [kW] | gemiddeld [kW] | maximaal [kN] | gemiddeld [kN] |
| 12. Eenparig bewegen | 243 | 192 | 34 | 26 | 189 | 154 |
| 13. Versnellen / vertragen | 275 | 219 | 39 | 30 | 194 | 161 |
| **Maxima:** | **275** | **219** | **39** | **30** | **194** | **161** |

**Bruikbaarheidsgrenstoestand: overschrijden remkoppel**

| Situatie | $M_{motoras}$ [Nm] | $F_{drijfstang}$ [kN] |
|---|---|---|
| 14. Vertragen (rem wordt gebruikt bij maken noodstop) | 348 | 228 |
| 15. Vasthouden (rem als vasthoudrem) | 597 | 431 |
| **Maxima:** | **597** | **431** |